



POLITECNICO DI TORINO

Corso di Laurea in Ingegneria Edile

Tesi di Laurea Magistrale

**Thermal-mechanical analysis for
structural response under the fire action:
operative methodologies**

Relatori

Prof. Ing. Roberto Vancetti

Correlatori

Prof. Ing. Marco Domaneschi

Ing. Antonio La Malfa

Ing. Emiliano Cereda

Candidato

Nicola Tunzi

ANNO ACCADEMICO 2020-21

Contents

| | | |
|----------|---|-----------|
| 1 | Introduction | 17 |
| 1.1 | Goals | 19 |
| 2 | Theory | 21 |
| 2.1 | The fire | 21 |
| 2.1.1 | Physics and chemistry of fire | 21 |
| 2.1.2 | The development of fire and flashover | 23 |
| 2.1.3 | Heat Release Rate | 25 |
| 2.2 | Fire Dynamics Simulator | 29 |
| 2.3 | Finite Element Method | 29 |
| 2.3.1 | ANSYS FEM Suite | 31 |
| 2.3.2 | APDL Theory Reference | 33 |
| 2.4 | Heat Transfer Analysis | 36 |
| 2.5 | Coupled thermal-mechanical analysis | 38 |
| 2.5.1 | Historical references | 38 |
| 2.5.2 | Adopted procedures | 40 |
| 3 | Reinforced concrete and fire | 43 |
| 3.1 | General | 43 |
| 3.2 | Physical and chemical response to fire | 44 |
| 3.3 | Effect on structural members | 48 |
| 4 | Standards | 51 |
| 4.1 | Eurocodes | 51 |
| 4.2 | National annexes | 53 |
| 4.3 | Italian Standards | 54 |
| 5 | Engineering Data | 59 |
| 5.1 | Eurocode 2 | 59 |
| 5.1.1 | Stress-strain diagram for concrete and reinforcement steel | 59 |

| | | |
|----------|---|------------|
| 5.1.2 | Thermal elongation for concrete and reinforcement steel | 64 |
| 5.1.3 | Density variation for concrete and reinforcement steel . | 66 |
| 5.1.4 | Specific heat variation for concrete | 68 |
| 5.1.5 | Thermal conductivity variation for concrete | 69 |
| 5.1.6 | Young modulus variation for reinforcement steel | 70 |
| 5.2 | Eurocode 3 | 71 |
| 5.2.1 | Specific heat variation for reinforcement steel | 71 |
| 5.2.2 | Thermal conductivity variation for reinforcement steel . | 72 |
| 5.3 | ASCE 78 | 72 |
| 5.3.1 | Young modulus variation for concrete | 72 |
| 5.4 | Literature papers | 74 |
| 5.4.1 | Poisson ratio variation for concrete | 74 |
| 5.4.2 | Poisson ratio variation for reinforcement steel | 75 |
| 6 | FDS2ANSYS | 77 |
| 6.1 | General | 77 |
| 6.2 | Fields of application and limitations | 78 |
| 6.2.1 | Sensitivity analysis | 79 |
| 6.2.2 | MPI Utility Engine | 80 |
| 6.2.3 | Reinforcing bars interface | 81 |
| 6.2.4 | Limitations | 81 |
| 6.3 | Processes | 82 |
| 6.3.1 | FDS Input File | 86 |
| 6.3.2 | /PREP7 Input File | 88 |
| 6.3.2.1 | Sequential coupled thermal-mechanical analysis | 88 |
| 6.3.2.2 | Direct coupled thermal-mechanical analysis . . | 91 |
| 6.3.3 | Coupled thermal-mechanical analysis | 93 |
| 7 | Validation | 95 |
| 7.1 | Case Study A. | 96 |
| 7.1.1 | Input Data | 96 |
| 7.1.2 | Heat transfer and endothermic analysis | 106 |
| 7.1.3 | Structural analysis | 129 |
| 8 | Considerations | 133 |
| 8.1 | VB.NET Framework | 133 |
| 8.2 | HPC | 134 |
| 8.3 | Software for analysis | 142 |
| 8.4 | Computing time | 144 |
| 9 | Conclusion | 147 |

| | |
|--|------------|
| A HRRSprinklerGen User Manual | 153 |
| A.1 Installation | 154 |
| A.2 Execution | 156 |
| A.3 Use | 158 |
| A.3.1 Parametric HRR - Advanced approach | 158 |
| A.3.1.1 Calculating the time of ignition of nearby items | 165 |
| A.3.1.2 Calculating additional information about the flashover | 166 |
| A.3.1.3 Exporting the HRR diagram as an image | 168 |
| A.3.1.4 Opening the HRR diagram on Microsoft Excel | 168 |
| A.3.1.5 Exporting the HRR diagram as data | 168 |
| A.3.1.6 Generating a HRR diagram with the correction of a sprinkler system | 169 |
| A.3.1.7 Example of generation of a parametric HRR using the complex approach | 173 |
| A.3.1.8 Data to be stored | 173 |
| A.3.1.9 Setting the software | 174 |
| A.3.1.10 Output of the software | 175 |
| A.3.1.11 Plotting modified diagrams | 178 |
| A.3.2 Parametric HRR - Simple approach | 179 |
| A.3.2.1 Generating a HRR diagram with the correction of a sprinkler system | 179 |
| A.3.2.2 Example of generation of a parametric HRR using simple approach | 180 |
| A.3.2.3 Data to be stored | 180 |
| A.3.2.4 Setting the software | 181 |
| A.3.2.5 Output of the software | 181 |
| A.3.3 Premade parametric HRR | 183 |
| A.3.4 Experimental HRR | 186 |
| A.3.4.1 Graph digitizer for an experimental HRR diagram | 187 |
| A.3.4.2 Generating a HRR diagram with the correction of a sprinkler system | 188 |
| A.3.4.3 Example of generation of an experimental HRR | 189 |
| A.3.4.4 Data to be stored | 189 |
| A.3.4.5 Setting the software | 189 |
| A.3.4.6 Output of the software | 189 |
| A.3.4.7 Plotting modified diagrams | 193 |
| A.4 Uninstallation | 194 |
| A.5 Error list | 195 |

| | | |
|----------|---|------------|
| B | FDS2ANSYS Manual | 197 |
| B.1 | Limitations | 200 |
| B.2 | Theory Reference | 201 |
| B.3 | Installation | 204 |
| B.4 | Execution and use | 206 |
| B.4.1 | FDS File Generation | 209 |
| B.4.1.1 | MSAT Utility | 211 |
| B.4.1.2 | FDS geometry | 213 |
| B.4.1.3 | MPI Utility Engine | 214 |
| B.4.1.4 | FDS file | 215 |
| B.4.2 | Thermal-mechanical analysis file generation | 216 |
| B.4.2.1 | 2D Views Panel | 217 |
| B.4.2.2 | Generation of /PREP7 files | 218 |
| B.4.2.3 | Material parameters | 224 |
| B.4.2.4 | Heat Transfer Analysis | 224 |
| B.4.2.5 | Rebar and stirrups settings | 226 |
| B.4.2.6 | Endothermic analysis | 228 |
| B.4.2.7 | Coupled thermal-mechanical analysis | 230 |
| B.5 | Validation | 231 |
| B.6 | Uninstallation | 232 |
| C | Scripts | 233 |
| C.1 | Case Study A. | 233 |
| C.1.1 | Case Study A. - Raw FDS Code | 233 |
| C.1.2 | Case Study A. - Pyrosim FDS Code | 234 |
| C.1.3 | Case Study A. - /PREP7 Code for ANSYS Mechanical APDL #1 | 237 |
| C.1.4 | Case Study A. - /PREP7 Code for ANSYS Mechanical APDL #2 | 241 |
| C.1.5 | Case Study A. - /PREP7 Code for ANSYS Mechanical APDL #3 | 245 |
| C.1.6 | Case Study A. - /PREP7 Code for ANSYS Mechanical APDL #4 | 247 |

List of Figures

| | | |
|-----|--|----|
| 2.1 | The fire triangle | 22 |
| 2.2 | Temperature development stages of a fire - Khoury's representation (2008) | 23 |
| 2.3 | Comparison between experimental and parametric HRR curves | 26 |
| 2.4 | Comparison between experimental and parametric HRR curves, both corrected with the use of a sprinkler system | 28 |
| 2.5 | Comparison between pre-processing and post-processing engines for FDS | 30 |
| 2.6 | Comparison between ANSYS engines | 33 |
| 2.7 | K. Prasad and H. Baum - World Trade Center thermal-structural analysis (2005) | 39 |
| 3.1 | Simplified global presentation of physic-chemical processes in Portland cement concrete during heating - Khoury (2008) | 48 |
| 3.2 | Rigid-supported beam with axial restraint thrust forces - Buchanan (2002) | 50 |
| 4.1 | Nominal fire curves | 52 |
| 5.1 | Stress-strain diagram - Kent and Park's model (1971) | 60 |
| 5.2 | Variation of concrete stress-strain diagram with temperature variation | 60 |
| 5.3 | Variation of reinforcement steel elasto-plastic stress-strain diagram | 62 |
| 5.4 | Rebar stress-strain diagram with temperature variation | 62 |
| 5.5 | Variation of concrete thermal elongation with temperature | 65 |
| 5.6 | Variation of reinforcement steel thermal elongation with temperature | 66 |
| 5.7 | Variation of concrete density with temperature | 67 |
| 5.8 | Variation of steel density with temperature | 67 |
| 5.9 | Variation of concrete specific heat with temperature | 69 |

| | | |
|------|---|-----|
| 5.10 | Variation of concrete thermal conductivity with temperature | 70 |
| 5.11 | Variation of reinforcement steel Young modulus with temperature | 70 |
| 5.12 | Variation of reinforcement steel specific heat with temperature | 71 |
| 5.13 | Variation of reinforcement steel thermal conductivity with temperature | 72 |
| 5.14 | Variation of concrete average Young modulus with temperature | 73 |
| 5.15 | Variation of concrete Poisson ratio with temperature | 74 |
| 5.16 | Variation of reinforcement steel Poisson ratio with temperature | 75 |
| 5.17 | Synthesis of the material properties - Eurocode 2 - Eurocode 3 - ASCE 78 - Literature papers | 76 |
| 6.1 | Generic flowchart for FDS2ANSYS procedures | 78 |
| 6.2 | FDS reading method of geometries. LEFT: how the element is - RIGHT: how the element is read by FDS | 79 |
| 6.3 | Original and equivalent cross-sections of structural members | 82 |
| 6.4 | Complete flowchart for sequential coupling procedures in FDS2ANSYS | 85 |
| 6.5 | Complete flowchart for direct coupling procedures in FDS2ANSYS | 86 |
| 6.6 | Flowchart for FDS2ANSYS procedures to write a FDS input file | 87 |
| 6.7 | Flowchart for FDS2ANSYS procedures to write /PREP7 ANSYS Mechanical APDL preprocessing input files for sequential coupled thermal-mechanical analysis | 91 |
| 6.8 | Flowchart for FDS2ANSYS procedures to write /PREP7 ANSYS Mechanical APDL preprocessing input files for sequential coupled thermal-mechanical analysis | 93 |
| 6.9 | Flowchart for FDS2ANSYS procedures to couple thermal and mechanical analysis for sequential coupled thermal-mechanical analysis | 94 |
| 7.1 | Case Study A. geometrical features for validating the Heat Transfer and Endothermic analysis phases [quotes in millimeters] | 97 |
| 7.2 | C55/67 concrete stress-strain diagram and temperature variation | 98 |
| 7.3 | C55/67 concrete specific heat diagram for 3% of moisture content | 98 |
| 7.4 | C55/67 concrete density diagram | 99 |
| 7.5 | C55/67 concrete thermal conductivity diagram | 99 |
| 7.6 | C55/67 concrete Young modulus diagram | 100 |
| 7.7 | C55/67 concrete thermal elongation diagram | 100 |
| 7.8 | Rebar steel stress-strain diagram | 101 |
| 7.9 | Stirrups steel stress-strain diagram | 101 |

| | |
|---|-----|
| 7.10 Reinforcement steel thermal elongation diagram | 102 |
| 7.11 Reinforcement steel Young modulus diagram | 102 |
| 7.12 Reinforcement steel density diagram | 103 |
| 7.13 Reinforcement steel thermal expansion coefficient diagram . . | 103 |
| 7.14 Reinforcement steel thermal conductivity diagram | 104 |
| 7.15 Reinforcement steel specific heat diagram | 104 |
| 7.16 C55/67 concrete Poisson ratio diagram | 105 |
| 7.17 Reinforcement steel Poisson ratio diagram | 105 |
| 7.18 C55/67 concrete thermal expansion coefficient diagram | 106 |
| 7.19 Benchmark structure as modeled in Thunderhead Engineer- ing Pyrosim - Devices (DEV) for Adiabatic Surface Tempera- ture (AST) and Heat Transfer Coefficient (HTC) - [quotes in millimeters] | 108 |
| 7.20 FDS file configured for the analysis - Thunderhead Engineer- ing Pyrosim 2019 | 109 |
| 7.21 AST01 device - values from FDS and ANSYS Mechanical APDL | 109 |
| 7.22 AST02 device - values from FDS and ANSYS Mechanical APDL | 110 |
| 7.23 AST03 device - values from FDS and ANSYS Mechanical APDL | 110 |
| 7.24 AST04 device - values from FDS and ANSYS Mechanical APDL | 111 |
| 7.25 AST05 device - values from FDS and ANSYS Mechanical APDL | 111 |
| 7.26 AST06 device - values from FDS and ANSYS Mechanical APDL | 112 |
| 7.27 AST07 device - values from FDS and ANSYS Mechanical APDL | 112 |
| 7.28 AST08 device - values from FDS and ANSYS Mechanical APDL | 113 |
| 7.29 AST09 device - values from FDS and ANSYS Mechanical APDL | 113 |
| 7.30 AST10 device - values from FDS and ANSYS Mechanical APDL | 114 |
| 7.31 AST11 device - values from FDS and ANSYS Mechanical APDL | 114 |
| 7.32 AST12 device - values from FDS and ANSYS Mechanical APDL | 115 |
| 7.33 HTC01 device - values from FDS and ANSYS Mechanical APDL | 115 |
| 7.34 HTC02 device - values from FDS and ANSYS Mechanical APDL | 116 |
| 7.35 HTC03 device - values from FDS and ANSYS Mechanical APDL | 116 |
| 7.36 HTC04 device - values from FDS and ANSYS Mechanical APDL | 117 |
| 7.37 HTC05 device - values from FDS and ANSYS Mechanical APDL | 117 |
| 7.38 HTC06 device - values from FDS and ANSYS Mechanical APDL | 118 |
| 7.39 HTC07 device - values from FDS and ANSYS Mechanical APDL | 118 |
| 7.40 HTC08 device - values from FDS and ANSYS Mechanical APDL | 119 |
| 7.41 HTC09 device - values from FDS and ANSYS Mechanical APDL | 119 |
| 7.42 HTC10 device - values from FDS and ANSYS Mechanical APDL | 120 |
| 7.43 HTC11 device - values from FDS and ANSYS Mechanical APDL | 120 |
| 7.44 HTC12 device - values from FDS and ANSYS Mechanical APDL | 121 |
| 7.45 Adiabatic Surface Temperature error ratio | 123 |
| 7.46 Heat Transfer Coefficient error ratio | 124 |

| | | |
|------|---|-----|
| 7.47 | Thermal banded map | 125 |
| 7.48 | Control points along the axis of the beam | 126 |
| 7.49 | Comparison of temperature values over the time | 127 |
| 7.50 | Error ratio for the quarter depth control point | 128 |
| 7.51 | Error ratio for the mid depth control point | 128 |
| 7.52 | Four-point bending configuration for the beam [quotes in mil- limeters] | 129 |
| 7.53 | Comparison of mid-span deflection values over the time | 130 |
| 7.54 | Error ratio for the mid-span deflection | 130 |
| 7.55 | Mid-span displacement banded map | 131 |
| | | |
| 8.1 | WS01 CPU: Intel Xeon E5 2683 v3 – 2.00 GHz CPU x 14 cores (28 threads) | 135 |
| 8.2 | WS01 Mainboard: AsRock X99 Extreme 4 | 136 |
| 8.3 | WS01 Memory: 32 GB DDR4 | 136 |
| 8.4 | WS01 GPU: nVidia GeForce GTX 1060 – 6 GB GDDR5 | 137 |
| 8.5 | WS01 Local IP Address | 137 |
| 8.6 | SERVER01 CPU #1: AMD Opteron 6234 - 2.40 GHz CPU x 12 core (12 threads) | 138 |
| 8.7 | SERVER01 CPU #2: AMD Opteron 6234 - 2.40 GHz CPU x 12 core (12 threads) | 138 |
| 8.8 | SERVER01 Mainboard: HP Enterprise DL385P Gen 8 | 139 |
| 8.9 | SERVER01 Memory: 48 GB DDR3 | 139 |
| 8.10 | SERVER01 GPU: nVidia Quadro 4000 - 2 GB GDDR5 | 140 |
| 8.11 | SERVER01 Local IP Address | 140 |
| 8.12 | Microsoft Windows Server 2016 deployment environment | 141 |
| 8.13 | Thunderhead Engineering Pyrosim Cluster FDS | 143 |
| 8.14 | ANSYS Mechanical APDL Product Launcher - High Perform- ance Computing Setup | 143 |
| 8.15 | Computing time needed for the case CTSA01 | 145 |
| 8.16 | Computing time needed for the case CTSA02 | 145 |
| 8.17 | Needed storage for the monitored cases | 146 |
| | | |
| 9.1 | Complete flowchart for structural safety checks through thermal- mechanical using HRRSprinkler Gen and FDS2ANSYS | 150 |
| | | |
| A.1 | HRRSprinkler Gen - Installation steps | 155 |
| A.2 | HRRSprinkler Gen - Splash screen | 156 |
| A.3 | HRRSprinkler Gen - Main screen | 157 |
| A.4 | HRRSprinkler Gen - About screen | 158 |
| A.5 | HRRSprinkler Gen - Facade ventilation openings dimensions | 161 |

| | | |
|------|--|-----|
| A.6 | HRRSprinkler Gen - Roof ventilation openings features - only available in the Kawagoe approach | 162 |
| A.7 | HRRSprinkler Gen - End purpose of analysis selection | 164 |
| A.8 | HRRSprinkler Gen - Generation of HRR diagram | 164 |
| A.9 | HRRSprinkler Gen - Ignition of nearby items | 166 |
| A.10 | HRRSprinkler Gen - Additional flashover information | 168 |
| A.11 | HRRSprinkler Gen - HRR Sprinkler User Interface | 169 |
| A.12 | HRRSprinkler Gen - Software setting for the example 4.1.7 | 174 |
| A.13 | HRRSprinkler Gen - Output HRR diagram for the example 4.1.7 | 175 |
| A.14 | HRRSprinkler Gen - Output sprinkler diagrams for the example 4.1.7 | 177 |
| A.15 | HRRSprinkler Gen - Software instability for estimating sprinkler activation time with slower fire | 178 |
| A.16 | HRRSprinkler Gen - Output HRR diagram for the example 4.2.2 | 181 |
| A.17 | HRRSprinkler Gen - Output diagram for the example 4.2.2 | 183 |
| A.18 | HRRSprinkler Gen - Experimental HRR diagrams importing | 186 |
| A.19 | HRRSprinkler Gen - Importing an HRR diagram from an image using the Graph Digitizer | 188 |
| A.20 | HRRSprinkler Gen - Output HRR diagram for the example 4.4.2 | 191 |
| A.21 | HRRSprinkler Gen - Output sprinkler diagrams for the example 4.4.2 | 192 |
| A.22 | HRRSprinkler Gen - Successful estimation of the sprinkler activation time | 193 |
| A.23 | HRRSprinkler Gen - Uninstallation steps | 194 |
| | | |
| B.1 | Flowchart for one-way coupling | 199 |
| B.2 | Original and equivalent cross-sections of structural members | 200 |
| B.3 | FDS2ANSYS - Installation steps | 205 |
| B.4 | FDS2ANSYS - Splash screen | 206 |
| B.5 | FDS2ANSYS - Decimal separator alert | 206 |
| B.6 | Decimal separator setting tab - Microsoft Windows 10 Control Panel | 207 |
| B.7 | FDS2ANSYS - Welcome screen | 207 |
| B.8 | FDS2ANSYS - Main screen for Step I | 210 |
| B.9 | FDS2ANSYS - Control to find the geometry file | 210 |
| B.10 | FDS reading method of geometries. LEFT: how the element is - RIGHT: how the element is read by FDS | 212 |
| B.11 | FDS2ANSYS - Mesh Sensitivity Analysis Tool | 213 |
| B.12 | FDS2ANSYS - Check of the entity calculus | 214 |
| B.13 | FDS2ANSYS - MPI Utility Engine | 215 |
| B.14 | FDS2ANSYS - Smokeview file not found error | 215 |

| | |
|--|-----|
| B.15 FDS2ANSYS - Main screen for Step II | 217 |
| B.16 FDS2ANSYS - 2D View Panel, example for a simply supported beam | 218 |
| B.17 Complete flowchart for sequential coupling procedures in FDS2ANSYS | 220 |
| B.18 Complete flowchart for direct coupling procedures in FDS2ANSYS | 221 |
| B.19 FDS2ANSYS - Heat Transfer Analysis progress window | 225 |
| B.20 FDS2ANSYS - Rebar/stirrups settings panel | 226 |
| B.21 Running the Endothermic analysis in ANSYS Mechanical APDL | 229 |
| B.22 Flowchart for FDS2ANSYS procedures to couple thermal and mechanical analysis for sequential coupled thermal-mechanical analysis | 231 |
| B.23 FDS2ANSYS - Uninstallation message prompt | 232 |

English Abstract

The traditional approach in order to estimate the structural response to fire is by mean of prescriptive methods, based on parametric time-temperature curves. These mathematical laws should approximately describe the global behavior of the structural members when fire is occurring. Despite this method is much faster and simpler than the engineering-based one, it does not take into account of many relevant aspect, such as the geometrical features, the chemical reaction of the combustion and the position of the fire, that cannot be considered in a rigorous way. Several curves have been implemented by the current standards, in order to state the minimum requirements to satisfy security checks when the structure is subjected to fire. For this reason, this research has the goal to find a way, using advanced mathematical methods, to check the local and global structural behavior performing coupled thermal-mechanical analysis. Furthermore, a subsequent phase of study may focus the attention on the displacement-based failure criteria, through the execution of a force-control structural analysis. Indeed, through a profitable collaboration with the Italian National Fire Brigade (CNVVF – Corpo Nazionale dei Vigili del Fuoco) - Piedmont Division -, this research has been carried on to find an automatized method to perform thermal-structural using a commercial FEM codes – ANSYS Mechanical APDL, which is one of the most used Finite Element Method code worldwide, which allows all purposes engineering analysis - and FDS - a Computational Fluid Dynamic simulator for fire scenarios -, through a force-control static structural analysis. Since the exothermic analysis is not performed under the same calculation engine of the FEM code, the available procedures are not always automatized and this is a relatively new field of research. Nevertheless, the needed computing time and the Information Technology knowledge and resources may be very onerous. In order to do this and to optimize the needed time for studying the structural behavior of a building, an experimental interface called FDS2ANSYS has been developed – under Microsoft Windows Visual Basic .NET Framework 4.7.2 Environment - as a bridge-software between FDS and ANSYS Mechanical APDL.

Nevertheless, the FDS setting phase should be also considered: in order to simulate realistic scenarios, a preliminary study on the characterization of the HRR curves has been done and a software, called HRRSprinkler Gen, has been deployed. Through this simple software – developed under Microsoft Windows Visual Basic. NET Framework 4.7.2 Environment -, it is possible to generate parametric or experimental HRR curves from the insertion of typical parameters or through images and to correct them with the sprinkler installation. This phase of study allowed to deploy FDS2ANSYS more easily.

Although steel structures are the ones which suffer more the fire load – due to the high thermal deformation rate, typical of metallic materials -, a statistical survey carried on by the Italian National Fire Brigade (CNVVF – Corpo Nazionale dei Vigili del Fuoco) showed that the activities, for which a fire prevention analysis (both thermal and structural) may be required, are located mostly in concrete structures, both with ordinary and prestressed rebar configuration.

Thus, this research has been carried on to find the strategies to investigate on local collapses of reinforced concrete structures exposed to fire and, for this reason, FDS2ANSYS has been developed to study the structural behavior only for concrete structures.

Keywords: FDS, Structural Fire Resistance, Reinforced Concrete, FEM, ANSYS Mechanical APDL

Abstract Italiano

L'approccio tradizionale per la stima del comportamento delle strutture esposte al fuoco avviene attraverso metodi prescrittivi, basati su curve di incendio di tipo parametrico. Queste leggi matematiche dovrebbero approssimativamente descrivere il comportamento globale delle membrature strutturali durante un incendio. Nonostante questo metodo sia molto più veloce e semplice di quello prestazionale, ha la limitazione di non tener conto di diversi aspetti rilevanti, come la configurazione geometrica del compartimento antincendio, la reazione chimica della combustione e la posizione del focolaio. Le normative cogenti riportano diverse curve di incendio, al fine di stabilire i requisiti minimi per soddisfare le verifiche di sicurezza quando una struttura è esposta al fuoco. Per tale motivo, i principali obiettivi riguardano la ricerca di metodi numerici avanzati finalizzati alla verifica del comportamento strutturale locale e globale, eseguendo analisi termo-meccaniche accoppiate. Inoltre, un conseguente studio potrebbe riguardare la determinazione di un criterio di collasso delle strutture, attraverso un'analisi statica strutturale in controllo di forze. Infatti, da una proficua collaborazione con il Corpo Nazionale dei Vigili del Fuoco - Direzione Regionale del Piemonte -, questa ricerca ha inoltre avuto come obiettivo quello di trovare un metodo automatizzato per condurre analisi termo-meccaniche, utilizzando un codice FEM commerciale – ANSYS Mechanical APDL, uno dei codici FEM più utilizzati al mondo per la sua trasversalità d'uso nelle analisi ingegneristiche – e FDS – un calcolatore per fluidodinamica computazionale CFD ottimizzato per gli scenari di incendio – per condurre analisi statiche strutturali in regime di controllo di forze. Dal momento che l'analisi esotermica d'incendio non è eseguita sotto lo stesso motore di calcolo del codice FEM, le procedure disponibili non sono sempre automatizzate e, nondimeno, si tratta di un settore della ricerca relativamente nuovo. Oltretutto, anche i tempi e le conoscenze informatiche, nonché le risorse, possono essere piuttosto onerosi. Al fine, quindi, di ottimizzare il tempo necessario per lo studio del comportamento strutturale di un edificio, è stata programmata un'interfaccia sperimentale chiamata FDS2ANSYS – sviluppata sotto ambiente Microsoft Windows Vi-

sual Basic .NET Framework 4.7.2. Questo software è un vero e proprio ponte tra FDS e ANSYS Mechanical.

Questione da non tralasciare è quella della fase di settaggio di FDS: al fine di simulare scenari d'incendio realistici, è stato affrontato uno studio preliminare sull'incendio e le curve HRR, da cui è stato sviluppato un software denominato HRRSprinkler Gen. Attraverso questo semplice programma – sviluppato sotto ambiente Microsoft Windows Visual Basic .NET Framework 4.7.2 – è possibile generare curve HRR parametriche o sperimentali, dall'inserimento di alcuni parametri o direttamente dalle immagini e di correggere tali diagrammi tramite l'installazione di un impianto sprinkler. Nondimeno, questa fase di studio ha permesso di conseguire lo sviluppo di FDS2ANSYS con più facilità e cognizione di causa.

Sebbene le strutture in acciaio siano quelle che risentono maggiormente delle sollecitazioni termiche, dovute all'alto tasso di deformabilità tipico dei materiali metallici, un'indagine statistica condotta dal Corpo Nazionale dei Vigili del Fuoco ha mostrato come le attività, per le quali è richiesta un'analisi termo-strutturale ai fini della prevenzione incendi, sono prevalentemente localizzate in strutture in calcestruzzo armato, ad armatura sia ordinaria che pretesa.

Dunque, questa ricerca ha come scopo la redazione di un insieme di strategie a comporre un metodo per lo studio dei meccanismi di collasso localizzati delle strutture in calcestruzzo armato esposte al fuoco e, per questa ragione, FDS2ANSYS è stato sviluppato per il solo studio del comportamento strutturale di edifici in conglomerato cementizio armato.

Keywords: FDS, Resistenza al fuoco delle strutture, Cemento armato, FEM, ANSYS Mechanical APDL

Chapter 1

A brief introduction to the fire resistance capacity of structures

The Italian ¹ and European ² Standards are based on prescriptive approaches about checking fire resistance capacity of structures. Several simplified methods are implemented in the most common codes and most of them are based on parametric time-temperature curves, such as the cellulosic fire curve or the hydrocarbon fire curve which are both reported in the EN 1991-1-2 Code. The use of these simplified curves do not take in account the randomness of fire and cannot accurately represent what happens in a fire compartment. The main reason is due to the adaptation of these curves to every situation, without considering the geometric boundary conditions and the fire evolution settings, if governed by oxygen supply or by fire distribution.

In order to have realistic scenarios about which is the structural behavior under the fire stress, this research focused the attention on advanced numerical models. In particular, two different calculus engines have been taken in account:

- **Fire Dynamics Simulator** engine, based on Computational Fluid Dynamics and capable of modelling accurately the fire propagation onto a three dimensional model;

¹Italian Technical Fire Prevention Standards - Ministerial Decree 3rd of August, 2015 and subsequent amendments and additions

²EN 1991-1-2:2004 Standard: "Eurocode 1: Actions on structures – Part 1-2: General actions – Actions on structures exposed to fire"

- **Finite Element Method** engine, used to predict local and global structural behavior.

Through the coupling of these two calculus engines, it is possible to predict accurately which is the effective structural behavior. What is needed to achieve this goal, is to perform coupled thermal-mechanical analysis, which is a relatively new area of research. The coupling procedure of these two kinds of analysis can be different.

- **One-way coupled analysis:** the fire scenario is modeled once and the temperature-time profiles are carried out from FDS. Then a time-history thermal-mechanical analysis is performed and all collapses configuration are considered;
- **Two-way coupled analysis:** the fire scenario is modeled once and the temperature-time profiles are carried out from FDS in order to perform thermal-mechanical analysis. During the structural analysis, when the first structural collapse occurs, the structure is remodeled, following the deformed-shape configuration and another FDS analysis is performed, restarting from the boundary condition of the collapse time-step. After this, the coupled thermal-mechanical analysis goes on until the second structural collapse occurs. This iterative procedure is carried on for a variable maximum number of structural collapses (which corresponds to the number of iterations).

In this research, a simplified method of monitoring the structural behavior has been developed, using a one-way coupled analysis methodology. Taking into account a statistical survey carried on by the Italian National Fire Brigade (CNVVF – Corpo Nazionale dei Vigili del Fuoco), in Italy the most widespread structural typologies on which fire resistance capacity analysis needs to be performed are concrete warehouses, both with ordinary and prestressed rebar configuration. This procedure has been studied only to a very limited number of cases, due to the many limitations that appeared during this study.

The main aim of this research is to study the feasibility of the coupling procedures of CFD fire simulation to finite element structural response analysis. In order to achieve this goal, a software called FDS2ANSYS has been developed on Microsoft Windows environment, using Visual Basic .NET programming language, implemented on the .NET Framework 4.7.2. This experimental interface has been developed only for concrete structures.

1.1 Main aims of this research

At first, the main goals of this research have been defined:

- Optimizing the quality of the obtained data;
- Understanding the techniques of coupling multi-field analysis;
- Facilitating and automating the procedure for coupling thermal and structural analysis by finding a method to perform coupled thermal-structural analysis;
- Stating the structural behavior under fire stress and defining strategies to achieve safety conditions for occupants;
- Understanding which parameters affect the structural behavior.

Chapter 2

Preliminary theory references

Several theory references have been explored, in order to fully understand all the aspect on which this research work is based on.

2.1 Analytical study of fire

Combustion is a complex matter, which needs to be studied carefully. Even if CFD modelers are automated and relatively simple to use, the phenomena on which the fire development is based on have to be explained as well. For this reason the physical and chemical aspects of combustion - which are the fundamentals of the conventions and the hypothesis of the Fire Engineering -, are described in the following paragraphs.

2.1.1 Physics and chemistry of fire

Combustion is an exothermic oxidation reaction which happens rapidly and generates high rates of thermal energy. According to Denoël ¹, it can be synthesized with the contemporary reaction of three elements - representing the fire triangle, [Figure 2.1] - which are essential for the initiation, continuation and diffusion of flames:

- **Input heat:** solid and liquid materials must be heated sufficiently to produce vapors to burn. In this way, several materials have been tested in laboratory under known condition to find the lowest temperature at which these vapors are produced in sufficient quantify to burn. This temperature is also known as ignition temperature;

¹DENOËL J.F. (2007): "Fire Safety and Concrete Structures", FEBELCEM - Federation of Belgian Cement Industry

- **Fuel:** materials, in form of solid, liquid or gas, subjected to combustion. In order to make the fuel burn, it needs to be heated sufficiently to produce vapors;
- **Oxygen:** the primary source of oxygen is atmosphere, with approximately 20% of it; experimental data demonstrates that at least 15% of oxygen is needed for the continuation of combustion.

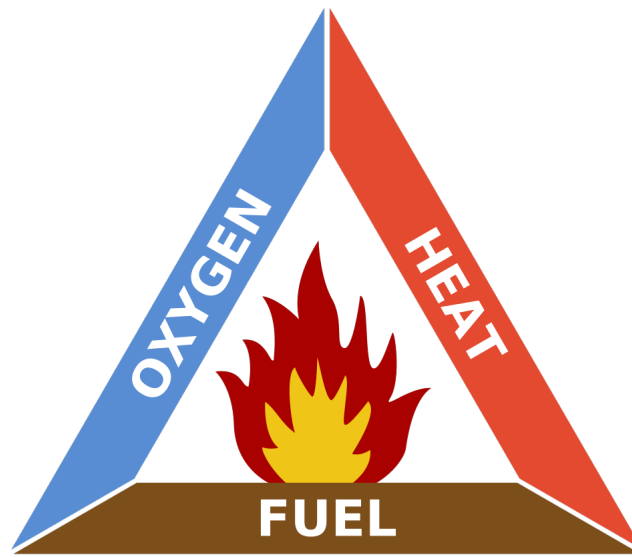
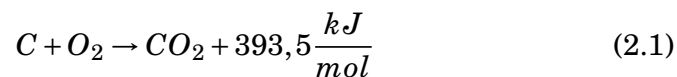


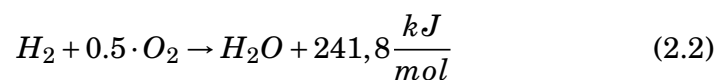
Figure 2.1: The fire triangle

The speed of oxidation, which depends on the speed of production of vapors, is the most important aspect because it influences the speed of decomposition of the fuel, the combination of combustion products and the released thermal energy, whose maximum value is obtained with the stoichiometric combustion - **Equations 2.1 - 2.3:**

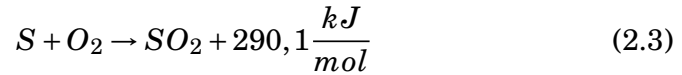
- **Oxidation reaction for carbon**



- **Oxidation reaction for hydrogen**



- **Oxidation reaction for sulfur**



2.1.2 The development of fire and flashover

In this section the behavior of fire and how it is analytically studied will be briefly explained. The development can be seen as the effect of combustion, by mean of a variation of temperature over the time. This distribution, on a XY-graph, is called fire curve, as previously said. Depending on the range-variation of temperature, it is possible to divide the development of the fire into several zones, according to the Khoury's representation of the temperature development stages² - **[Figure 2.2]**:

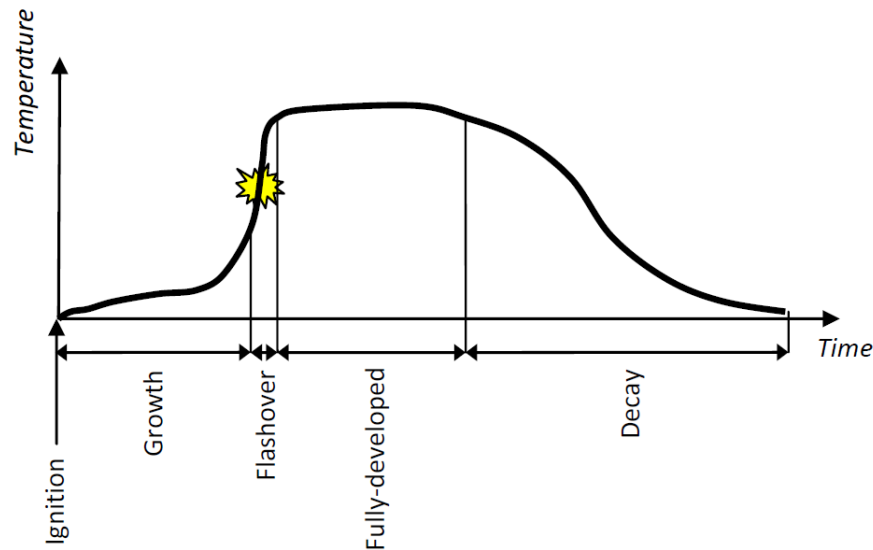


Figure 2.2: Temperature development stages of a fire - Khoury's representation (2008)

- **Ignition:** by the presence of a fuel, oxygen and an input heat, once the so-called temperature of ignition is reached, the combustion begins. The mostly diffused techniques of extinguishing fire are based on the subtraction of one of these three elements that causes the decay of the fire;

²KHOURY G. A. (2008): "Passive fire protection of concrete structures", Proceedings of the Institution of Civil Engineers, Structures & Buildings 161, Issue SB3, June 2008

- **Growth:** from the ignition, a small amount of material begins to burn and the first smoke are produced. The presence of oxygen supplies the fire and, in the environment, two layered zones begin to develop: a lower zone, with lower temperatures in which the coolest air is pumped, and an higher zone, with hotter smoke, called ceiling jet gasses³. While the fire develops, the cooler lower layer allows occupants to escape safely but the layer interface from these two zones becomes shorter, because of the saturation of the air with these gasses and smoke. During this phase, the temperature increases - more or less fast - and it is possible to approximate this phase with a quadratic or an exponential mathematical function on a fire curve. This assumptions are made on the hypotheses that a single object is burning but the presence of flammable items in the fire compartment may significantly increase the growth-speed of the fire. With this phase, the pre-flashover fire regime ends;
- **Flashover:** this name comes from the flash that occurs during a fire when the critical radiant heat flux value is reached. This situation usually occurs around 500-600°C and all the exposed combustible materials in a fire compartment start to burn⁴. This phase is usually characterized by a rapid increase of the temperature that is the boundary condition for the beginning of the fully-developed fire phase;
- **Fully-developed Fire:** from this phase, the post-flashover fire regime begins and the global behavior of the fire is completely different: there are no more two layered zones but an only one zone where the flows of the air become highly turbulent and, for this reason, a two-zone modeling technique cannot be adopted anymore. In this phase, the temperature can reach values over 1000°C and, together with the radiant heat fluxes, pyrolyse produces a very large amount of combustion gasses. In addition, this phase shows differences depending on the ventilation amount and, for this reason, fuel-controlled and ventilation-controlled fires can be distinguished.
- **Decay:** when the available fuel or oxygen, inside a fire compartment, is lacking, the decay phase occurs, with the natural extinguishing of the fire and the consequent temperature decreasing phase.

³BUCHANAN A. H. (2002): "Structural Design for Fire Safety", John Wiley and Sons, New York, USA

⁴DRYSDALE D. (1998): "An introduction to fire dynamics, second edition", John Wiley and Sons, New York, USA

2.1.3 Heat Release Rate

As previously described, the most basic way to study the fire development is through a fire curve and this approach has been largely implemented by the prescriptive methods, reported in the current Standards. Unfortunately, the temperature distribution is highly influenced by the availability of combustible materials and the geometric features of the fire compartment and these aspects can be taken in account only through an engineering-based method. This approach is based on the total energy rate released during a fire and it is described by the Heat Release Rate curve. An HRR curve is the representation, on a XY graph, of the released energy of a fire (a burner) over the time⁵. The HRR value can also be seen as the thermal steady-state balance of a fire compartment - **Equation 2.4**:

$$RHR = RHR_C + RHR_W + RHR_{GAS} + RHR_{RAD} \quad (2.4)$$

where:

- RHR_C : is the leakage convective thermal power through the ventilation openings;
- RHR_W : is the leakage convective and radiative thermal power through the surrounding structures;
- RHR_{GAS} : is the leakage radiative thermal power through the ventilation openings;
- RHR_{RAD} : is the thermal power of the combustion gasses.

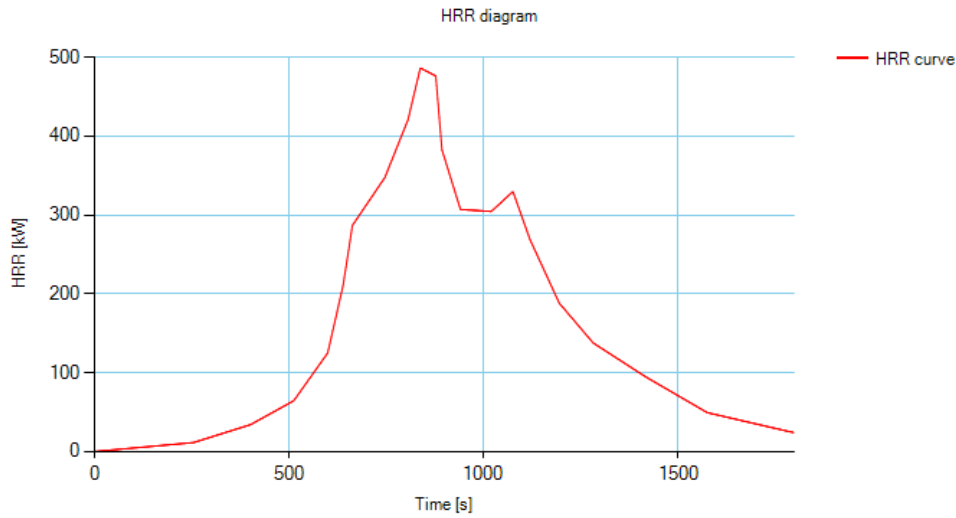
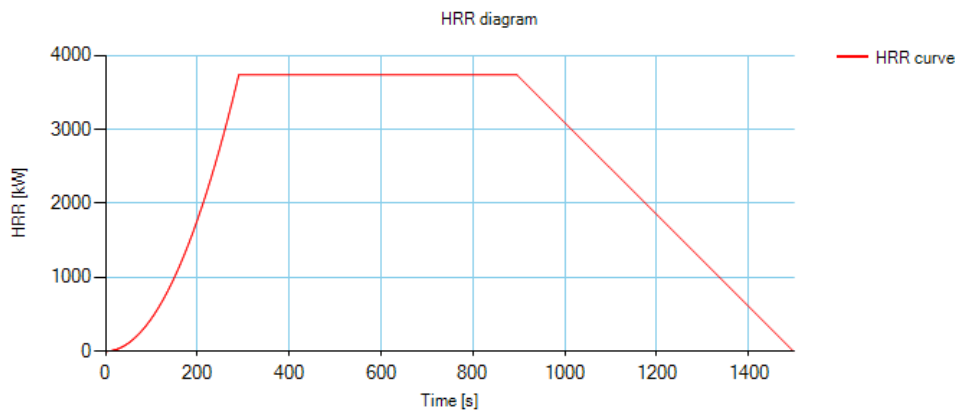
Furthermore, the air mass balance of a fire compartment can be defined as follows - **Equation 2.5**:

$$m_{out} = m_{in} + m_c \quad (2.5)$$

where:

- m_{out} : is the outgoing gasses and smoke mass flow;
- m_{in} : is the ingoing gasses and smoke mass flow;
- m_c : is the fuel mass flow, due to pyrolysis.

⁵LA MALFA A., LA MALFA S., LA MALFA R. (2020): "Ingegneria della Sicurezza Antincendio", Legislazione Tecnica, Rome, Italy

(a) *Experimental HRR curve*(b) *Parametric HRR curve***Figure 2.3:** Comparison between experimental and parametric HRR curves

These curves are widely diffused in the literature, for example the *SFPE Handbook of Fire Protection Engineering*⁶ reports several HRR curves which have been built from experimental tests in fire-simulation rooms. These curves can take in account if the fire is fuel controlled or ventilation controlled and, for these reason, several mathematical functions have been formulated to this purpose. There are two kinds of HRR curves:

- **Experimental HRR curves:** as previously said, these curves are the

⁶HURLEY M.J (2016); "SFPE Handbook of Fire Protection Engineering - Fifth edition", Springer, United States

result of experimental tests on fire-simulation rooms. Usually, these curves represent the energy rate released by a certain item or material. An example of experimental HRR curve is shown in the [Figure 2.3a];

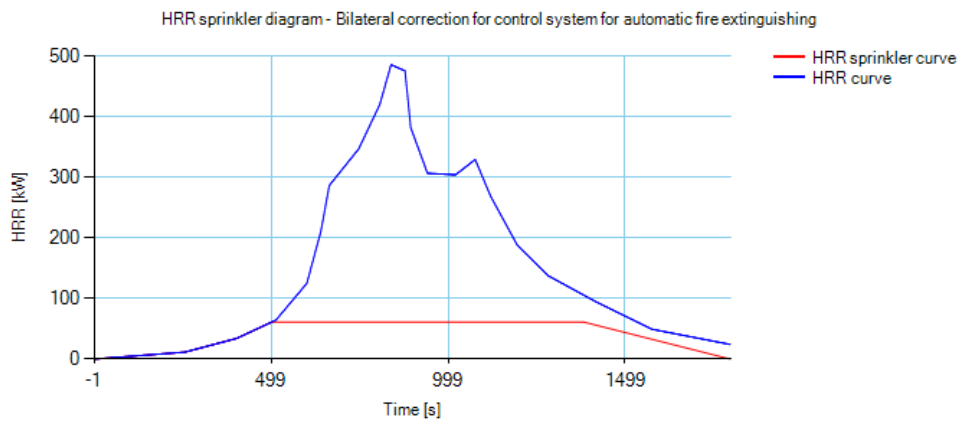
- **Parametric HRR curves:** curves that describe the released energy from a fire, through mathematical laws. Usually, these curves are made of four parts:
 - **Growth:** often described with a quadratic function until the flashover HRR value is reached;
 - **Flashover:** once the flashover HRR value is reached, a linear curve - with an high angular coefficient - reaches the fully-developed fire HRR value. This part is often skipped and the HRR curve is described by a quadratic function until the fully-developed fire HRR value;
 - **Fully-developed fire:** this part of the fire is represented by a plateau, whose lower and upper bound are respectively represented by the starting and the ending timings of the fully-developed fire phases;
 - **Decay:** usually described by a linear descending curve with a null value of HRR at the decay timing value.

The Italian Technical Fire Prevention Standards⁷ reports the mathematical laws to build this curve from the fire growth speed and the specific fire load value. Besides, in order to achieve the life safety goal, it is possible to quantify the fire propagation of nearby items through the methods reported in the NFPA 92B and NFPA 555 Standards. An example of experimental HRR curve is shown in the [Figure 2.3b].

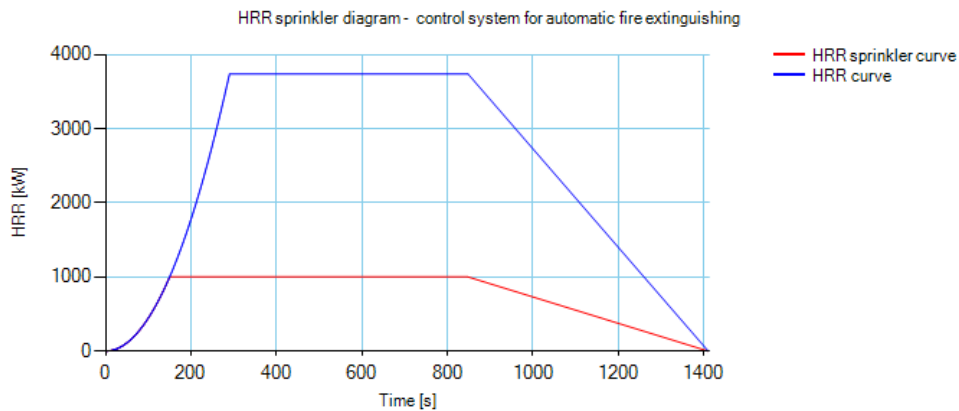
Another important aspect, since these curves describe the released energy rate of a fire, is about sprinkler systems, which break the released energy of the fire and nowadays are more and more requested by the current Codes. These systems, which can work both with water and inert gases in order to control or extinguish the fire, are activated by a temperature device when the target temperature of the sprinkler is reached. The activation of this system usually limits the energy released rate of a fire, allowing the occupants to escape safely and avoiding or retarding the structural collapse. In order to automate the building procedures of the HRR curves, a software

⁷Italian Technical Fire Prevention Standards - Ministerial Decree 3rd of August, 2015 and subsequent amendments and additions

called HRRSprinklerGen has been developed on Microsoft Windows environment, using Visual Basic .NET programming language, implemented on the .NET Framework 4.7.2. This software has been used to build the HRR curves and to correct them with the activation time of a sprinkler system - **[Figure 2.4]**. In order to fully understand the functionalities and the potentialities of this software, the user manual is reported in the **Appendix A: HRRSprinklerGen User Manual**, at the end of this essay.



(a) *Experimental HRR curve*



(b) *Parametric HRR curve*

Figure 2.4: Comparison between experimental and parametric HRR curves, both corrected with the use of a sprinkler system

2.2 Simulating with Fire Dynamics Simulator (FDS)

Fire Dynamics Simulator (FDS) is a computational fluid dynamics (CFD) engine, specific to model fire-driven fluid flow⁸⁹. This Large Eddy Simulator (LES) numerically solves the differential form of the Navier-Stokes equations in a simplified form, suitable for low-speed reactions (Mach number less or equal to 0.3), thermally-driven flow, with an emphasis on smoke and heat transport from fires. FDS is a free command-prompt Fortran-based software developed by the American National Institute of Standards and Technology (NIST) and it reads input parameters from a text files, calculates a numerical solution and writes user-specified output data to files. The first version of FDS was released in February 2000 and during the years several third-party pre-processors GUI embedded have been developed. One of the most used is blenderFDS, which is a Python interface for blender, an open-source 3D modeling software. Instead, a commercial graphical interface for creating FDS input files is Pyrosim, developed from the Thunderhead Engineering software-house - [Figure 2.5a]. The FDS post-processing engine is called Smokeview, a companion software with a simple graphical interface for reading FDS output files and producing smoke animations on the computer screen¹⁰¹¹ - [Figure 2.5b]. At the moment, FDS is available for download with the version 6.x.

2.3 Simulating with A Finite Element Method Calculator

The finite element method (FEM) is a widely diffused procedure for numerically solving partial differential equations for the resolution of mathematical and engineering problems. The base concept of the FEM analysis is to have a discrete 1D, 2D or 3D workspace, in which boundary conditions at the edge interface of the discrete element are filled into a system of algebraic

⁸MCGRATTAN K., HOSTIKKA S., FLOYD J., MCDERMOTT R., VANELLA M. (2020): "Fire Dynamics Simulator User's Guide - Sixth Edition", NIST Special Publication 1019

⁹MCGRATTAN K., HOSTIKKA S., FLOYD J., MCDERMOTT R., VANELLA M. (2020): "Fire Dynamics Simulator Technical Reference Guide - Volume 1: Mathematical Model", NIST Special Publication 1018-1

¹⁰FORNEY G.P. (2020): "Smokeview, A Tool for Visualizing Fire Dynamics Simulation Data - Volume I: User's Guide", NIST Special Publication 1017-1

¹¹FORNEY G.P. (2020): "Smokeview, A Tool for Visualizing Fire Dynamics Simulation Data - Volume II: Technical Reference Guide", NIST Special Publication 1017-2

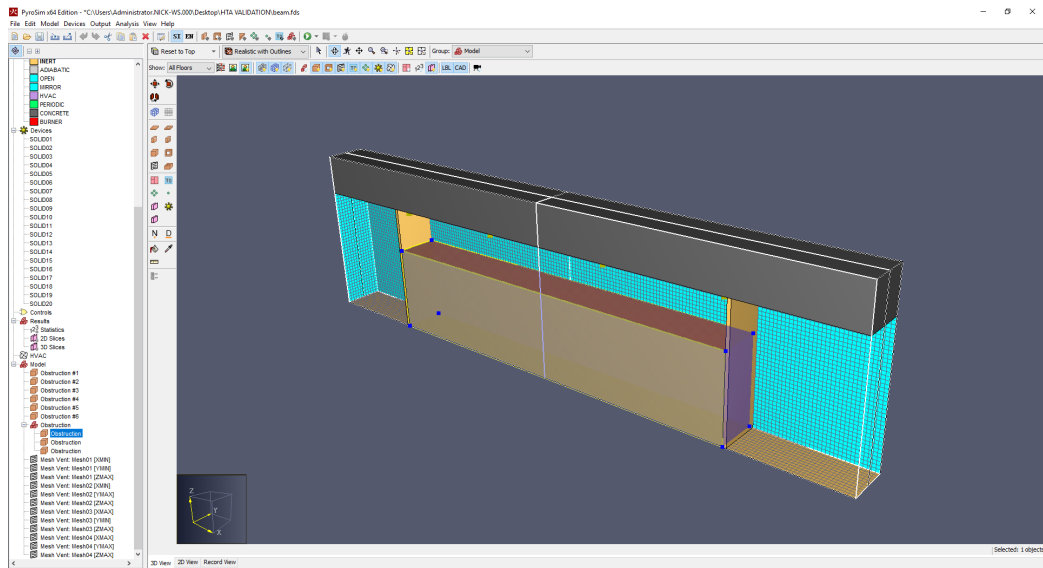
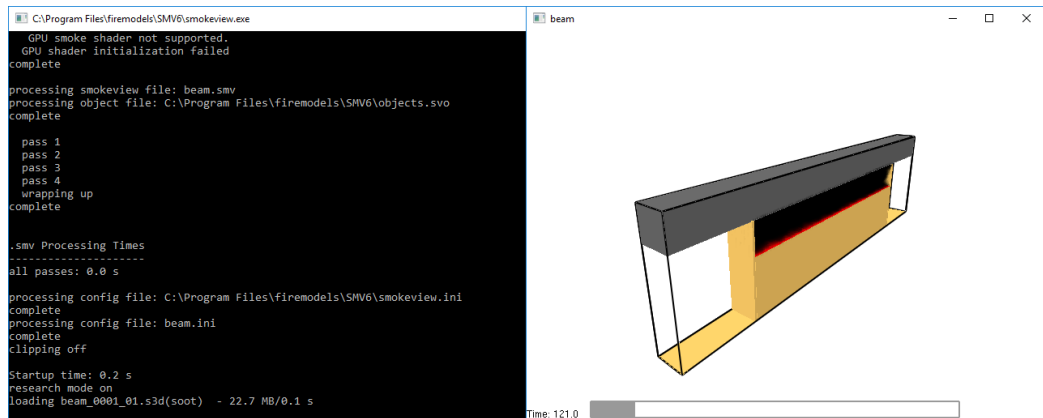
(a) *Thunderhead Engineering Pyrosim*(b) *NIST Smokeview*

Figure 2.5: Comparison between pre-processing and post-processing engines for FDS

equations. Since the real function of the domain is unknown, the calculator approximates it through an iterative calculus procedure which stops when convergence is achieved (a relative variation of the error ratio that is minor than a defined threshold value). The purposes of these analysis can be various and several engineering fields are often included by the most common FEM commercial suites. For this research, ANSYS Mechanical APDL

v19.0¹²¹³¹⁴¹⁵ has been used, in order to perform three different steps of Finite Element Analysis:

- **Heat Transfer Analysis:** assuming to have performed an exothermic analysis with FDS, the Heat Transfer Analysis is the transport procedure for temperature and heat transfer coefficient time-histories, as boundary conditions, that each point of the structural elements reach during the fire simulation;
- **Thermal Analysis:** after the Heat Transfer analysis is completed, this step is necessary to understand the propagation of the temperature gradient through the section of the structural member. This kind of thermal analysis can be defined as endothermic;
- **Structural Analysis:** the endothermic analysis is adopted to obtain the forces, due to the thermal deformation. By applying these forces and the static structural loads (permanent and non-permanent loads, live load, wind load, snow load) on the structural model, it is possible to perform a coupled thermal-mechanical analysis. On the coupling procedure, a description is reported in the next paragraphs.

2.3.1 ANSYS FEM Suite

ANSYS is one of the most diffused commercial multi-purpose finite element analysis engine worldwide. It allows several kind of engineering analysis, such as structural, thermal, electric, and it is possible to couple two or more of them in order to perform hybrid analysis. The first commercial version of ANSYS FEM suite was labeled as 2.0 and it was released in 1971. In 1979 the version 3.0 was endowed of a command-prompt console like the MS-DOS interface. In 1980 the version 5.0 was released and it was the first that integrated in the software a CAD interface too. The version 8.0 was published in 2005 and it was the first version to implement a fluid-structure interaction software and a multi-field solver. The version 10.0 was the first ANSYS version to implement a new graphical interface, called Workbench. Further updates of the suite have the possibility to have both the Workbench than the Classic interface. Nowadays, ANSYS is available for Linux, Microsoft

¹²MADENCI E., GUVEN I. (2015): "The Finite Element Method and Applications in Engineering Using ANSYS", Springer US

¹³ANSYS Mechanical APDL Command Reference Guide (2019)

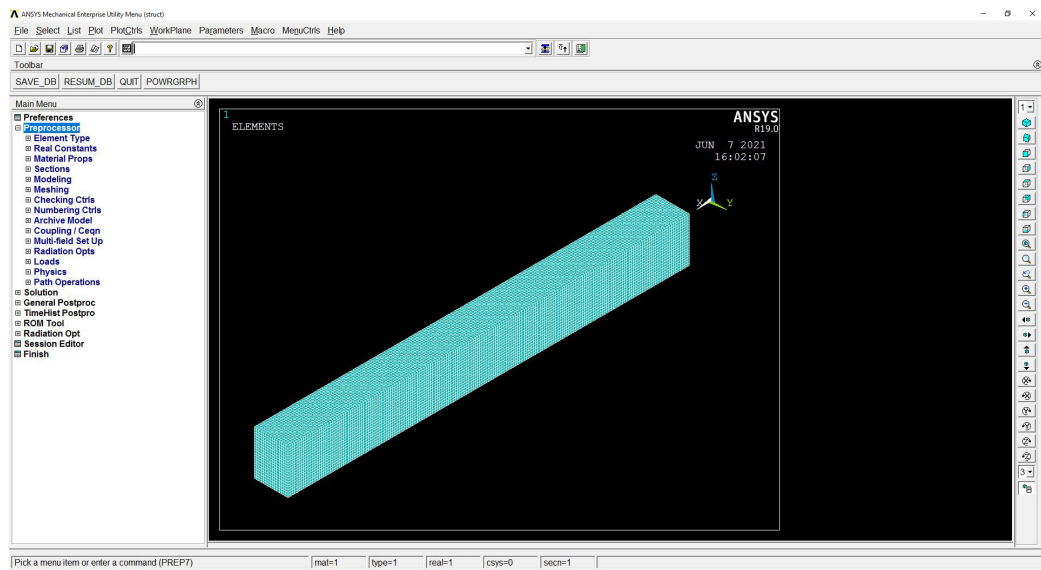
¹⁴ANSYS Mechanical APDL Theory Reference Guide (2019)

¹⁵ANSYS Mechanical APDL Element Reference Guide (2019)

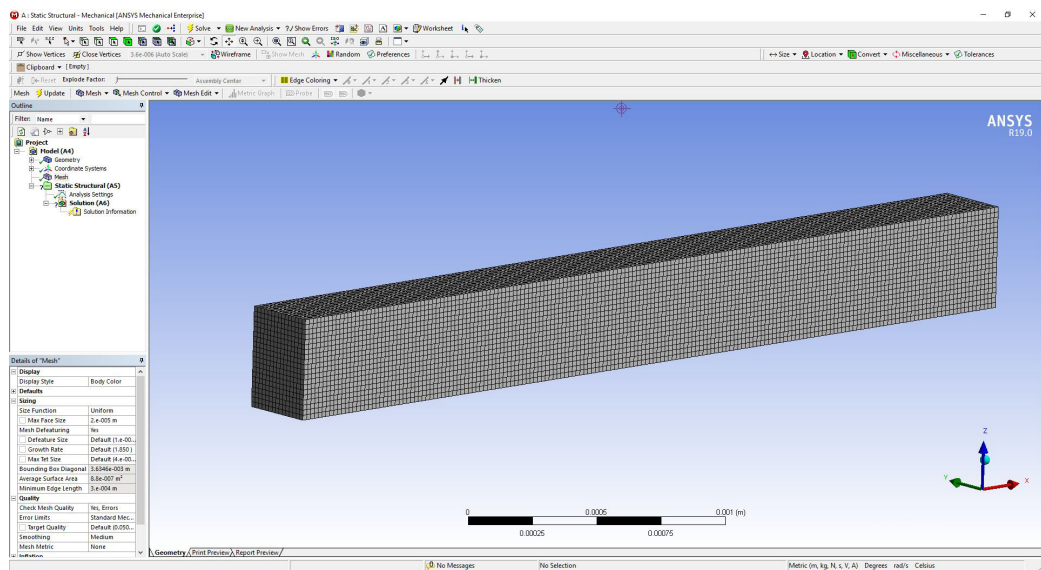
Windows and Unix-based operative systems. As previously said, two different ways of starting ANSYS are provided:

- **ANSYS Mechanical APDL:** also known as ANSYS Classic, APDL is the ANSYS Parametric Design Language and this acronym is used to point out the command-line prompt that is still present in the current releases of ANSYS. A graphic interface is also implemented - [**Figure 2.6a**] -, even if it is possible to start and work with APDL using the batch mode, from the Unix or Microsoft Windows terminal command prompt. APDL is used in order to perform analysis for which unconventional solving algorithms may be required, because the "Read input from" command makes the calculator working in a completely-free way. This function allows also the user to work with macros, written in ANSYS Parametric Design Language. It is possible to start APDL with two different solvers:
 - **ANSYS Mechanical APDL Classic Solver:** which is the only one used for this research;
 - **LS-DYNA:** which until 2019 - the year of the acquisition of the Livermore Software Technology Corporation from ANSYS.Inc - was a stand-alone Finite Element solver, mainly used for automotive, aerospace and military engineering analysis.
- **ANSYS Workbench:** as previously said, this interface was introduced with the version 10.0, released in 2007. Workbench is a dashboard interface which, depending on the type of analysis that needs to be performed, allows the user to define easily the engineering data of the model (also because a wide database of material properties is implemented) and to choose the pre-processing and post-processing engines in a easier way - [**Figure 2.6b**]. From Workbench, many different pre-processors can be executed, which usually are used to perform analysis with conventional solving algorithms (such as the modified Newton-Raphson). The version 15.0 allows the user to perform hybrid analysis, from Workbench to Mechanical-APDL and vice-versa.

It is also possible to solve analysis by importing APDL scripts into Workbench. Unfortunately, if this procedure is not checked in the right way, it may cause numerical error and instabilities, preventing the convergence to be reached correctly. For this reason, this procedure is advised only with a large knowledge of both ANSYS Mechanical APDL and ANSYS Workbench.



(a) ANSYS Mechanical APDL



(b) ANSYS Workbench

Figure 2.6: Comparison between ANSYS engines

2.3.2 Theory references about thermal and mechanical modelling for concrete and rebar

In order to understand the capability of this software, ANSYS Mechanical APDL, in the Help Section, is endowed of a Theory Reference where the theoretical definitions are explained. It is also important to distinguish two

different ways of performing coupled thermal-mechanical analysis¹⁶:

- **Sequential coupling approach:** it consists in performing the endothermic analysis and then the structural analysis, which is obtained with the results of the first one. Furthermore, this technique allows users to take into consideration the non-linearity for both thermal - conductivity, specific heat, density - and mechanical material - stress-strain relationship for concrete compressive strength and reinforcement steel ultimate tension strength - properties. Even geometric non-linearity can be considered - $P\Delta$ effects. Despite this aspect, this approach does not take into account of the change of the temperature field, that may cause, once a failure occur - an extra-exposition of the inner core of the structural elements to the thermal stress.
- **Direct coupling approach:** it consists in a step-by-step thermal-mechanical analysis. In other words a thermal and then a mechanical analysis for the single time-step is performed. Unfortunately, with this technique, concrete cracking and crushing behavior may be neglected. On the other hand, it is possible to take into account of the variation of the after-failure temperature field, while the fire is still occurring.

To obtain reliable results from a sequential coupled thermal-mechanical model of a reinforced concrete structure, four different types of finite element needs to be defined:

- **Thermal behavior of concrete:** a **SOLID70** element type needs to be defined. It is a 3D thermal conductive element, with eight nodes and a single degree of freedom, temperature, at each node. This element is also capable of both steady-state and transient thermal analysis and it can compensate for mass transport heat flow from a constant velocity field. For this kind of analysis, the material properties for concrete that need to be defined are thermal conductivity, density and specific heat.
- **Thermal behavior of rebar and stirrups:** a **LINK33** element type is capable of representing the thermal behavior of rebar and stirrups. It is a uniaxial conductive element with two nodes, a starting one and an ending one, with a single degree of freedom per node - temperature. Besides, a section needs to be defined for this element, in order to set

¹⁶M. ELSHORBAGY, M. ABDEL-MOOTY (2019), "The coupled thermal-structural response of RC beams during fire events based on nonlinear numerical simulation", Engineering Failure Analysis, Volume 109

the cross section surface of the bar. For this kind of analysis, the material properties for reinforcing steel that need to be defined are thermal conductivity, density and specific heat.

- **Mechanical behavior of concrete:** a **SOLID65** element type needs to be defined, because it is the most suitable way to simulate and calculate the nonlinear structural behavior of concrete. It is a 3D solid element, with eight nodes and three degrees of freedom per each node - translations along X, Y and Z direction. Rotational DOFs can be added by calling an instance of the specific command. The SOLID65 element type is capable of foreseeing cracking - in tension - and crushing - in compression - of concrete. For this kind of analysis, the material properties for concrete that need to be defined are Young modulus, Poisson ratio, cylindrical compression strength and thermal elongation. The stress-strain diagram is represented by a Multilinear Kinematic Hardening model. Therefore, some parameters are needed to be defined for the cracking/crushing concrete behavior. Thus, ANSYS is also capable of allowing spalling parameters - that for these analysis are set equal to zero. These mechanical features are not related to Standard and Codes and the values are referred to guidelines, forum threads and tutorials¹⁷ and for this reason are not editable from the FDS2ANSYS GUI. Here follow the list:

- **Open Shear Transfer Coefficient:** 0.3
- **Closed Shear Transfer Coefficient:** 1
- **Uniaxial Cracking Stress:** 2.7E+6 [Pa]
- **Uniaxial Crushing Stress:** -1
- **Biaxial Crushing Stress:** 0
- **Hydrostatic Pressure:** 0
- **Hydrostatic Biaxial Cracking Stress:** 0
- **Hydrostatic Uniaxial Crushing Stress:** 0
- **Tensile Cracking Factor:** 0

- **Mechanical behavior of rebar and stirrups:** a **LINK180** element type needs to be defined. It is a two-node element, with three degrees of freedom per each node - translations along X, Y and Z direction. It is the LINK33 homologue element for modeling mechanical behavior and, so, LINK180 too needs the definition of a section to quantify the

¹⁷<https://www.youtube.com/watch?v=0JiKNWt095I>

cross section surface. For this kind of analysis, the material properties for reinforcing steel that need to be defined are Young modulus, Poisson coefficient, yielding strength and thermal elongation. The stress-strain diagram is represented by a Multilinear Isotropic Hardening model.

In order to obtain reliable results from a direct coupled thermal-mechanical analysis, another element type needs to be defined:

- **Thermal-mechanical behavior of concrete:** a **SOLID226** element type needs to be defined in order to perform a direct-coupled thermal mechanical analysis. It is a twenty-node element, with up to six degrees of freedom per each node - for this analysis, only four of them are considered: translations along X, Y and Z direction and temperature. Even in this case, rotational DOFs can be added by invoking an instance of the specific command. For this kind of analysis, the material properties are the same to the ones defined for both the **SOLID70** and **SOLID65** element types;
- **Thermal-mechanical behavior of rebar and stirrups:** it is defined with a **LINK180**, neglecting the thermal behavior of the reinforcement steel.

Thus, there is a sixth element type that needs to be defined in order to couple the FDS output solution with ANSYS Mechanical APDL and it is the **SURF152** element type, that has neither thermal nor mechanical behavior, but it is needed just to perform the Heat Transfer Analysis. It is a 2D planar thermal element, with variable number of nodes - from four to eight, depending on the element type keyoptions. Since this is a thermal element, temperature is the main degree of freedom per each node. It has also a top temperature and a bottom temperature, that may be enabled or disabled, depending on the element type keyoptions. To allow the heat transfer, a real constant for this element type needs to be defined and it is equal to the Stefan-Boltzmann constant: $\sigma = 5.67 \cdot 10^{-8} \frac{W}{m^2 \cdot K^4}$

2.4 Performing an Heat Transfer Analysis

The Heat Transfer Analysis is the procedure that allows the temperature transfer from FDS to a FEM code. This has been possible using a Fortran

experimental interface called FDS2FTMI and developed by the NIST^{18 19}. This so-called Fire Thermal Mechanical Interface is based on the creation of a point cloud - from the Smokeview output file of the FDS analysis, in which each node has a temperature time-history, for the entire simulation time in FDS. Therefore, this script is capable of reproducing the net heat flux, evaluated in FDS, through the transfer of the Adiabatic Surface Temperature (T_{AST}) and of the heat transfer coefficient (h) at each time-step. As explained in the **Chapter 1. A brief introduction to the fire resistance capacity of structures**, it is possible to perform two kinds of thermal-mechanical analysis and FDS2FTMI is projected for this purpose. This interface has also been programmed for LS-DYNA pre-processing engine. Nevertheless, just the APDL interface has been used. For this research a one-way coupling interface of FDS2FTMI has been used for the following main reasons:

- **Unavailability of the two-way code:** during a coupled thermal-mechanical analysis, when a structural collapse occurs, the deformed shape of the structure needs to be exported as a new FDS input file, with the time and temperature information of the failure time-step. Since a structural deformed shape is not regular as the undeformed one, it is not possible to reproduce reliable deformed shapes, due to geometric limitations of FDS 6. Despite this aspect, FDS 7 - in plan to be released soon - may support the generation of complex geometries this could allow to perform a "multi-collapses" coupled thermal-mechanical analysis;
- **Concrete spalling:** a two-way code would have allowed to consider in which condition the explosive spalling of concrete would have occurred. The EN 1992-1-2²⁰ allows to neglect this behavior for moisture content less than 3% - Italian Standards²¹ suggest 2-2.5% of moisture content for concrete and it is a common value. From a research, a 2% of moisture content is reported in the American Standards²².

¹⁸SILVA J.C. (2017), "FDS2FTMI User's Guide - An automated code to one-way coupling between FDS and FEM using FTMI", National Institute of Standards and Technology

¹⁹ZHANG C., SILVA J.C., WEINSCHENK C., KAMIKAWA D., HEASEMI Y. (2017), "Simulation Methodology for Coupled Fire-Structure Analysis: Modeling localized fire tests on a steel column", National Institute of Standards and Technology

²⁰EN 1992-1-2:2019 Standard: "Eurocode 2: Actions on concrete structures – Part 1-2: General actions – Actions on structures exposed to fire"

²¹Italian Technical Building Standards - Ministerial Decree 17th of January, 2018 and subsequent amendments and additions

²²ASTM F2170-18: "Standard Test Method for determining Relative Humidity in Concrete Floor Slabs Using in Situ Probes"

The validation of this interface has been provided both from Silva and Zhang et. al. From the FDS exothermic conditions, the heat transfer analysis is obtained by a combination of three different forms of thermal exchange:

- **Conduction:** is the transfer of energy between items that are in direct contact with each other;
- **Convection:** is the transfer of energy between an item and the surrounding environment. It occurs when warmer areas of gasses or liquid rise to cooler areas;
- **Radiation:** is the transfer of energy involving electromagnetic radiation, without relying any contact between the heat source and the exposed item. During a fire, this is often the dominating component of the heat transfer.

2.5 A short dissertation on the coupled thermal-mechanical analysis

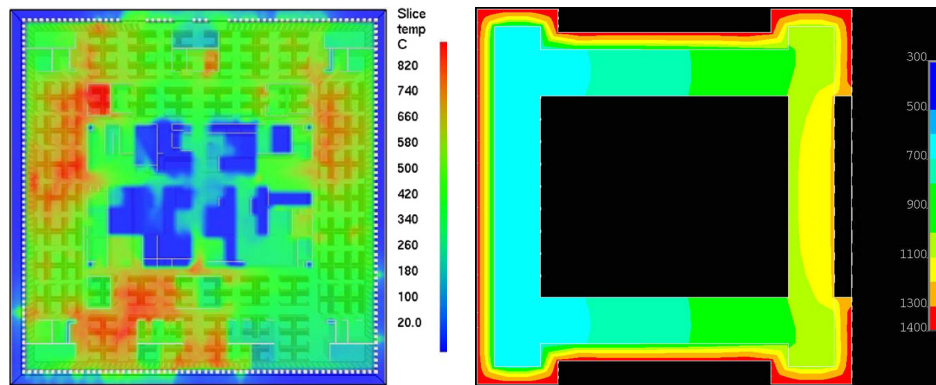
The procedure of coupling multi-field engineering analysis is needed to investigate on particular situation for which the laboratory simulations may be expensive or difficult to realize. To achieve this goal, it is necessary to define mathematical models, in order to have all the boundary conditions that allow to perform a coupled engineering analysis. As previously said, for this research the coupled thermal-mechanical analysis is necessary in order to state the structural behavior of concrete when subjected to high temperature. A brief historical background on the coupling procedure of thermal and structural field is reported in the next paragraph.

2.5.1 Historical references

Since the coupling procedure of thermal and structural finite element analysis is a relatively new field of research, all of the reported references are really modern and come from experimental researches of the last twenty years. Thus, the first time that investigating on the structural collapse due to a thermal stress has been about the September 11 attacks, at the World Trade Center in New York City. On this matter, a reliable paper²³ is the

²³BAUM H. R., PRASAD K. (2005): "Coupled fire dynamics and thermal response of complex building structures", Combustion Symposium 30, Building and Fire Research Laboratory of the National Institute of Standards and Technology

first step towards the comprehension of the mechanisms of structural collapse due to large thermal stresses. With one of the first released versions of FDS - [Figure 2.7a] -, a 3D model of the Twin Towers area has been analyzed in order to simulate the range of temperature that the structure reached after the collision of the airplane. At this point, a coupling procedure with a structural FEM code was needed, since a direct link between FDS and structural analysis codes was not available yet. The adopted FEM suite was ANSYS APDL - [Figure 2.7b] -, version 7.1, and the use of macros automated the heat transfer procedure, reducing the needed time.



(a) FDS Simulation - Layered temperature at Tower 1 - Floor 96. 1000 s after the collision of the airplane

(b) ANSYS APDL Simulation - thermal analysis of core column. Cross section

Figure 2.7: K. Prasad and H. Baum - World Trade Center thermal-structural analysis (2005)

In 2008 an experimental interface for coupled thermal-mechanical analysis, from FDS to FEM engines, has been developed. It is called FIRESTRUC²⁴ and implements both one-way and two-way coupling modes and it is available for several FEM codes.

Another interesting work about the thermal and structural interaction regards the use of ABAQUS/CAE as FEM code for the thermal-structural analysis. In particular, two different utilities, which exploit the ABAQUS FEM Engine, have been developed and are named Abaqus Fire Interface Simu-

²⁴CHAN A., KUMAR S., LEMAIRE T., WELCH S. (2009): "FIRESTRUC – Integrating Advanced Three-dimensional Modelling Methodologies for Predicting Thermo-mechanical Behaviour of Steel and Composite Structures Subjected to Natural Fires", Fire Safety Science 9

lator Toolkit (AFIST)²⁵ and FDS-2-ABAQUS²⁶. Both of them are capable of two-way coupling interfaces for handling thermal-mechanical analysis. In order to exploit the ANSYS FEM Engine through an automated procedure, an ad hoc interface has been deployed.

2.5.2 Adopted procedures

Since the one-way coupling procedure has been adopted, in order to study the local behavior of concrete structure the following steps have been followed:

- **FDS Exothermic Analysis:** an FDS file, with the base structural geometries, is generated. The structural obstructions come on a surface-layer named "concrete" and it is endowed with Adiabatic Surface Temperature and Heat Transfer Coefficient boundary functions. If the model is very wide, it is advisable to split the mesh for the FDS Parallel engine (using a MPI interface). Then it is imported into a GUI FDS-based model engine (e.g. Thunderhead Engineering Pyrosim) and modeled with burners, reactions and devices. Once the modeling procedure is completed, the exothermic analysis is performed;
- **Heat Transfer Analysis:** through the Silva's FDS2FTMI interface for ANSYS APDL, the temperature and heat transfer coefficient profiles over time are carried out and transferred into the FEM modeler;
- **FEM Endothermic Analysis:** once the temperature and heat transfer coefficient profiles over time are imported, a thermal analysis is performed in order to understand the propagation of the differential temperature inside the solid structural elements. Furthermore, for the sequential analysis, at the end of the analysis, a file, containing the output results with .rth extension, is exported and can be used for the coupling procedure of the analysis;
- **FEM Coupled Thermal-Mechanical Analysis:** the coupling procedure needed to link the thermal and structural fields of analysis. Two kinds of coupling procedures can be distinguished:
 - **Sequential coupling:** the coupling procedure between thermal and structural analysis is done by running the whole thermal

²⁵CHEN L., LIU P., LUA J., LUO C. (2010): "Abaqus Fire Interface Simulator Toolkit (AFIST) For Coupled Fire and Structural Response Prediction", Global Engineering and Materials Inc.

²⁶FEENSTRA J. (2016): "FDS-2-Abaqus, C++ Managed automated Python scripted CFD-FEM Coupling", Master of Science Degree Thesis, Eindhoven University of Technology

analysis and then linking it to the mechanical field through the .rth output results file, loaded onto ANSYS APDL as overload due to the differential temperature. Once defined the self-weight of the structural elements and other overloads (as disposed by the current Standards), it is possible to perform the analysis. Once completed, safety checks on the structural elements can be done;

- **Direct coupling:** the coupling procedure between thermal and structural analysis is done before running the analysis, since the thermal and structural analysis are run simultaneously, in a step-by-step way.

Even if the described methods seem to be similar, the sequential coupling has the advantage to predict the cracking behavior of the structural elements. On the other hand, the direct coupling procedure has the advantage to take into account the variation of the inner core temperature field when a collapse occurs.

Chapter 3

Reinforced concrete structural behavior under the fire action

Structures exposed to fire are usually checked in terms of fire resistance, which is the period of time under exposure to a parametric fire curve - ISO 834, hydrocarbon or nominal external curves. According to this definition, the current European Standard ¹ defines the general prescription about the stress due to the fire exposition. Focusing attention on reinforced concrete, the current European Standard ² defines also the mechanical and thermal features of materials and the variation of these parameters over the temperature. The main limitations of these approaches are due to the extreme simplification of the experimental tests from which these methods are based on: usually, a simple supported beam is tested according to the ISO 834 temperature profile and, for real structures, all the members are checked with the hypothesis of "distributed fire". To overcome this limitation, the EN-1992-1-2:2019 - Appendix C provides a simplified numerical method for the safety checks for localized fire. Nevertheless, it is not a performance-based method.

3.1 General dissertation on the reinforced concrete behavior under the fire action

Reinforced concrete is an excellent material for its price, speed of construction and architectural appearance and, for this reason, is widely used for

¹EN 1991-1-2:2004 Standard: "Eurocode 1: Actions on structures – Part 1-2: General actions – Actions on structures exposed to fire"

²EN 1992-1-2:2019 Standard: "Eurocode 2: Actions on concrete structures – Part 1-2: General actions – Actions on structures exposed to fire"

all kind of buildings and civil-engineering projects. According to Denoël's dissertation ³, concrete is a non-combustible material, so it does not propagate fire and does not give off smoke or toxic gases. However, it has a high thermal inertia, since concrete structural members are highly massive. This feature allows to withstand high temperatures and to continue bearing load, - since the inner core remains cooler - for relatively long time and the reinforcing steel remains protected while the fire is occurring. Nevertheless, even if advantages are various, concrete remains a complex material and its properties can dramatically change during the fire. Indeed, while temperature rises, the loss of compressive strength and the ejection of chunks of concrete may occur. This phenomenon causes the reduction of the resistant cross-section and the exposing of the reinforcing steel. Moreover, the exposure of a concrete to fire causes a stratification of temperature inside the cross section, due to the massiveness of concrete structural members, which leads to different mechanical and thermal behavior depending on the values of "depth". Furthermore, it is not possible to simplify a concrete mass matrix as a lumped parameter.

3.2 Physical and chemical response of concrete under the fire action

While exposed to fire, concrete is subjected to micro-structural, thermal, mechanical changes. According to the works of Denoël ³, Fletcher et. al. ⁴ and Khoury ⁵, internal cracks and degradation of the cement paste lead to the loss of compressive strength. Furthermore, the differential temperature is the cause of the compromise of cohesion between the aggregates and the cement paste. However, the physical and chemical changes inside the concrete may be reversible or non-reversible upon cooling. The latter phenomenon is the most dangerous, since, even if no damage can be visually detected, the weakness after a fire may be significantly. This aspect can also be helpful in order to state the critical range of exposure temperature. Anyway, the most common used aggregates can bear temperatures up to 300°C.

³DENOËL J.F. (2007): "Fire Safety and Concrete Structures", FEBELCEM - Federation of Belgian Cement Industry

⁴FLETCHER I. A., WELCH S., TORERO J. L., CARVEL R. O., USMANI A. (2007): "Behaviour of Concrete Structures in Fire", Thermal Science, Vol. 11, No. 2, 2007, pp. 37-52

⁵KHOURY G. A. (2008): "Passive fire protection of concrete structures", Proceedings of the Institution of Civil Engineers, Structures & Buildings 161, Issue SB3, June 2008, pp. 135-145

While the temperature arises, the first change that occurs in concrete is the evaporation of the free water, with a boiling range temperature from 100 to 140°C (depending on the relative pressure condition ⁶). From 300°C, the aggregates expand, the cement past begins to shrink and if heated for a long time, the loss of tensile strength occurs because the calcium hydroxide ($Ca(OH)_2$) loses the water molecule (H_2O), breaking down in to calcium oxide (CaO). The aggregates are affected by the fire too: calcareous ones decompose at approximately 800°C, instead siliceous ones are subjected to a volume expansion at around 575°C. The cooling phase of the concrete after a fire causes a new physical and chemical change: cracks may develop along the structural element, the moisture content may increase or the calcium oxide may be subjected to re-hydration. However, during the design phase, most of these phenomena are conservatively neglected. In general, the parameters that may affect the concrete behavior while a fire is occurring are the type of cement paste, the type of aggregate and the bond region and Khoury ⁷ - **[Figure 3.1]** - analyzed these features to state a method for which a smart choice of aggregates and cement blend would be made in order to improve structural performance. Many other aspects need to be taken into consideration, as the heating/cooling rate, the cyclic thermal stress or the speed of heating and, since this phenomenon is related to several parameters, usually predetermined heating regimes may not be representative of a realistic fire ^{8 9 10}. Due to these physical and chemical reactions, a phenomenon is particularly discussed and it takes the name of **spalling** ¹¹. It consists, in the most general form, as the ejecting of layer or pieces of concrete from the surface of the structural members which are exposed to fire. Nevertheless, spalling is a very complex phenomenon and the its mechani-

⁶JANSSON R. (2008): "Material properties related to fire spalling of concrete", Licentiate thesis, Lund institute of technology and Lund university, 120 pp.

⁷KHOURY G. A. (2008): "Passive fire protection of concrete structures", Proceedings of the Institution of Civil Engineers, Structures & Buildings 161, Issue SB3, June 2008, pp. 135-145

⁸KHOURY G. A. (2000): "Effect of fire on concrete and concrete structures", Progress in Structural Engineering and Materials, 2, pp. 429-447

⁹HANDOO S. K., AGARWAL S. and AGARWAL S. K. (2002): "Physicochemical, mineralogical, and morphological characteristics of concrete exposed to elevated temperatures", Cement and concrete research, Volume 32, Issue 7, July 2002, pp. 1009-1018

¹⁰HUSEM M. (2006): "The effects of high temperature on compressive and flexural strengths of ordinary and high-performance concrete", Fire Safety Journal, Volume 41, Issue 2, March 2006, pp. 155-163

¹¹KHOURY G. A. and ANDERBERG Y. (2000), "Concrete spalling review", Report submitted to the Swedish National Road Administration, June 2000

cal stress configuration is still poorly understood. From several studies¹²¹³, four main kinds of spalling have been identified:

- **Aggregate spalling:** hollows develop, producing a popping sound;
- **Surface spalling:** usually violent ejection of portion of concrete, especially for pressure stressed walls;
- **Corner spalling**
- **Explosive spalling:** usually violent, with a loud bang.

Furthermore, other studies¹⁴ carried on two more types of spalling:

- **Sloughing-off spalling:** the concrete is not sufficient to bear the self-weight load;
- **Post-cooling spalling:** occurring during and after the cooling.

Several factors influence explosive spalling and over years have been summarized¹⁵¹⁶:

- **Heating rate:** higher is the heating rate and higher is the probability and severity that a concrete element does spall;
- **Heating exposure:** the more faces of a member are exposed to fire, the more likely spalling is to occur;
- **Section size:** thin structural members have low probability to spalling and explosion are less likely in thick sections greater than 200 mm;
- **Section shape:** explosive spalling is more likely in structural members where cross-sections change rapidly;

¹²JANSSON R. (2008): "Material properties related to fire spalling of concrete", Licentiate thesis, Lund institute of technology and Lund university, 120 pp.

¹³GARY M. (1916), "Fire tests on reinforced concrete bases", German Committee for Reinforced Concrete, Issue 33, Berlin, Germany

¹⁴KHOURY G. A. (2008): "Passive fire protection of concrete structures", Proceedings of the Institution of Civil Engineers, Structures & Buildings 161, Issue SB3, June 2008, pp. 135-145

¹⁵KHOURY G. A. and ANDERBERG Y. (2000), "Concrete spalling review", Report submitted to the Swedish National Road Administration, June 2000

¹⁶MAJORANA C. E., SALOMONI V. A., MAZZUCCO G. and KHOURY G. A. (2010): "An approach for modelling concrete spalling in finite strains", Mathematics and Computers in Simulation, Volume 80, Issue 8, April 2010, pp. 1694-1712

- **Moisture content:** explosive spalling is usually unlikely with a moisture content less than 2%;
- **Permeability:** experimental tests showed that spalling is unlikely for permeability values less than $5 \times 10^{-11} \text{ cm}^2$;
- **Age of concrete:** the effect of this parameter is debated: however the majority of the reports stated that the risk of spalling may reduce with increasing age;
- **Strength of concrete:** paradoxically, as the concrete quality is poorer, the risk of spalling is more unlikely;
- **Compressive stress and restraint:** as the compressive stress increases - by reduction of cross section or increasing in loading -, explosive spalling may be more likely to occur;
- **Aggregates:** spalling decreases with low thermal expansion aggregates. Furthermore, the use of great-size aggregates encourages explosive spalling;
- **Cracking:** the presence of crack may have two effects: it may facilitate moisture migration but it may make the crack propagating;
- **Reinforcement:** usually, the unreinforced zone of a structural member should be the one where spalling is more likely but, in the reinforced zone, the corner rebar is the one that can become exposed due to spalling;
- **Concrete cover:** in order to avoid or retard spalling, a nominal cover bigger than 40 mm for dense aggregates or 50 mm for lightweight aggregates concrete is highly recommended.

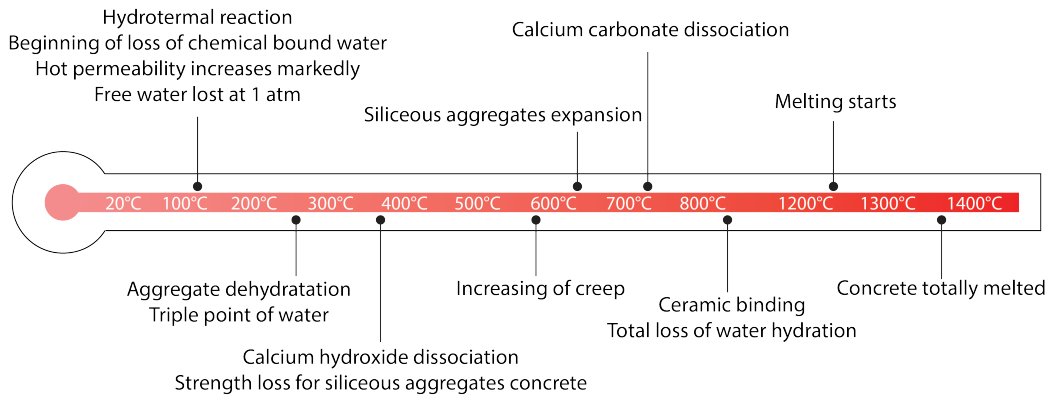


Figure 3.1: Simplified global presentation of physic-chemical processes in Portland cement concrete during heating - Khoury (2008)

Since this phenomenon is really complex and several experimental tests have been done to understand it, the EN 1992-1-2:2019¹⁷ indicates that the spalling may be neglected for content of moisture less than 3% - in Italy¹⁸ the common value of moisture content is 2-2.5%. In America¹⁹ a 2% of moisture content is commonly considered.

3.3 Effect of fire on structural members

Several reliable publications²⁰ report the material behavior under the fire action and in this paragraph a summary of them follows.

When the temperature rises, both the thermal and the mechanical features are modified. The strength and the stiffness of both concrete and steel is reduced and the whole stress-strain diagram is modified: both the compressive strength for the concrete and the yielding strength for the steel decrease as the temperature rises. Deformation features may also change as the temperature changes. In the **Chapter 5. Engineering Data**, all the variation relationships have been explained, taking into consideration - where

¹⁷EN 1992-1-2:2019 Standard: "Eurocode 2: Actions on concrete structures – Part 1-2: General actions – Actions on structures exposed to fire"

¹⁸Italian Technical Building Standards - Ministerial Decree 17th of January, 2018 and subsequent amendments and additions

¹⁹ASTM F2170-18: "Standard Test Method for determining Relative Humidity in Concrete Floor Slabs Using in Situ Probes"

²⁰fib Bulletin 46 (2008): "Fire Design of concrete structures – structural behavior and assessment", Fédération internationale du béton, 209 pp.

possible - the current Standards^{21 22 23} and reliable papers^{24 25}. Besides spalling, another important effect is thermal lateral deflections - that may degenerate in thermal bowing -, due to an high averaged thermal gradient. This phenomenon depends on the exposed surface of a structural member to fire. Thus, if a concrete column is heated from four sides, this effect may not occur, because the extent of this behavior is influenced by the average gradient.

However, the structural behavior of members exposed to fire can be correlated to the whole structural assembly²⁶ - [Figure 3.2] -, of which many types can be found:

- **Redundancy:** if the failure of a single element occurs, the collapse of the whole structure does not occur, because, through the so-called "load sharing", loads are redistributed to the other undamaged, stiffer and stronger members. Furthermore, although this technique is similar to the continuity one, the redistribution of the internal forces is carried from a member to another. Thus, the efficiency of this typology is highly influenced by a load factor, which is needed to individuate the undamaged members which are capable of carrying the overload due to the structural collapse. Ductility may influence a redundant structural assembly too - in particular for metallic and reinforced concrete structure;
- **Continuity:** constraint configuration for which a member is hyperstatic and endowed with a greater fire resistance. The discrete representation of this mechanism is based on a concentrated plasticity model, based on the formation of plastic hinges which allow the portions of the member to have large displacements without significant increase in bending moment. For this reason, this plasticity model represents the mechanical behavior of ductile materials, such as steel or reinforced concrete;

²¹EN 1992-1-2:2019 Standard: "Eurocode 2: Actions on concrete structures – Part 1-2: General actions – Actions on structures exposed to fire"

²²EN 1993-1-2:2005 Standard: "Eurocode 3: Actions on steel structures – Part 1-2: General actions – Actions on structures exposed to fire"

²³American Society of Civil Engineers, Manual of Practice no.78

²⁴GERNAY T., MILLARD A., FRANSENSEN J.M. (2013): "A multiaxial constitutive model for concrete in the fire situation: Theoretical formulation", International Journal of Solids and Structures

²⁵YANG. Y (2015): "Temperature-dependent thermoelastic analysis of multidimensional functionally graded materials", Ph.D. Thesis, University of Pittsburgh, Pennsylvania

²⁶BUCHANAN A. H. (2002): "Structural Design for Fire Safety", John Wiley and Sons, New York, USA

- **Axial restraint:** this mechanism may have a positive or negative influence on the structure, while a fire is occurring. These effects are evaluated by taking into consideration several aspects, as the concrete cover size, the shape and the size of the structural member, the reinforcement type, the aggregates type and the load intensity²⁷. This phenomenon is obtained by a global rigid surrounding structure, where is possible to obtain non-negligible restraining reactions - due to the high thermal gradient. When the heating phase starts, the member develops a volume increase - due to the thermal expansion. The restraint configuration prevent the elongation with a reaction force T and the eccentricity between its point of application and the neutral axis is called e . From this configuration, the bending moment $T \cdot e$ is generated and must be considered in the global bending resistance capacity of the structural member - **Equation 3.1:**

$$M_{R,total} = M_{R,fire} + (T \cdot e) \quad (3.1)$$

The developed eccentricity may also be negative - if the line of the action of the axial forces develops near the upper surface of a beam - and may reduce the bending moment $M_{R,fire}$ - which is the flexural resistance while a fire is occurring - which depends on the surrounding structure stiffness and may influence the global behavior negatively too. However, it is possible that the axial restraint may lead to additional failure models that should be considered during the design phase.

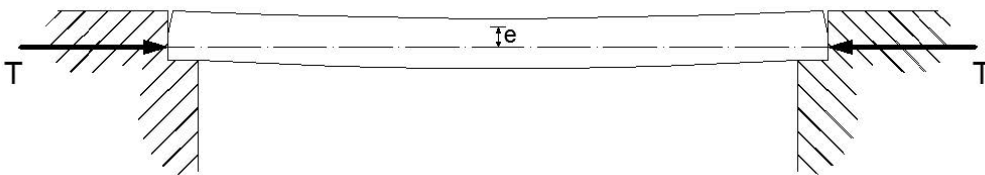


Figure 3.2: Rigid-supported beam with axial restraint thrust forces - Buchanan (2002)

²⁷FELLINGER J. and BREUNESE A. (2004): "Fire Safe Design: Make it Concrete!", Paper published in (Gambarova et al., 2004)

Chapter 4

Available Standards on reinforced concrete structural behavior under fire

This brief dissertation is on the current Standards – from both structural and fire prevention point of view - about the fire-resistance capacity of concrete structures. As shown in the next paragraphs, most of the reported methods are prescription-based and the performance-based ones are just mentioned or briefly argued. Since one of the main aims of this research is to investigate on the available methods and to study in deep which can be the strategies to carry on structural analysis while the fire is occurring, this approach is needed in order to have a wider knowledge of the available procedures.

4.1 Eurocode 1, 2 and 3 for structures exposed to fire

The first Standard that has been considered is the Eurocode 1¹, whose **Chapter 3.2** reports the nominal temperature time-histories - [**Figure 4.1**], **Equations 4.1 - 4.3**:

- **ISO 834 fire curve:** for which the heat transfer coefficient by convection is $\alpha_c = 25 \frac{W}{m^2 \cdot K}$

$$\theta_g = 20 + 345 \cdot \log_{10}(8 \cdot t + 1) \quad (4.1)$$

¹EN 1991-1-2:2004 Standard: "Eurocode 1: Actions on structures – Part 1-2: General actions – Actions on structures exposed to fire"

- **Nominal external fire curve:** for which the heat transfer coefficient by convection is $\alpha_c = 25 \frac{W}{m^2 \cdot K}$

$$\theta_G = 660 + (1 - 0.687 \cdot e^{-0.32 \cdot t} - 0.313 \cdot e^{-3.80 \cdot t}) \quad (4.2)$$

- **Hydrocarbon fire curve:** for which the heat transfer coefficient by convection is $\alpha_c = 50 \frac{W}{m^2 \cdot K}$

$$\theta_G = 1080 + (1 - 0.325 \cdot e^{-0.167 \cdot t} - 0.675 \cdot e^{-2.50 \cdot t}) \quad (4.3)$$

where:

- θ_g : is the gas temperature in the fire compartment;
- t : is the time.

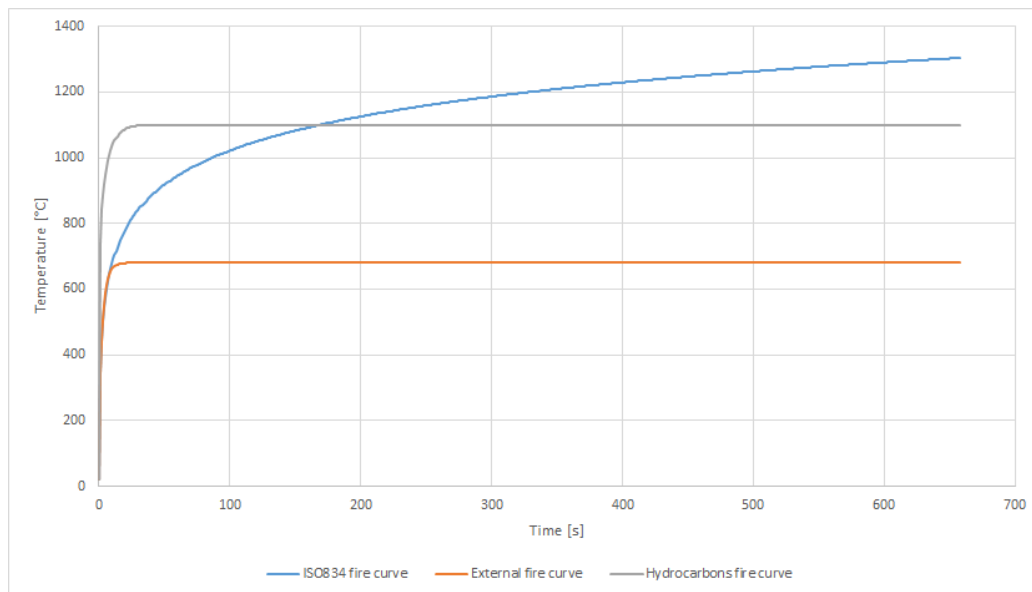


Figure 4.1: Nominal fire curves

Moreover, this Standard takes into consideration both simplified numerical methods - for which some of the appendixes of the Standards are dedicated - and advanced fire models. Focusing attention on the latter, the parameters that must be taken into account are:

- **Gas properties**
- **Mass exchange**
- **Energy exchange**

To this purpose, a Computational Fluid Dynamic model, whose main output is the time dependent temperature distribution in the fire compartment, may be used.

On the specific rules for the safety checks for concrete structures, the Eurocode 2² and Eurocode 3³ may be considered.

In this section the load combinations are reported and the variation of them with the temperature gradient. Material features are largely reported in this Standard - **Chapter 5. Engineering Data**.

4.2 Italian National Annexes - Ministerial Decree 31th of July, 2012

The Italian National Annexes⁴ contain several indication for structural design by using the Eurocodes. From this Decree, the aforementioned Eurocodes^{5 6} annexes have been taken into account.

The Eurocode 1 has been integrated with an explanation of the fire load density and the nominal fire load - both reported in the Italian Technical Fire Prevention and Technical Building Standards⁷ yet.

For the Eurocode 2 no additional information on methods or equation have been proposed.

²EN 1992-1-2:2019 Standard: "Eurocode 2: Actions on concrete structures – Part 1-2: General actions – Actions on structures exposed to fire"

³EN 1993-1-2:2005 Standard: "Eurocode 3: Actions on steel structures – Part 1-2: General actions – Actions on structures exposed to fire"

⁴Italian National Annexes for the application of Eurocodes - Ministerial Decree 31th of July, 2012

⁵EN 1991-1-2:2004 Standard: "Eurocode 1: Actions on structures – Part 1-2: General actions – Actions on structures exposed to fire"

⁶EN 1992-1-2:2019 Standard: "Eurocode 2: Actions on concrete structures – Part 1-2: General actions – Actions on structures exposed to fire"

⁷Italian Technical Building Standards - Ministerial Decree 17th of January, 2018 and subsequent amendments and additions

4.3 Italian Technical Fire Prevention and Technical Building Standards

In the Italian Technical Fire Prevention Standards⁸ three evaluation methods for the structural fire resistance capacity are illustrated - [Table 4.1]:

- **Experimental method:** protected or non-protected specimens are tested in furnace, respectively with the prescription of the EN 13501 Standard and of the EN 13381 Standard;
- **Tabular method:** based on the ISO 834 temperature time-history. It is a rigorous method which can be used just for some structural members reported in the table below and that cannot consider any change of the boundary conditions;
- **Analytical method:** which could be used in two different ways:
 - **Simplified analytical method:** based on simplifying hypothesis for safety, it is used for checking single structural members⁹. This method may be used just for single elements or parts of structures;
 - **Advanced analytical method:** based on the application of the performance-based approach for the safety checks of structural members, it can be used to verify single elements, parts of a structure or the whole structure. This is the most accurate method that leads to both global and local structural analysis. An high-detailed model is required to these methods, considering the degradation of the materials while the fire is occurring. Then, the collapse security checks - Ultimate Limit State - may be calculated with the exceptional load combination - **Equation 4.4**¹⁰:

$$G_1 + G_2 + P + A_d + \psi_{21} \cdot Q_{k1} + \psi_{22} \cdot Q_{k2} + \dots \quad (4.4)$$

where:

* G_1 : permanent structural load

⁸Italian Technical Fire Prevention Standards - Ministerial Decree 3rd of August, 2015 and subsequent amendments and additions - Chapter S.2.6 (Verification of fire resistance performance with natural fire curves)

⁹EN 1991-1-2:2004 Standard: "Eurocode 1: Actions on structures – Part 1-2: General actions – Actions on structures exposed to fire"

¹⁰Italian Technical Building Standards - Ministerial Decree 17th of January, 2018 and subsequent amendments and additions - Chapter 2.5.3

- * G_2 : permanent non-structural load

- * P : prestress load

- * A_d : exceptional load, such as fire or explosion

- * Q : variable load, such as live load, wind load or snow load

Then the following three different criteria can be used to verify the structural behavior:

- * **Time:** the required time (for the evacuation or for the intervention of the rescue teams)

- * **Strength:** the needed strength to bear all the action for the required time

- * **Temperature:** the temperature over the required time may be less than the critical value of the material.

| Structural members to check | Available checking methods | ISO 834 temperature time-history | Natural temperature time-history |
|------------------------------------|-------------------------------------|---|---|
| Single elements | <i>Tabular method</i> | Allowed | Not allowed |
| | <i>Simplified analytical method</i> | Allowed | Allowed (if available) |
| | <i>Advanced analytical method</i> | Allowed | Allowed |
| Parts of the structure | <i>Tabular method</i> | Not allowed | Not allowed |
| | <i>Simplified analytical method</i> | Allowed (if available) | Not allowed |
| | <i>Advanced analytical method</i> | Allowed | Allowed |
| Whole structure | <i>Tabular method</i> | Not allowed | Not allowed |
| | <i>Simplified analytical method</i> | Not allowed | Not allowed |
| | <i>Advanced analytical method</i> | Allowed | Allowed |

Table 4.1: Italian Technical Fire Prevention Standards - Ministerial Decree 3rd of August, 2015 and subsequent amendments and additions - Chapter S.2.6 (Fire resistance) - Verification of fire resistance performance with natural fire curves

For the evaluation method about the exothermic analysis, the Chapter M.2¹¹ invokes the use of FDS and the Fire Engineering Methods - **Chapter 2.1 - The Fire; Chapter 2.2 - Fire Dynamics Simulator**. Furthermore, the Chapter M.1.9¹² reports some suggested Finite Element Codes - such as ABAQUS, Adina, ANSYS, DIANA and SAFIR calculation codes.

For the structural analysis, the Italian Technical Building Standards¹³ is invoked. The nominal¹⁴ and natural temperature time-histories are mentioned the concept of bearing capacity - as the time, expressed in minutes, for which the fire compartment features may have guaranteed - is introduced. The determination of this parameter is obtained through a tabular method and defines the **fire resistance class**. Furthermore, it is function of the **design specific fire heat load**, which may be the function of the contained materials in the fire compartment or averaged values, typical of the intended use.

Structural security checks for this Standard are achieved by checking that the exceptional load combination - **Equation 4.4** - are less than the strength at the specified temperature.

Other references on the structural behavior security check from this Standard are to the Eurocode 1¹⁵ and to the Italian Fire Prevention Standard¹⁶.

¹¹Italian Technical Fire Prevention Standards - Ministerial Decree 3rd of August, 2015 and subsequent amendments and additions - Chapter M.2 - Fire scenarios for performance design

¹²Italian Technical Fire Prevention Standards - Ministerial Decree 3rd of August, 2015 and subsequent amendments and additions - Chapter M.1.9 - Criteria for choosing and using models and calculation codes

¹³Italian Technical Building Standards - Ministerial Decree 17th of January, 2018 and subsequent amendments and additions - Chapter 3.6.1 - Fire action

¹⁴ISO 834, hydrocarbon and external fire curves.

¹⁵EN 1991-1-2:2004 Standard: "Eurocode 1: Actions on structures – Part 1-2: General actions – Actions on structures exposed to fire"

¹⁶Italian Technical Fire Prevention Standards - Ministerial Decree 3rd of August, 2015 and subsequent amendments and additions

Chapter 5

Standards for the definition of the engineering data

In this chapter, all the Standards considered for the definition of the material properties - both thermal and mechanical - are reviewed. In order to have the most complete scenario as possible the Eurocodes 2 and 3 and American Society of Civil Engineers vol. 78 Standards have been taken into account. Where the Codes are lacking of information, these have been integrated with literature papers considered reliable. In the following dissertation, the emissivity has been omitted, since it has a constant value and it has been considered as 0.8 both for concrete and reinforcement steel.

5.1 Material properties from the EN 1992-1-2:2019 Standard

The **EN 1992-1-2:2019 Standard** reports several materials parameter. Since this Standard regards the reinforced concrete structures, information for both concrete and reinforcement steel are mentioned.

5.1.1 Stress-strain diagram for concrete and reinforcement steel

First of all, the **stress-strain relationship for concrete**, whose variation over the temperature depends the kind of aggregates, is defined. The considered stress-strain diagram is the one proposed for unconfined concrete

by Kent and Park ¹ - **[Figure 5.1]** -, approximated with a bi-linear relationship with a cubic function fillet between the elastic and plastic behavior, according to the Eurocode 2 - **[Figure 5.2]** -. Then, the **[Table 5.1]** for the stress and strain variation with the thermal gradient is reported and all the stress-strain diagrams at fixed temperature can be calculated.

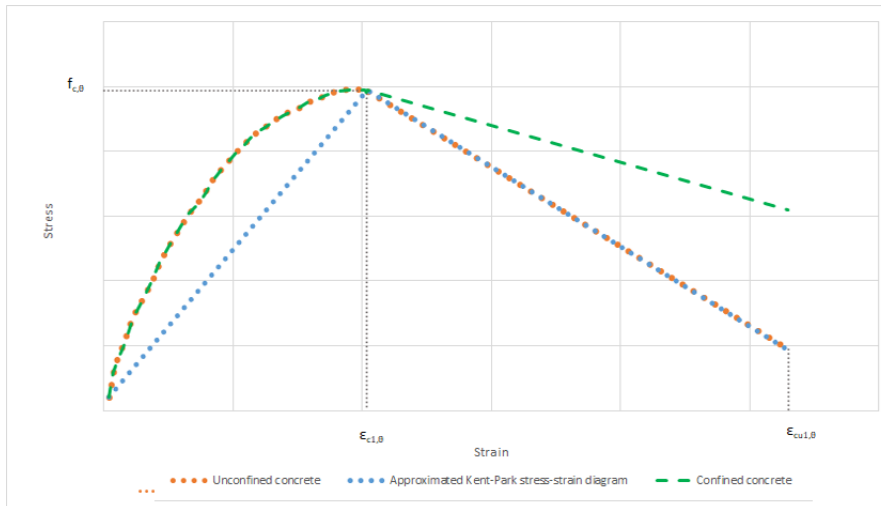


Figure 5.1: Stress-strain diagram - Kent and Park's model (1971)

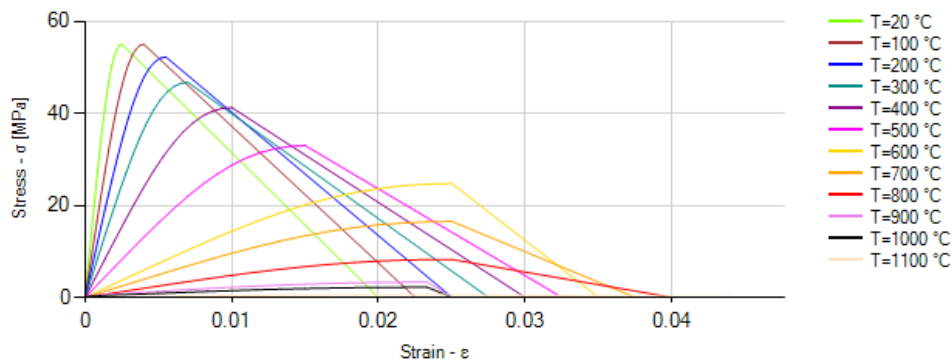


Figure 5.2: Variation of concrete stress-strain diagram with temperature variation

¹KENT, D.C., PARK, R., 11 Flexural Members with Confined Concrete 11, Journal of the Structural Division, ASCE, Vol. 97, ST7, July 1971, pp.1969-1990

| Concrete temperature [°C] | Siliceous aggregates | | | Calcareous aggregates | | |
|---------------------------|--------------------------------|------------------------|-------------------------|--------------------------------|------------------------|-------------------------|
| | $\frac{f_{c,\theta}}{f_{c,k}}$ | $\epsilon_{c1,\theta}$ | $\epsilon_{cu1,\theta}$ | $\frac{f_{c,\theta}}{f_{c,k}}$ | $\epsilon_{c1,\theta}$ | $\epsilon_{cu1,\theta}$ |
| 20 | 1.00 | 0.0025 | 0.0200 | 1.00 | 0.0025 | 0.0200 |
| 100 | 1.00 | 0.0040 | 0.0225 | 1.00 | 0.0040 | 0.0225 |
| 200 | 0.95 | 0.0055 | 0.0250 | 0.97 | 0.0055 | 0.0250 |
| 300 | 0.85 | 0.0070 | 0.0275 | 0.91 | 0.0070 | 0.0275 |
| 400 | 0.75 | 0.0100 | 0.0300 | 0.85 | 0.0100 | 0.0300 |
| 500 | 0.60 | 0.0150 | 0.0325 | 0.74 | 0.0150 | 0.0325 |
| 600 | 0.45 | 0.0250 | 0.0350 | 0.60 | 0.0250 | 0.0350 |
| 700 | 0.30 | 0.0250 | 0.0375 | 0.43 | 0.0250 | 0.0375 |
| 800 | 0.15 | 0.0250 | 0.0400 | 0.27 | 0.0250 | 0.0400 |
| 900 | 0.08 | 0.0250 | 0.0425 | 0.15 | 0.0250 | 0.0425 |
| 1000 | 0.04 | 0.0250 | 0.0450 | 0.06 | 0.0250 | 0.0450 |
| 1100 | 0.01 | 0.0250 | 0.0475 | 0.02 | 0.0250 | 0.0475 |
| 1200 | 0.00 | - | - | 0.00 | - | - |

where:

- $f_{c,\theta}$: is the cylinder compressive strength at the temperature θ .
- $\epsilon_{c1,\theta}$: is the strain corresponding to $f_{c,\theta}$.
- $\epsilon_{cu1,\theta}$: is the rupture strain.

Table 5.1: EN 1992-1-2:2019 Standard: values for the main parameters of stress-strain relationships of normal weight concrete with siliceous or calcareous aggregates concrete at elevated temperatures

As safety, the tensile strength of the concrete has been neglected. For the **reinforcing steel**, an linear-quadratic-linear elasto-plastic stress-strain diagram has been considered and shown in the [Figures 5.3, 5.4]. An explanation on the symbols follows:

- $E_{s,\theta}$: is the slope of the linear elastic range at the temperature θ .
- $f_{sp,\theta}$: is the proportional limit at the temperature θ .
- $f_{sy,\theta}$: is the maximum stress level at the temperature θ .
- f_{yk} : is the yielding stress limit at environment temperature.

Then the [Table 5.2] shows the variation parameters for the calculation of the stress-strain diagram for the ordinary steel and the [Table 5.3] shows the ones for the prestressing steel.

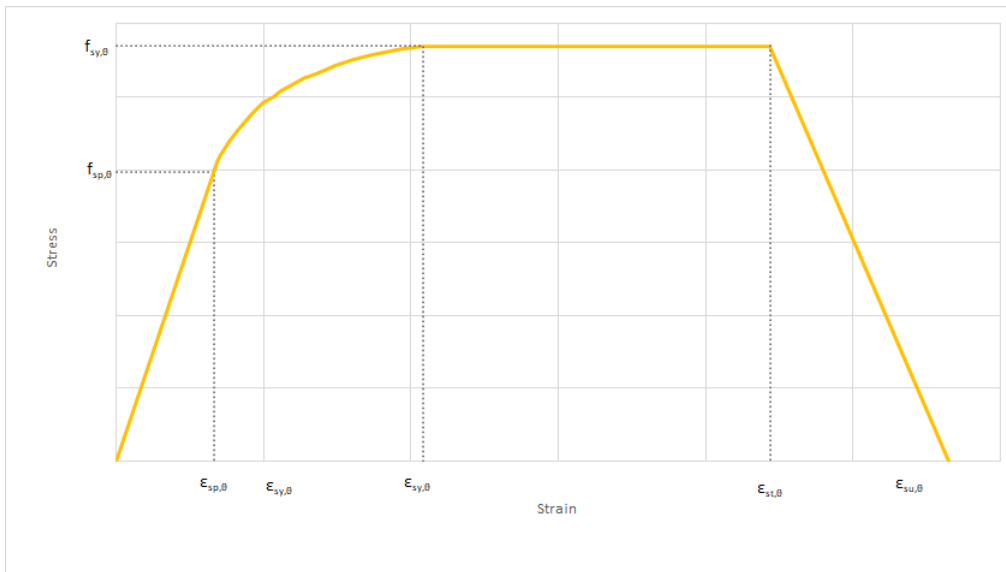


Figure 5.3: Variation of reinforcement steel elasto-plastic stress-strain diagram

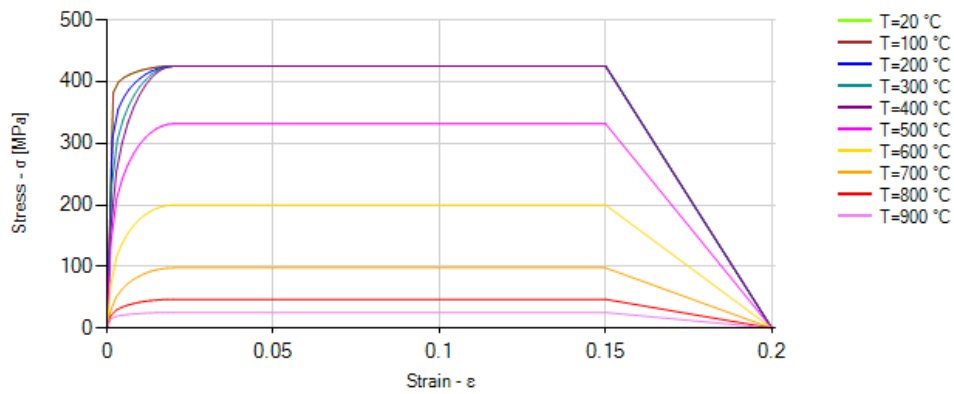


Figure 5.4: Rebar stress-strain diagram with temperature variation

| Class N ordinary reinforcement steel | | | | | | |
|---|-----------------------------------|--------------------|-----------------------------------|--------------------|-----------------------------------|--------------------|
| Steel temperature [°C] | Hot rolled | Cold worked | Hot rolled | Cold worked | Hot rolled | Cold worked |
| | $\frac{f_{sy,\theta}}{f_{yk}}$ | | $\frac{f_{sp,\theta}}{f_{yk}}$ | | $\frac{E_{s,\theta}}{E_s}$ | |
| 20 | 1.00 | 1.00 | 1.00 | 1.00 | 1.00 | 1.00 |
| 100 | 1.00 | 1.00 | 1.00 | 0.96 | 1.00 | 1.00 |
| 200 | 1.00 | 1.00 | 0.81 | 0.92 | 0.90 | 0.87 |
| 300 | 1.00 | 1.00 | 0.61 | 0.81 | 0.80 | 0.72 |
| 400 | 1.00 | 0.94 | 0.42 | 0.63 | 0.70 | 0.56 |
| 500 | 0.78 | 0.67 | 0.36 | 0.44 | 0.60 | 0.40 |
| 600 | 0.47 | 0.40 | 0.18 | 0.26 | 0.31 | 0.24 |
| 700 | 0.23 | 0.12 | 0.07 | 0.08 | 0.13 | 0.08 |
| 800 | 0.11 | 0.11 | 0.05 | 0.06 | 0.09 | 0.06 |
| 900 | 0.06 | 0.08 | 0.04 | 0.05 | 0.07 | 0.05 |
| 1000 | 0.04 | 0.05 | 0.02 | 0.03 | 0.04 | 0.03 |
| 1100 | 0.02 | 0.03 | 0.01 | 0.02 | 0.02 | 0.02 |
| 1200 | 0.00 | 0.00 | 0.00 | 0.00 | 0.00 | 0.00 |
| Class X ordinary reinforcement steel | | | | | | |
| Steel Temperature [°C] | Hot rolled and cold worked | | Hot rolled and cold worked | | Hot rolled and cold worked | |
| | $\frac{f_{sy,\theta}}{f_{yk}}$ | | $\frac{f_{sp,\theta}}{f_{yk}}$ | | $\frac{E_{s,\theta}}{E_s}$ | |
| 20 | 1.00 | | 1.00 | | 1.00 | |
| 100 | 1.00 | | 1.00 | | 1.00 | |
| 200 | 1.00 | | 0.87 | | 0.95 | |
| 300 | 1.00 | | 0.74 | | 0.90 | |
| 400 | 0.90 | | 0.70 | | 0.75 | |
| 500 | 0.70 | | 0.51 | | 0.60 | |
| 600 | 0.47 | | 0.18 | | 0.31 | |
| 700 | 0.23 | | 0.07 | | 0.13 | |
| 800 | 0.11 | | 0.05 | | 0.09 | |
| 900 | 0.06 | | 0.04 | | 0.07 | |
| 1000 | 0.04 | | 0.02 | | 0.04 | |
| 1100 | 0.02 | | 0.01 | | 0.02 | |

Table 5.2: EN 1992-1-2:2019 Standard: values for the main parameters of stress-strain relationships of ordinary reinforcement steel at elevated temperatures

| Steel Temperature [°C] | $\frac{f_{py,\theta}}{\beta f_{pk}}$ | | $\frac{f_{pp,\theta}}{\beta f_{pk}}$ | | $\frac{E_{p,\theta}}{E_p}$ | | $\epsilon_{pt,\theta}$ | $\epsilon_{pu,\theta}$ | |
|------------------------|--------------------------------------|---------|--------------------------------------|---------------------------------|------------------------------|---------------------------------|------------------------------|-----------------------------------|-----------------------------------|
| | Cold worked (wires and strands) | | Quenched and tempered (bars) | Cold worked (wires and strands) | Quenched and tempered (bars) | Cold worked (wires and strands) | Quenched and tempered (bars) | Cold worked Quenched and tempered | Cold worked Quenched and tempered |
| | Class A | Class B | | | | | | | |
| 20 | 1.00 | 1.00 | 1.00 | 1.00 | 1.00 | 1.00 | 1.00 | 0.050 | 0.100 |
| 100 | 1.00 | 0.99 | 0.98 | 0.68 | 0.77 | 0.98 | 0.76 | 0.0500 | 0.100 |
| 200 | 0.87 | 0.87 | 0.92 | 0.51 | 0.62 | 0.95 | 0.61 | 0.050 | 0.100 |
| 300 | 0.70 | 0.72 | 0.86 | 0.32 | 0.58 | 0.88 | 0.52 | 0.055 | 0.105 |
| 400 | 0.50 | 0.46 | 0.69 | 0.13 | 0.52 | 0.81 | 0.41 | 0.060 | 0.110 |
| 500 | 0.30 | 0.22 | 0.26 | 0.07 | 0.14 | 0.54 | 0.20 | 0.065 | 0.115 |
| 600 | 0.14 | 0.10 | 0.21 | 0.05 | 0.11 | 0.41 | 0.15 | 0.070 | 0.120 |
| 700 | 0.06 | 0.08 | 0.15 | 0.03 | 0.09 | 0.10 | 0.10 | 0.075 | 0.125 |
| 800 | 0.04 | 0.05 | 0.09 | 0.02 | 0.06 | 0.07 | 0.06 | 0.080 | 0.130 |
| 900 | 0.02 | 0.03 | 0.04 | 0.01 | 0.03 | 0.03 | 0.03 | 0.085 | 0.135 |
| 1000 | 0.00 | 0.00 | 0.00 | 0.00 | 0.00 | 0.00 | 0.00 | 0.090 | 0.140 |
| 1100 | 0.00 | 0.00 | 0.00 | 0.00 | 0.00 | 0.00 | 0.00 | 0.095 | 0.145 |
| 1200 | 0.00 | 0.00 | 0.00 | 0.00 | 0.00 | 0.00 | 0.00 | 0.100 | 0.150 |

where:

- β : is a parameter equal to:

$$- \text{ for Class A, } \beta = \left[\left(\frac{\epsilon_{ud} - \frac{f_{p0,1k}}{E_p}}{\epsilon_{uk} - \frac{f_{p0,1k}}{E_p}} \right) \cdot \left(\frac{f_{pk} - f_{p0,1k}}{f_{pk}} \right) + \frac{f_{p0,1k}}{f_{pk}} \right]$$

- for Class B, $\beta = 0.9$

- E_p : is the slope of the linear elastic range at the temperature θ .
- $f_{p0,1k}$: is the proof strength at 1% of deflection.
- f_{pk} : is the tensile strength at the temperature θ .
- ϵ_{uk} : is the elongation at maximum load at environment temperature.

Table 5.3: EN 1992-1-2:2019 Standard: values for the main parameters of stress-strain relationships of prestressed reinforcement steel at elevated temperatures

5.1.2 Thermal elongation for concrete and reinforcement steel

Unlike the previous cases, the temperature variation of the **thermal elongation of the concrete** is introduced by mean of two different equations - per each kind of aggregates -, without any tabular correlation methods. This variation is shown in the **[Figure 5.5]** (where θ is the steel temperature in Celsius degrees):

- **Siliceous aggregates:**

- $\epsilon_c(\theta) = -1.8 \cdot 10^{-4} + 9 \cdot 10^{-6} \cdot \theta + 2.3 \cdot 10^{-11} \cdot \theta^3$
for $20^\circ\text{C} \leq \theta \leq 700^\circ\text{C}$
- $\epsilon_c(\theta) = 14 \cdot 10^{-3}$ for $700^\circ\text{C} < \theta \leq 1200^\circ\text{C}$

- **Calcareous aggregates:**

- $\epsilon_c(\theta) = -1.2 \cdot 10^{-4} + 6 \cdot 10^{-6} \cdot \theta + 1.4 \cdot 10^{-11} \cdot \theta^3$
for $20^\circ\text{C} \leq \theta \leq 805^\circ\text{C}$
- $\epsilon_c(\theta) = 12 \cdot 10^{-3}$ for $805^\circ\text{C} < \theta \leq 1200^\circ\text{C}$

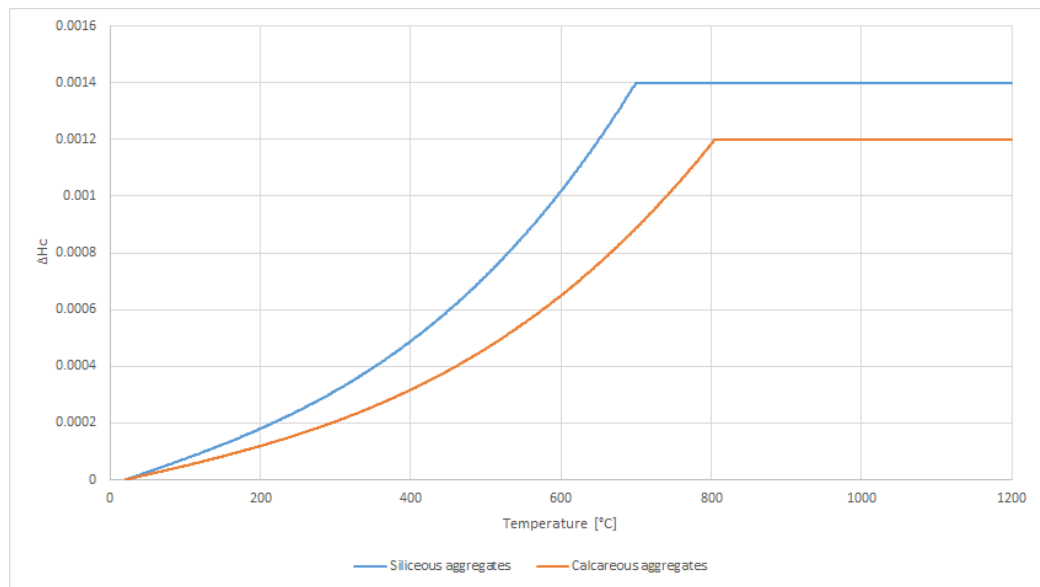


Figure 5.5: Variation of concrete thermal elongation with temperature

Even for **reinforcement steel**, the variation of the thermal elongation is calculated by some equations - **[Figure 5.6]**:

- **Ordinary reinforcement steel:**

- $\epsilon_s(\theta) = -2.416 \cdot 10^{-4} + 1.2 \cdot 10^{-5} \cdot \theta + 0.4 \cdot 10^{-8} \cdot \theta^2$
for $20^\circ\text{C} \leq \theta \leq 750^\circ\text{C}$
- $\epsilon_s(\theta) = 11 \cdot 10^{-3}$ for $750^\circ\text{C} < \theta \leq 860^\circ\text{C}$
- $\epsilon_s(\theta) = -6.2 \cdot 10^{-3} + 2 \cdot 10^{-5} \cdot \theta$ for $860^\circ\text{C} < \theta \leq 1200^\circ\text{C}$

- **Prestressed reinforcement steel:**

$$- \epsilon_p(\theta) = -2.416 \cdot 10^{-4} + 1.2 \cdot 10^{-5} \cdot \theta + 0.4 \cdot 10^{-8} \cdot \theta^2$$

for $20^\circ\text{C} \leq \theta \leq 750^\circ\text{C}$

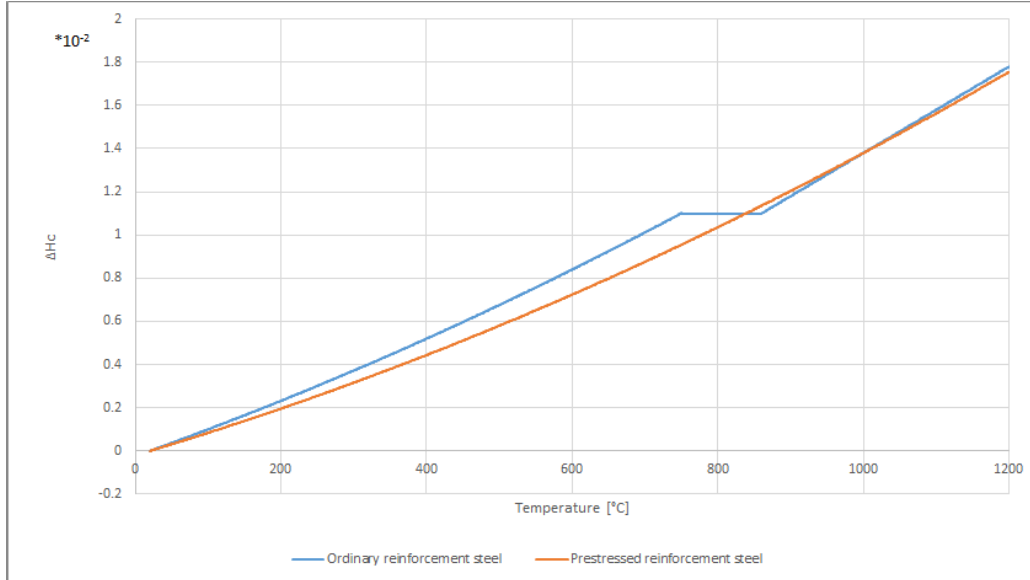


Figure 5.6: Variation of reinforcement steel thermal elongation with temperature

5.1.3 Density variation for concrete and reinforcement steel

The temperature depending variation of the **density of concrete** is influenced from the evaporation of the interstitial water and it is described by the following equations - **[Figure 5.7]:**

- $\rho(\theta) = \rho(20^\circ\text{C}) \left[\frac{\text{kg}}{\text{m}^3} \right]$ for $20^\circ\text{C} \leq \theta \leq 115^\circ\text{C}$
- $\rho(\theta) = \rho(20^\circ\text{C}) \cdot \left[1 - \frac{0.02 \cdot (\theta - 115)}{85} \right] \left[\frac{\text{kg}}{\text{m}^3} \right]$ for $115^\circ\text{C} < \theta \leq 200^\circ\text{C}$
- $\rho(\theta) = \rho(20^\circ\text{C}) \cdot \left[0.98 - \frac{0.03 \cdot (\theta - 200)}{200} \right] \left[\frac{\text{kg}}{\text{m}^3} \right]$ for $200^\circ\text{C} < \theta \leq 400^\circ\text{C}$
- $\rho(\theta) = \rho(20^\circ\text{C}) \cdot \left[0.95 - \frac{0.07 \cdot (\theta - 400)}{800} \right] \left[\frac{\text{kg}}{\text{m}^3} \right]$ for $400^\circ\text{C} < \theta \leq 1200^\circ\text{C}$

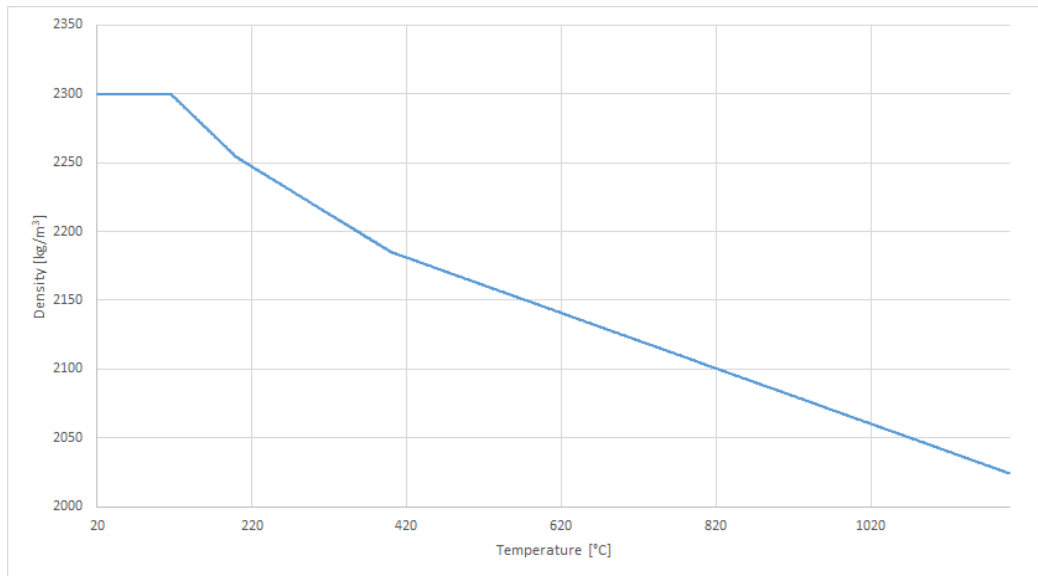


Figure 5.7: Variation of concrete density with temperature

Instead, the variation of the **density of reinforcement steel** does not occur, since this parameter is not influenced from the thermal gradient and it remains constant - **[Figure 5.8]**.

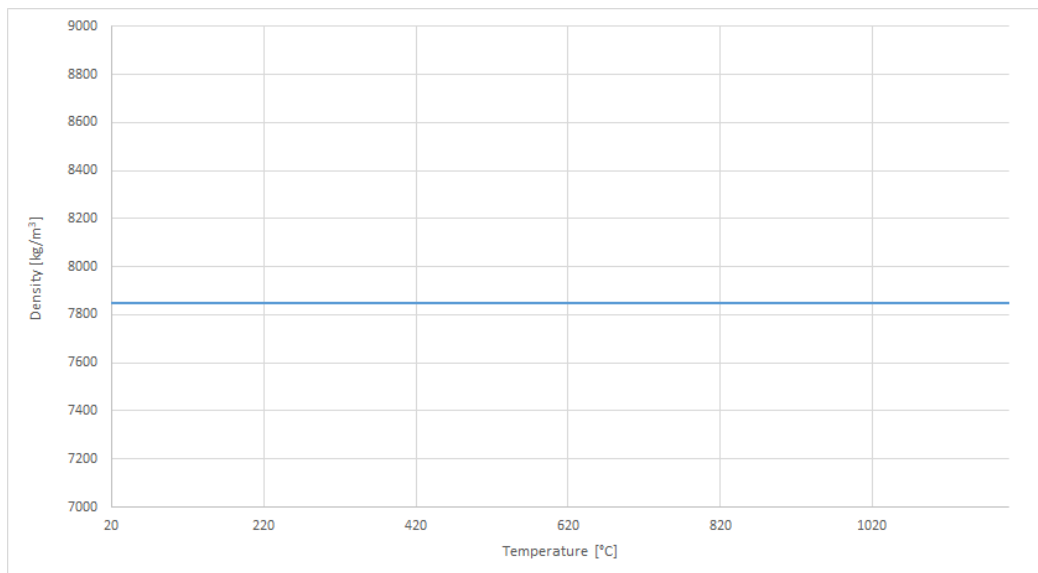


Figure 5.8: Variation of steel density with temperature

5.1.4 Specific heat variation for concrete

In this paragraph just the **specific heat variation for concrete** is reported, since the homologue parameter for the reinforcement steel is reported in the Eurocode 3 Standard. This parameter is influenced by the moisture content of the cement paste and its variation is reported - [Figure 5.9]:

- $c_p(\theta) = 900 \left[\frac{J}{kg \cdot K} \right]$ for $20 < \theta \leq 100^\circ C$
- *for 0% of moisture content*
 - $c_p(\theta) = 900 + (\theta - 100) \left[\frac{J}{kg \cdot K} \right]$ for $100^\circ C < \theta \leq 200^\circ C$
- *for 1.5% and 3% of moisture content*
 - $c_p(\theta) = c_{p,peak} \left[\frac{J}{kg \cdot K} \right]$ for $100^\circ C < \theta \leq 115^\circ C$
 - $c_p(\theta) = c_{p,peak} + \frac{(1000 - c_{p,peak}) \cdot (\theta - 115)}{85} \left[\frac{J}{kg \cdot K} \right]$ for $115^\circ C < \theta \leq 200^\circ C$
- $c_p(\theta) = 1000 + \frac{\theta - 200}{2} \left[\frac{J}{kg \cdot K} \right]$ for $200^\circ C < \theta \leq 400^\circ C$
- $c_p(\theta) = 1100 + (\theta - 100) \left[\frac{J}{kg \cdot K} \right]$ for $400^\circ C < \theta \leq 1200^\circ C$

where:

- θ is the temperature of the concrete
- $c_{p,peak} = 900 \left[\frac{J}{kg \cdot K} \right]$ for 0% of moisture content
- $c_{p,peak} = 1470 \left[\frac{J}{kg \cdot K} \right]$ for 1.5% of moisture content
- $c_{p,peak} = 2020 \left[\frac{J}{kg \cdot K} \right]$ for 3% of moisture content

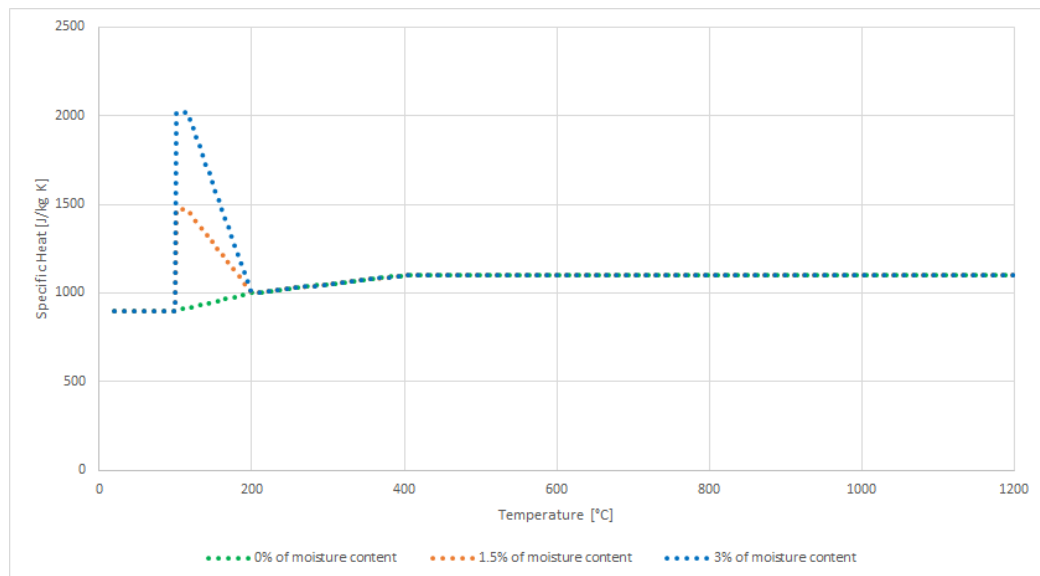


Figure 5.9: Variation of concrete specific heat with temperature

5.1.5 Thermal conductivity variation for concrete

Even in this paragraph, the **thermal conductivity variation** is reported just for concrete, since the homologue parameter for the reinforcement steel is reported in the Eurocode 3 Standard. This parameter has not a fixed value, but a range in which it is defined. For this research the lower bound of the thermal conductivity of concrete has been considered - **[Figure 5.10]**.

- $\lambda_c = 1.36 - (0.136 \cdot \frac{\theta}{100}) + (0.0057 \cdot (\frac{\theta}{100})^2) \frac{W}{m \cdot K}$
where:

– θ is the temperature of the concrete

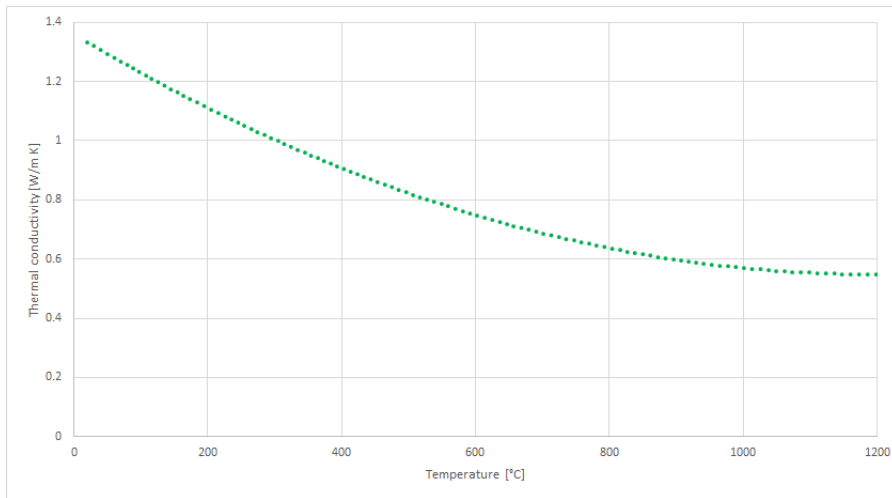


Figure 5.10: Variation of concrete thermal conductivity with temperature

5.1.6 Young modulus variation for reinforcement steel

The temperature variation of the **Young modulus of reinforcement steel** - both ordinary and prestressed rebar - has been introduced yet - [Tables 5.2, 5.3], [Figure 5.11]. Furthermore, the homologue parameter variation for concrete is reported in the ASCE 78 Standards.

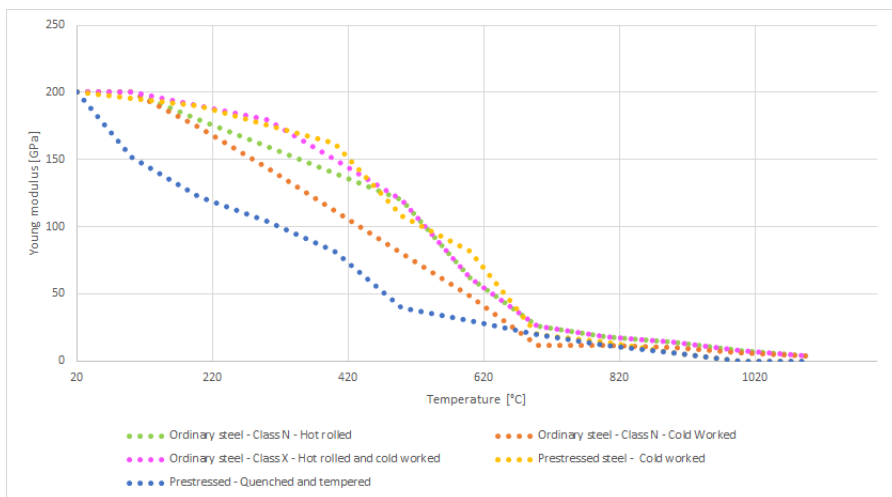


Figure 5.11: Variation of reinforcement steel Young modulus with temperature

5.2 Material properties from the EN 1993-1-2:2005 Standard

The EN 1993-1-2:2005 Standard reports several steel parameters.

5.2.1 Specific heat variation for reinforcement steel

The **specific heat variation of the reinforcement steel** is defined through four different equations, depending on the values of the temperature - [Figure 5.12]:

- $c_s = 425 + 7.73 \cdot 10^{-1} \cdot \theta - 1.69 \cdot 10^{-3} \cdot \theta^2 + 2.22 \cdot 10^{-6} \cdot \theta^3$ [$\frac{J}{kg \cdot K}$] for $20^\circ C \leq \theta \leq 600^\circ C$
- $c_s = 666 + \frac{13002}{738 - \theta}$ [$\frac{J}{kg \cdot K}$] for $600^\circ C < \theta \leq 735^\circ C$
- $c_s = 545 + \frac{17820}{\theta - 731}$ [$\frac{J}{kg \cdot K}$] for $735^\circ C < \theta \leq 900^\circ C$
- $c_s = 650$ [$\frac{J}{kg \cdot K}$] for $900^\circ C < \theta \leq 1200^\circ C$

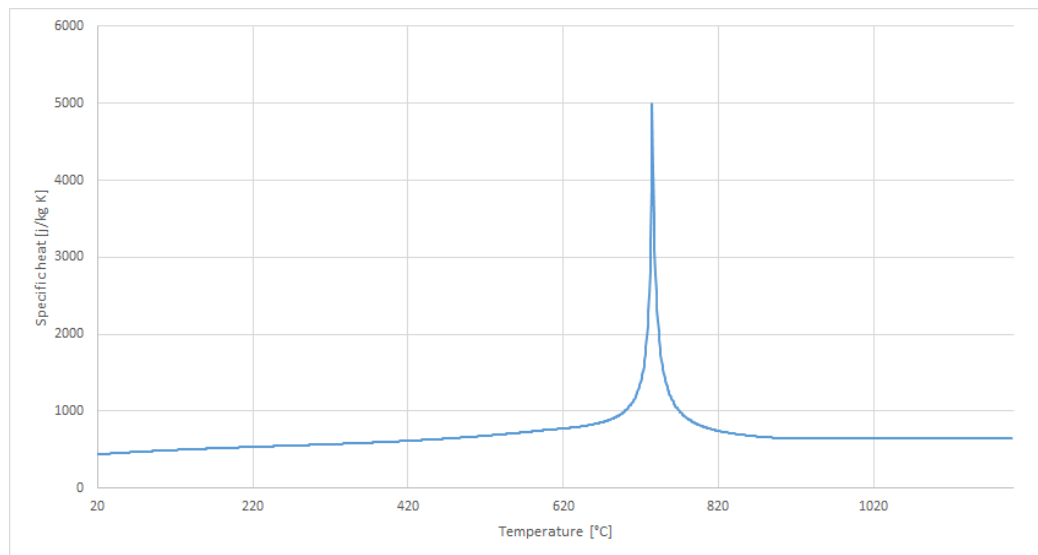


Figure 5.12: Variation of reinforcement steel specific heat with temperature

5.2.2 Thermal conductivity variation for reinforcement steel

Even the **thermal conductivity variation for reinforcement steel** is depending on the values of the temperature and it is defined through two equations - [Figure 5.13]:

- $\lambda_s = 54 - (3.33 \cdot 10^{-2} \cdot \theta) [\frac{W}{m \cdot K}]$ for $20^\circ\text{C} \leq \theta \leq 800^\circ\text{C}$
- $\lambda_s = 27.3 [\frac{W}{m \cdot K}]$ for $800^\circ\text{C} < \theta \leq 1200^\circ\text{C}$

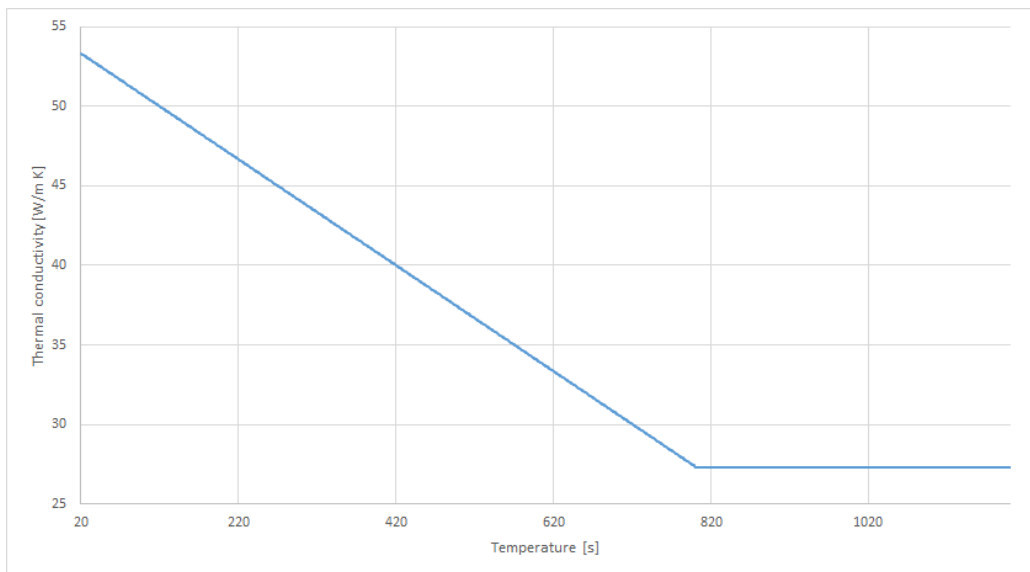


Figure 5.13: Variation of reinforcement steel thermal conductivity with temperature

5.3 Material properties from the ASCE 78 Standard

The **ASCE 78 Standard** reports the variation of the needed parameters which are not mentioned in the Eurocode 2 and 3.

5.3.1 Young modulus variation for concrete

The American Standard illustrates the variation relationships for the **average Young modulus of the concrete**. This parameter is assumed to be

equal to the formula reported in the Italian Technical Building Standard²:

$$E_{cm} = 22000 * \left(\frac{f_{ck}}{10}\right)^{0.3} [MPa] \quad (5.1)$$

The variation of the Young modulus is different, depending on the f_{ck} value - cylinder compressive strength - **[Figure 5.14]**:

- **Normal Strength Concrete - NSC:** defined for f_{ck} values less than 55 MPa

- $E_{cm}(\theta) = E_{cm}$ for $20 \leq \theta \leq 100$
- $E_{cm}(\theta) = E_{cm} \cdot \left(1 + \frac{100-\theta}{500}\right)$ for $100 < \theta \leq 600$

- **High Strength Concrete - HSC:** defined for f_{ck} values equal or major than 55 MPa

- $E_{cm}(\theta) = E_{cm}$ for $20 \leq \theta \leq 100$
- $E_{cm}(\theta) = E_{cm} \cdot (1.06 - (0.003 \cdot \theta))$ for $100 < \theta \leq 330$

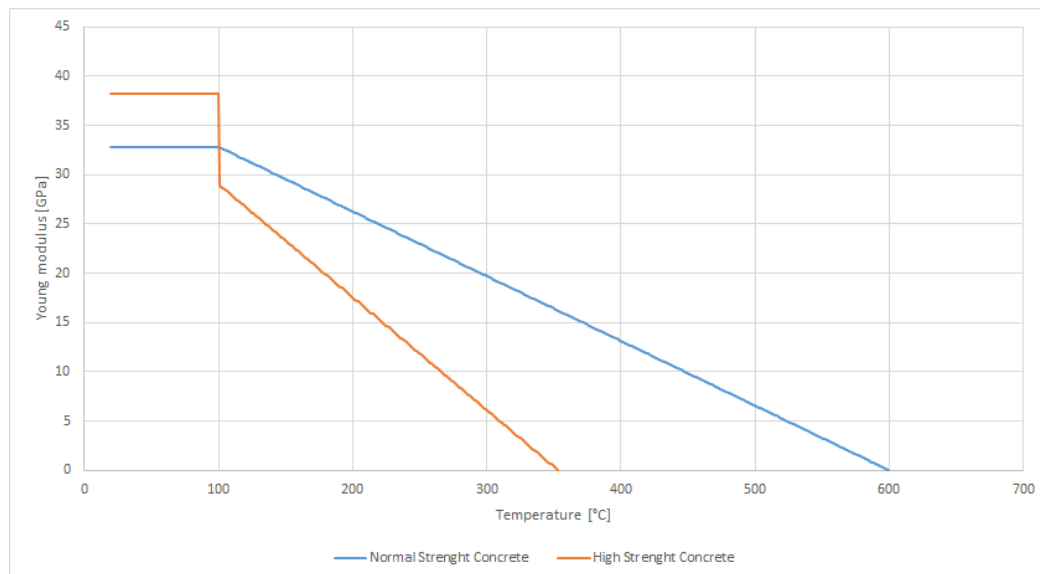


Figure 5.14: Variation of concrete average Young modulus with temperature

²Italian Technical Building Standards - Ministerial Decree 17th of January, 2018 and subsequent amendments and additions

5.4 Reliable papers for other material properties

The Eurocode 2 and 3 and the ASCE 78 Standards are actually lacking of information on the Poisson ratio. For this reason, a research work has been done in order to find one or more mathematical relationships to describe the variation over the temperature of the aforementioned parameter. Actually, there are no Standards reporting any variation laws for the Poisson ratio, instead there are some papers reporting experimental-based equations.

5.4.1 Poisson ratio variation for concrete

In order to find the variation of the **Poisson ratio for concrete**, a reliable paper ³ has been considered. This research focused attention on experimental tests on concrete specimens, in order to find a mathematical law for the variation of the Poisson ratio - **[Figure 5.15]**:

- $\nu_c(\theta) = \nu_c \cdot (0.2 + 0.8 \cdot \frac{500-\theta}{500-20})$ for $20^\circ\text{C} \leq \theta \leq 500^\circ\text{C}$
- $\nu_c(\theta) = 0.2 \cdot \nu_c$ for $500^\circ\text{C} \leq \theta \leq 1200^\circ\text{C}$

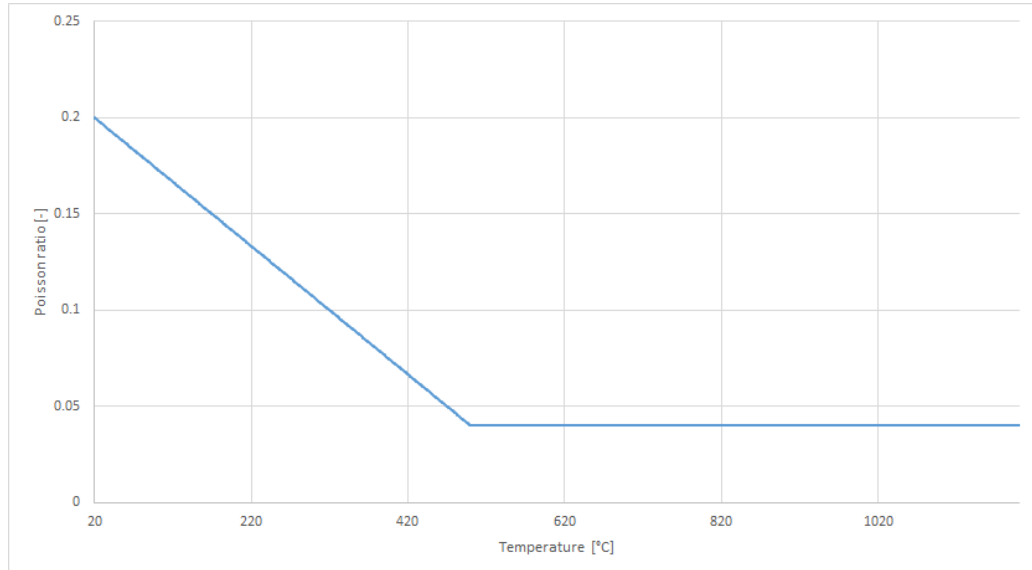


Figure 5.15: Variation of concrete Poisson ratio with temperature

³GERNAY T., MILLARD A., FRANSSSEN J.M. (2013): "A multiaxial constitutive model for concrete in the fire situation: Theoretical formulation", International Journal of Solids and Structures

5.4.2 Poisson ratio variation for reinforcement steel

Since the aforementioned paper regarded just the behavior of the concrete, another reliable paper⁴ has been considered for the **variation of the Poisson ratio for the reinforcement steel**. For this parameter, a linear distribution over the time has been predicted - [Figure 5.16].

- $v_c(\theta) = v_c \cdot (3.2 \cdot 10^{-5} \cdot \theta)$

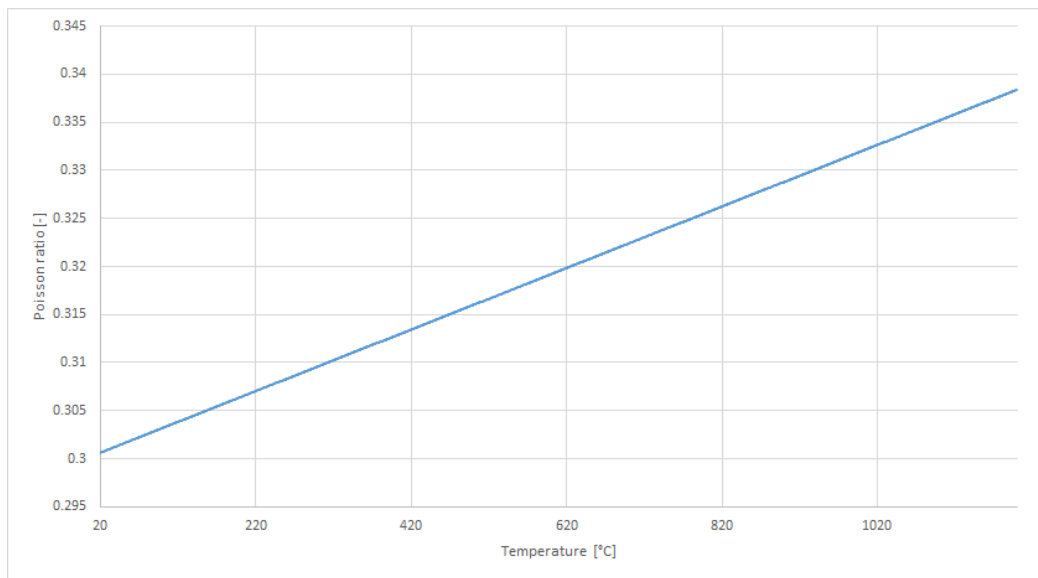


Figure 5.16: Variation of reinforcement steel Poisson ratio with temperature

⁴YANG, Y (2015): "Temperature-dependent thermoelastic analysis of multidimensional functionally graded materials", Ph.D. Thesis - University of Pittsburgh, Pennsylvania

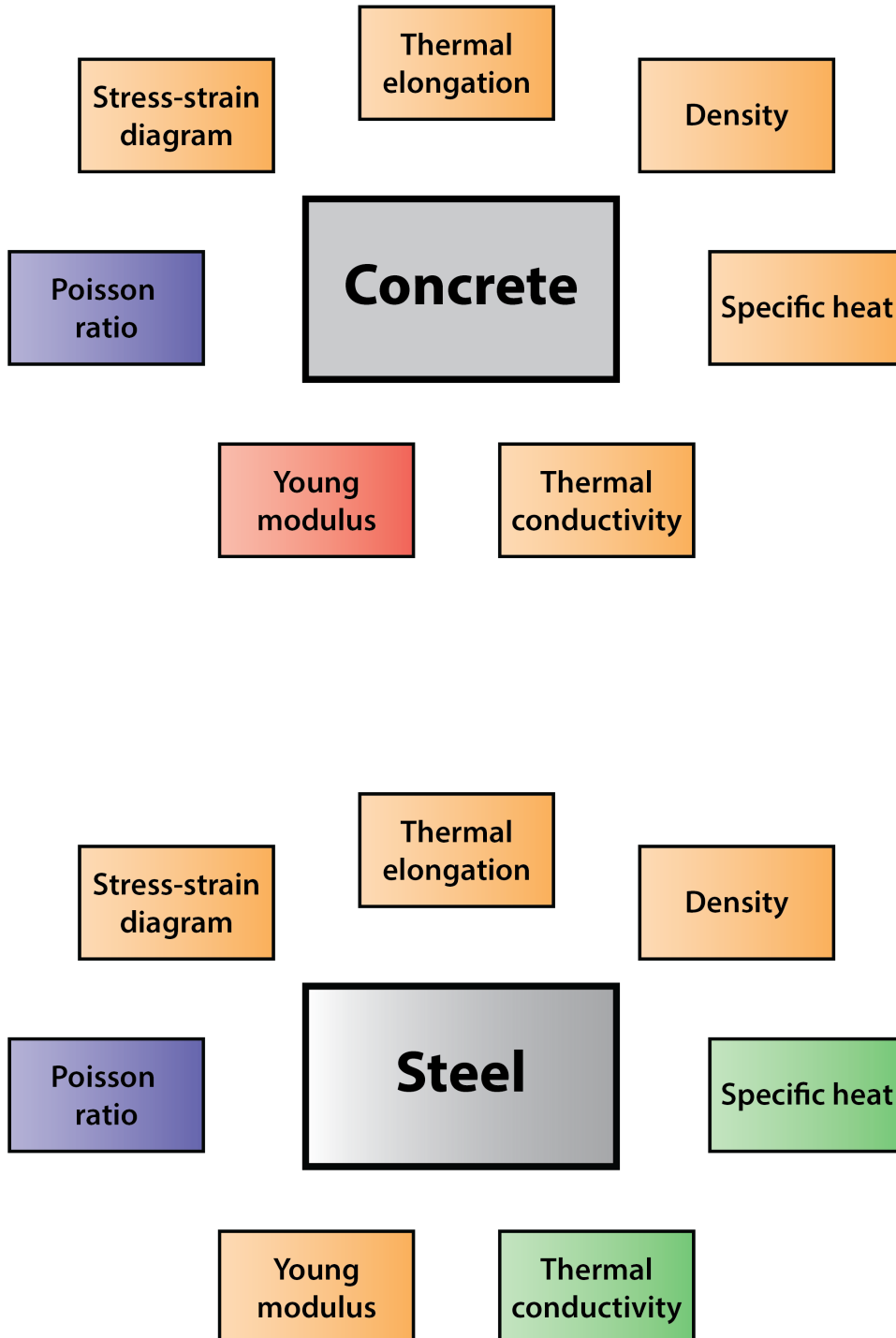


Figure 5.17: Synthesis of the material properties - Eurocode 2 - Eurocode 3
- ASCE 78 - Literature papers

Chapter 6

Introduction to FDS2ANSYS

After having analysed the main subjects of this research, this chapter introduces FDS2ANSYS, the solution to the problem of simplifying and automatizing the procedures for the generation of the input files for coupled thermal-mechanical analysis.

6.1 General dissertation on FDS2ANSYS

FDS2ANSYS is an experimental bridge-software, developed on Microsoft Windows environment using Visual Basic .NET programming language, implemented on the .NET Framework 4.7.2, which links the results of exothermic analysis – performed through FDS – in order to perform endothermic and mechanical analysis – through ANSYS Mechanical APDL. This association is possible through the NIST FDS2FTMI interface, developed by professor Julio Cesar Silva^{1 2}, which needs to be compiled and launched with a specific Command-Prompt Batch script each time an analysis is run. In this way the software automatizes this procedure, with a graphical interface, just typing some data useful to perform the analysis, without handling any script. Furthermore, this software completely automatizes the APDL-preprocessing file generation, with the analysed geometries in FDS, the Engineering Data – as described in the **Chapter 5. Engineering Data** and the features of the analysis, through setting the keyoptions for the element types – as described in the **Chapter 2. Theory** and the simulation time. Since ANSYS Mechanical APDL can be launched from the Microsoft Windows Command-Prompt

¹SILVA J.C. (2017), "FDS2FTMI User's Guide - An automated code to one-way coupling between FDS and FEM using FTMI", National Institute of Standards and Technology

²ZHANG C., SILVA J.C., WEINSCHENK C., KAMIKAWA D., HEASEMI Y. (2017), "Simulation Methodology for Coupled Fire-Structure Analysis: Modeling localized fire tests on a steel column", National Institute of Standards and Technology

in Batch mode – GUI disabled -, the generated input files too are loaded into the FEM code through specific Command-Prompt Batch script. In order to understand all the functionalities of this software, the FDS2ANSYS User manual can be found in the **Appendix B: FDS2ANSYS User Manual**, at the end of this essay - **[Figure 6.1]**.

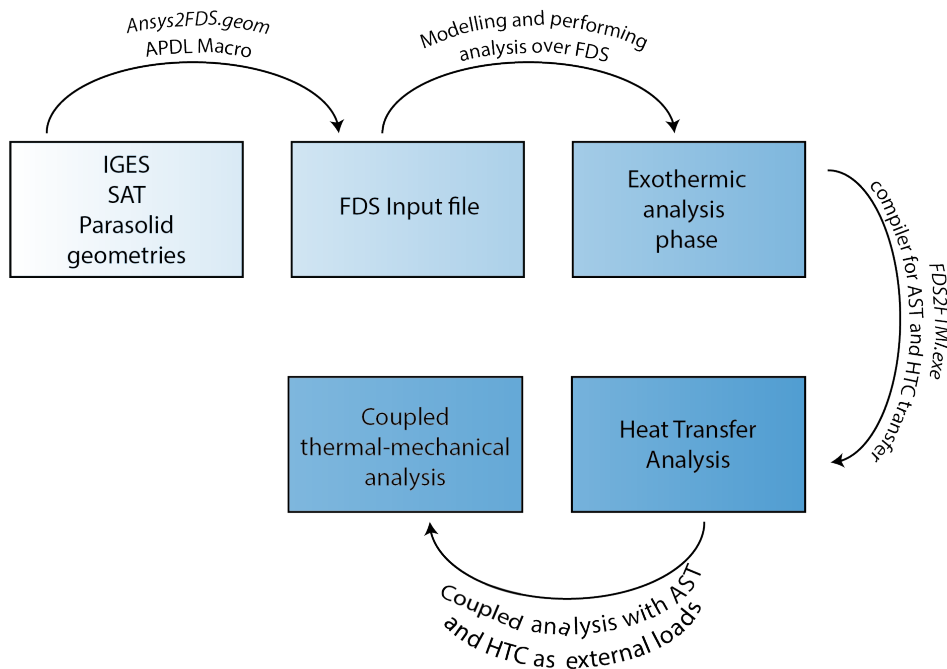


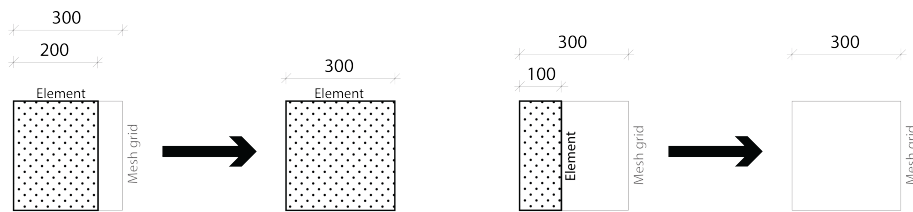
Figure 6.1: Generic flowchart for FDS2ANSYS procedures

6.2 Fields of application and limitations of FDS2ANSYS

Since this research has been carried out taking into account just **reinforced concrete structures**, FDS2ANSYS has been developed only for this kind of buildings, both with ordinary and prestressed reinforcement steel. For this reason, the software is endowed of a material property tab, in which all the parameters showed in the **Chapter 5. Engineering Data**. In the next sub-paragraphs, main aspect of the functionalities of this software have been shown.

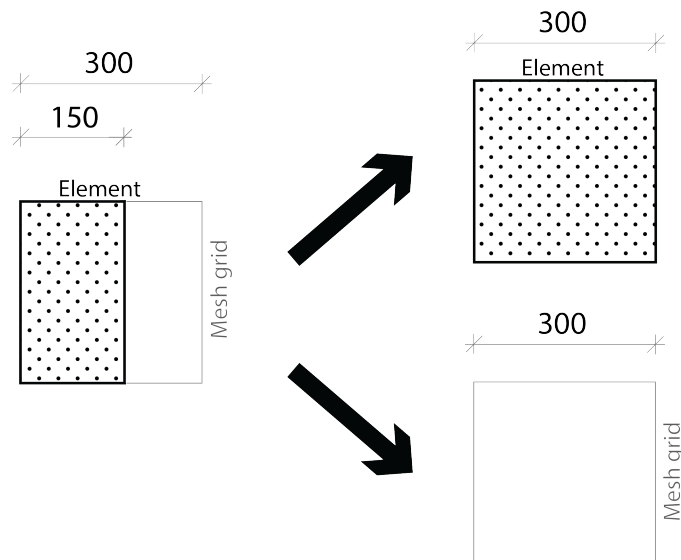
6.2.1 Mesh sensitivity analysis of the mesh for FDS

Since the FDS calculus engine is based on mesh cells, the geometries are read as multiples of cells. This means that if a 30 cm mesh size is set and the geometry has a side of 20 cm, FDS would read 30 cm - [Figure 6.2a]. The same situation happens with a side that is less long than the half of the mesh size: if the geometry has a size of 10 cm with a mesh cell size equal to 30 cm, the measure would be 0 cm - [Figure 6.2b] - and a surface with no thickness is placed in the zero-vertex. If the geometry has a size equal to the half of the mesh cell size, the geometry read from FDS could be a surface with no thickness or a 30 cm-sided solid, depending on the allocation method of numbers on the RAM of the PC - [Figure 6.2c].



(a) Element longer than the half of the mesh cell

(b) Element shorter than the half of the mesh cell



(c) Element as long as the half of the mesh cell

Figure 6.2: FDS reading method of geometries. LEFT: how the element is - RIGHT: how the element is read by FDS

This means that, in order to perform reliable analysis without the deformation of the structural members, a very small mesh size may be needed to run FDS properly. To this purpose, the MSAT - Mesh Sensitivity Analysis Tool - has been programmed. This algorithm finds the proper mesh cell size - assuming a cubic mesh - calculating the greatest common factor between the provided data. The properties that the user may provide are:

- **Side of structural members**
- **Clear spans**
- **Concrete cover**
- **Spacing between stirrups**

It is possible to provide some or all of the requested parameters. More of these are provided, more the output mesh size is reliable. Despite this means that analysis which should be with a very low error ratio, could be very time-consuming and expensive in terms of needed hardware. For this reason, another utility has been developed, in order to split the model and performing the analysis on more than one thread - logical processor - of the CPU.

6.2.2 Splitting the mesh and exploiting the MPI Utility Engine

By default, an FDS analysis run on only one logical processor of the CPU. It is possible to model more than one mesh and run the analysis in parallel onto the number of the modeled meshes of threads of the CPU. This is possible through FDS Parallel, which exploits the Intel MPI Engine. In order to reduce the needed time for the analysis, a Python script³ has been transposed on Visual Basic .NET Language and implemented. This script divides the geometry in a user-defined parts and this number needs to be higher than the employed logical processors - user-defined. This interface can be run from FDS2ANSYS in two ways:

- **Local resources:** a runtime control founds the number of the logical processors, which is the maximum allowable number;

³COLLINS D.C. (2015), "Dividing and Conquering Meshes within the NIST Fire Dynamics Simulator (FDS) on Multicore Computing Systems", Master of Science Degree Thesis, University of Tennessee, Knoxville

- **Remote resources:** all the files are prepared to be copied in a workstation/server/cluster which is not the PC that is running FDS2ANSYS. To this purpose, a maximum number of 64 threads can be set.

The latter is the chosen method, since to perform this kind of analysis, an HPC - High Performance Computing - cluster has been used. To the technical features, in the **Chapter 8. Further consideration on the experimented results** all these aspects are shown.

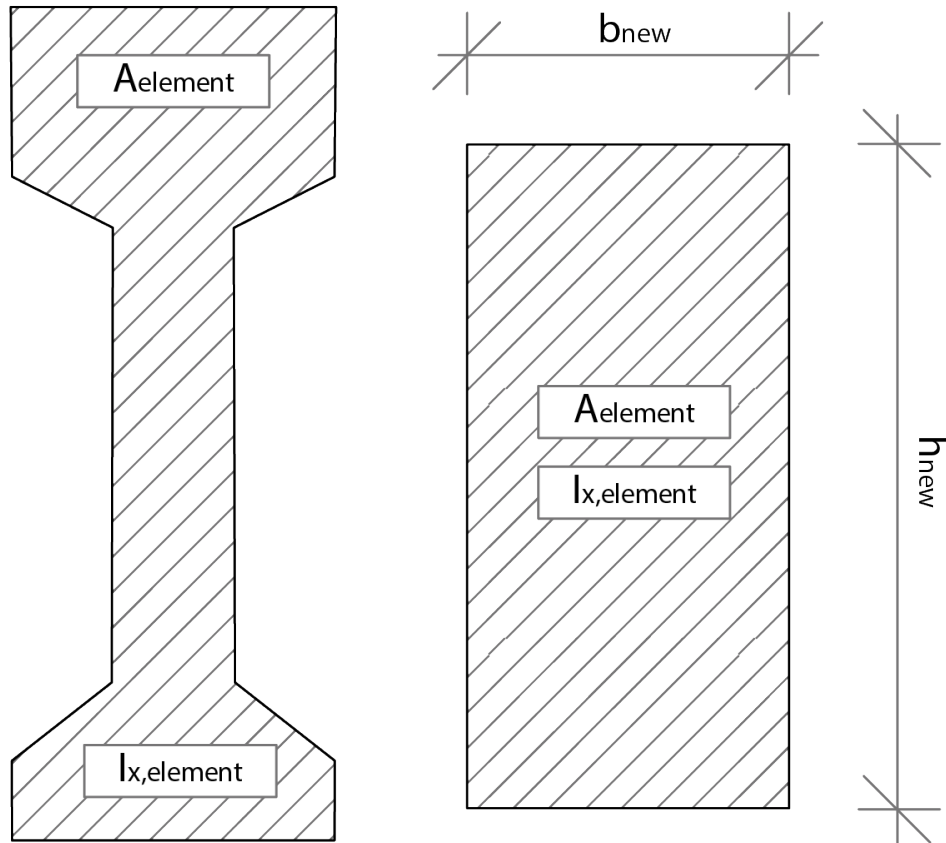
6.2.3 Interface for reinforcement steel bars

Since the complexity of modeling manually the reinforcement bars, a specific interface to this purpose has been implemented. With this utility, the user is allowed to model automatically both the rebar and the stirrups. To further information on this aspect, see the **Appendix B. FDS2ANSYS User Manual**

6.2.4 Limitations of FDS2ANSYS

On the FDS setting-up analysis phase, FDS2ANSYS has two main limitations: a cubic mesh is assumed for the calculus and it is not possible to place any mesh refinement areas. In other words, all the geometrical model is studied with the same cubic mesh cell size and this is a limitation, since the CPU time may increase significantly. On the FEM side, the main limitation of this software is due to the section of the structural members. Indeed, FDS2ANSYS is capable of recognizing rectangular or squared sections only. In case of more complex sections, it is advisable to calculate an equivalent cross-section as follows, by knowing the section surface and the moment of inertia - **[Figure 6.3]**:

$$\begin{cases} b_{new} \cdot h_{new} \approx A_{element} \\ \frac{b_{new} \cdot h_{new}^3}{12} \approx I_{x,element} \end{cases} \quad (6.1)$$



(a) Cross-section of the structural member (b) Cross-section of the equivalent structural member

Figure 6.3: Original and equivalent cross-sections of structural members

Another limitation is due to the FDS method of reading geometries. It is not allowed to model slopes (roof slabs, diagonal beams or braces). To overcome this limitation, an equivalent height of the structural members may be calculated. An advised method may be the averaged height of the columns.

6.3 Overall disquisition on the processes

In this paragraph, the processes that lead to the main goals of this research are described. Furthermore, before considering this aspect, it is important to remember that the whole coupled thermal-mechanical analysis may be

processed in two different ways, which differ on the thermal and structural analysis phases:

- **Sequential coupling approach:** this technique allows users to take into consideration the non-linearity for both thermal - conductivity, specific heat, density - and mechanical material features - stress-strain relationship for concrete compressive strength and reinforcement steel ultimate strength properties - and, so, to model the thermal-mechanical behavior with an high precision. This approach is achieved by performing separately the whole time-history thermal analysis, for the entire simulation time, and then, for the same time interval, the whole time-history mechanical analysis needs to be performed by coupling the results of the thermal analysis. For this reason, on the FEM code, appropriate finite element types need to be chosen, both for thermal and mechanical behavior. Despite this technique is really accurate on the results, it does not take into account of the change of the temperature field, that may occur with collapses - which may expose more the inner core of the structural elements to the thermal stress;
- **Direct coupling approach:** this technique consists in a step-by-step thermal-mechanical analysis. The coupling procedure, indeed, is not reached at the end of the endothermic analysis but at each time-step. In other words, whereas in the sequential coupled analysis appropriate finite element types need to be chosen, both for thermal and mechanical behavior, in the direct coupling technique a single element type - one for the concrete and one for the rebar - needs to be chosen and it may be capable of performing both thermal and structural analysis. This would mean that the concrete cracking and crushing behavior may be neglected with this kind of coupling procedure. On the other hand, it is possible to take into account any variation of the temperature field while the fire is occurring.

In order to start these processes, some features needs to be defined, as:

- **CHID:** name of the file;
- **Simulation time;**
- **Mesh cell size;**
- **Dump frames:** for the time interval of data output;
- **Time interval:** for the heat transfer;

In the next sub-paragraphs, some flowcharts are shown to simplify and synthesize the FDS2ANSYS procedures to sequential and direct coupling of thermal and mechanical analysis.

The sequential coupling technique can be divided in the following steps - **[Figure 6.4]**:

- **Procedures for exothermic analysis**: to generate a FDS input file needed to the exothermic analysis;
- **Procedures for heat transfer analysis**: to transfer the temperature profile over time in ANSYS Mechanical APDL;
- **Procedures for endothermic analysis**: to analyze - for the whole simulation time - the heat propagation into the concrete inner core;
- **Procedures for coupling thermal and mechanical analysis**: from the temperature field, it is possible to carry on a mechanical analysis with the thermal and inertial forces.

On the direct coupling technique, several steps may be identified - **[Figure 6.5]**:

- **Procedures for exothermic analysis**: performed in the same way of the sequential coupling approach;
- **Procedures for heat transfer analysis**: performed in the same way of the sequential coupling approach;
- **Procedures for direct-coupled thermal-mechanical analysis**: thermal and structural analysis are performed together step-by-step.

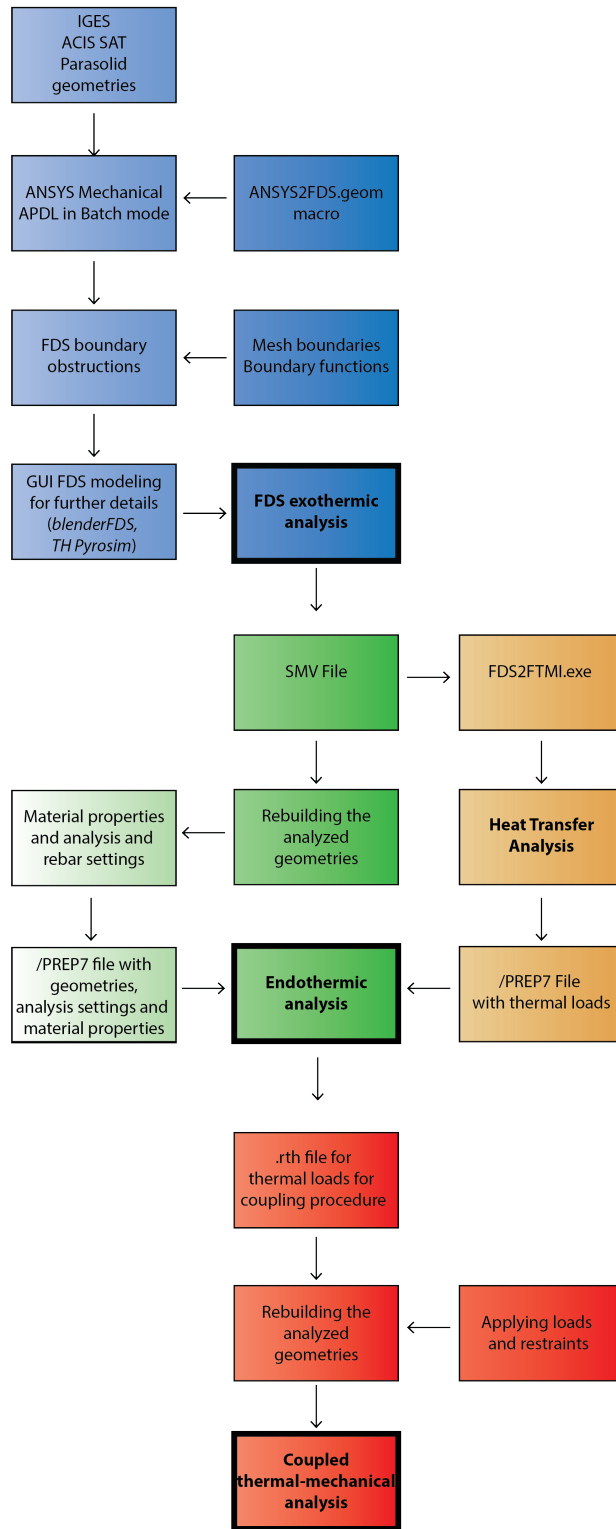


Figure 6.4: Complete flowchart for sequential coupling procedures in FDS2ANSYS

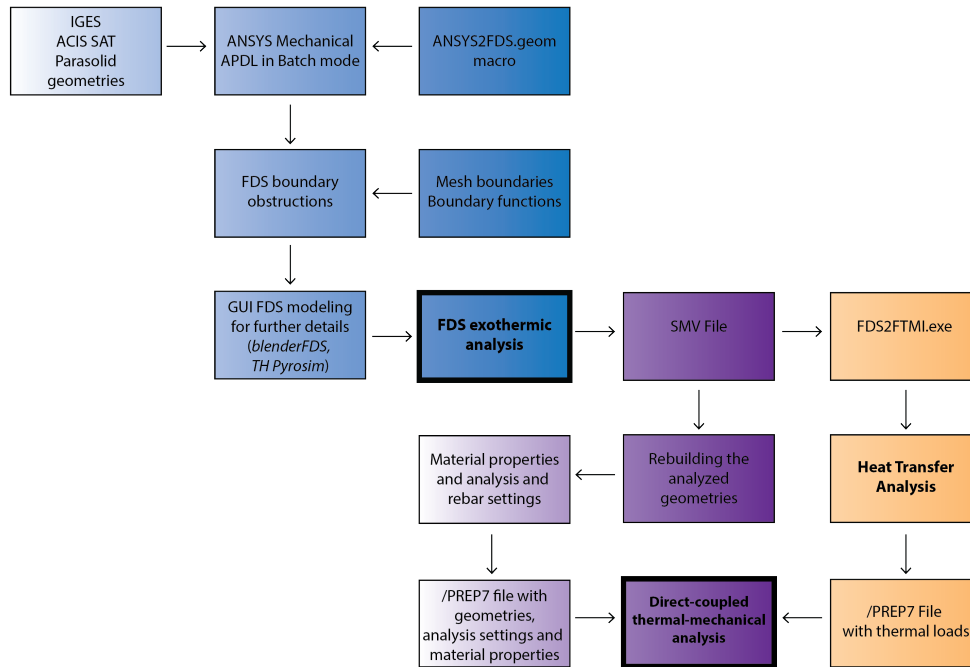


Figure 6.5: Complete flowchart for direct coupling procedures in FDS2ANSYS

6.3.1 Writing a FDS input file

As previously said, the exothermic analysis phase is performed with input files which are generated from FDS2ANSYS in the same way for both sequential and direct coupling techniques. The FDS input file is generated from FDS2ANSYS through a geometric model, which may be in IGES, ACIS SAT or Parasolid extension - because these are the supported formats from ANSYS Mechanical APDL. In this case, an APDL macro contained in the FDS2FTMI⁴ Git directory was implemented in the software and it is called "ANSYS2FDS.geom". Through this macro, a series of strings that describe the obstruction surfaces are generated. Then, the FDS file is added of some needed details, as the extension of the mesh - taking into account of the geometry file and the mesh cell size - and the boundary functions - for Adiabatic Surface Temperature and Heat Transfer Coefficient. In the **Appendix C.1.1. Case Study A. - Raw FDS Code** an example of code generated

⁴SILVA J.C (2017), "FDS2FTMI User's Guide - An automated code to one-way coupling between FDS and FEM using FTMI", National Institute of Standards and Technology

from FDS2ANSYS is reported. Then the FDS file may be imported in a GUI Model engine for FDS - blenderFDS or Thunderhead Engineering Pyrosim - to add further details, as burners, devices, slices, reaction and many other. A flowchart of these processes is shown in the [Figure 6.6]. In the **Appendix C.1.2. Case Study A. - Pyrosim FDS Code** an example of code edited in Pyrosim is reported. Furthermore it has been noticed that for long simulation timings - over 5000s -, the FDS analysis may not achieve convergence because of numerical instability. By contacting the FDS-SMV Google Discussions Forum, one of the main developer of FDS - Kevin McGrattan - suggested to model the geometries assuming pressure zones and modeling the single structural member as six separated surface obstructions or modeling it as a unique obstruction - instead of six separated surface obstructions. Actually, both of provided solution have been capable of solving these issues by rearranging the geometries or setting an additional pressure zone. For the reported examples of input files, this edit has not been done, since the simulation time has been set to 1000s and the aforementioned issue did not appear.

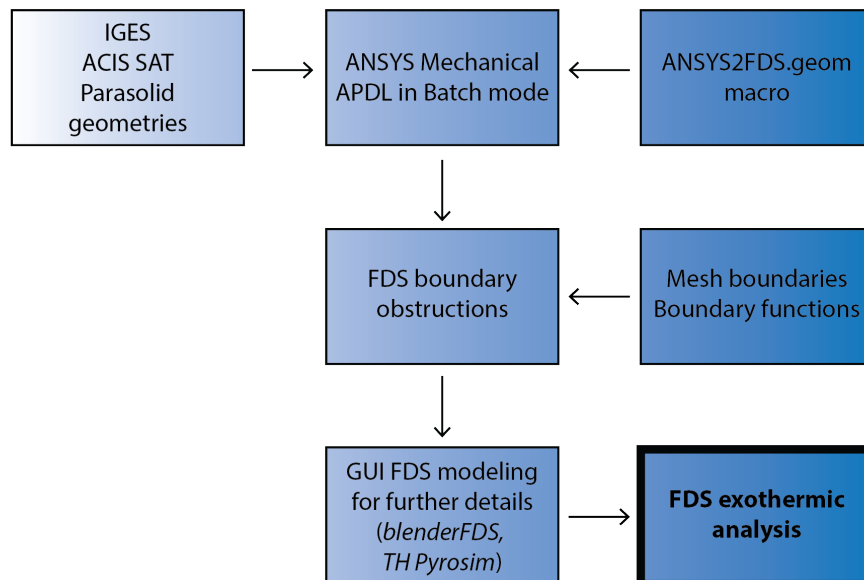


Figure 6.6: Flowchart for FDS2ANSYS procedures to write a FDS input file

6.3.2 Writing a /PREP7 ANSYS Mechanical APDL pre-processing input file

The "/PREP7" preamble in ANSYS Mechanical APDL means to run the pre-processing engine. Depending on the chosen coupling procedure, this input file can be generated in different ways.

6.3.2.1 Sequential coupled thermal-mechanical analysis

The /PREP7 file is generated from FDS2ANSYS in order to "build" the geometrical model to perform an Endothermic analysis. A flowchart of these processes is shown in the [Figure 6.7]. An example of the generated code can be found in **Appendix C.1.3. Case Study A. - /PREP7 Code for ANSYS Mechanical APDL #1.**

The contained features are:

- **Concrete structure with thermal behavior:** respecting the FDS mesh discretization;
- **Concrete and reinforcement steel thermal behavior:** according to the **Chapter 5. Engineering Data.**

In this phase, the keyoptions for both thermal and mechanical analysis needs to be set. This features are editable from a specific graphical interface contained in FDS2ANSYS. The available options are reported below:

- **Concrete thermal behavior - SOLID70 element type:**
 - **Evaluation of film coefficient** can be set as:
 - * Evaluate film coefficient (if any) at average film temperature, $(TS + TB)/2$ (KEYOPT(2)=0)
 - * Evaluate at element surface temperature, TS (KEYOPT(2)=1)
 - * Evaluate at fluid bulk temperature, TB (KEYOPT(2)=2)
 - * Evaluate at differential temperature $|TS-TB|$ (KEYOPT(2)=3)
 - **Element coordinate system defined** can be set as:
 - * Element coordinate system is parallel to the global coordinate system (KEYOPT(4)=0)
 - * Element coordinate system is based on the element I-J side (KEYOPT(4)=1)
 - **Nonlinear fluid option** can be set as:
 - * Standard heat transfer element (KEYOPT(7)=0)

- * Nonlinear steady-state fluid flow analogy element - Temperature degree of freedom interpreted as pressure - (KEYOPT(7)=1)
- **Mass transport effects** can be set as:
 - * No mass transport effects (KEYOPT(8)=0)
 - * Mass transport with VX, VY, VZ (KEYOPT(8)=1)
- **Reinforcement thermal behavior - LINK33 element type:** no keyoptions needed to be set.
- **Concrete mechanical behavior - SOLID65 element type:**
 - **Extra displacement shapes** can be set as:
 - * Including extra displacement shapes (KEYOPT(1)=0)
 - * Suppressing extra displacement shapes (KEYOPT(1)=1)
 - **Behavior of totally crushed unreinforced elements** can be set as:
 - * Base behavior (KEYOPT(3)=0)
 - * Suppress mass and applied loads, and warning message (KEYOPT(3)=1)
 - * Features of 1 and apply consistent Newton-Raphson load vector (KEYOPT(3)=2)
 - **Concrete linear solution output** can be set as:
 - * Print concrete linear solution only at centroid (KEYOPT(5)=0)
 - * Repeat solution at each integration point (KEYOPT(5)=1)
 - * Nodal stress printout (KEYOPT(5)=2)
 - **Concrete nonlinear solution output** can be set as:
 - * Print concrete nonlinear solution only at centroid (KEYOPT(6)=0)
 - * Print solution at each integration point (KEYOPT(6)=1)
 - **Stress relaxation after cracking** can be set as:
 - * No tensile stress relaxation after cracking (KEYOPT(7)=0)
 - * Include tensile stress relaxation after cracking to help convergence (KEYOPT(7)=1)
 - **Warning message for totally crushed unreinforced element** can be set as:
 - * Print the warning (KEYOPT(8)=0)
 - * Suppress the warning (KEYOPT(8)=1)

- **Reinforcement mechanical behavior - LINK180 element type:**
 - **Cross-section scaling** (which applies only if large-deflection effects - NLGEOM,ON - are specified) can be set as:
 - * By default, enforce incompressibility; cross section is scaled as a function of axial stretch (KEYOPT(2)=0)
 - * Section is assumed to be rigid (KEYOPT(2)=1)

 - **Hydrodynamic output** can be set as:
 - * By default, none (KEYOPT(12)=0)
 - * Additional hydrodynamic printout (KEYOPT(12)=1)

In the aforementioned /PREP7 file, just the concrete thermal features (element type with keyoptions and material properties) are reported. Later in the text, a description for reinforcement steel properties is reported. For the mechanical features, the specific /PREP7 input file is generated and shown in the next paragraph.

Then, a second /PREP7 input file is generated automatically, exploiting the FDS2FTMI interface, which contains all the heat loads and is the result of solving the Heat Transfer Analysis. An example of this code can be found in **Appendix C.1.4. Case Study A. - /PREP7 Code for ANSYS Mechanical APDL #2**. In this case, several keyoptions - typical of the SURF152 element type - are set but no user-defined properties can be set to this section, since the optimal keyoptions has been chosen yet from Silva.

Finally, another /PREP7 input file is generated, containing all the information on the reinforcement bars, as LINK33 element type - for reinforcement steel thermal behavior. This phase has been separated from the generation of the first input file, in order to be sure that the Heat Transfer Analysis is performed properly. An example of this code can be found in **Appendix C.1.5. Case Study A. - /PREP7 Code for ANSYS Mechanical APDL #3**. Once the reinforcement settings have been generated and automatically imported in ANSYS Mechanical APDL, it is possible to perform the Endothermic Analysis.

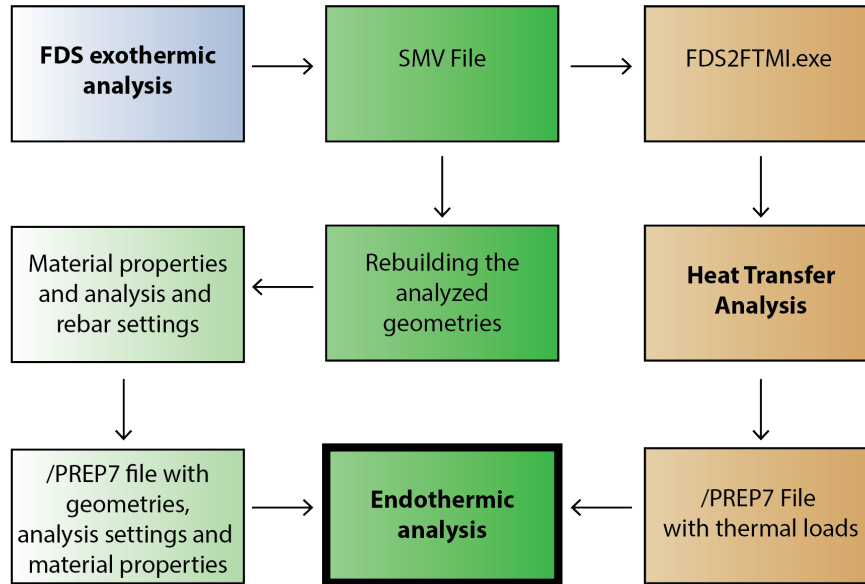


Figure 6.7: Flowchart for FDS2ANSYS procedures to write /PREP7 ANSYS Mechanical APDL preprocessing input files for sequential coupled thermal-mechanical analysis

6.3.2.2 Direct coupled thermal-mechanical analysis

The /PREP7 file for the direct analysis is generated from FDS2ANSYS in order to "build" the geometrical model which is capable of performing both the thermal and the structural analysis. A flowchart of these processes is shown in the [Figure 6.8].

The contained features are:

- **Concrete structure with reinforcement, with thermal-mechanical behavior:** respecting the FDS mesh discretization set with a SOLID226 element type - and with a LINK180 element type respectively - and whose keyoptions are described below;
- **Concrete and reinforcement steel thermal and mechanical properties:** according to the **Chapter 5. Engineering Data**

In this phase, the keyoptions for both thermal and mechanical analysis needs to be set. This features are editable from a specific graphical interface contained in FDS2ANSYS. The available options are reported below:

- **Concrete thermal-structural behavior - SOLID226 element type:**
 - **Element degrees of freedom for coupled-field analysis** always set for coupled thermal-structural analysis (KEYOPT(1)=11);
 - **Coupling DOFs matrix** can be set equal to:
 - * **Strong (matrix) coupling:** produces an unsymmetric matrix. In a linear analysis, a coupled response is achieved after one iteration (KEYOPT(2)=0);
 - * **Weak (load vector) coupling:** produces a symmetric matrix and requires at least two iterations to achieve a coupled response (KEYOPT(2)=1);
 - **Integration method** can be set equal to:
 - * **Full integration:** it uses 14 integrations points. This method can cause volumetric locking in the models with nearly incompressible materials. It is primary employed for purely linear analyses (KEYOPT(6)=0);
 - * **Uniform reduced integration:** it uses a 2 x 2 x 2 integration scheme. This method helps prevent volumetric mesh locking in the models with nearly incompressible materials. It is recommended for analyses with structural nonlinearities. To avoid the propagation of hourglass mode associated with the reduced integration, the model must have at least two layers of elements in each direction (KEYOPT(6)=1);
 - **Specific heat matrix** can be set equal to:
 - * **Consistent:** (KEYOPT(10)=0);
 - * **Diagonalized:** (KEYOPT(10)=1);
 - * **Diagonalized:** in this case, the specific heat or enthalpy is evaluated at element centroid (KEYOPT(10)=2);
 - **Element formulation** can be set equal to:
 - * **Pure displacement:** (KEYOPT(11)=0);
 - * **Mixed displacement-forces formulation:** (KEYOPT(11)=1);

This /PREP7 file contains all the required information and it is imported into ANSYS Mechanical APDL with another /PREP7 file, which is generated from the Heat Transfer Analysis in the same way of the sequential coupling procedure. An example of this file for ANSYS Mechanical APDL can be found in the **Appendix C.1.4. Case Study A: /PREP7 Code for**

ANSYS Mechanical APDL #2. Even in this case, the reinforcement settings are imported separately in order to prevent any mismatch during the Heat Transfer phase.

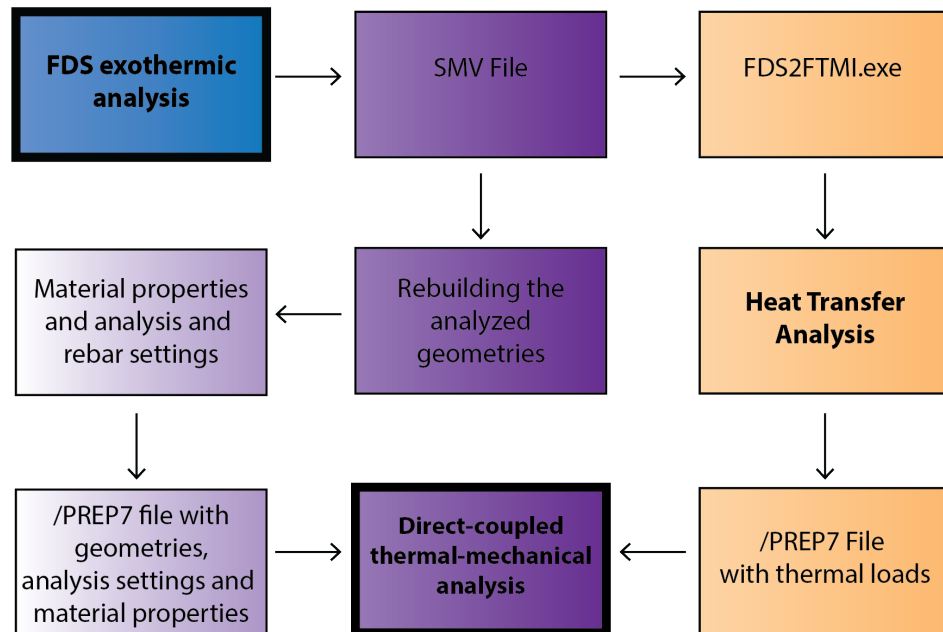


Figure 6.8: Flowchart for FDS2ANSYS procedures to write /PREP7 ANSYS Mechanical APDL preprocessing input files for sequential coupled thermal-mechanical analysis

6.3.3 Coupling thermal and mechanical analysis and post-processing

Since the direct coupling procedure is finished with the previous step of generation of the /PREP7 files, this paragraph regards only the sequential coupling approach. This procedure is done once the Endothermic Analysis phase is completed. The coupling procedure between thermal and mechanical analysis is achieved through another /PREP7 input file, which is generated automatically. A flowchart of these processes is shown in the [Figure 6.9]. An example of this code can be found in **Appendix C.1.6. Case Study A. - /PREP7 Code for ANSYS Mechanical APDL #4.** This input source is needed to:

- **Switching the analysis from thermal to mechanical:** this is done through the switching options which converts the geometries from thermal behavior - SOLID70 for concrete and LINK33 for reinforcement steel and relative keyoptions - to structural behavior - SOLID65 for concrete and LINK180 for reinforcement steel and relative keyoptions;
- **Material properties:** for mechanical behavior of both concrete and reinforcement steel;
- **Coupling the analysis:** the .rth file, which reports the results of the thermal analysis, is imported onto ANSYS Mechanical APDL as load.

Then, load and restraint conditions needs to be set. This phase has not been automatized from FDS2ANSYS and it can be done directly on ANSYS Mechanical APDL, by prompting in the command-line or by the graphical interface. Once done this, the coupled-thermal analysis can be performed and the result may be discussed.

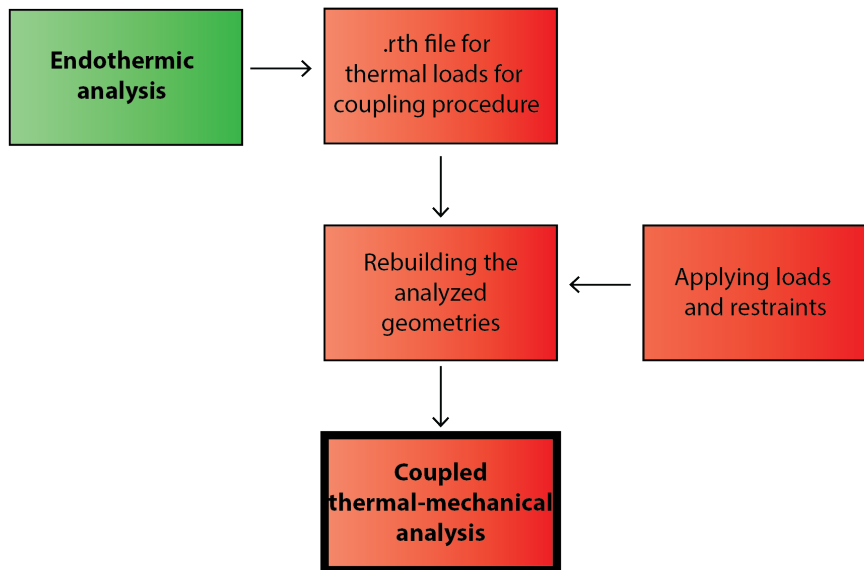


Figure 6.9: Flowchart for FDS2ANSYS procedures to couple thermal and mechanical analysis for sequential coupled thermal-mechanical analysis

Chapter 7

Dissertation on validation procedures for FDS2ANSYS

Since FDS2ANSYS has been introduced to the reader, this chapter is a report of the procedures that have been followed in order to state the reliability of the data and of the settings to perform the thermal and structural analysis on ANSYS Mechanical APDL that the software generates. Since the reported Case Study has been set with a sequential analysis, here follows the three different steps of testing that have been performed:

- **Validation of Heat Transfer Analysis:** this phase is needed in order to understand if the temperature and heat transfer coefficient profiles over time report reliable values;
- **Validation of Endothermic Analysis:** this phase is needed to verify if all the required parameters in ANSYS Mechanical APDL, for the thermal analysis, are set correctly by FDS2ANSYS (e.g. solver features and boundary conditions);
- **Validation of Mechanical Analysis:** by coupling the results of the thermal analysis, this phase is needed to check if all the required parameters by ANSYS Mechanical APDL, for the structural analysis, are set correctly (e.g. solver features, thermal and static structural loads, constraint and restraint settings).

To achieve this goal, a benchmark structure has been considered. Geometrical and material features, output data and validation processes are discussed in the following paragraphs.

7.1 Contextualization on the Case Study A.

The Case Study A. is the benchmark structure chosen for the validation procedures. It is a simple supported reinforced concrete beam, on which a reliable paper ¹ is based on. This beam has been tested from the experimentation teams in several configurations - with increasing concrete compressive strength, increasing concrete cover and the effect of increasing the lateral stiffness of the beam - and the tests have been both executed in laboratory and analytically reproduced on ANSYS Mechanical APDL engine, in order to compare the obtained results.

7.1.1 Geometrical, thermal and mechanical features

The specimen in object has a 240 mm wide and 380 mm high cross-section and it is 3600 mm long. The beam is reinforced both to resist to the bending moment and to the shear stress with longitudinal five bending-resistant rebar (two 12 mm-diameter rebar at the top of the cross-section and three 18 mm-diameter rebar at the bottom) - **[Figure 7.1a]** - and 8 mm-diameter stirrups every 200 mm - **[Figure 7.1b]**.

On the material parameters, an high resistance concrete - C55/67 class - with siliceous aggregates has been chosen for the specimen and the temperature-dependent variation has been taken from the EN 1992-1-2:2019 Standard - **[Figure 7.2]**. The concrete paste has been assumed with 3% of moisture content and the variation mathematical law of specific heat - the only one parameter depending on the moisture content - is reported on the EN 1992-1-2:2019 Standard - **[Figure 7.3]**. A value of $2300 \frac{kg}{m^3}$ of density of concrete has been considered and the temperature variation of it comes from the EN 1992-1-2:2019 Standard - **[Figure 7.4]**. On the concrete thermal conductivity variation mathematical relationship, the lower bound value has been chosen from the EN 1992-1-2:2019 Standard - **[Figure 7.5]**. The concrete Young modulus variation mathematical law is from the ASCE 78 Standard - **[Figure 7.6]**. For the bending-resistant rebar, a value of 425 MPa for yielding strength has been considered, instead for the stirrups a value of 275 MPa for yielding strength has been taken and the variation with temperature is from the EN 1992-1-2:2019 Standard - **[Figures 7.8, 7.9]**. The reinforcement steel thermal elongation - **[Figure 7.10]** -, Young modulus - **[Figure 7.11]** -, density - **[Figure 7.12]** - and thermal deformation - **[Figure 7.13]** - variation relationships come from the EN 1992-1-2:2019 Standard. The thermal

¹M. ELSHORBAGY, M. ABDEL-MOOTY (2019), "The coupled thermal-structural response of RC beams during fire events based on nonlinear numerical simulation", Engineering Failure Analysis, Volume 109

conductivity - [Figure 7.14] - and specific heat - [Figure 7.15] - variation mathematical laws instead have been taken from the Eurocode 3 Standard. On the Poisson ratio, two reliable paper, regarding experimental tests done on concrete and steel specimens, have been take into consideration both for concrete - [Figure 7.16] - and reinforcement steel - [Figure 7.17] -, since the current Standards do not report any temperature-depending mathematical relationships for this parameter^{2 3}.

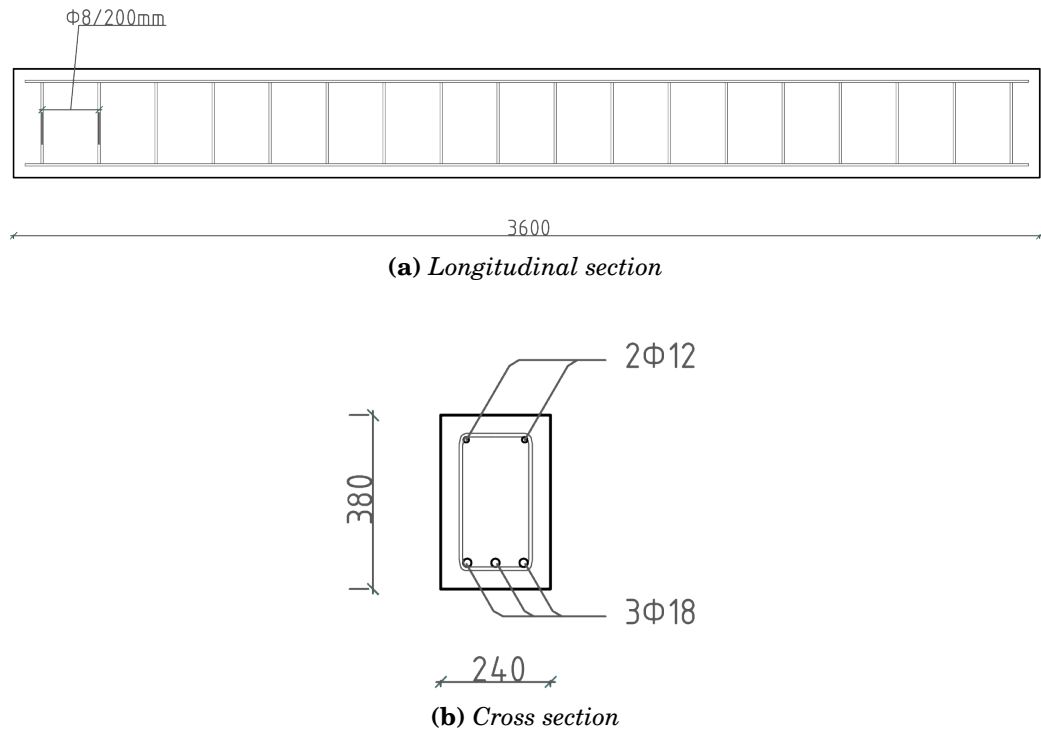


Figure 7.1: Case Study A. geometrical features for validating the Heat Transfer and Endothermic analysis phases [quotes in millimeters]

²GERNAY T., MILLARD A., FRANSSSEN J.M. (2013): "A multiaxial constitutive model for concrete in the fire situation: Theoretical formulation", International Journal of Solids and Structures

³YANG. Y (2015): "Temperature-dependent thermoelastic analysis of multidimensional functionally graded materials", Ph.D. Thesis - University of Pittsburgh, Pennsylvania

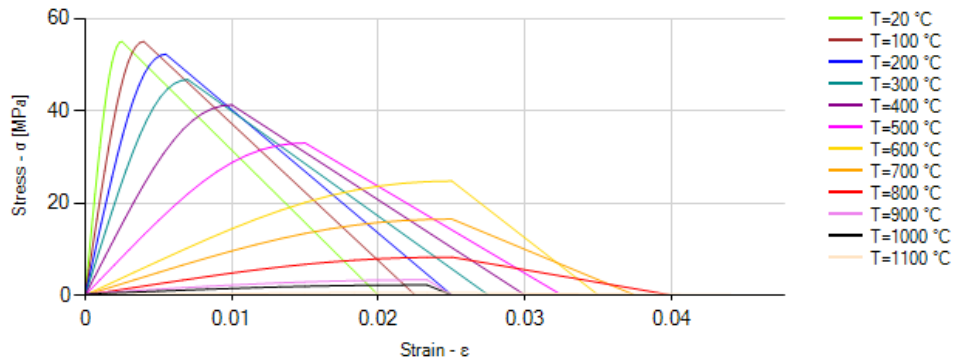


Figure 7.2: C55/67 concrete stress-strain diagram and temperature variation

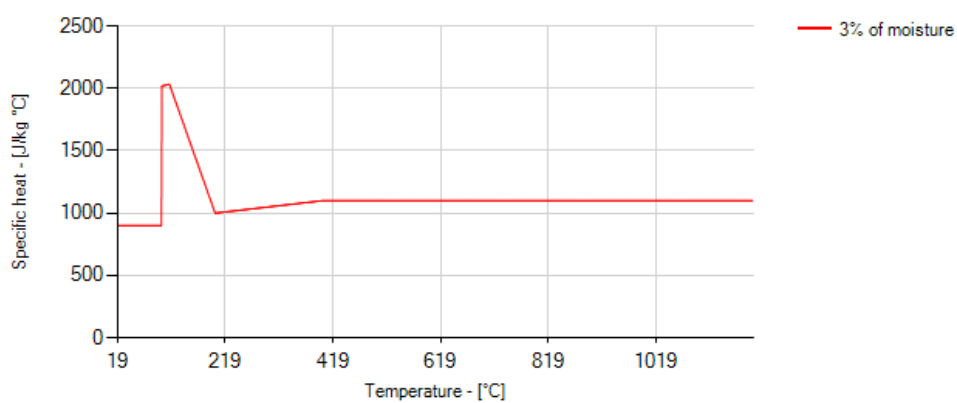


Figure 7.3: C55/67 concrete specific heat diagram for 3% of moisture content

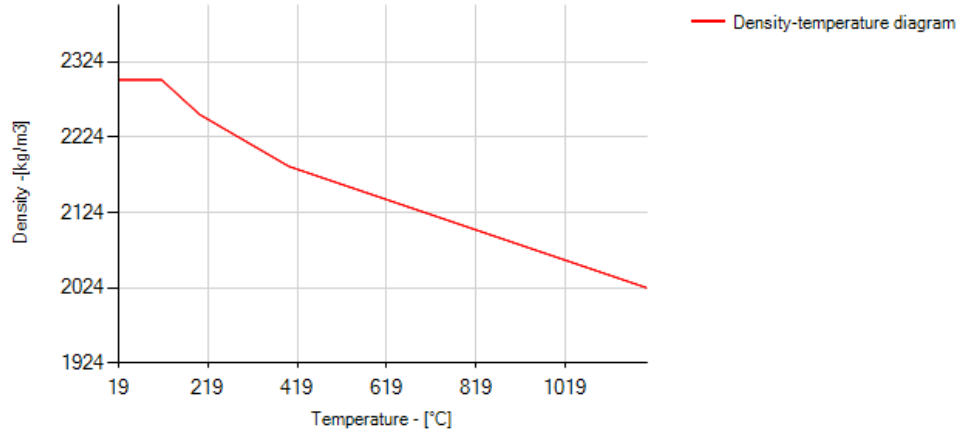


Figure 7.4: C55/67 concrete density diagram

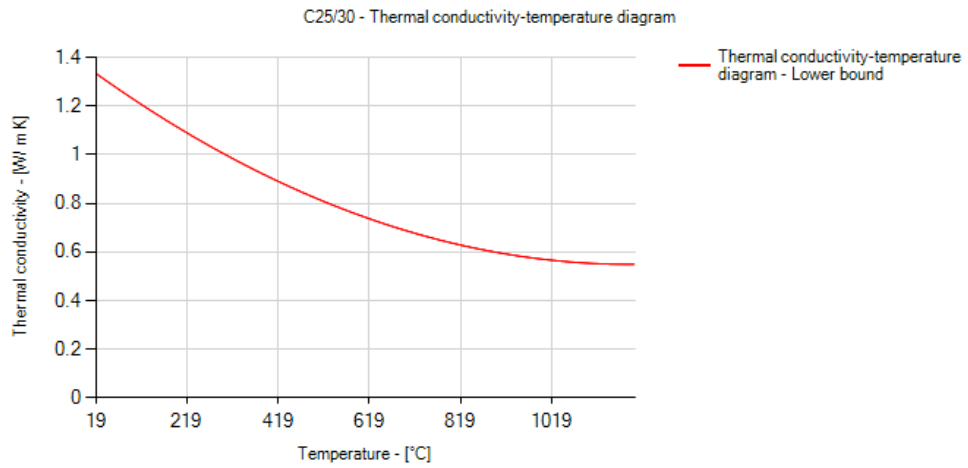


Figure 7.5: C55/67 concrete thermal conductivity diagram

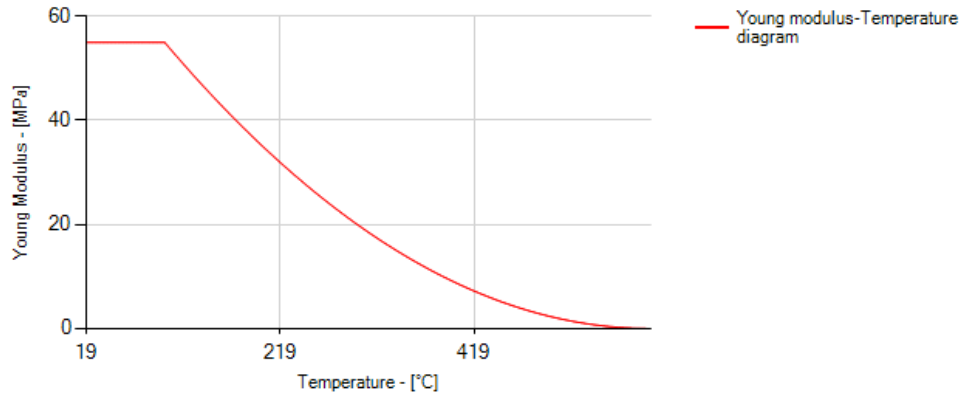


Figure 7.6: C55/67 concrete Young modulus diagram

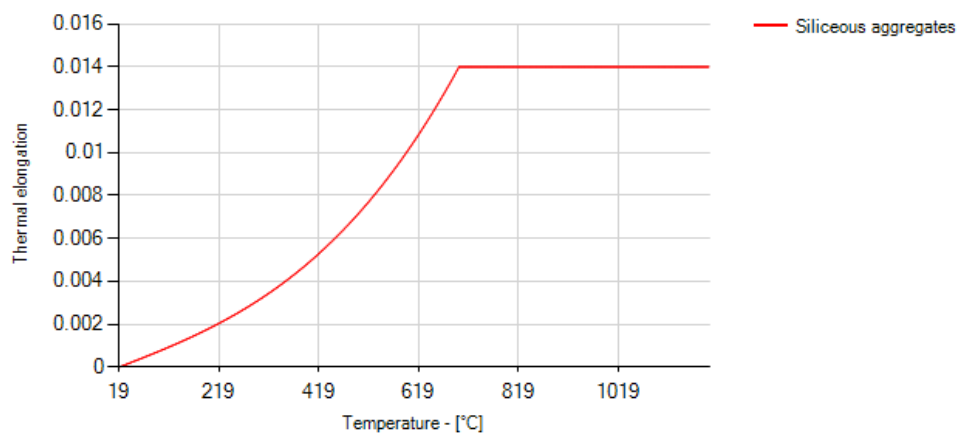


Figure 7.7: C55/67 concrete thermal elongation diagram

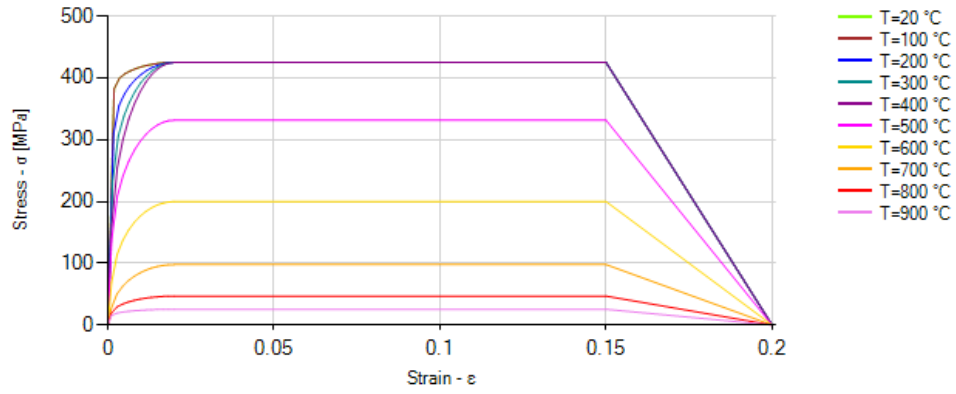


Figure 7.8: Rebar steel stress-strain diagram

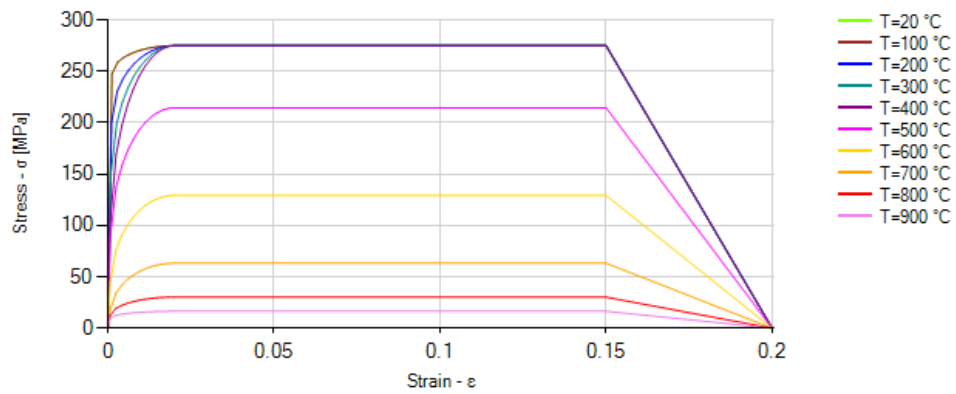


Figure 7.9: Stirrups steel stress-strain diagram

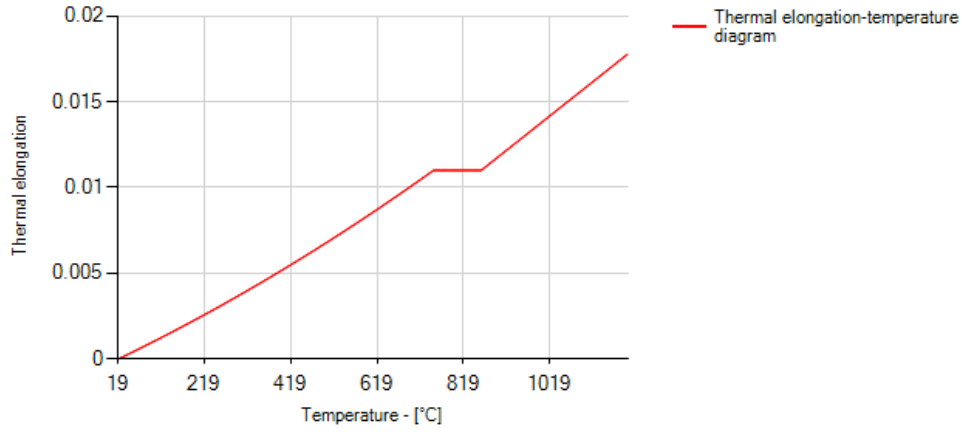


Figure 7.10: Reinforcement steel thermal elongation diagram

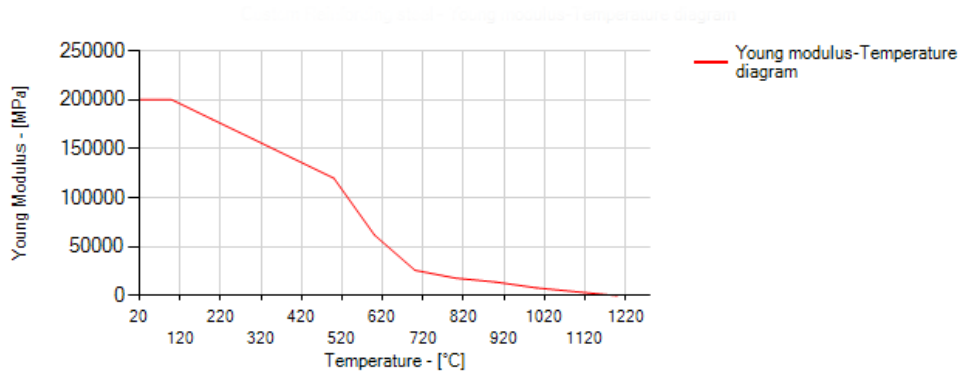


Figure 7.11: Reinforcement steel Young modulus diagram

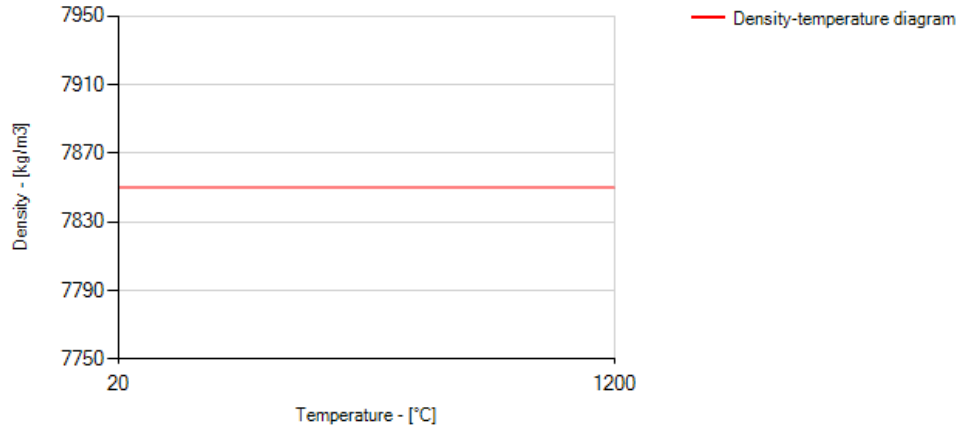


Figure 7.12: Reinforcement steel density diagram

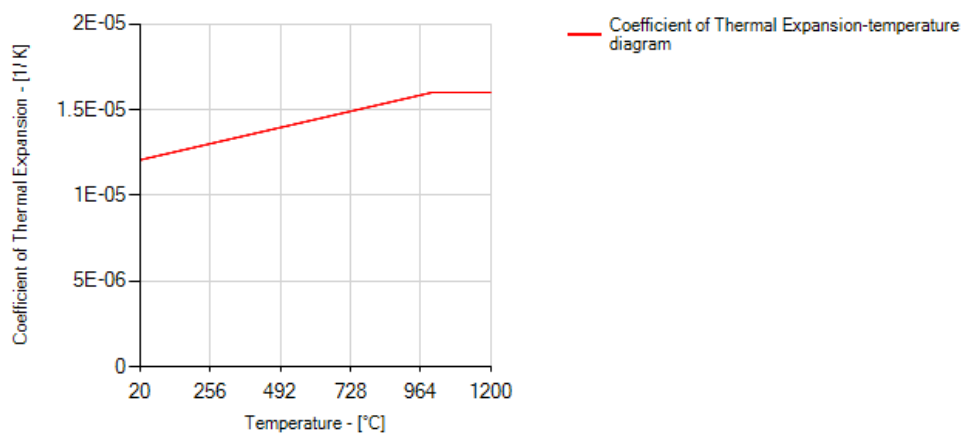


Figure 7.13: Reinforcement steel thermal expansion coefficient diagram

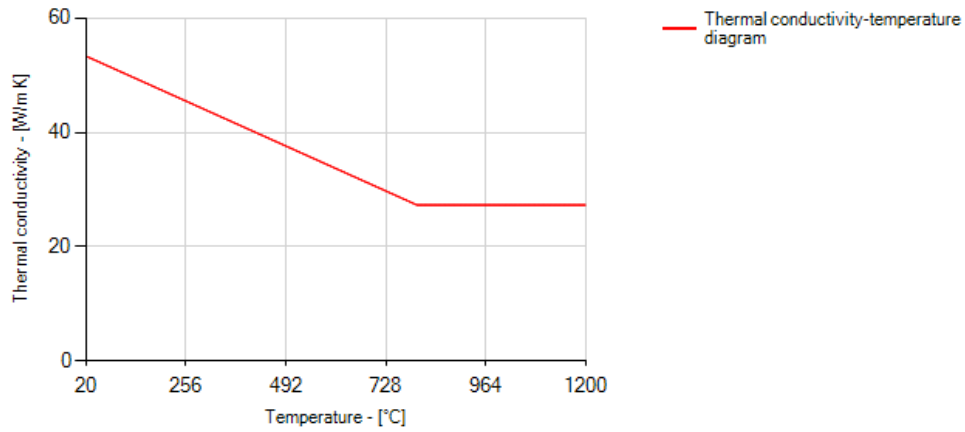


Figure 7.14: Reinforcement steel thermal conductivity diagram

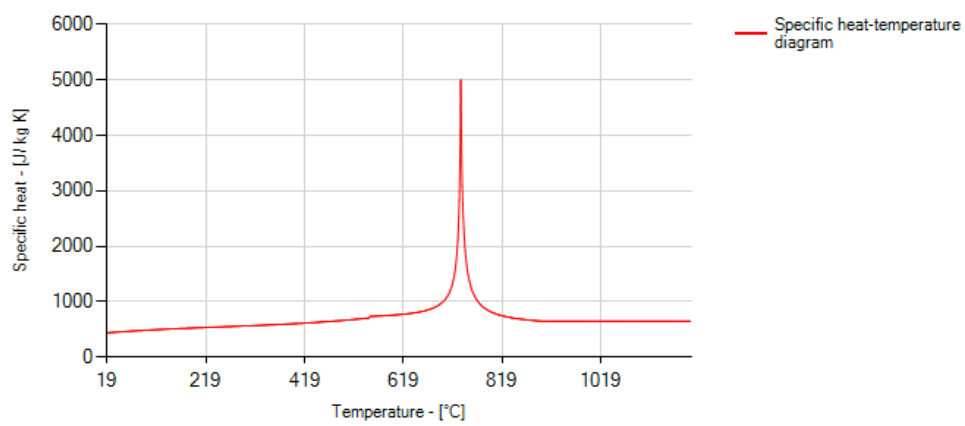


Figure 7.15: Reinforcement steel specific heat diagram

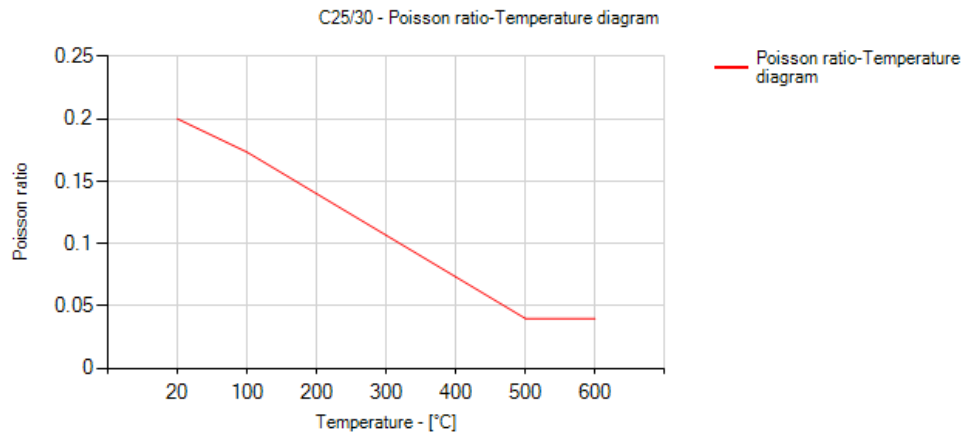


Figure 7.16: C55/67 concrete Poisson ratio diagram

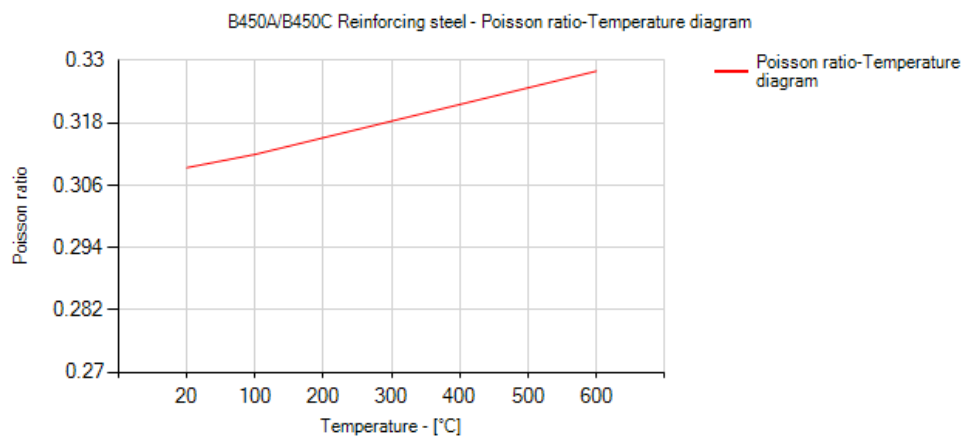


Figure 7.17: Reinforcement steel Poisson ratio diagram

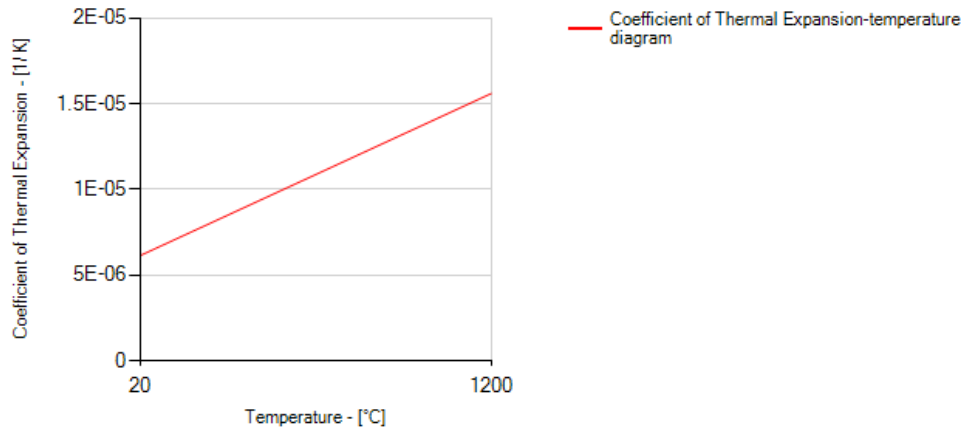


Figure 7.18: C55/67 concrete thermal expansion coefficient diagram

7.1.2 Validation of heat transfer and endothermic analysis

This validation phase consists in emulating without replying the experiment reported in the paper, because the test has been done with a fixed time-temperature profile - typical of a prescriptive approach to check the structural fire resistance -, without considering the heat transfer analysis phase. Furthermore, the heat transfer analysis is verified only once a thermal analysis is performed and for this reason the reliability of the output data of the heat transfer and the endothermic analysis are checked contemporary.

To achieve this goal, a simple supported beam has been three-dimensionally modeled and imported in FDS2ANSYS, in order to import it in ANSYS Mechanical APDL, launch the "ANSYS2FDS.geom" macro and generate the FDS file. Then this file has been imported in Thunderhead Engineering Pyrosim - **[Figure 7.20]** - and additional features have been modeled. By default, two boundary functions - Adiabatic Surface Temperature and Heat Transfer Coefficient - are enabled. Then, at first, two inert compartment walls have been added and between these two obstructions a generic burner surface - $HRR_{PUA} = 1000 \frac{kW}{m^2}$ with a constant ramp-up time - has been placed. Furthermore, a polyurethane GM27 reaction has been set. In order to verify that the two parameters that allow the Heat Transfer Analysis by enabling the dedicated boundary functions in FDS - Adiabatic Surface Temperature (AST) and the Heat Transfer Coefficient (HTC) -, twenty-four solid-phase devices - twelve for the AST and twelve for the HTC - have been

added - **[Figure 7.19]** - and the output data from FDS have been compared to the ones obtained from ANSYS Mechanical APDL. At first, the total heat flux concept - which is the sum of both a radiative and a convective parcels - is introduced as follows - **Equation 7.1**:

$$q_{tot} = q_r + q_c = \epsilon \cdot (e_{inc} + \sigma \cdot \theta_W^4) + h \cdot (\theta_G - \theta_W) \quad (7.1)$$

where:

- q_{tot} : is the total heat flux [$\frac{W}{m^2}$];
- q_r : is the radiative heat flux [$\frac{W}{m^2}$] - exported from ANSYS Mechanical APDL;
- q_c : is the convective heat flux [$\frac{W}{m^2}$] - exported from ANSYS Mechanical APDL;
- ϵ : is the emissivity;
- e_{inc} : is the incident radiative thermal energy;
- σ : is the Stefan-Boltzmann constant, equal to $5.67 \cdot 10^{-11} \frac{kW}{m^2 \cdot K^4}$;
- θ_W : is the wall temperature [K];
- h : is the heat transfer coefficient- object of verification [$\frac{W}{m^2 \cdot K}$];
- θ_G : is the gas temperature [K].

Since with the aforementioned approach is not possible to predict accurately the incident radiant thermal energy, the total heat flux may be calculated by a different approach, with the introduction of the Adiabatic Surface Temperature concept. A real surface can be replaced by an ideal one, perfectly insulated and exposed to the same heating conditions of the real one. Thus, the ideal surface has a zero total heat flux and it has a temperature - called T_{AST} - which can be exported from an FDS analysis.

$$\epsilon \cdot (e_{inc} + \sigma \cdot \theta_{AST}^4) + h \cdot (\theta_G - \theta_{AST}) \quad (7.2)$$

where:

- T_{AST} : is the Adiabatic Surface Temperature - object of verification [K]

Furthermore, the heating conditions of both the ideal and the real surfaces are the same and what stated so far can be synthesized as:

$$q_{tot} = \epsilon \cdot \sigma \cdot (\theta_{AST}^4 - \theta_w^4) + h \cdot (\theta_{AST} - \theta_w) \quad (7.3)$$

Hence, the simulation time has been set to 1000 s and the mesh size has been set to 0.02 m.

The results are shown below - [Figures 7.21 - 7.44].



Figure 7.19: Benchmark structure as modeled in Thunderhead Engineering Pyrosim - Devices (DEV) for Adiabatic Surface Temperature (AST) and Heat Transfer Coefficient (HTC) - [quotes in millimeters]

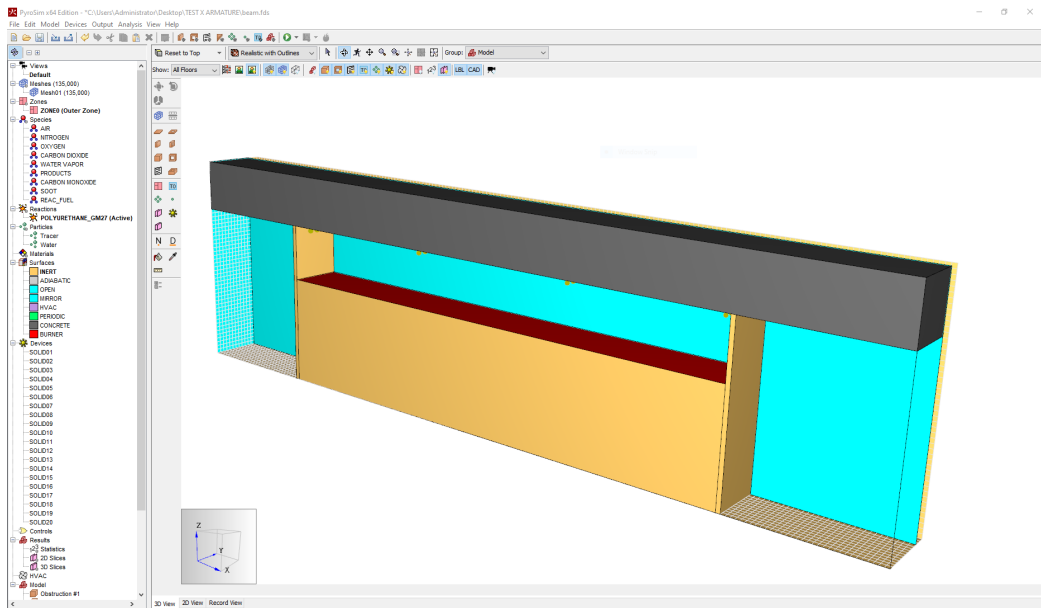


Figure 7.20: FDS file configured for the analysis - Thunderhead Engineering Pyrosim 2019

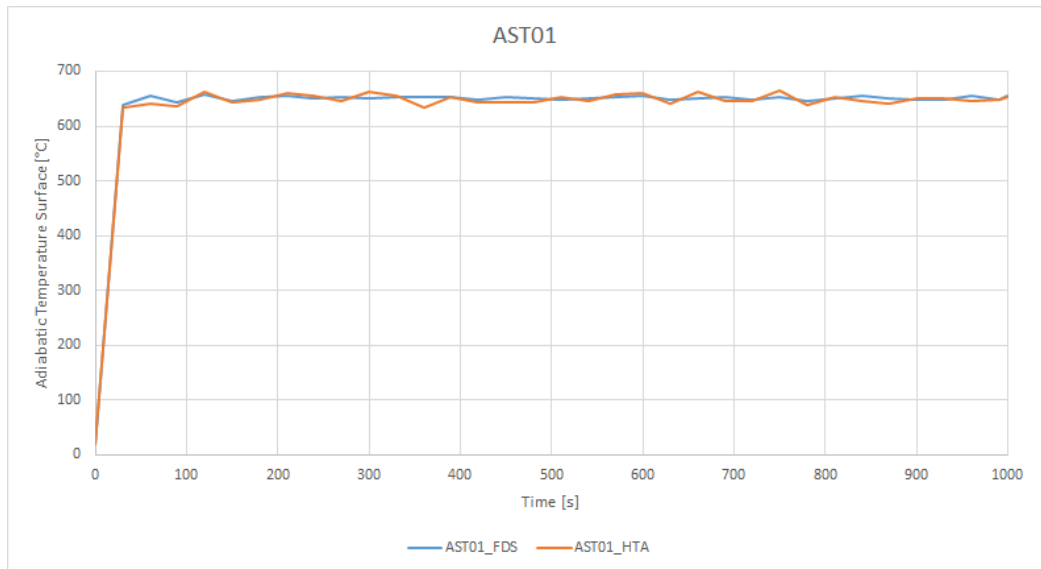


Figure 7.21: AST01 device - values from FDS and ANSYS Mechanical APDL

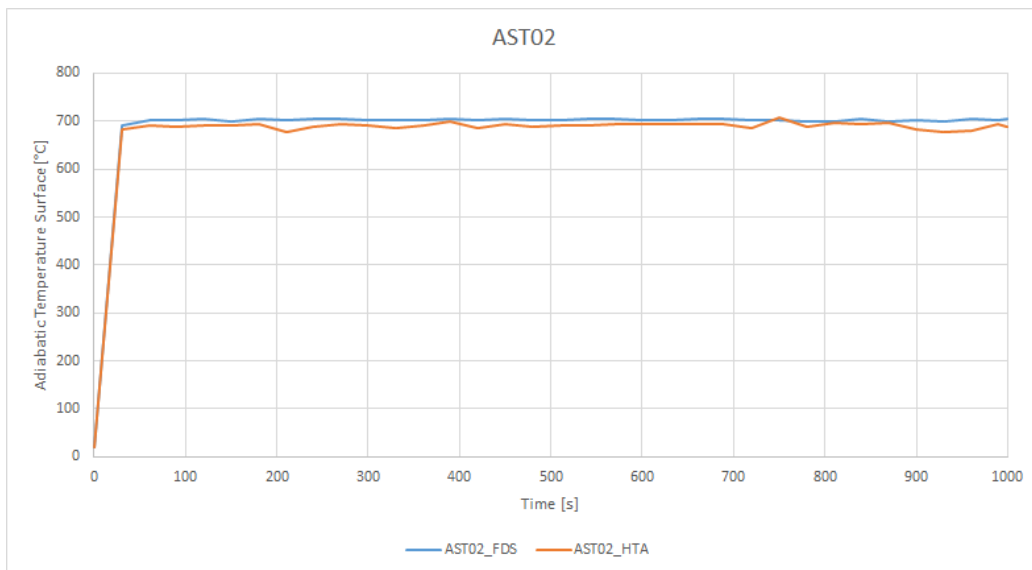


Figure 7.22: AST02 device - values from FDS and ANSYS Mechanical APDL

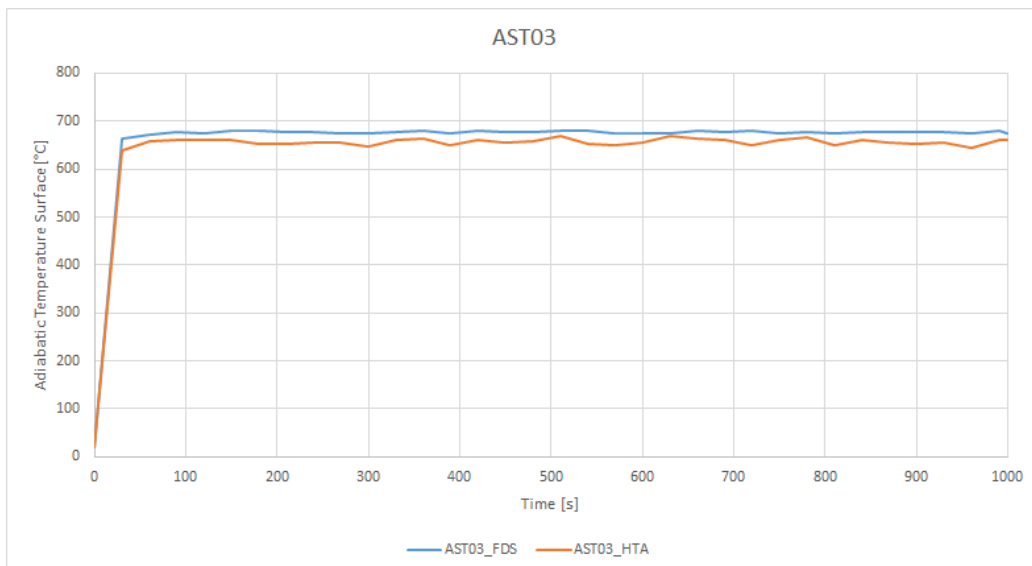


Figure 7.23: AST03 device - values from FDS and ANSYS Mechanical APDL

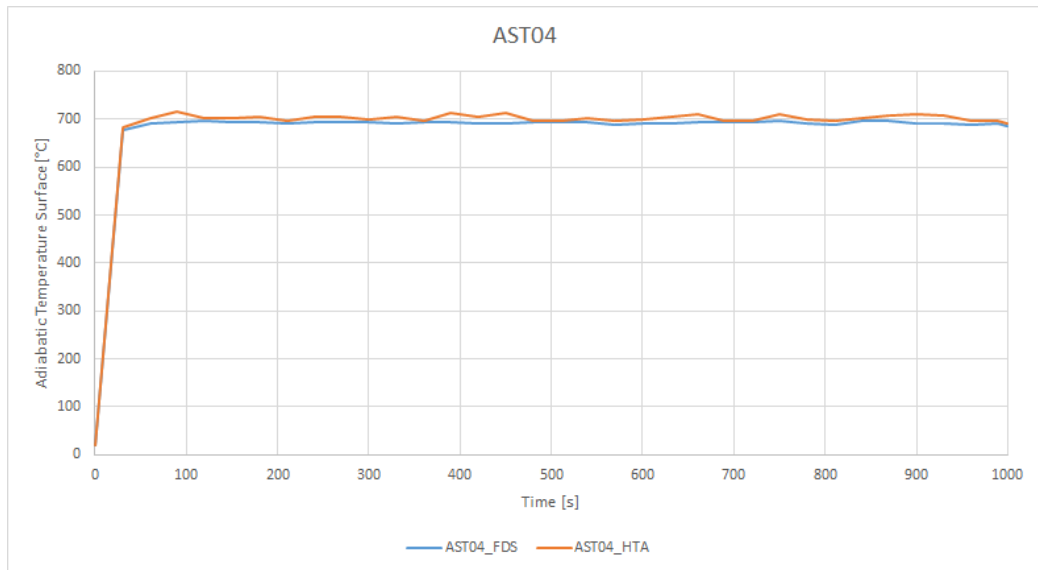


Figure 7.24: AST04 device - values from FDS and ANSYS Mechanical APDL

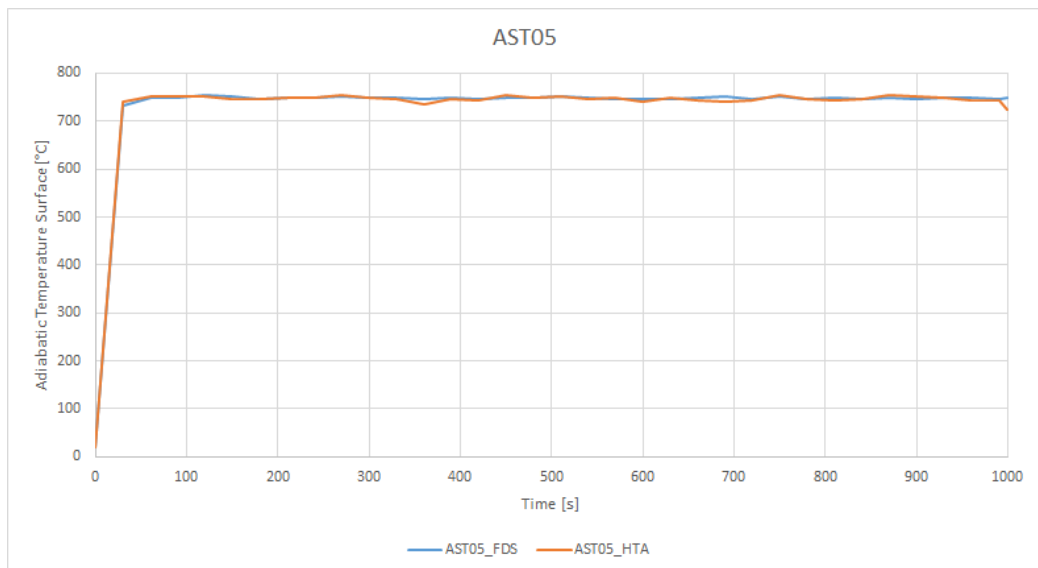


Figure 7.25: AST05 device - values from FDS and ANSYS Mechanical APDL

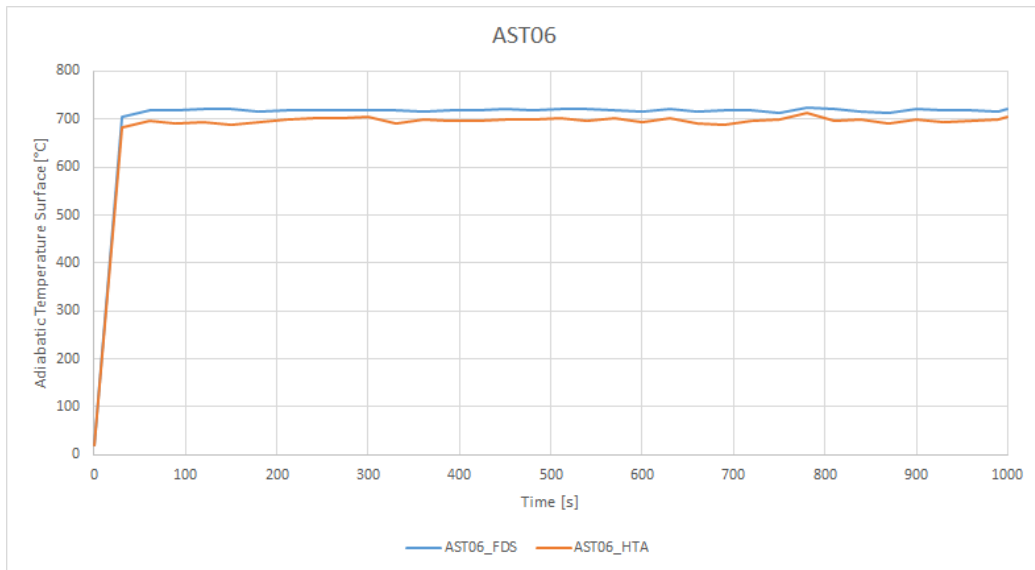


Figure 7.26: AST06 device - values from FDS and ANSYS Mechanical APDL

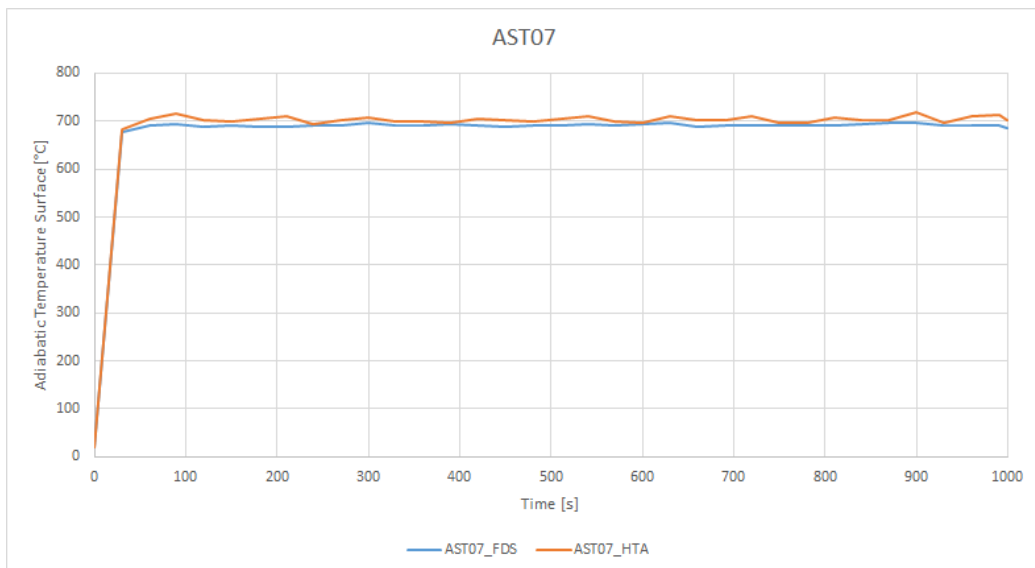


Figure 7.27: AST07 device - values from FDS and ANSYS Mechanical APDL

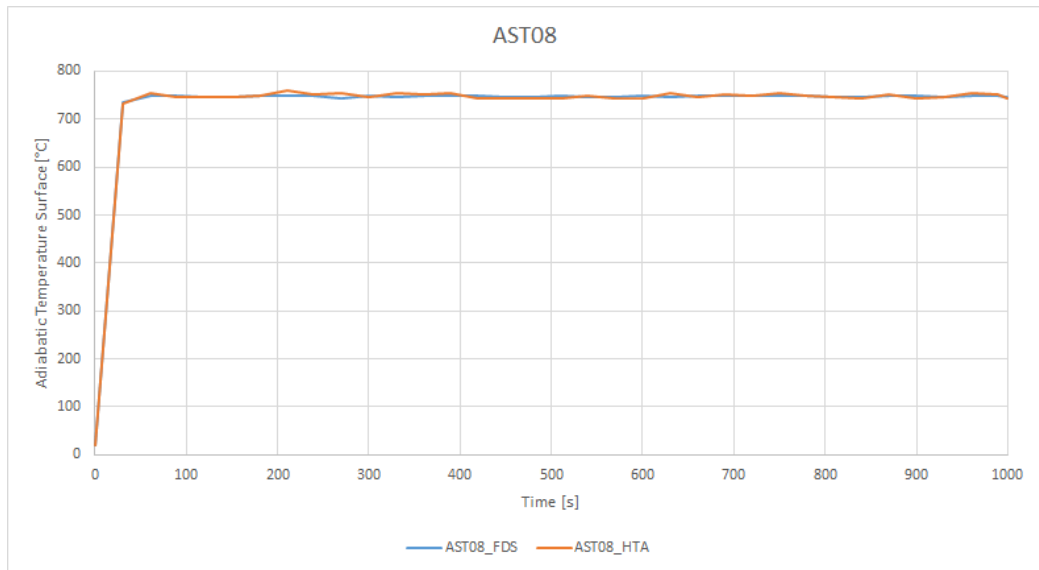


Figure 7.28: AST08 device - values from FDS and ANSYS Mechanical APDL

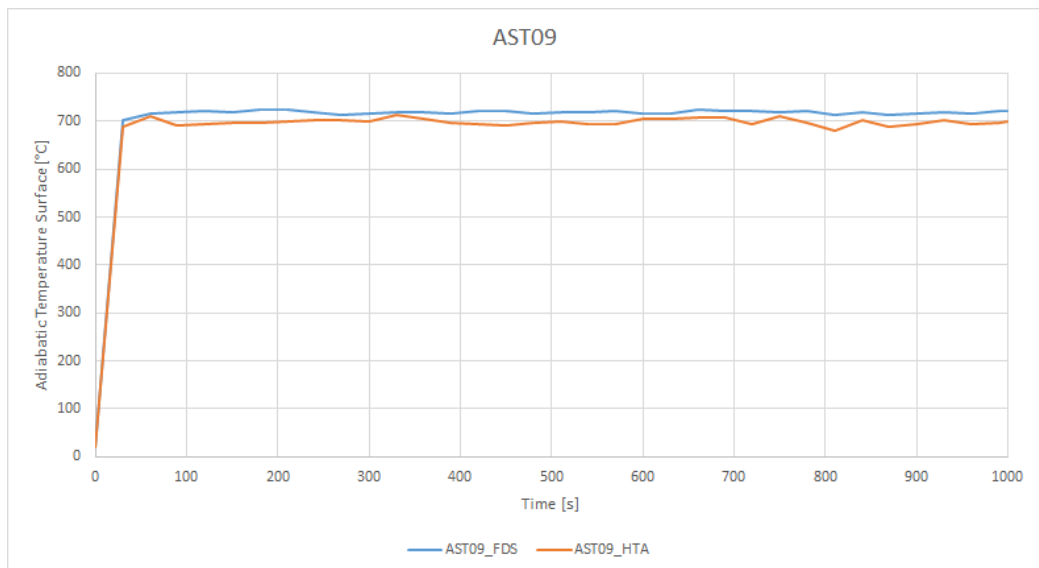


Figure 7.29: AST09 device - values from FDS and ANSYS Mechanical APDL

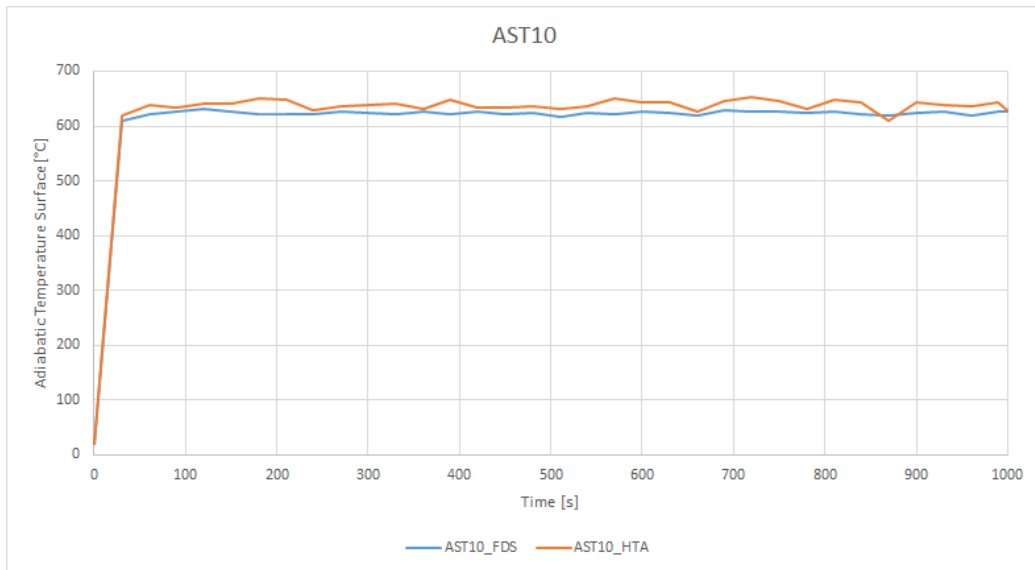


Figure 7.30: AST10 device - values from FDS and ANSYS Mechanical APDL

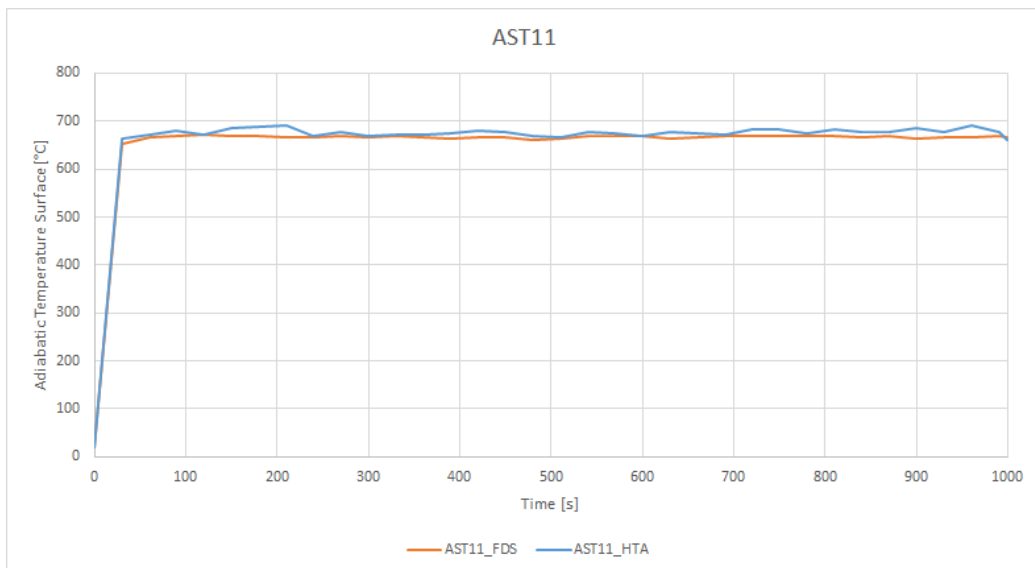


Figure 7.31: AST11 device - values from FDS and ANSYS Mechanical APDL

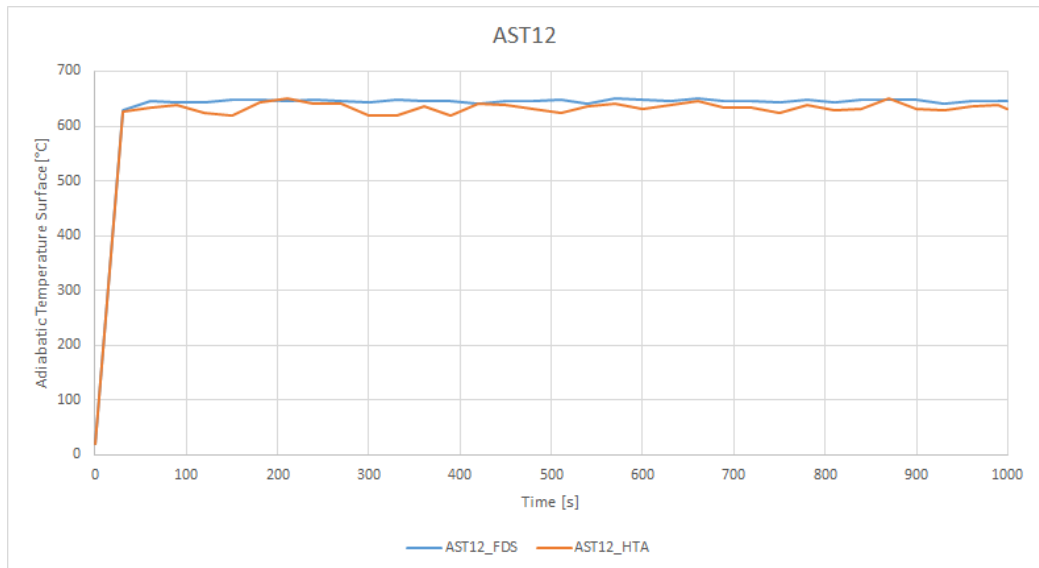


Figure 7.32: AST12 device - values from FDS and ANSYS Mechanical APDL

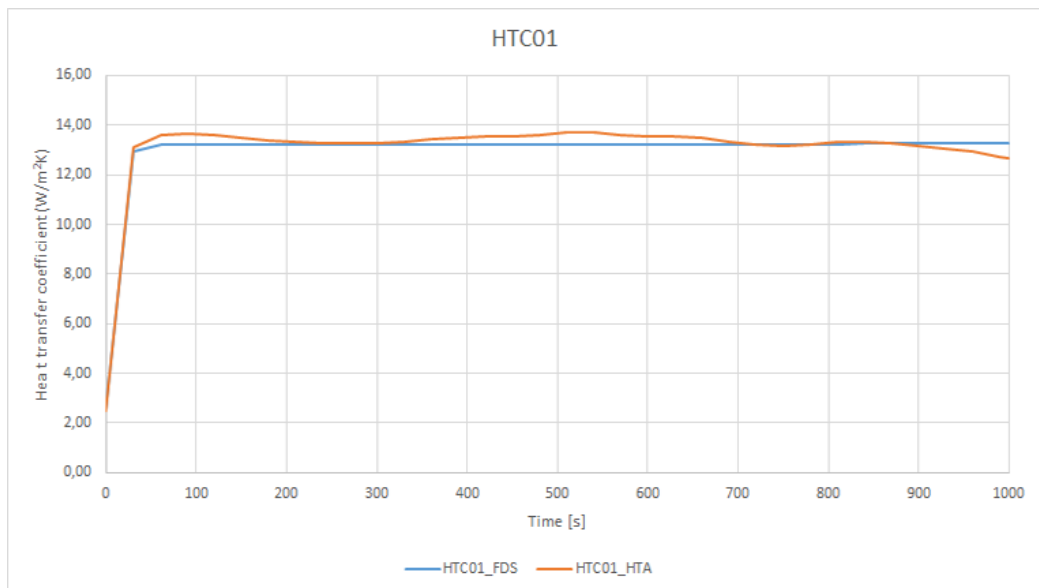


Figure 7.33: HTC01 device - values from FDS and ANSYS Mechanical APDL

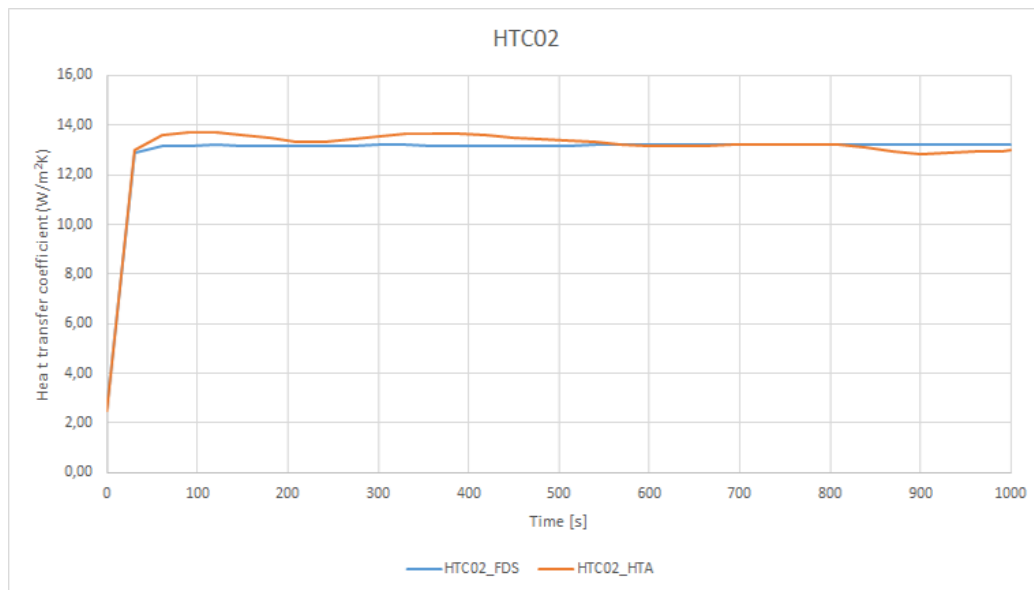


Figure 7.34: HTC02 device - values from FDS and ANSYS Mechanical APDL

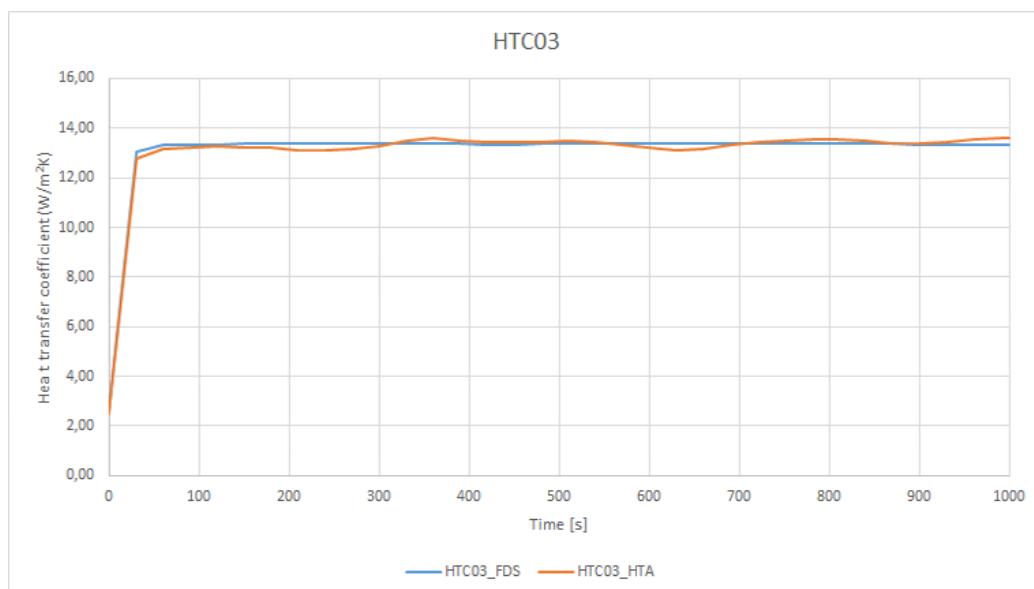


Figure 7.35: HTC03 device - values from FDS and ANSYS Mechanical APDL

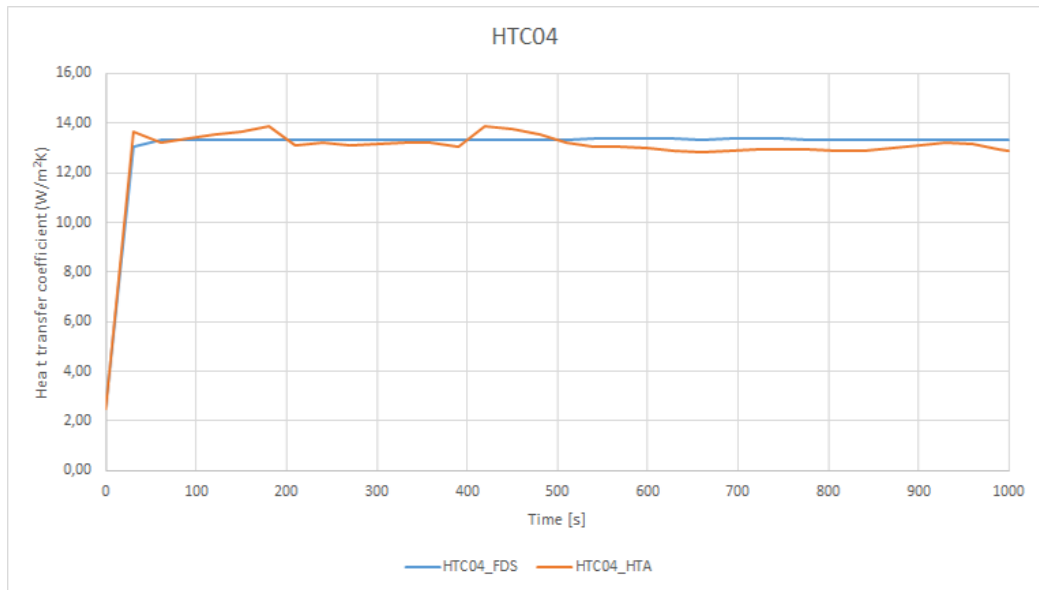


Figure 7.36: HTC04 device - values from FDS and ANSYS Mechanical APDL

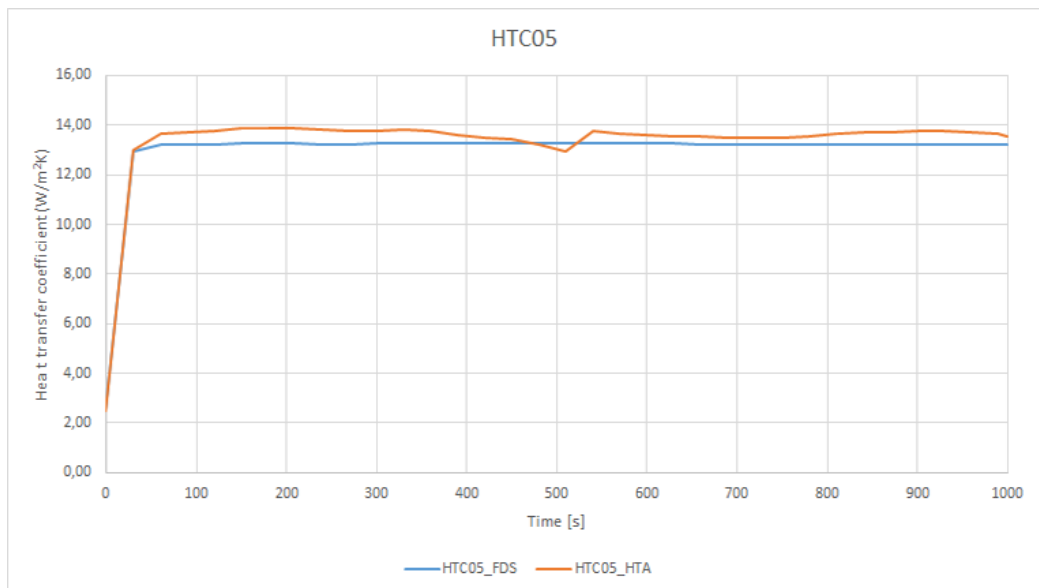


Figure 7.37: HTC05 device - values from FDS and ANSYS Mechanical APDL

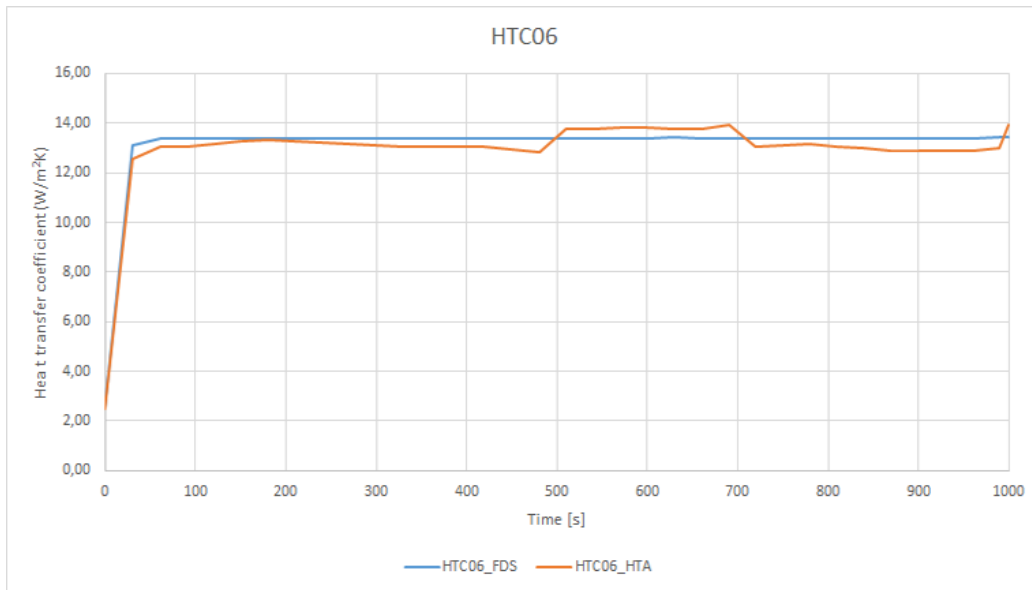


Figure 7.38: HTC06 device - values from FDS and ANSYS Mechanical APDL

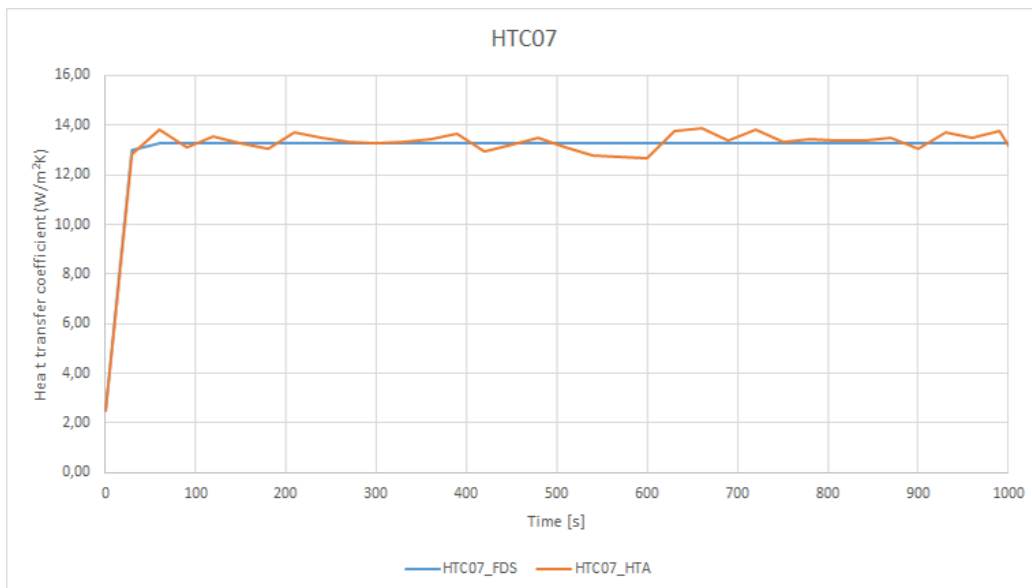


Figure 7.39: HTC07 device - values from FDS and ANSYS Mechanical APDL

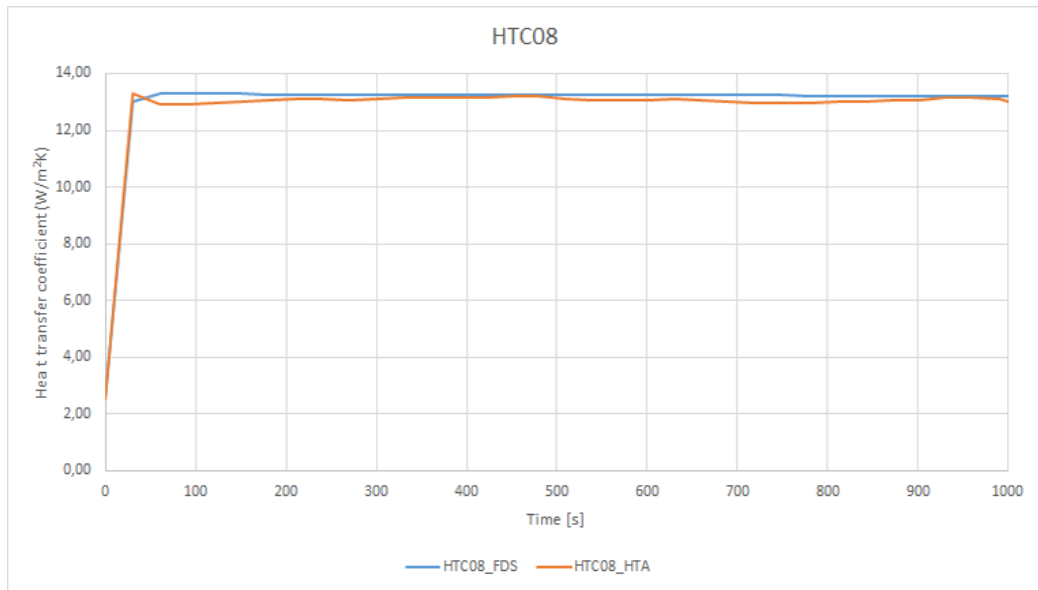


Figure 7.40: HTC08 device - values from FDS and ANSYS Mechanical APDL

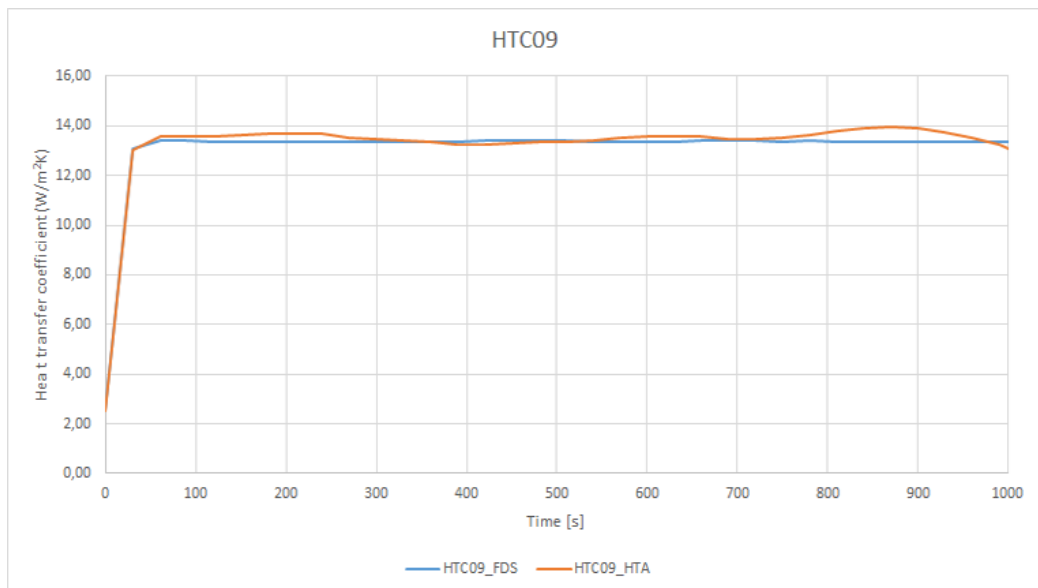


Figure 7.41: HTC09 device - values from FDS and ANSYS Mechanical APDL

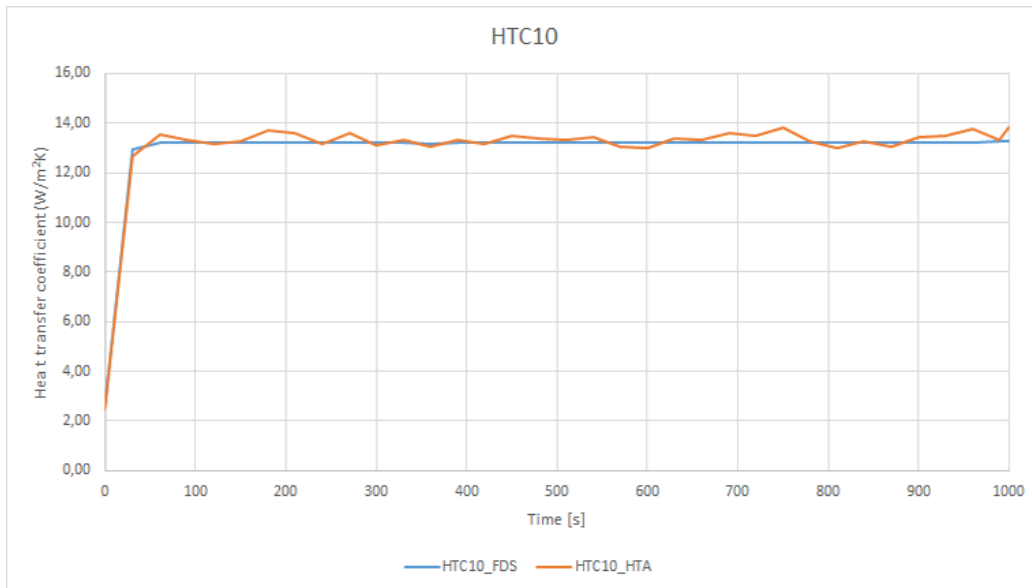


Figure 7.42: HTC10 device - values from FDS and ANSYS Mechanical APDL

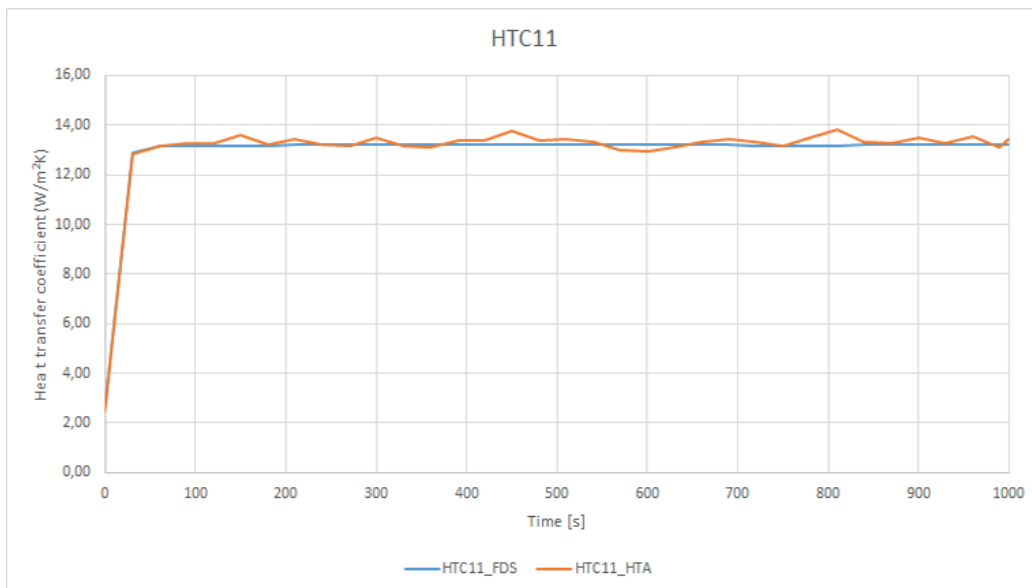


Figure 7.43: HTC11 device - values from FDS and ANSYS Mechanical APDL

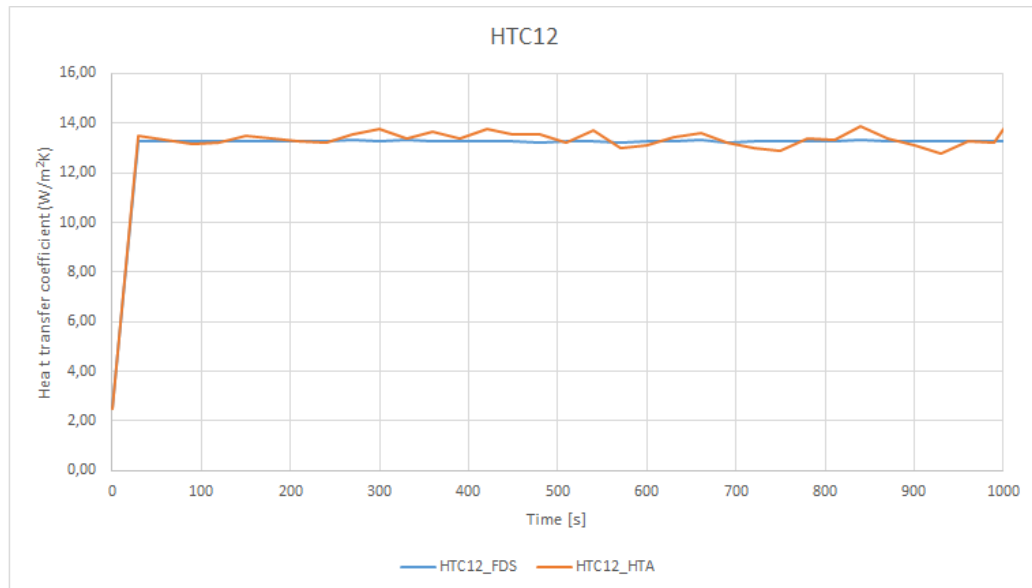


Figure 7.44: HTC12 device - values from FDS and ANSYS Mechanical APDL

From the results it is possible to state that both the Adiabatic Surface Temperature and the Heat Transfer Coefficient time-histories are not showing the same values. This may occur for two main reasons:

- **Location of the devices on the FDS simulation:** in order to avoid any calculus instabilities, the device have not been directly located on the bottom face of the beam but 0.02 m - a mesh cell - below. This trick may allow to obtain reliable result, without risking any issues because of the location of the devices. In this case, since the mesh has a very small cell, the temperature may be assumed as the surface temperature;
- **Endothermic analysis:** the heat transfer analysis is done by performing the endothermic analysis with ANSYS Mechanical APDL. This analysis has been executed using both the values of the Adiabatic Surface Temperature - considered as time-history loads - and the Heat Transfer coefficients, which depend on a view factor - exposure coefficient of the surfaces to the fire. For this reason the values may be slightly different.

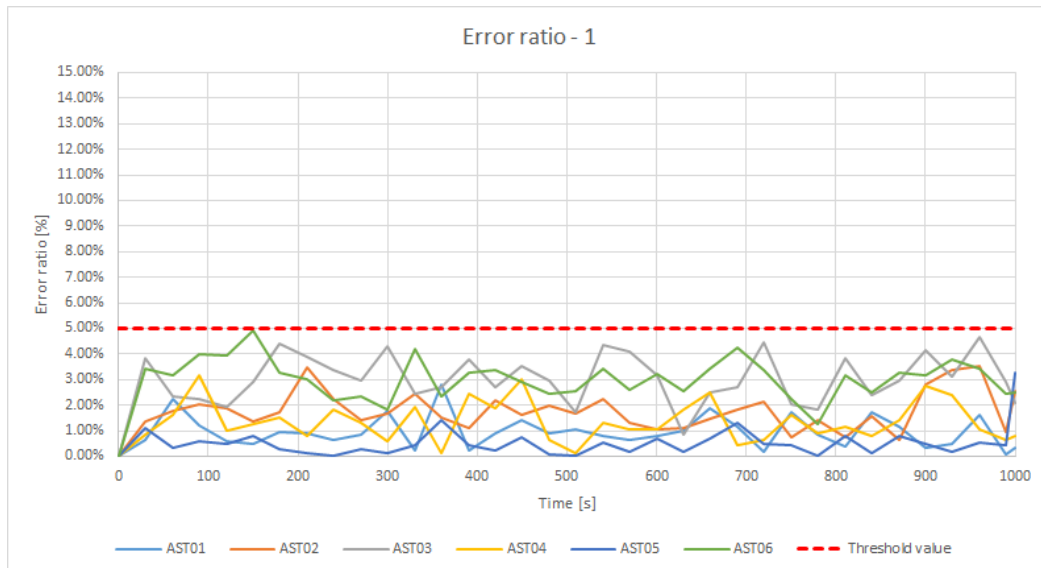
With respect of both the Adiabatic Surface Temperatures and the Heat Transfer Coefficients obtained with FDS, since the output values from ANSYS Mechanical APDL change, a deeper study on the error ratio - calculated as the

relative error with respect of the obtained value from FDS - has been done, in order to understand if these fluctuations of these parameters remain in an acceptable range. In order to monitor the variation of the aforementioned parameters, a threshold value for the error has been set to 5%, a reasonable value, since this is the typical threshold of the allowable error ratio for problems solved with the Finite Element Method - [Figures 7.45, 7.46] .

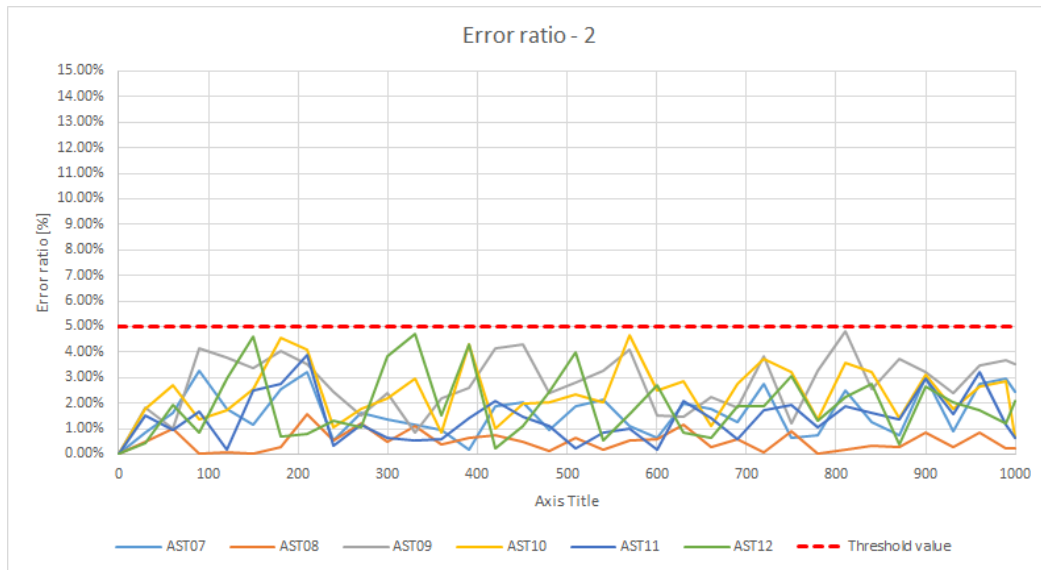
However, from the variation of the error ratio, it has not been possible to predict any trend for any device. Nevertheless, the relative difference has shown values minor than the threshold limit, at all. For this reason, it is possible to state that the Heat Transfer Analysis phase has been **validated successfully**.

In order to perform an endothermic analysis on structural members, the Heat Transfer Analysis phase may be already executed. Since the obtained values from the heat transfer are time-history boundary conditions, the endothermic analysis phase is performed at the same time. About this, FDS2ANSYS - based on the NIST's FDS2FTMI - writes the pre-processing input file, by applying the thermal loads and setting the thermal analysis features. Since FDS2FTMI has been already validated⁴, these loads - that are directly exported from FDS - are assumed to be reliable and the thermal analysis has been set with the same settings of the Silva's verification cases. The other parameters that may affect thermal analysis are the thermal properties of the material, which are taken from current Standards or reliable publications. For this reason, it is possible to state that the Endothermic Analysis phase has been **validated successfully**.

⁴SILVA J.C (2017), "FDS2FTMI User's Guide - An automated code to one-way coupling between FDS and FEM using FTMI", National Institute of Standards and Technology

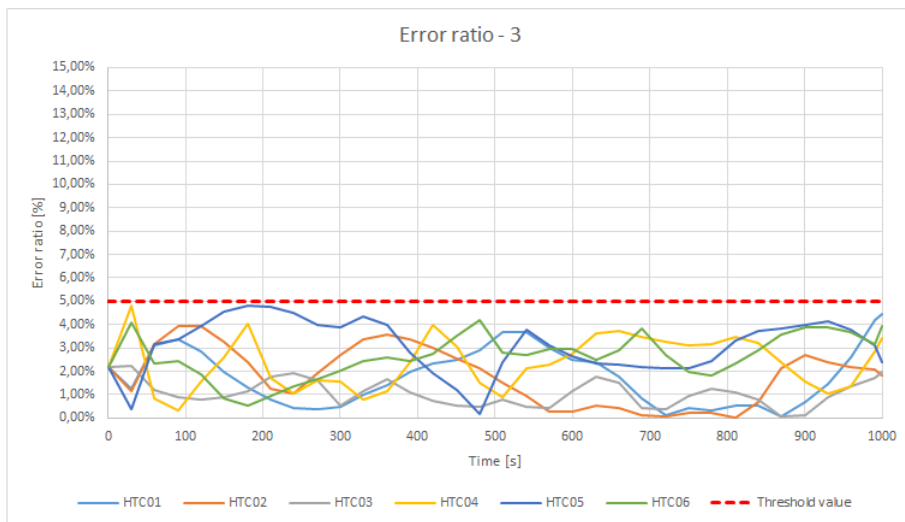


(a) Devices from 1 to 6

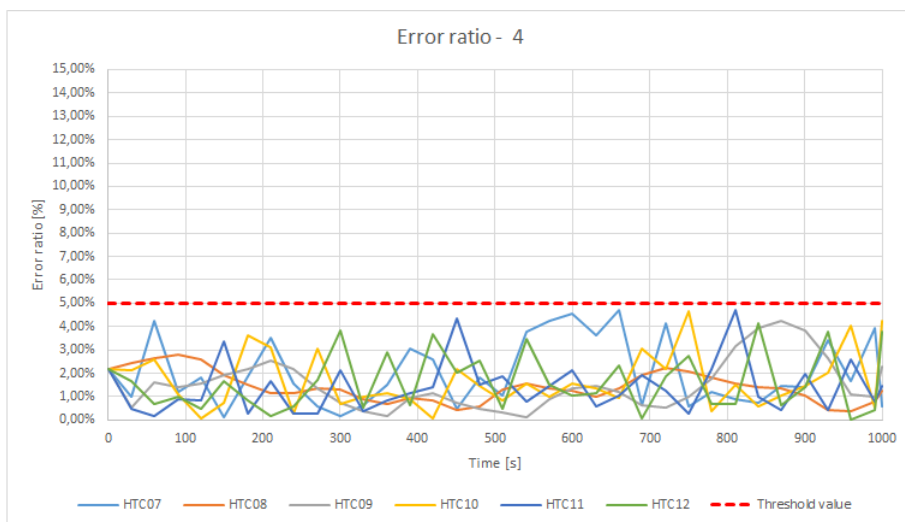


(b) Devices from 7 to 12

Figure 7.45: Adiabatic Surface Temperature error ratio



(a) Devices from 1 to 6



(b) Devices from 7 to 12

Figure 7.46: Heat Transfer Coefficient error ratio

Moreover, this Case Study have been remodeled with a 0.04 m mesh cell size - obtaining a 400 mm high and 240 mm wide cross section - and setting the simulation time for 240 minutes (14400 seconds). This configuration has been chosen for two reasons: replicating the Abdel-Mooty test with an sufficient precision and performing the analysis in an acceptable CPU time - [Figure 7.47] .

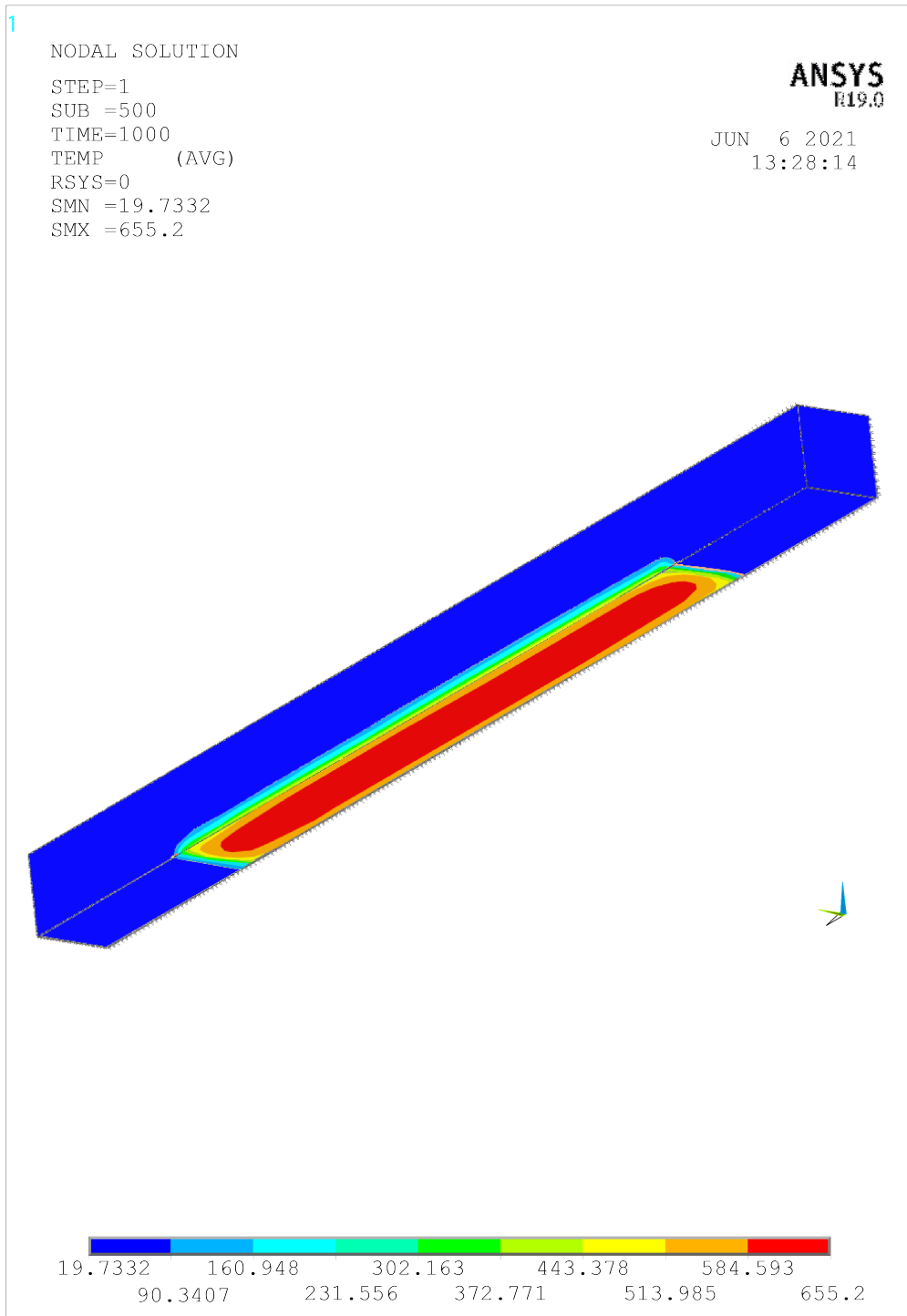


Figure 7.47: Thermal banded map

The concrete cover is 40 mm and the reinforcement steel configuration has not been changed. This further analysis is needed to understand if the heat model has been arranged in the right way. Furthermore, the Abdel-Mooty paper refers to the Kodur experience⁵ that has also been taken as term of comparison. Then, two points of control along the axis of the beam - on the cross section - have been taken to verify the thermal stress - [Figures 7.48, 7.49].

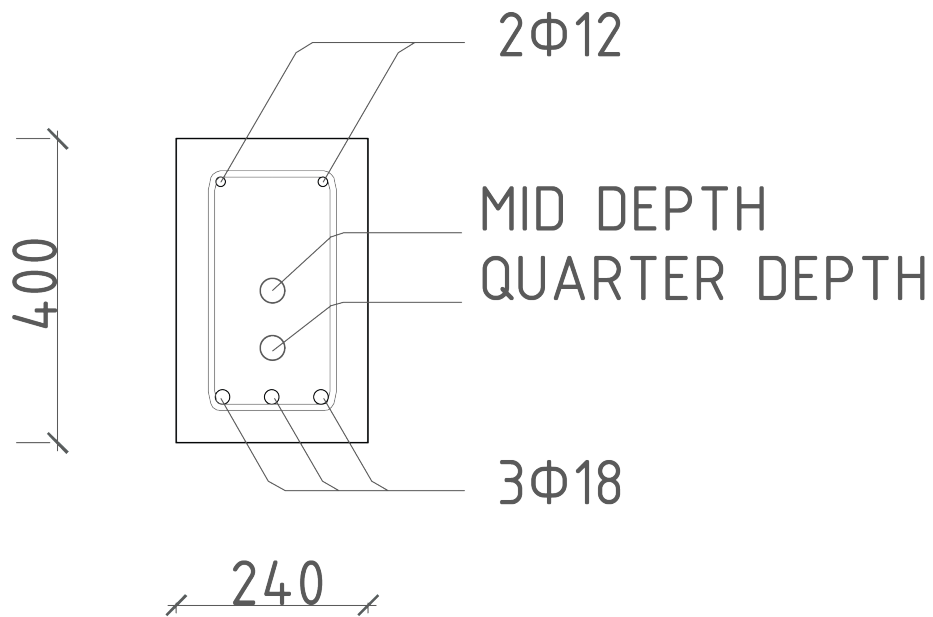


Figure 7.48: Control points along the axis of the beam

⁵KODUR V.K.R., ANGRAWAL A. (2016), "An approach for evaluating the residual capacity of reinforced concrete beams exposed to fire", J. Eng. Struct. 110 293–306

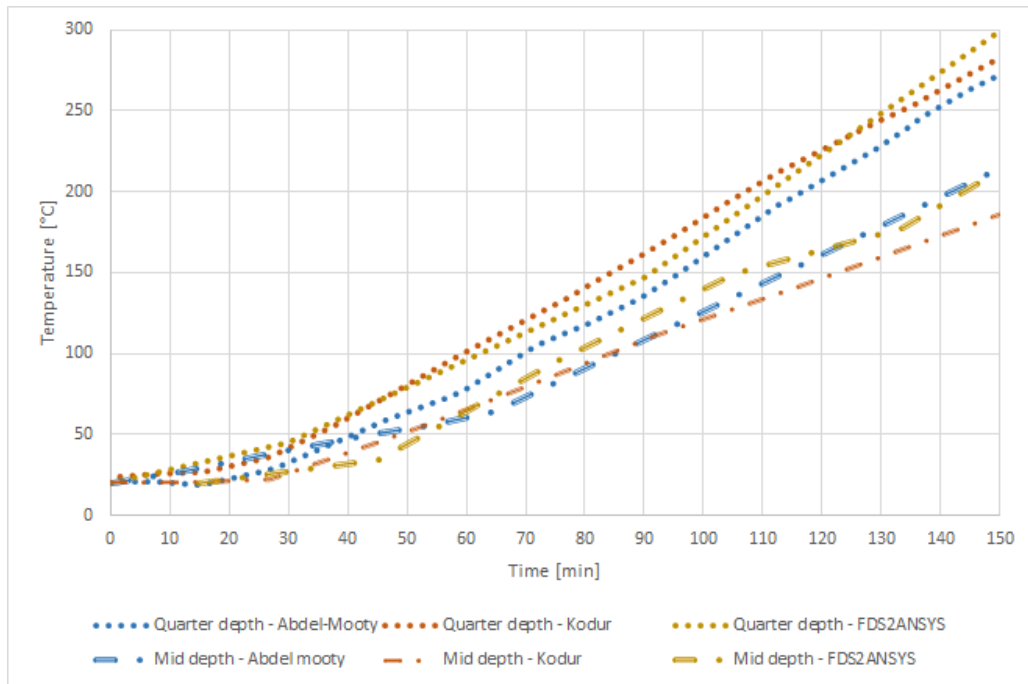


Figure 7.49: Comparison of temperature values over the time

It is possible to see from the error distribution - [Figures 7.50,7.51] - that the error has an overall trending that is similar for both the control points with respect of both the reference literature studies. It may imply that these trends may represent a sort calibration mathematical functions. Anyway, from a check over the simulation time, the threshold value - set equal to 5 % of error ratio - has never been overcome, for both the quarter depth and the mid depth control points. For this reason, it is possible to state that the Endothermic Analysis phase has been **validated successfully**.

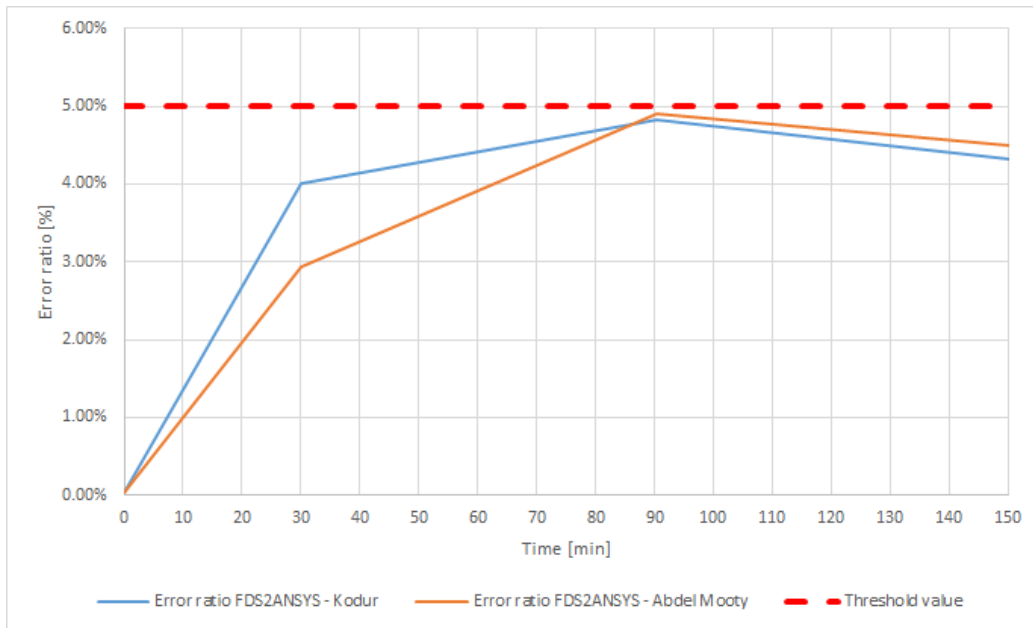


Figure 7.50: Error ratio for the quarter depth control point

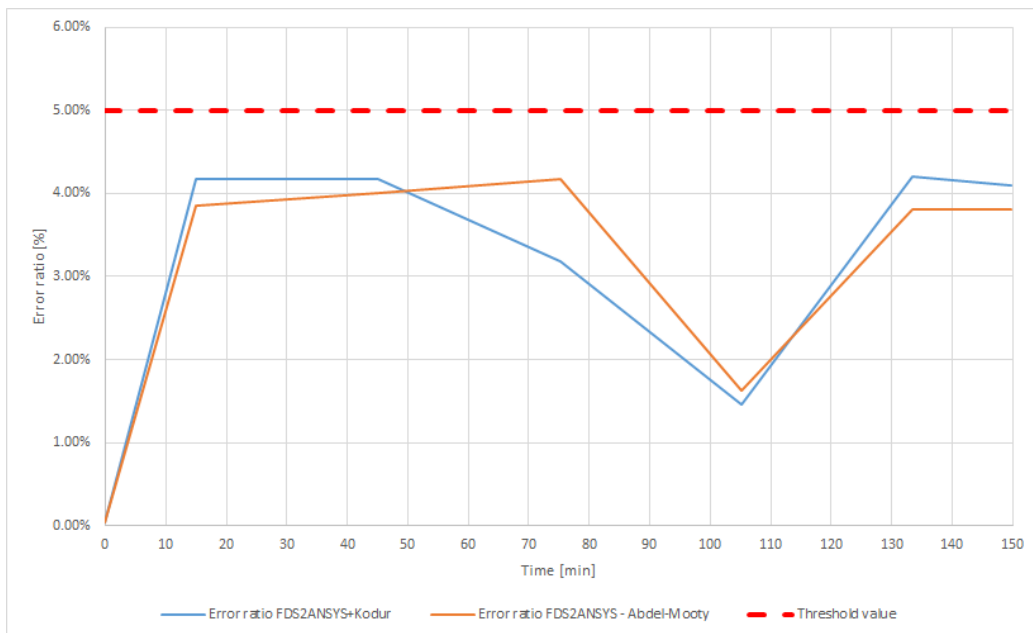


Figure 7.51: Error ratio for the mid depth control point

7.1.3 Validation of structural analysis

The validation of the structural analysis settings has been done on the simply supported beam case study, following the sequential coupling method for the thermal and the structural analysis. All the mechanical and geometrical features have been defined in the **Chapter 7.1.1. Geometrical, thermal and mechanical feature**. The sample code provided for this analysis can be found in the **Appendix C.1.6. Case Study A. - /PREP7 Code for ANSYS Mechanical APDL # 4**. In order to reproduce the applied mechanical stress during the test, FDS2ANSYS exports another input file which contains the structural model, with all the aforementioned geometrical and mechanical properties and with the coupled results from the thermal analysis. At this point, FDS2ANSYS closes and it is possible to set manually the mechanical loads and the restraining conditions. Indeed, a four-point bending configuration with two 50 kN-module vertical concentrated forces have been applied to the model. The restraint condition are represented by a simple support and a hinge, making isostatic the beam - **[Figure 7.52]** .

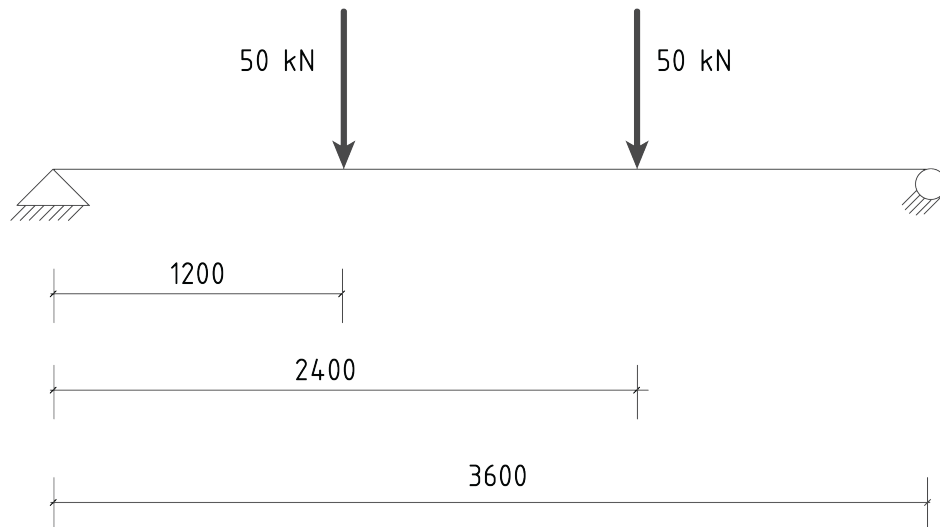


Figure 7.52: Four-point bending configuration for the beam [quotes in millimeters]

The parameter that has been chosen to make the comparison between the reported experiments is the vertical displacement, along the Z-direction. Here is reported the mid-span deflection over the time and the displacement

map at the moment of the collapse (calculus convergence no more achieved at 9128 s) - [Figure 7.53]. The mid-span deflection remains in an acceptable range of error ratio - equal to the 5% - [Figures 7.54, 7.55]. Even in this case the error distribution has a similar distribution for both the case study. For this reason, it is possible to state that the Structural Analysis phase too has been **validated successfully**.

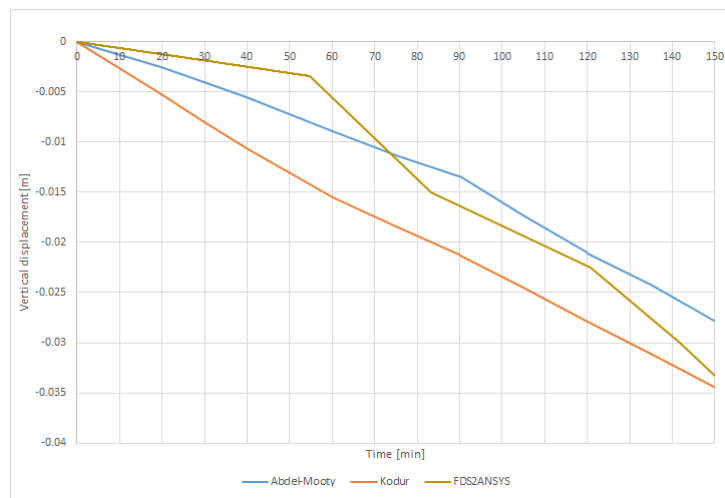


Figure 7.53: Comparison of mid-span deflection values over the time

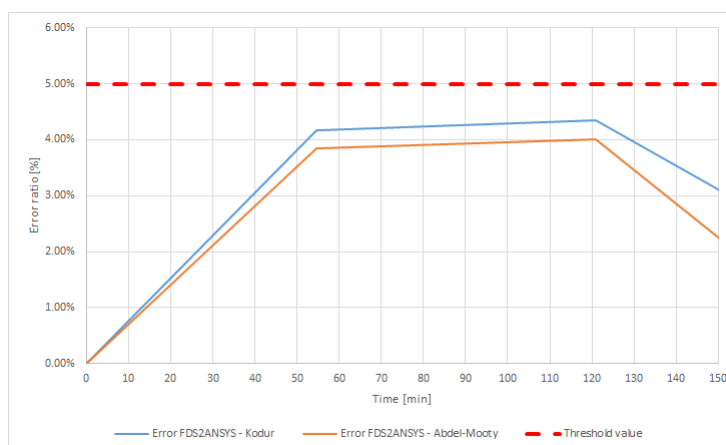


Figure 7.54: Error ratio for the mid-span deflection

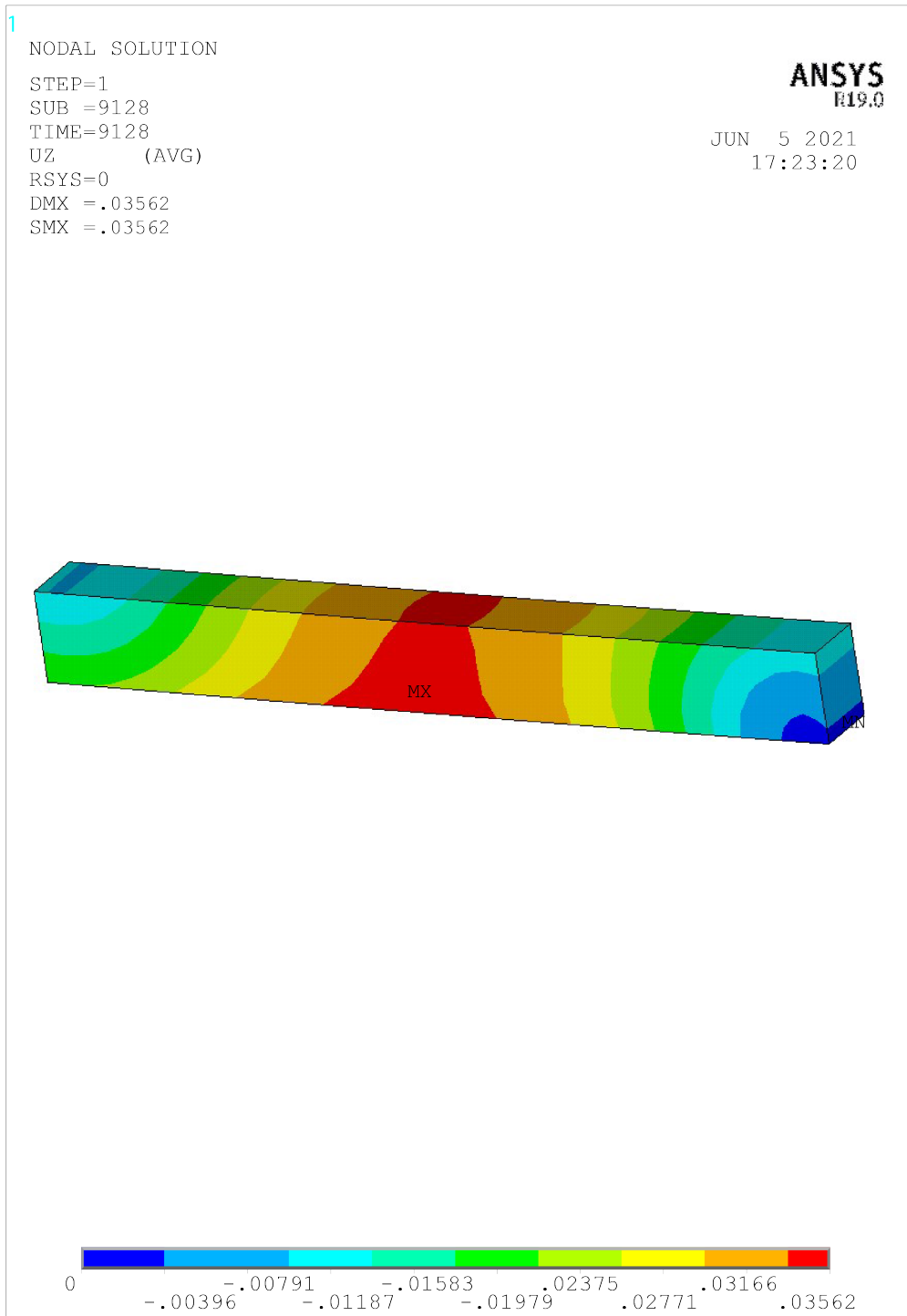


Figure 7.55: Mid-span displacement banded map

Chapter 8

Further consideration on the experimented results

The results may suggest an encouraging input to the world of the thermal-structural analysis. Despite this aspect, several secondary aspects may be considered, such as the technical matter on the deployment of the software.

8.1 VB.NET Framework under Microsoft Windows Environment

FDS2ANSYS has been developed in VB.NET language, implemented with .NET Framework 4.7.2, without considering the .NET Core Visual Basic version, under Microsoft Visual Studio 2019 integrated development environment on Microsoft Windows 10. It has been successfully tested both on Microsoft Windows 10 and Microsoft Windows Server 2016, but despite this, FDS2ANSYS is compatible with Microsoft Windows 7 and newer Operating System too. The simplicity of this programming language allowed the development of the software in a very simple way, in particular for those links needed for the data exchange between the software. Besides, since ANSYS Mechanical APDL may be run from terminal instances, the needed processes has been scheduled through the use of batch scripts, which are compiled in the right way to make something happen and then run from the software. **For this reason it is asked to run FDS2ANSYS with Administrator privileges.** Furthermore, VB.NET has a very-simple scripting engine, which has allowed to compile easily the ANSYS Mechanical APDL preprocessing files too. At last, the requirement needed to start the software is that the decimal separator is set as point ".".

8.2 High Performance Computing

On the commercial hierarchy, two main types of Personal Computer – independently from the Operating System – can be found: desktop and notebook PC. On the notebooks, four categories can be found:

- Cheap price;
- Averaged price;
- High-end price;
- Portable workstations.

On the desktop computers, a cheaper and an higher price range may be considered. Focusing the attention on the high-end price ones, four categories may be found:

- **Workstations:** high-end price desktop computer for calculus, engineering purposes and rendering; nevertheless gaming or crypto-mining;
- **Server:** high-end price desktop computer for calculus, engineering purposes, rendering, storage, business cloud, mail and print server;
- **Clusters:** link between computers. An MPI interface and a Network Ethernet Switch LAN may be required in order to establish a connection between the nodes. A DHCP setting of the IP address of the cluster nodes may have to be disabled, by setting a Static Local IP Address. It has the advantage to attach additional nodes to the network;
- **Supercomputers:** computers needed for very-high computational charge.

The CFD calculus engine settings may require a very onerous hardware in terms of power of calculus. The deployment of FDS2ANSYS and the most common experiments have been done on daily-use notebooks but the most onerous analysis have been performed on an High Performance Computing cluster. An HPC – High Performance Computing – cluster is the link established between computers in a local network, through the Server Protocol called Failover Clustering. This connection is usually established with at least a server computer – called master node – and one or more server or workstation or common-use computers- called slave nodes - that are associated in order to perform analysis exploiting the computing power of all nodes. In order to do this research, a two-nodes failover cluster has been deployed under Microsoft Windows Server 2016 environment - **[Figure 8.12]** . The first node is an assembled workstation - named as WS01 - with the following features - **[Figures 8.1 - 8.5]** :

- **CPU:** Intel Xeon E5 2683 v3 – 2.00 GHz CPU x 14 cores (28 threads)
- **Mainboard:** AsRock X99 Extreme 4
- **Memory:** 32 GB DDR4
- **GPU:** nVidia GeForce GTX 1060 – 6 GB GDDR5
- **SSD:** Kingston 960 GB
- **Local IP Address:** 192.168.1.115

The second node is a commercial enterprise server - named as SERVER01 - with the following features - [Figures 8.6 - 8.11] :

- **CPU:** 2 x AMD Opteron 6234 - 2.40 GHz CPU x 12 core (24 threads)
- **Mainboard:** HP Enterprise Proliant DL385P Gen 8
- **Memory:** 48 GB DDR3
- **GPU:** nVidia Quadro 4000 – 2 GB GDDR5
- **SSD:** Silicon Power 240 GB
- **Local IP Address:** 192.168.1.51

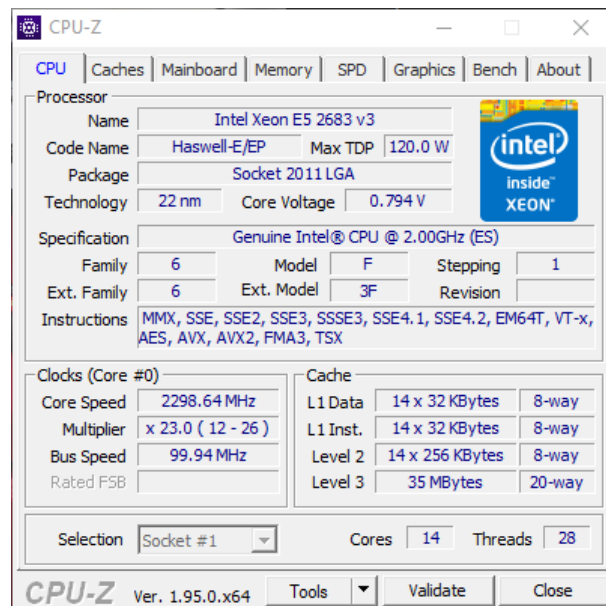


Figure 8.1: WS01 CPU: Intel Xeon E5 2683 v3 – 2.00 GHz CPU x 14 cores (28 threads)

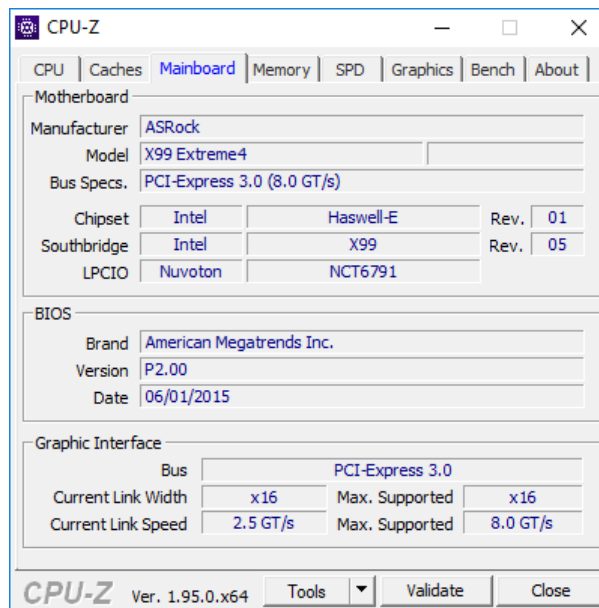


Figure 8.2: WS01 Mainboard: AsRock X99 Extreme 4

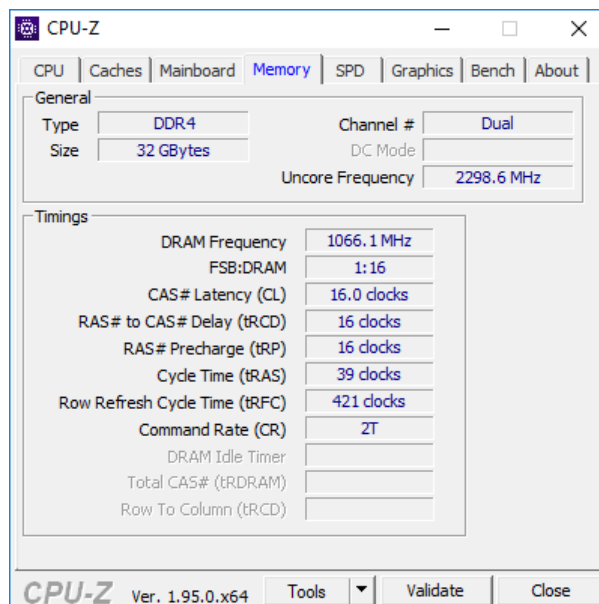


Figure 8.3: WS01 Memory: 32 GB DDR4

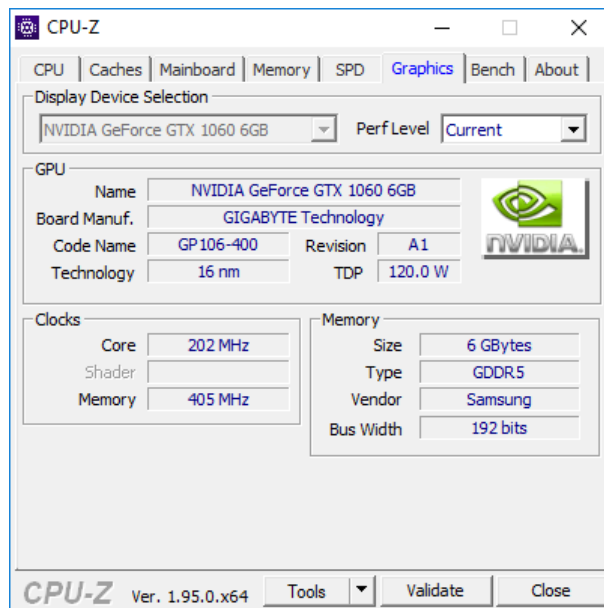


Figure 8.4: WS01 GPU: nVidia GeForce GTX 1060 – 6 GB GDDR5

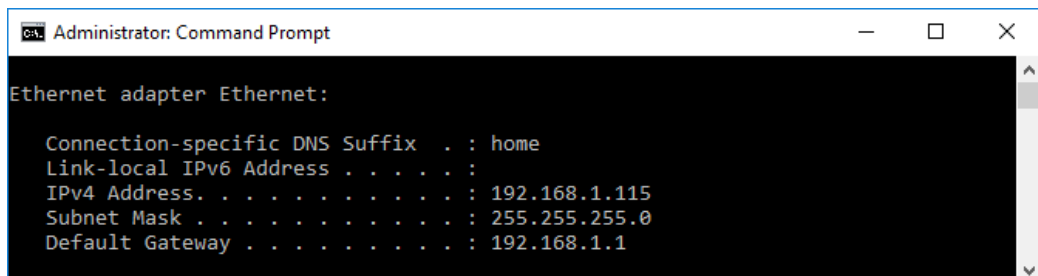


Figure 8.5: WS01 Local IP Address

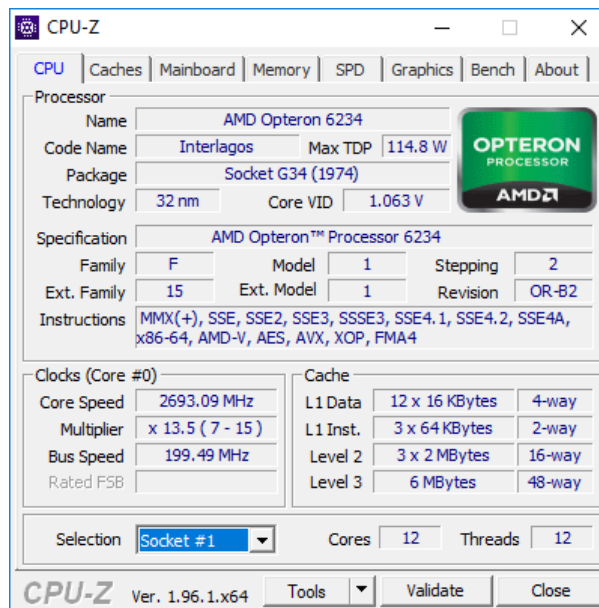


Figure 8.6: SERVER01 CPU #1: AMD Opteron 6234 - 2.40 GHz CPU x 12 core (12 threads)

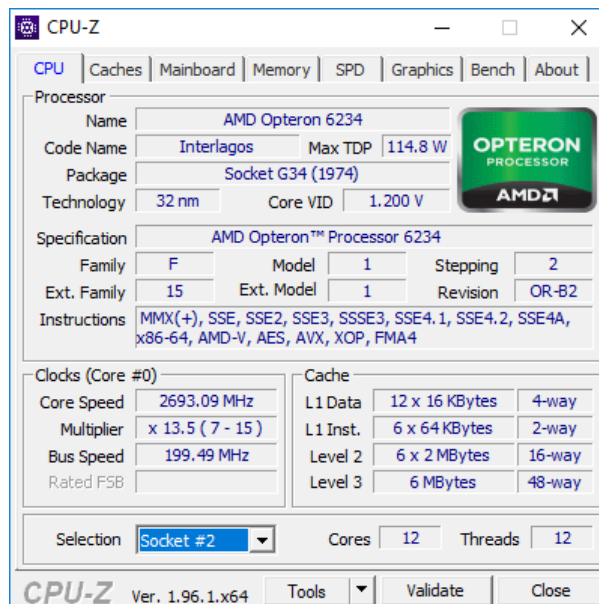


Figure 8.7: SERVER01 CPU #2: AMD Opteron 6234 - 2.40 GHz CPU x 12 core (12 threads)

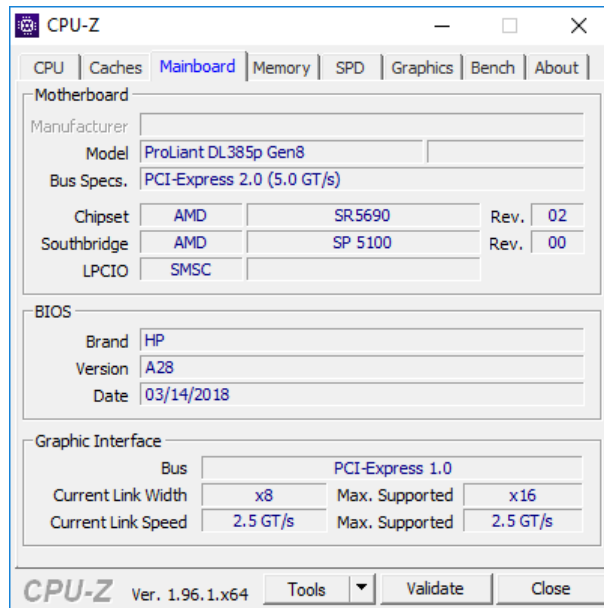


Figure 8.8: SERVER01 Mainboard: HP Enterprise DL385P Gen 8

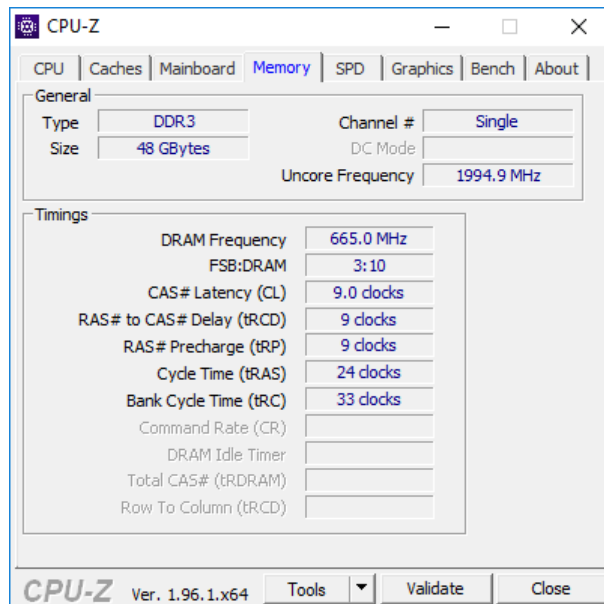


Figure 8.9: SERVER01 Memory: 48 GB DDR3

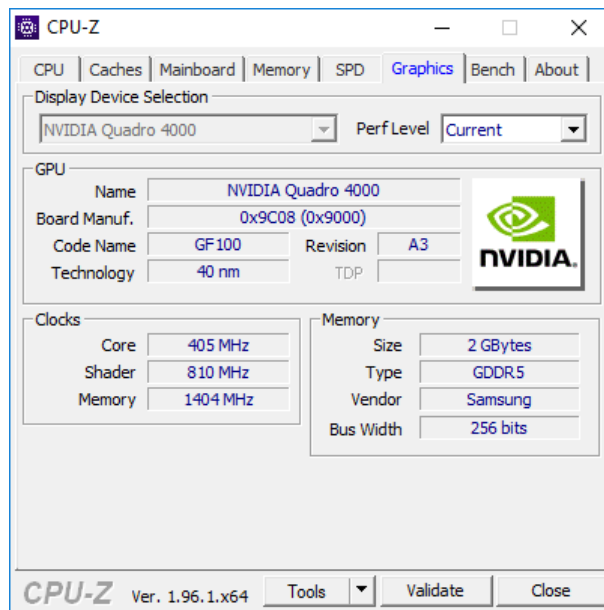


Figure 8.10: SERVER01 GPU: nVidia Quadro 4000 - 2 GB GDDR5

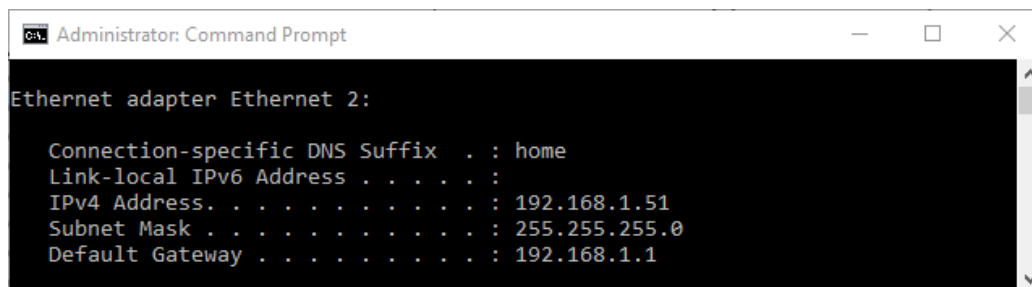


Figure 8.11: SERVER01 Local IP Address

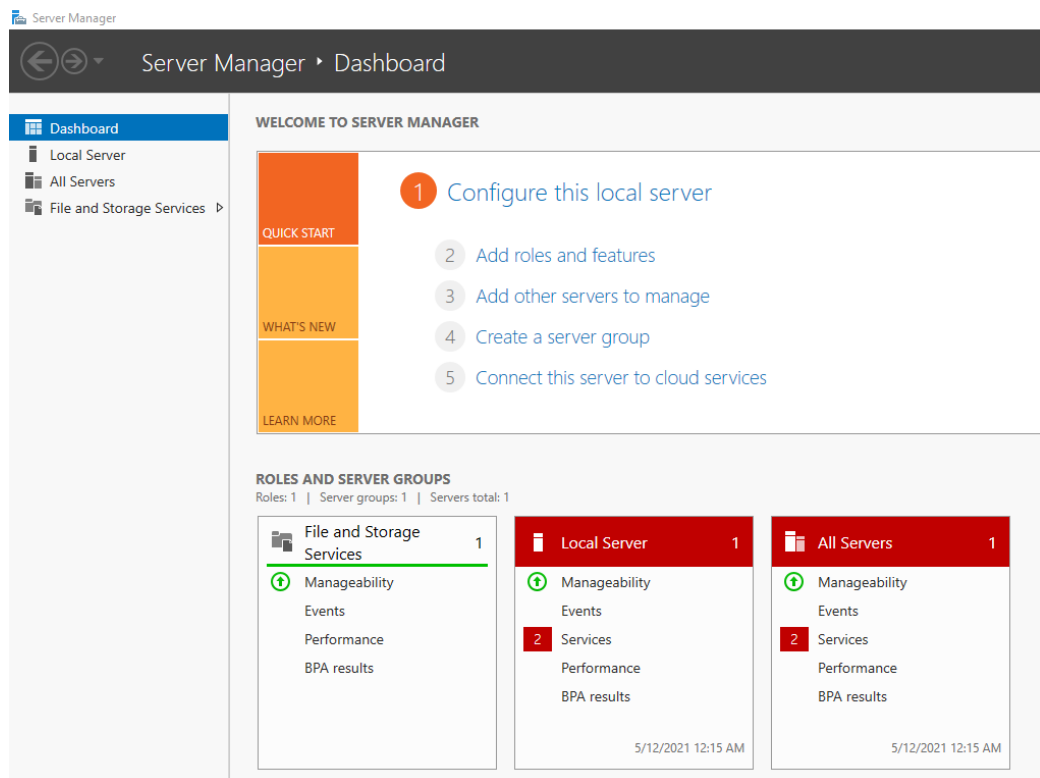


Figure 8.12: Microsoft Windows Server 2016 deployment environment

The Failover Clustering concept applies to a group of computer which, appropriately connected one to the other, allows to virtualize a PC environment which has the power equal to the sum of the technical specification of all the connected nodes. Usually, this kind of systems are used for the IT business management, in order to have a common storage which users can access and which keeps data even if a disk becomes corrupted - for this reason the name is Failover Cluster - applying redundancy data security protocols. This concept has been fitted to the necessity of computing power by "summing" the RAM memory and the CPU threads of the aforementioned nodes. Indeed, CPU power and RAM amount are the most important features for running CFD and FEM analysis, because the CPU clock indicates the "speed" of calculation - since each core of a CPU works at an averaged frequency equal to the one declared commercially; if needed some CPU are provided of a turbo-boost frequency which exceeds the declared one -, the CPU threads indicate the maximum number of parallel processes that can be run - since the MPI console, which works both for FDS and for ANSYS Mechanical APDL, assigns one process per logical thread - and the RAM amount, since the cal-

ulation results are temporarily stored on the RAM but it may be needed to "unload" the RAM by saving data onto the Hard Drive. For this reason, at least a 500 GB Solid-State Drive is recommended, because enough space on this may be guaranteed and also the data exchange speed is acceptable.

8.3 Employed software for the performed analysis

Without taking consideration of the aforementioned Integrated Development Environment, a brief discussion on the employed software in this research. At the beginning, a geometric model may be provided. Considering the IGES, ACIS SAT and Parasolid extension formats for allowed geometries, it is suggested to use a Mechanical Engine Modeler, such as Rhinoceros or SOLIDWORKS. Even the BIM models may be supported from this interface. If isolating the structural geometries workset, an ACIS SAT model may be exported and analysed¹. The software which have been employed to perform the analysis are the two main calculus engines: FDS, for the Fire CFD analysis, and the FEM Code, ANSYS Mechanical APDL. Both of them support the Intel MPI Engine which allows to run the analysis on a cluster with more or less nodes. For the FDS platform, the Thunderhead Engineering Pyrosim GUI has been chosen. The great advantage is to set the FDS Cluster - **[Figure 8.13]** - in a very simplified way, just by assigning a mesh on a CPU thread. On the FEM side, ANSYS Mechanical APDL allows, from the Product Launcher - **[Figure 8.14]**, to set the analysis onto a cluster through the Intel MPI Utility. For this cluster configuration, at the top of the computing power, a maximum of 13 cores (26 threads) for the WS01 node and of 22 cores (22 threads) for the SERVER01 node have been assigned. This phase is not provided from FDS2ANSYS: the Intel MPI features have been set on the ANSYS Mechanical APDL Product Launcher - High Performance Computing Setup. Instead, the multi-thread calculation processing for FDS can be also set from FDS2ANSYS.

¹This functionality has not been tested and may require some editing procedures before loading the geometries onto FDS2ANSYS.

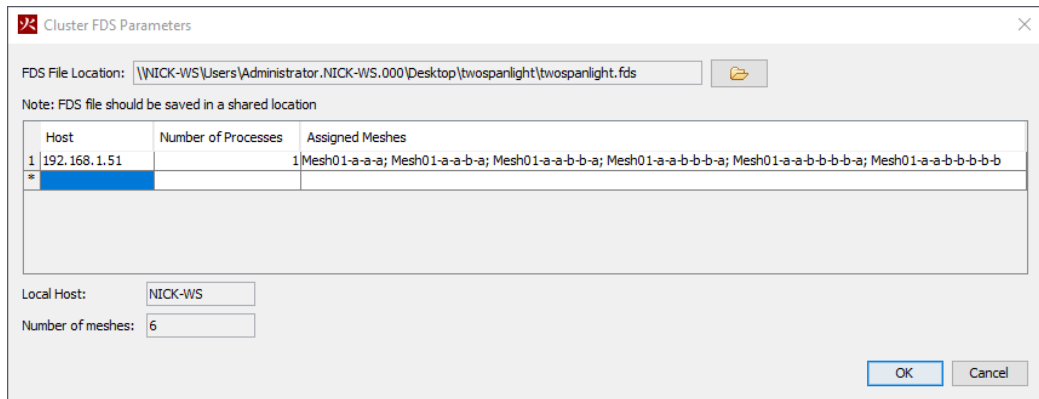


Figure 8.13: Thunderhead Engineering Pyrosim Cluster FDS

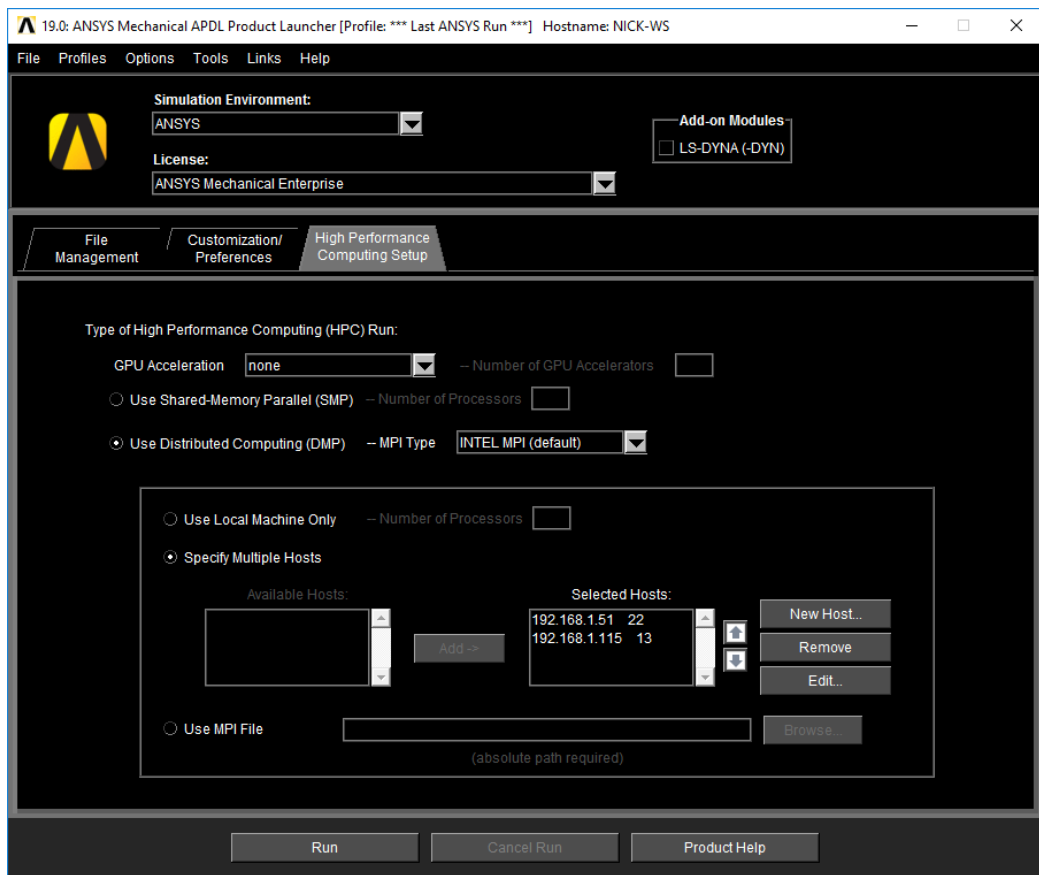


Figure 8.14: ANSYS Mechanical APDL Product Launcher - High Performance Computing Setup

8.4 A brief dissertation on the computing time

The major critical issue of this research regards the computing time, which may be very long. The need to perform analysis with a very high level of detail - small mesh cell size -, makes the number of computed cells increasing exponentially. Non-linear problems usually have a cubic distribution of the computing time with respect of the computed cells. Another important aspect is related to the simulation time, which has not shown a linear correlation with the computing time. It is necessary to precise that, by enabling the boundary functions exporting, all the cells are computed, not only the ones where there are obstructions. Below are reported the features of the performed analysis described in the **Chapter 7. Validation**, which have been monitored:

- **CTSA01**

- Simulation Time: 1000 s
- Mesh cell size: 0.02 m
- Mesh cell number: 108000
- Threads: 16

- **CTSA02**

- Simulation Time: 14400 s
- Mesh cell size: 0.04 m
- Mesh cell number: 150000
- Threads: 6

The most important aspect of the needed computing time sensibly increases with the simulation time and the nodes increasing. Nevertheless, even the needed storage is not neglectible: the case CTSA01 needed 25.0 GB of storage and the case CTSA02 needed 800.0 GB of storage - [**Figure 8.17**]. Here follow the graphs of the needed computing time - [**Figures 8.15, 8.16**].

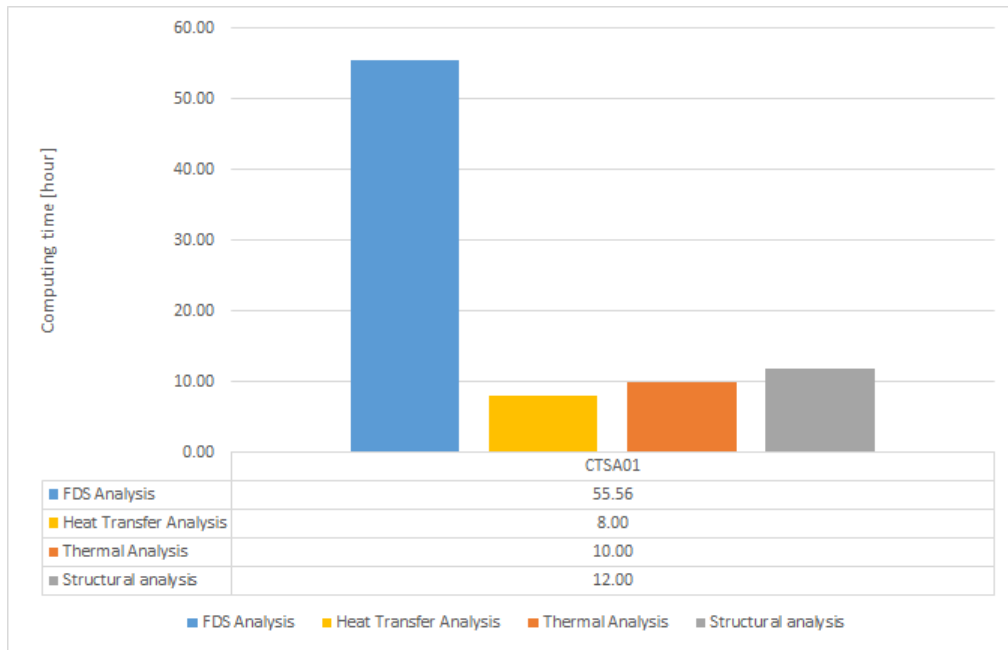


Figure 8.15: Computing time needed for the case CTSA01

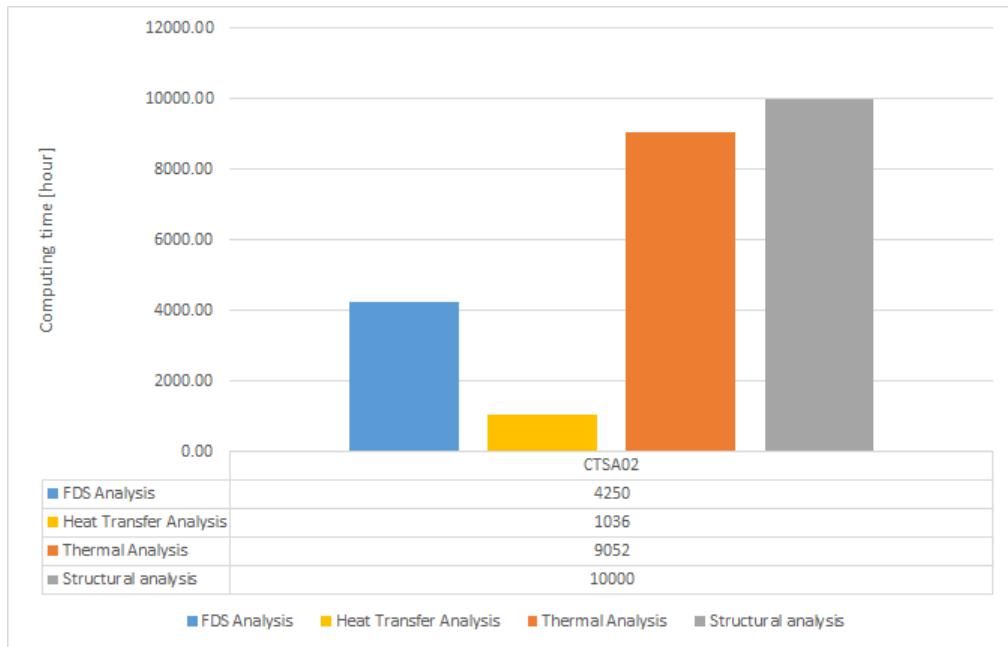


Figure 8.16: Computing time needed for the case CTSA02

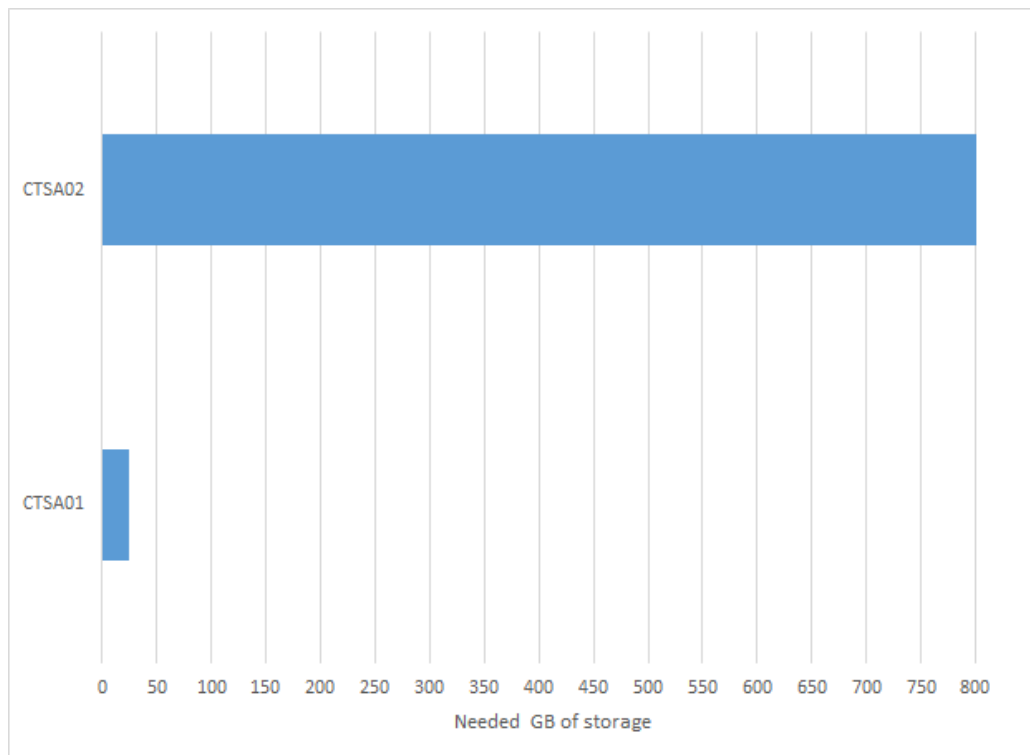


Figure 8.17: Needed storage for the monitored cases

Chapter 9

Conclusion: reached objectives, improvements and further researches

At this point of the essay, it is possible to state which objectives have been reached and, then, how to focus the attention on the further researches. At the beginning of this research, the fixed objectives were:

- Optimizing the quality of the obtained data;
- Understanding the techniques of coupling multi-field analysis;
- Facilitating and automating the procedure for coupling thermal and structural analysis by finding a method to perform coupled thermal-structural analysis;
- Stating the structural behavior under fire stress and defining strategies to achieve safety conditions for occupants;
- Understanding which parameters affect the structural behavior;

In order to reach the first objective, a large amount of FDS analysis have been performed in order to find a way to obtain high-quality results in an acceptable computing time. This has not been simple, since the FDS way of processing geometric obstructions is often the main reason of the long computing-time, due to the mesh cell size. Unfortunately, on ANSYS Mechanical APDL too the needed computing time is influenced on the aforementioned parameter. For this reason, this method is applicable to local structural members which may suffer more the heat load, such as single beams or columns or L, T or + beam-column nodes. Since the calculation

of a suitable value of mesh cell size may be complex, the Mesh Sensitivity Analysis Tool has been introduced into FDS2ANSYS with the goal of simplifying this operation. This means that as much the structure is geometrically regular, the mesh cell size should be bigger and the needed time may be less. Another test that has been done regards the mesh refinement after importing the /PREP7 files onto ANSYS Mechanical APDL. This technique may be optimal by hand-setting the nodes of which the results are needed, since the needed storage availability may be very onerous. Even the computing time is very long. Some algorithms of optimization of the exported data may significantly improve the efficiency of this coupling interface. **The first objective has been reached**, but several researches on this aspects are needed.

On the second objective, a large documentation has been consulted on the coupling techniques between thermal and mechanical fields analysis. Here follow the procedures that have been considered in this research:

- **Sequential coupling technique:** the whole time-history thermal analysis is performed and then the time-history structural one is executed by a coupling command;
- **Direct coupling technique:** the thermal and structural time-history analysis are performed in the order step-by-step.

At this point, the element types need to be set, considering that for the sequential coupling technique, four elements are needed and for the direct one just two:

- **Sequential coupling technique:**
 - **SOLID70:** thermal behavior of concrete;
 - **LINK33:** thermal behavior of reinforcement;
 - **SOLID65:** mechanical behavior of concrete;
 - **LINK180:** mechanical behavior of reinforcement.
- **Direct coupling technique:**
 - **SOLID226:** thermal-mechanical behavior of concrete;
 - **LINK180:** mechanical behavior of reinforcement.

The second objective has been reached.

The third objective has been reached, since FDS2ANSYS generates the needed scripts for coupled thermal-mechanical analysis with a user-friendly GUI. This does not mean that the user can model a structure for this purpose

without knowing ANSYS Mechanical APDL: a large knowledge of the Command Reference¹ and of the Theory Reference² notions is required. Furthermore, the objective has been reached, since this research can be synthesized with the following steps - **[Figure 9.1]**:

- Modeling phase;
- Research on the burner and reaction of the fire;
- Employment of a Sprinkler System;
- *HRRSprinkler Gen*;
- FDS Analysis for global temperature distribution;
- Check of the Adiabatic Surface Temperature Boundary function;
- *FDS2ANSYS*;
- Local FDS analysis on a part of the structure;
- Heat Transfer Analysis;
- Coupled Thermal Mechanical Analysis;
- Security structural safety checks.

¹ANSYS Mechanical APDL Command Reference Guide

²ANSYS Mechanical APDL Theory Reference Guide

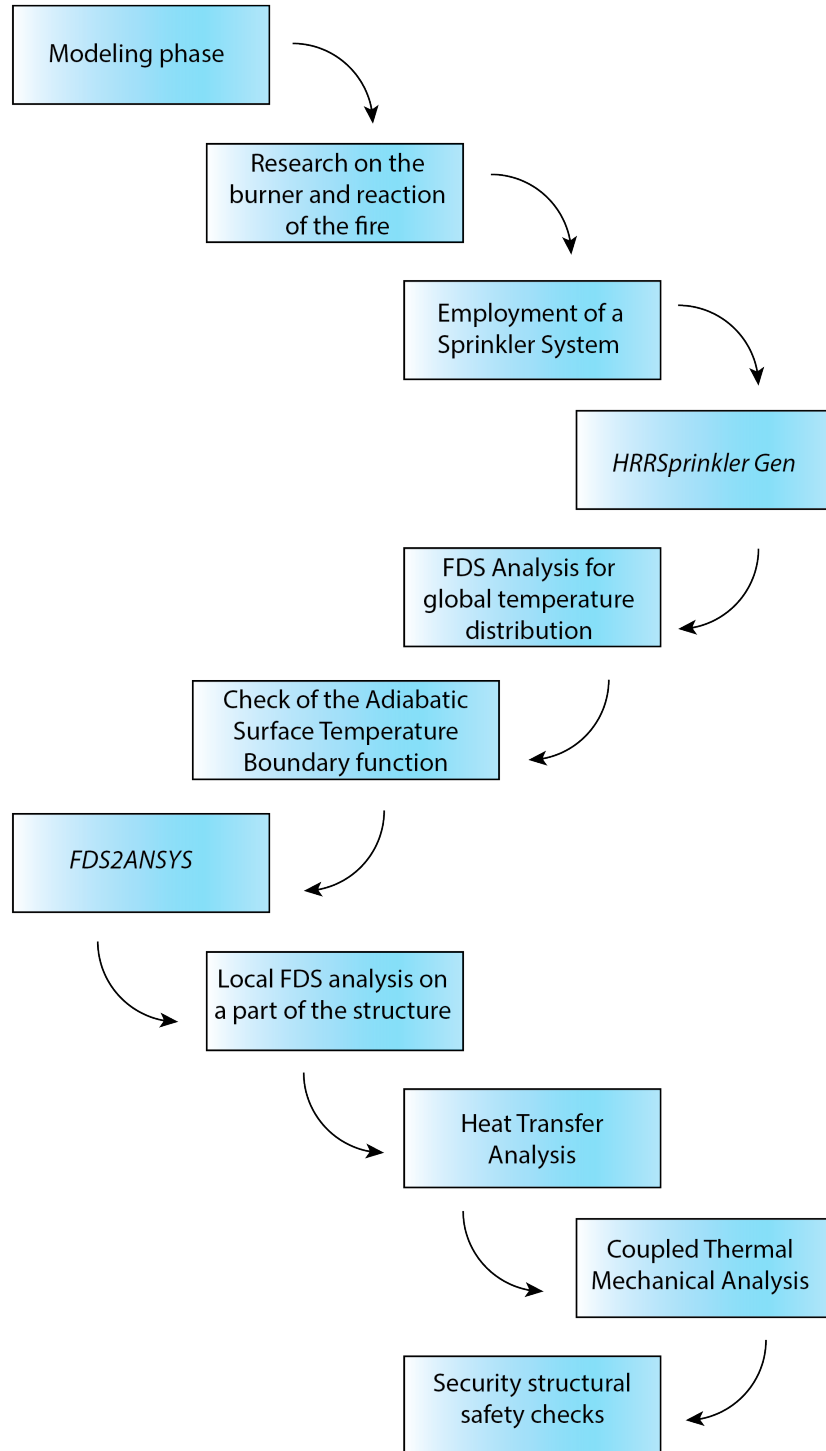


Figure 9.1: Complete flowchart for structural safety checks through thermal-mechanical using HRRSprinkler Gen and FDS2ANSYS

Then, once the thermal analysis has been executed, the results showed that the concrete structures resist optimally to the fire, by the formation of an inner core in the cross section which remains at lower temperatures. The parameter that affects mainly the structural behavior is the concrete cover, which as the distance increases, the inner core temperature decreases, during the time-histories. Even the moisture content influences the structural behavior under the fire action. It is possible to state that **the fourth objective has been reached**, but further researches are needed on the strategies to achieve safety conditions for occupants. A solution may be achieved with the ASET/RSET criteria - considering the safety occupants or the Rescue Team Intervention -, reported in several standards³⁴, coordinated with the safety checks as results of coupled thermal-mechanical analysis. Then, in order to understand which parameters affect the structural behavior, it is necessary to develop further studies.

After these considerations, and despite the aspect of the computing time which is the most influential issue, it is possible to carry on the research through some improvements that can be done on FDS2ANSYS:

- **Different mesh cell size values:** actually FDS2ANSYS is working with a single mesh cell size value. In some zones, a small mesh size may not be needed and allowing different mesh cell size values may reduce the needed computing time. The reason of the lack of this functionality is due to some instabilities that have been shown on the FDS2FTMI interface by providing different mesh cell sizes;
- **Radiative Heat Flow:** actually FDS2FTMI allows the heat transfer taking into account both of the convective and the radiative heat flow. Some commercial software, such as SAFIR, allow the analysis considering the only radiative phase, reducing the needed computing time;
- **Complex geometries and slopes implementation:** this limitation is due to the FDS discretization method. With the use of correction algorithms or with FDS 7 - which is in plan to be released soon - complex geometries - complex sections, slopes, structural bracings and diagonal beams - may be computed;
- **Two-way coupling method:** actually FDS2ANSYS works for a one-way coupling procedure but, linked to the FDS 7 Release, a two-way

³ISO TR 16738:2009

⁴Italian Technical Fire Prevention Standards - Ministerial Decree 3rd of August, 2015 and subsequent amendments and additions

coupling method may be implemented, since it could be possible to model the deformed shape at each collapse;

- **ANSYS Mechanical APDL and Intel MPI Engine:** a next release of FDS2ANSYS may prevent the necessity of hand-setting the Intel MPI Engine on the ANSYS Mechanical APDL Product Launcher.
- **Memory allocation and resources:** with further researches, new ways of allocation of memory and resources - but also wiping memory subroutines which may optimize the use of the hardware.

Despite the previous considerations, the results of this research are very encouraging: one of the main aim at the beginning of this work was to simplify the procedure to perform coupled thermal-mechanical analysis and this is why FDS2ANSYS may be used, even considering the aforementioned limitations. This objective is the beginning point of the study of a collapse criteria for the structural behavior under the fire stress.

Furthermore it is needed to consider that the Information Technology trade is developing and improving constantly and the needed computing power that now may seems prohibitive, in two or three years may become more accessible. Moreover, main newer components can be chosen for configuring a cluster node. Then the configuration may be replied with a variable number of nodes. Even if this kind of analysis requires an high number of threads for parallel computing, an high CPU clock (higher than 3.5 GHz per each core) may reduce the time of analysis. Approximately, not less than 64 GB of DDR4 NON-ECC RAM should be provided on each node and, on the storage specifications, a RAID configuration with a variable number of Solid State Drives may be required, in order to have a larger storage with high read/write speed ratio. There are not particular specification for the Graphic Card, but at least 4 GB GDDR5 of video RAM should be provided.

Appendix A

A brief introduction to HRRSprinkler Gen

HRRSprinkler Gen is a freeware software made for helping users whose purpose is to use Fire Safety Engineering methods for Civil Engineering applications. As the name suggests, this program is designed to be used to **generate heat release ratio diagrams**, to correct them when an **automatic or control fire extinguish system** (commonly known as a sprinkler system) is employed and to gain more information about the fire – such as ignition of nearby items, flashover time and temperature, behaviour of the heat release ratio with ventilation openings. Thus, HRRSprinkler Gen is meant to be used both with a computational source for calculation of fires – as NIST's CFAST or FDS platforms - and as a standalone software, without the need to use a finite element calculator. Depending on the situation, the use of a computational calculator is always advised, since the numerical models of heat collected in the software – more or less complex – are obviously approximated solutions, while Computational Fluid Dynamics systems are based on the resolution of the differential form of Navier-Stokes equations. The advantage of using this program is to **obtain useful information, without knowing how to use a finite element calculator**.

In order to compare the consequences of fires according to various models in different types of legislation, the physical models here proposed are looked at in turn. The main laws on which this software is based on are European and Italian, but also British and American Standards are taken into consideration.

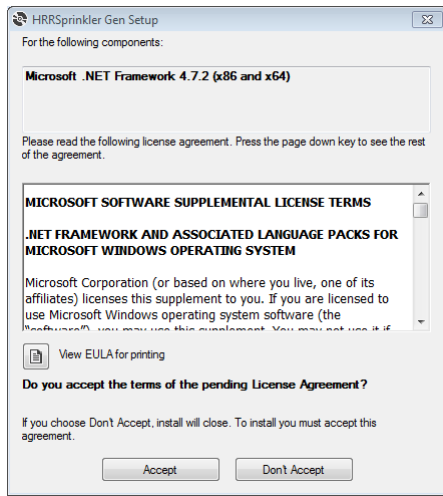
A.1 Installing HRRSprinkler Gen

HRRSprinkler Gen can be easily downloaded from <https://github.com/NicTunFSE/HRRSprinklerGen>. On this page, it is possible also to updated the software and consulting changelog. It is also possible to report any bugs or issues about the program by sending an email to: nictunfse@engineer.com.

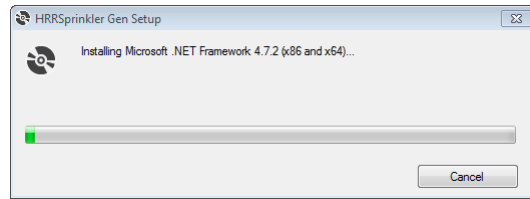
In order to exploit all the functionalities, here follows the **system requirements** for HRRSprinkler Gen:

- OS: Microsoft Windows 7, Microsoft Windows 8, Microsoft Windows 8.1, Microsoft Windows 10
- CPU: AMD or Intel 1 GHz processor - both x86 and x64 builds are allowed
- RAM: 512 MB
- Graphics: 128 MB of video RAM
- Screen resolution: at least 1280x960 pixels
- HDD: at least 4.5 GB of free space
- .NET Framework 4.7.2
- An internet connection is required
- Highly recommended to have installed Microsoft Excel or similar
- *Optional: a CFAST or FDS finite element calculator*

The installation proceeds with the simple following steps: once opened, the setup asks the user - if needed - to install the .NET Framework 4.7.2. By clicking on accept, the download process starts - duration depends on the Internet connection speed. After download and installation of the Framework ends, the system verifies the application and it asks the user the confirm to install HRRSprinkler Gen. Press "Install" button. Finally the installation process begins. Once installation is completed, HRRSprinkler Gen starts automatically.



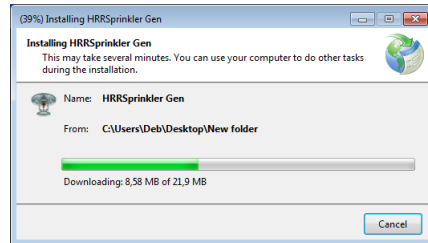
(a) .NET Framework 4.7.2 installation



(b) .NET Framework 4.7.2 download



(c) HRRSprinkler Gen installation confirm



(d) HRRSprinkler Gen installation process

Figure A.1: HRRSprinkler Gen - Installation steps

A.2 Running HRRSprinkler Gen

Once running with the splash screen visible, HRRSprinkler Gen starts.



Figure A.2: HRRSprinkler Gen - Splash screen

On the main screen, the user can choose between four kinds of approach for generating a heat release ratio diagram. Here we report only the main functionalities of the software for each approach but, later, the theoretical physical heat models - on which these features are based - will be described in depth. Each approach generates a diagram, allowing the user to save a picture of it or export it as an .xls/.xlsx workbook or as a data file (.txt or .csv). Besides, the software is equipped with a convergence check for the maximum heat released quantity, which is useful in case of fires which do not reach the steady-state phase. The four main approaches:

- **Parametric HRR – Complex approach:** the complex approach for generating HRR diagrams is based on two different models of heat generation – the Eurocode 1 one and the Kawagoe one – and takes into consideration several aspects which can affect fire behaviour: burning material – with several materials and their specific thermal features - and ventilation openings – both on the external façade and on the roof. In this section, in order to generate the correct HRR diagram for a sprinkler system, there is also an iterative algorithm to estimate the time of activation of the fire extinguishing system – which is commonly calculated with a CFD calculator. Three models of fire extinguishing systems are provided – as many algorithms of diagrams correction:

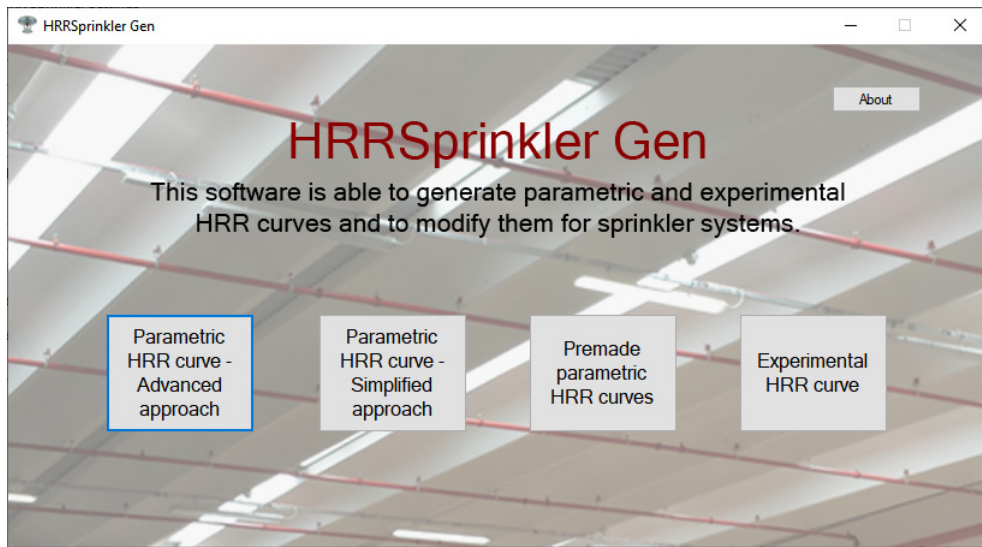


Figure A.3: HRRSprinkler Gen - Main screen

automatic fire extinguishing using water, automatic fire extinguishing using an inert gas and control system for fire extinguishing using water.

- **Parametric HRR - Simple approach:** the simple approach for generating HRR diagrams is based on the Eurocode 1 approach and is designed to build these diagrams with only a few input parameters, such as maximum heat release ratio (or completely developed fire time), combustion speed, specific heat load, fire area and time of activation for sprinkler systems.
- **Premade parametric HRR:** this section contains several premade HRR diagrams, taken from literature, for environments - whose specific heat loads are taken from the Italian ClaRaF 3.0 Database - and for items or materials. The user has only to type the area of the fire compartment (or the burner floor area) and the fire growth ratio - recognised in several legislations as t_{α} .
- **Experimental HRR:** this section has been made for users that want to work with experimental HRR diagrams and to correct them for the activation of a sprinkler system. In this section - as in the "Parametric HRR - Complex approach" section - the user can decide to correct the generated HRR graph with three different models of fire extinguishing: an automatic fire extinguishing system using water, an automatic

fire extinguishing system using inert gas and a control system for fire extinguishing using water.



Figure A.4: HRRSprinkler Gen - About screen

Finally, on the main screen, there is the About button, useful to check which version of the software is running, to visit the GitHub page for bug-fixes and changelogs and also to have support for troubleshooting.

A.3 Using HRRSprinkler Gen

This chapter browses the sections of the software, mentioned in **Chapter 3 - Running HRRSprinkler Gen**, focusing on heat models which the software is based on. Mathematical expressions and physical hypotheses are explained in order to understand how this application works for calculating results and diagrams.

A.3.1 Parametric HRR - Advanced approach

The parametric advanced approach focuses attention first on the calculation of the maximum heat released ratio, considering that ventilation can drastically modify heat distribution in the environment. To do this, two different approaches, embedded in the software, can be chosen as shown:

- **The Eurocode 1 approach:** this algorithm calculates HRR_{max} with the approach reported on EN 1991-1-2 standard for structures:

$$RHR_{max} = 0.10 \cdot m \cdot H \cdot A_v \cdot \sqrt{h_{eq}} \quad (\text{A.1})$$

where:

- **m:** combustion participation coefficient: it is equal to 0.8 for cellulosic or wooden materials and is equal to 1.0 for all the other materials;
- **H:** wood heat power, equal to $17.5 \frac{MJ}{kg}$;
- **A_v :** sum of each ventilation opening area, expressed in [**m²**], calculated as $A_v = \sum_{i=1}^n A_{v,i}$;
- **h_{eq} :** equivalent height, expressed in [**m**], calculated as weighted average of heights of ventilation openings: $h_{eq} = \sum_{i=1}^n \frac{A_{v,i} \cdot h_i}{A_v}$;
- **The Kawagoe approach:** this approach is a little bit more complex than Eurocode 1. There are two versions: one which takes into consideration roof openings - which are never considered in the EN 1991-1-2 approach - and one which does not. Another aspect of this approach concerns the burning material - which is not assumed to be necessarily wood, even if common materials usually have values of energy released while burning approximately around $3000 \frac{kJ}{kg_{air}}$. The Kawagoe approach - for building with wall ventilation openings only - for calculating HRR_{max} is based on the following formula:

$$RHR_{max} = \chi_A \cdot P_c \cdot 0.5 \cdot A_{v_{equiv}} \cdot \sqrt{h_{v_{equiv}}} \quad (\text{A.2})$$

where:

- **χ_A :** combustion efficiency; when Kawagoe approach is selected, this value is equal to 1.0 by default - 100 % of entering oxygen in the fire compartment is burned -, but user can change this value from 0 to 1 in order to modify the burned oxygen fraction;
- **P_c :** energy released while burning expressed in [$\frac{MJ}{kg_{air}}$]; the selected value is "User defined" by default, but values of several

materials are available:

| Material | P_c - Energy released while burning [$\frac{MJ}{kg_{air}}$] |
|--------------------|---|
| Methane | 2.91 |
| Propane | 2.97 |
| Ethanol | 2.99 |
| Acetone | 3.25 |
| Cellulose | 3.15 |
| Wood | 3.07 |
| Polyethylene | 2.93 |
| Polypropylene | 2.94 |
| Polyvinyl chloride | 2.98 |
| Polystyrene | 3.01 |
| Nylon | 2.94 |
| Polyurethane | 3.56 |
| Benzene | 3.03 |
| n - Pentane | 2.97 |
| Polycarbonate | 3.04 |

– h_{vequiv} : the difference between the highest point and the shortest point of all ventilation facade openings, expressed in [m];

– A_{vequiv} : calculated as the product $w_{vequiv} \cdot h_{vequiv}$, which are respectively the width and the height of the ventilation equivalent

opening; w_{vequiv} is calculated as:
$$w_{vequiv} = \frac{\sum_{i=1}^n w_{vent,i} \cdot h_{vent,i}^{1.5}}{h_{vequiv}^{1.5}}$$

In order to calculate ventilation factors, both for the Eurocode 1 and for the Kawagoe approach, facade ventilation openings dimensional features are required.

Insert opening area dimensions

| | w,vent [m] | h,vent [m] | z0 [m] |
|---|------------|------------|--------|
| * | | | |

Roof openings

Add row

Delete row

Clear Data

Paste Data

X dimension of the fire compartment [m]

Y dimension of the fire compartment [m]

Z dimension of the fire compartment [m]

Figure A.5: HRRSprinkler Gen - Facade ventilation openings dimensions

On the right side of the windows, there is the explanation of the required terms:

- w_{vent} : width of the single facade ventilation opening, expressed in [m];
- h_{vent} : height of the single facade ventilation opening, expressed in [m];
- z_0 : distance from the floor of the single facade ventilation opening, expressed in [m];
- **X dimension of fire compartment**: the width of the fire compartment - along the X axis - expressed in [m];
- **Y dimension of fire compartment**: the depth of the fire compartment - along the Y axis - expressed in [m];
- **Z dimension of fire compartment**: the height of the fire compartment - along the Z axis - expressed in [m];

The advantage of the Kawagoe approach is that it allows user to consider the effect of roof openings. By selecting this approach, in fact, the user will notice that, on the User Interface shown in Figure 4.1, the Roof Openings button is active. By clicking on it, it is possible to set the roof ventilation openings dimensional features as follows:

- w_{roof} : width of the single roof ventilation opening, expressed in [m];
- h_{roof} : height of the single roof ventilation opening, expressed in [m];
- w_{vent} : width of the single facade ventilation opening, expressed in [m];
- h_{vent} : height of the single facade ventilation opening, expressed in [m];
- d_H : distance from the roof ventilation opening to half height of the facade ventilation opening, expressed in [m];

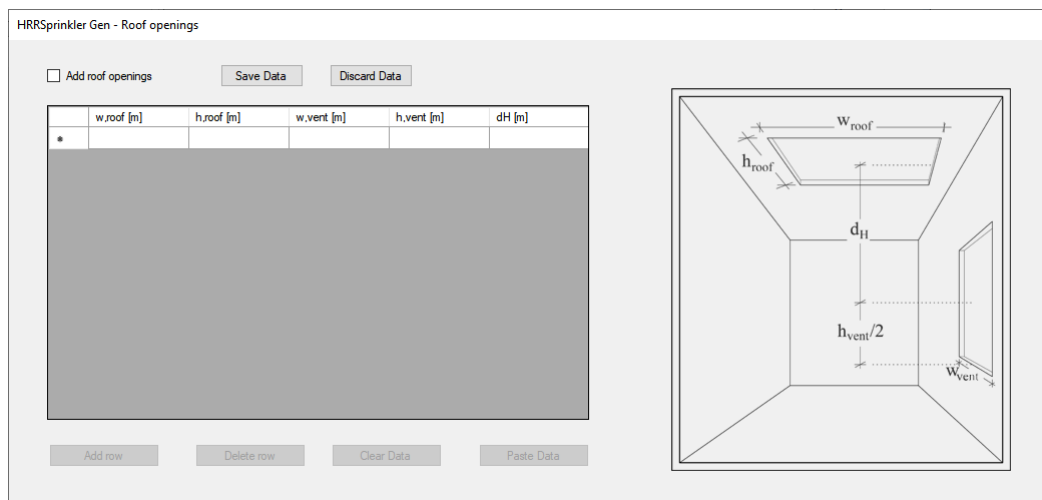


Figure A.6: HRRSprinkler Gen - Roof ventilation openings features - only available in the Kawagoe approach

In order to activate this feature, the user must tick the "Add roof openings" checkbox, insert the roof openings dimensions and click to "Save Data" button. When "Save Data" is pressed, the software makes a convergence control, in order to give the user reliable results. If the ratio $\frac{A_v \cdot \sqrt{d_H}}{A_v \cdot \sqrt{h}}$ returns a value between 0.3 to 1.5, a success message box will be shown, otherwise a message box will notify the user that roof openings cannot be calculated because of calculus instability.

Another important parameter to be set is the fire growth speed - recognised in several legislations as t_α - in order to generate the heat release ratio diagram. The user can type manually this parameter manually:

- **Ultra-fast combustion** corresponds to a value of t_α equal to 75 s;
- **Fast combustion** corresponds to a value of t_α equal to 150 s;

- **Medium combustion** corresponds to a value of t_α equal to 300 s;
- **Slow combustion** corresponds to a value of t_α equal to 600 s;

The last required input concerns the end purpose of the analysis. In other words, the user has to select for what the generated diagram will be used for:

- **Eurocode 1 - Appendix A, Eurocode 1 - Appendix B, CFAST model:** this entry is chosen for numerical simplified fire models, reported in Eurocode 1 - Appendix A and Eurocode 1 - Appendix B, and for advanced numerical zone models (such as a CFAST model tool). In order to generate the diagram, the user must type the specific design fire load, calculated as:

$$q_{f,d} = \delta_{q_1} \cdot \delta_{q_2} \cdot \delta_n \cdot q_f \quad (\text{A.3})$$

expressed in [$\frac{MJ}{m^2}$], where:

- δ_{q_1} : is the fire risk factor, depending on the floor area of the fire compartment;
 - δ_{q_2} : is the fire risk factor, depending on the type of activity done inside the fire compartment;
 - δ_n : is the coefficient to consider the management of the protective measures;
 - q_f : is the specific fire load, expressed in [$\frac{MJ}{m^2}$];
- **Eurocode 1 - Appendix C, FDS model:** this entry is chosen for localised fire models, reported in Eurocode 1 - Appendix C, and for advanced numerical CFD model (such as a FDS model tool). In order to generate the diagram, the user must type the specific fire load, calculated as:

$$q_f = \frac{\sum_{i=1}^n g_i \cdot H_i \cdot m_i \cdot \psi_i}{A} \quad (\text{A.4})$$

expressed in [$\frac{MJ}{m^2}$], where::

- g_i : is the i-th combustible material weight, expressed in [kg];
- H_i : is the i-th combustible material lower heat power, expressed in [$\frac{MJ}{kg}$];

- m_i : is the i-th combustible material participation coefficient: it is equal to 0.8 for cellulosic or wooden materials and is equal to 1.0 for all the other materials;
- ψ_i : is the i-th combustible material limit participation coefficient: it is equal to 0 for materials in fire-resistant containers, is equal to 0.85 for materials in containers which are not fire-resistant and is equal to 1.0 for all the other situations;

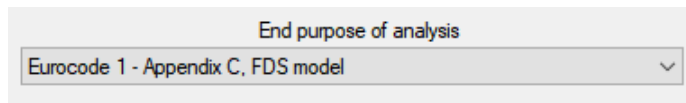


Figure A.7: HRRSprinkler Gen - End purpose of analysis selection

When the user has typed all the aforementioned parameters, by pressing the button "Generate HRR", the software will plot the diagram. Once the diagram has been generated, the values of important parameters are shown:

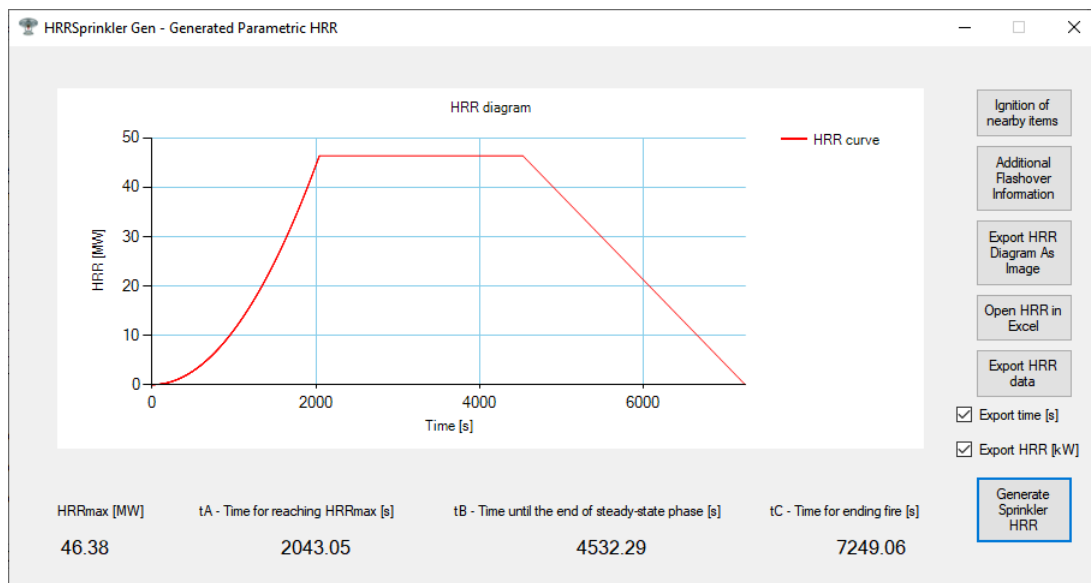


Figure A.8: HRRSprinkler Gen - Generation of HRR diagram

- HRR_{max} : maximum heat release rate, calculated as previously said, expressed in [MW]
- t_A : time for reaching the maximum heat release rate - the beginning of the steady-state phase of the fire, expressed in [s] and calculated as

$$t_A = \sqrt{\frac{RHR_{max} \cdot t_a^2}{1000}};$$

- t_B : time until the end of the steady-state phase of the fire, expressed in [s] and calculated as $t_B = t_A + \frac{0.7 \cdot q_f \cdot A - 0.333 \cdot \alpha \cdot t_a^2}{RHR_{max}}$;
- t_C : time for the ending of the fire, expressed in [s] and calculated as $t_C = t_B + \frac{0.6 \cdot q_f \cdot A}{RHR_{max}}$;

From this window, the user is able to:

- **Calculating the time of ignition of nearby items**
- **Calculating additional information about the flashover**
- **Exporting the HRR diagram as an image**
- **Opening the HRR diagram on Microsoft Excel**
- **Exporting the HRR diagram as data**
- **Generating a HRR diagram with the correction of a sprinkler system**

A.3.1.1 Calculating the time of ignition of nearby items

The American NFPA 555 legislation reports three different equations to estimate the minimum heat release rate for ignition of nearby items; then the value of the time is calculated as $t_{ignition} = \sqrt{\frac{RHR_{min}}{\alpha}}$. This approach is mathematically stable for values of distance - called D in the following expressions - equal or less than 2 meters and values of RHR_{min} not higher than RHR_{max} ; for this reason the software is endowed with a convergence check to calculate the maximum distance - which is shown to the user - in order to obtain reliable results. If a distance higher than this value is typed, a message box will notify the user that the calculus is unstable. The equations from the NFPA 555 are for:

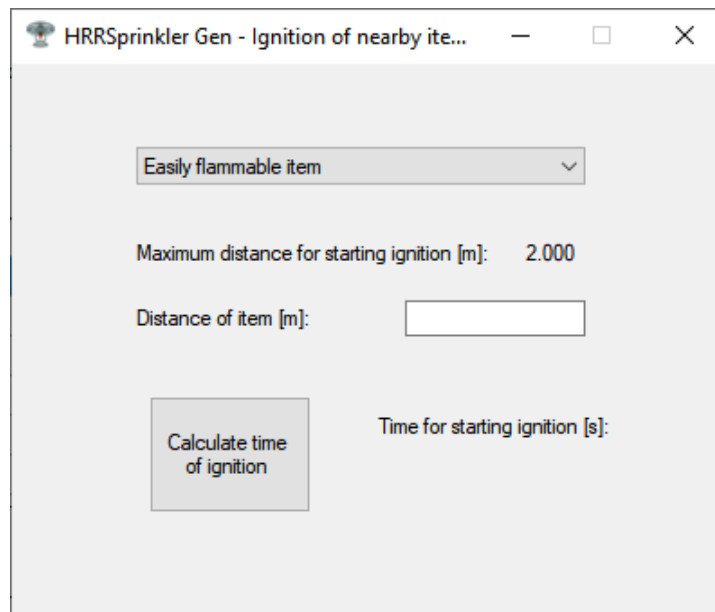


Figure A.9: HRRSprinkler Gen - Ignition of nearby items

- **Easily flammable items:** such as curtains, mats, newspapers, etc., that are invested with values of thermal flows of around $10 \frac{kW}{m^2}$; for this kind of material, $RHR_{min} = 30 \cdot 10^{\frac{D+0.08}{0.89}}$;
- **Standard ignition resistant item:** such as sofas or materials with a low thermal inertia, that are invested with values of thermal flows of around $20 \frac{kW}{m^2}$; for this kind of material, $RHR_{min} = 30 \cdot \frac{D+0.05}{0.019}$;
- **Hardly flammable items:** such wood, thermosetting plastic or materials with high thermal inertia, that are invested with values of thermal flows of around $40 \frac{kW}{m^2}$; for this kind of material, $RHR_{min} = 30 \cdot \frac{D+0.02}{0.0092}$;

A.3.1.2 Calculating additional information about the flashover

The American NFPA 555 legislation reports two different approaches, both based on the energetic balance of hot gases on the ceiling of a fire compartment. These approaches are useful to understand which thermal power causes flashover and the time in which it occurs. Here are the methods:

- **The Thomas Method:** for this method, no parameters are requested to be typed by the user and the flashover time and HRR are calculated

only by pressing the "Calculate" button; the method is based on the following equation:

$$RHR_{flashover} = 7.8 \cdot A_T + 378 \cdot A_{v_{equiv}} \cdot h_{v_{equiv}} \quad (A.5)$$

where:

- A_T : the difference between the total surface of the fire compartment and $A_{v_{equiv}}$, expressed in m^2 ;
 - $A_{v_{equiv}}$: calculated as above;
 - $h_{v_{equiv}}$: calculated as above;
- **The Babrauskas Method:** this method requires that the user types several values; to help the user, default values are suggested; according to this approach, $RHR_{flashover}$ is calculated as follows:

$$RHR_{flashover} = c_p \cdot m_u \cdot (T_g - T_{env}) + \varepsilon \cdot \sigma \cdot (T_g^4 - T_{env}^4) \quad (A.6)$$

where:

- c_p : hot gases specific heat - set by default to $1 \frac{kJ}{kg \cdot K}$;
- m_u : combustion products mass flow - set by default to $0.5 \cdot A_{v_{equiv}} \cdot \sqrt{h_{v_{equiv}}}$;
- T_g : hot gases temperature - set by default to $600^\circ C$;
- T_{env} : environment temperature - set by default to $20^\circ C$;
- ε : surface emissivity - set by default to 0.5;
- σ : Stefan–Boltzmann constant - $5.67 \cdot 10^{-11} \frac{kW}{m^2 \cdot K^4}$;

If *Eurocode 1 - Appendix A*, *Eurocode 1 - Appendix B*, *CFAST model* is selected as end purpose of analysis, it possible, from this interface, to calculate the maximum gas temperature, reached during the fire, with the following Eurocode 1 formula:

$$T_{g,max} = 6000 \cdot (1 - e^{-\frac{0.1}{O}}) \cdot \sqrt{O} \cdot [1 - e^{-0.00286 \cdot A \cdot \frac{q_{f,d}}{\sqrt{(A_v \cdot A_T)}}}] \quad (A.7)$$

where:

- O : is the opening factor, calculated as $O = \frac{A_v \cdot \sqrt{h_{eq}}}{A_T}$;
- A : is the floor area, expressed in m^2 ;
- A_v : calculated as previously said;
- A_T : calculated as previously said;

HRRSprinkler Gen - Additional Flashover Information

Flashover Babrauskas approach

Surface emissivity: 0.5

Specific heat capacity [kJ/kg K]: 1

Percentage of Radiative Power Loss: 40

Combustion Gas Temperature [°C]: 600

Environment Temperature [°C]: 20

Reached maximum gas temperature [°C]: -

Calculate

Flashover Heat Release Ratio [MW]: -

Flashover Time [s]: -

Figure A.10: HRRSprinkler Gen - Additional flashover information

A.3.1.3 Exporting the HRR diagram as an image

The user is allowed to save diagrams as images, with the format shown in the chart window. The user can save these graphs as PNG, JPEG, Bitmap and TIFF image formats.

A.3.1.4 Opening the HRR diagram on Microsoft Excel

In this section, the software implements an interoperability feature with Microsoft Excel, in order to directly export diagrams by points. It is recommended to have a working installation of Microsoft Office, version 2007 or newer. Compatibility with older versions of Microsoft Office could not be granted because of different format compilation of .xlsx files from .xls ones. If the user has installed alternative version of Microsoft Office Suite - such as Open Office or Libre Office - this feature will not work and, in order to export these diagrams by point, the "Exporting Diagram As Data" function must be used. The next paragraph is about this function.

A.3.1.5 Exporting the HRR diagram as data

In order to have a wider compatibility with common-use applications, the diagrams by points can be saved as the most versatile file format:

- **Workbook files:** diagrams can be saved as Microsoft Excel 2000-2003 files - .xls - and as Microsoft Excel 2007 or newer files - .xlsx;
- **Data files:** diagrams can be saved as Comma Separated Values files - .csv - and as a text file - .txt.

A.3.1.6 Generating a HRR diagram with the correction of a sprinkler system

The generation of a HRR diagram with a sprinkler system depends on several settings, reported on the HRR Sprinkler User Interface.

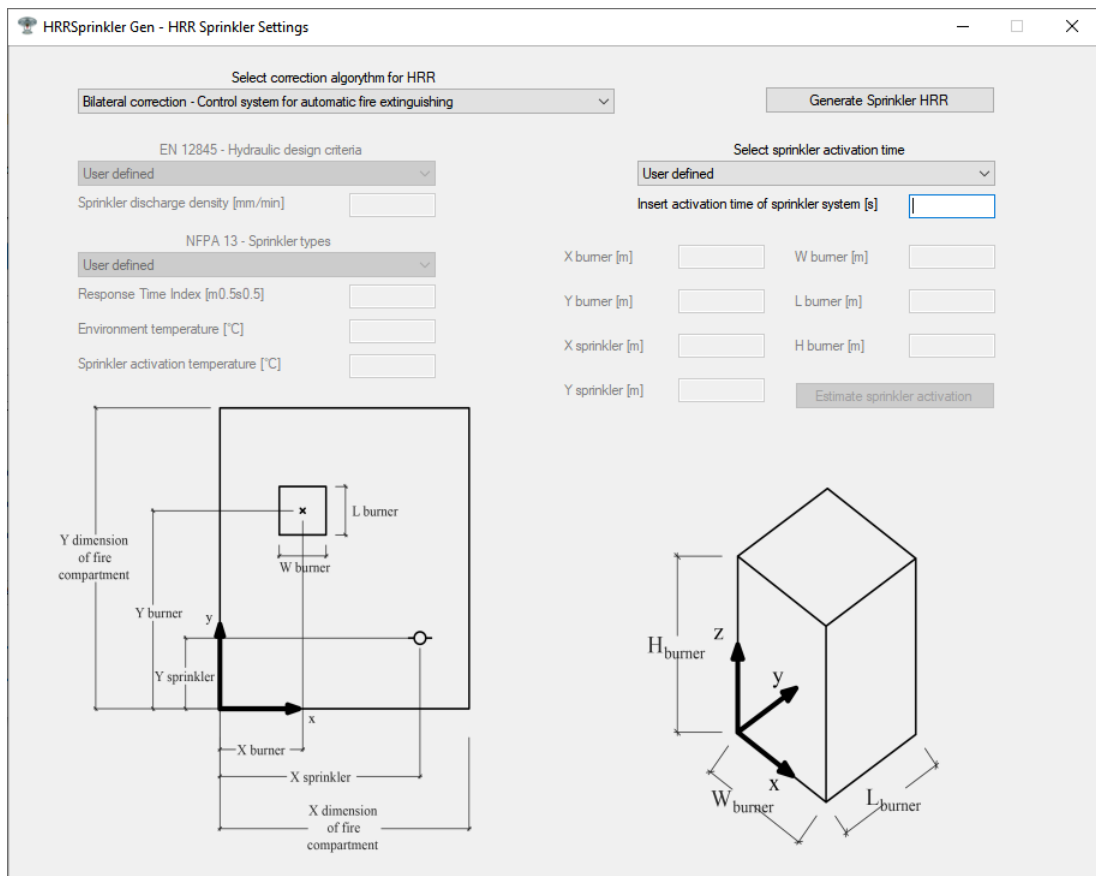


Figure A.11: HRRSprinkler Gen - HRR Sprinkler User Interface

First of all, the sprinkler activation time can be set in two different ways:

- **User defined:** maybe the most common way to know the time of activation of the sprinkler system is to perform an analysis on an advanced numeric calculator - such as FDS - of a 3D building model,

endowed with a sprinkler, and to read its activation time; once this is done, typing this time into this software generates the modified HRR;

- **Iterate calculus for estimated sprinkler activation time:** this function makes this software work as a standalone software too: if the user wants to by-pass the first FDS analysis, an iterative calculus is embedded in the software, in order to calculate the activation time of the sprinkler system. This time is calculated with regard to the temperature that, when it reaches the sprinkler target temperature, activates the sprinkler system:

$$T_{sprinkler}(t_{i+1}) = T_{sprinkler}(t_i) + [T_{jet}(t_{i+1}) - T_{sprinkler}(t_i)] \cdot (1 - e^{-\frac{1}{\tau}}) + [T_{jet}(t_{i+1}) - T_{jet}(t_i)] \cdot t \cdot (e^{-\frac{1}{\tau}} + \frac{1}{\tau} - 1) \quad (\text{A.8})$$

where:

- $T_{sprinkler}$: is the activation sprinkler temperature - set by default to 74°C;
- r : is the radial distance from the burner to the sprinkler, expressed in [m];
- H : is the distance from the top of the burner to the ceiling, expressed in [m];
- T_{jet} : is the ceiling jet hot gases temperature, expressed in °C; if $\frac{r}{H}$ is higher than 0.18, T_{jet} is calculated as $T_{jet} = T_{env} + \frac{5.38 \cdot (\frac{HRR}{r})^{0.666}}{H}$; otherwise T_{jet} is calculated as $T_{jet} = T_{env} + \frac{16.9 \cdot HRR^{0.666}}{H^{1.666}}$;
- u_{jet} : is the ceiling jet hot gases maximum speed, expressed in $\frac{m}{s}$; if $\frac{r}{H}$ is higher than 0.15, u_{jet} is calculated as $u_{jet} = \frac{0.197 \cdot HRR^{0.333} \cdot \sqrt{H}}{r^{0.833}}$; otherwise u_{jet} is calculated as $u_{jet} = 0.947 \cdot (\frac{HRR}{H})^{0.333}$;
- **RTI**: Response Time Index, calculated in $\sqrt{m \cdot s}$, whose values are indicated from NFPA 13 American Standard - or set as User Defined:

| Sprinkler sensibility | Average RTI Values $\sqrt{m \cdot s}$ |
|-----------------------|---------------------------------------|
| Quick response | 50 |
| Special response | 65 |
| A Standard response | 140 |
| B Standard response | 275 |

- τ : time constant, calculated as $\frac{RTI}{\sqrt{u_{jet}}}$;

In order to define r and H , the user must type the X-location and the Y-location of the burner center of mass, the X-location and Y-location of the sprinkler and the width, the depth and the height of the burner.

The other important aspect about the generation of the modified HRR concerns the choice of a correction algorithm. The construction of the modified diagram occurs in two parts: before the time of activation of the sprinkler system, the correct diagram has the same distribution as the native one; when the activation time is reached, a correction algorithm is applied. As previously said, in this section there are three models for correction of the HRR diagram, which correspond to three extinguish sprinkler systems:

- **Automatic system for complete fire extinguishing using inert gas:** this algorithm is taken from the British Standard BS PD 7974-3 and it is representative of situations in which inert gas sprinkler system are installed. This correction is made with the following formula:

$$HRR(t) = HRR(t_{sprinkler}) \cdot e^{\frac{t_{sprinkler} - t_{env}}{3 \cdot \delta - 1.85}} \quad (A.9)$$

where:

- δ : is the discharge density of the sprinkler, expressed in $\frac{mm}{s}$; please note: the input, in the software is expressed in $\frac{mm}{min}$, in accordance with legislation; in this section, the software implements several values of sprinkler discharge density, taken from the European Standard EN 12845:

| Hydraulic design criteria | Sprinkler density discharge [$\frac{mm}{min}$] |
|---------------------------|--|
| LH | 2.25 |
| OH1 | 5 |
| OH2 | 5 |
| OH3 | 5 |
| OH4 | 5 |
| HHP1 | 7.5 |
| HHP2 | 10 |
| HHP3 | 12.5 |
| HHS-ST1-1 | 7.5 |
| HHS-ST1-2 | 10 |
| HHS-ST1-3 | 12.5 |
| HHS-ST1-4 | 15 |
| HHS-ST1-5 | 17.5 |
| HHS-ST1-6 | 20 |
| HHS-ST1-7 | 22.5 |
| HHS-ST1-8 | 25 |
| HHS-ST1-9 | 27.5 |
| HHS-ST1-10 | 30 |
| HHS-ST2-ST4-1 | 7.5 |
| HHS-ST2-ST4-2 | 10 |
| HHS-ST2-ST4-3 | 12.5 |
| HHS-ST2-ST4-4 | 15 |
| HHS-ST2-ST4-5 | 17.5 |
| HHS-ST2-ST4-6 | 20 |
| HHS-ST2-ST4-7 | 22.5 |
| HHS-ST2-ST4-8 | 25 |
| HHS-ST2-ST4-9 | 27.5 |
| HHS-ST2-ST4-10 | 30 |
| HHS-ST3-ST5-ST6-1 | 7.5 |
| HHS-ST3-ST5-ST6-2 | 10 |
| HHS-ST3-ST5-ST6-3 | 12.5 |
| HHS-ST3-ST5-ST6-4 | 15 |
| HHS-ST3-ST5-ST6-5 | 17.5 |

- **Exponential correction - Automatic system for complete fire extinguishing using water:** this algorithm - as above - decreases with an exponential function:

$$HRR(t) = HRR(t_{sprinkler}) \cdot e^{0.0023 \cdot (t_{sprinkler} - t_{env})} \quad (A.10)$$

- **Bilateral correction - Control system for automatic fire extinguishing:** this is the most common algorithm to modify a HRR diagram. When $t_{sprinkler}$ is reached, the value of $HRR(t_{sprinkler})$ remains constant for all the duration of the fire, until the fire begins to abate. In other words, the curve is obtained replacing $t_{sprinkler}$ to t_A and $HRR(t_{sprinkler})$ to HRR_{max} ; then t_B and t_C are the same values of the native curve.

A.3.1.7 Example of generation of a parametric HRR using the complex approach

This is performed on an industrial warehouse, assumed to be a single fire compartment.

A.3.1.8 Data to be stored

- **Dimensions of the fire compartment:** 30 m wide, 25 m deep, 4.50 m high;
- **Specific fire load:** assuming $q_f = 300 \frac{MJ}{m^2}$;
- **Fire growth rate:** the fire is assumed to have a medium speed growth;
- **Kind of combustible:** combustible is a cellulosic material;
- χ_A : 100% of oxygen is burned;
- **Ventilation openings:** there are two doors, both are 2.20 m high but one is 1.80 m wide and the other is 3.00 m wide; six facade ventilation windows are provided, 1.11 m wide, 1.90 m high and positioned 1.10 m from the ground; four roof ventilation openings are provided, 1.00 m wide, 1.00 m deep;
- **End purpose of analysis:** the diagram is going to be modified in order to be imported in a FDS calculator.

HRRSprinkler Gen - Parametric HRR - Complex Approach

HRR calculus approach: Kawagoe Approach Home

q_f - Specific fire load [MJ/m²]
 $q_{f,d}$ - Specific design fire load [MJ/m²]
 x_A - Combustion efficiency [%]

t_{gr} - Fire growth rate coefficient [s] Medium
 A_f - Fire area [m²]
 Wooden or cellulosic material

Insert opening area dimensions

| | w.vent [m] | h.vent [m] | z0 [m] |
|--|------------|------------|--------|
| | 1.11 | 1.9 | 1.1 |
| | 1.11 | 1.9 | 1.1 |
| | 1.11 | 1.9 | 1.1 |
| | 3 | 2.2 | 0 |
| | 1.8 | 2.2 | 0 |

Roof openings
 Add row
 Delete row
 Clear Data
 Paste Data

P_c - Lost Thermal Energy with combustion [MJ/kg of air]

Cellulose

X dimension of the fire compartment [m]
 Y dimension of the fire compartment [m]
 Z dimension of the fire compartment [m]

End purpose of analysis

Generate HRR Ready

(a) Burner and facade ventilation openings settings

HRRSprinkler Gen - Roof openings

Add roof openings Save Data Discard Data

| | w.roof [m] | h.roof [m] | w.vent [m] | h.vent [m] | dH [m] |
|---|------------|------------|------------|------------|--------|
| ▶ | 1 | 1 | 1.11 | 1.9 | 2.45 |
| | 1 | 1 | 1.11 | 1.9 | 2.45 |
| | 1 | 1 | 1.11 | 1.9 | 2.45 |
| | 1 | 1 | 1.11 | 1.9 | 2.45 |
| * | | | | | |

Add row Delete row Clear Data Paste Data

(b) Roof ventilation openings settings

Figure A.12: HRRSprinkler Gen - Software setting for the example 4.1.7

A.3.1.9 Setting the software

For this application, once HRRSprinkler Gen is opened, the user must choose "Parametric HRR curve - Advanced approach". In this case, both facade ventilation openings and roof ventilation openings are provided, so the calcu-

lus of the diagram must be done through Kawagoe approach. For this roof openings pattern, the convergence check is successful and roof openings are initialised. Once the software is set, the "Generate HRR" button must be pressed.

A.3.1.10 Output of the software

Once the diagram is generated, it is possible to export it or to calculate several details about the fire, as previously said. For this example:

- **HRR_{max}** : 9390 kW;
- **t_A** : 919.47 s for reaching maximum heat release rate;
- **t_B** : 16262.15 s for the end of the steady-state phase of the fire;
- **t_C** : 29675.47 s for the natural fire extinguish;

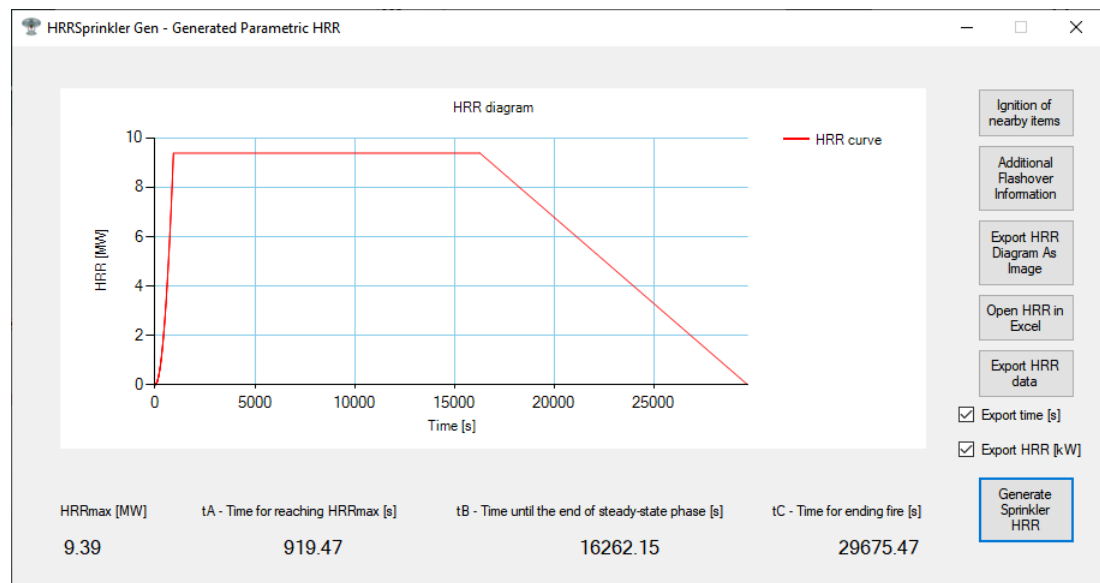
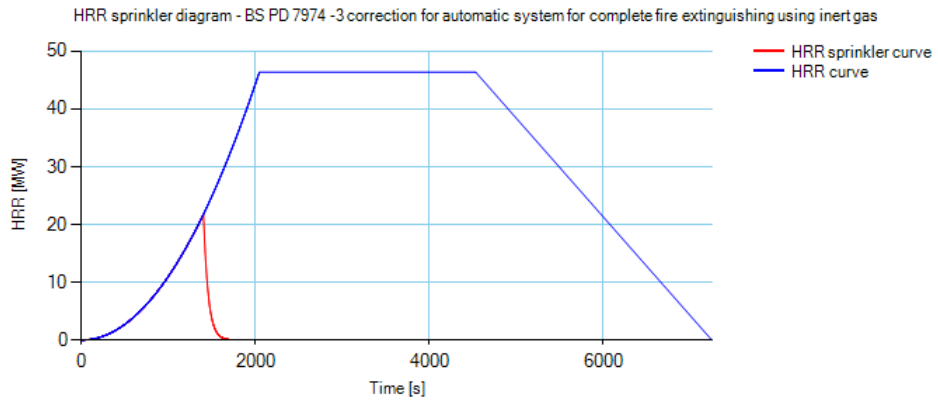


Figure A.13: HRRSprinkler Gen - Output HRR diagram for the example 4.1.7

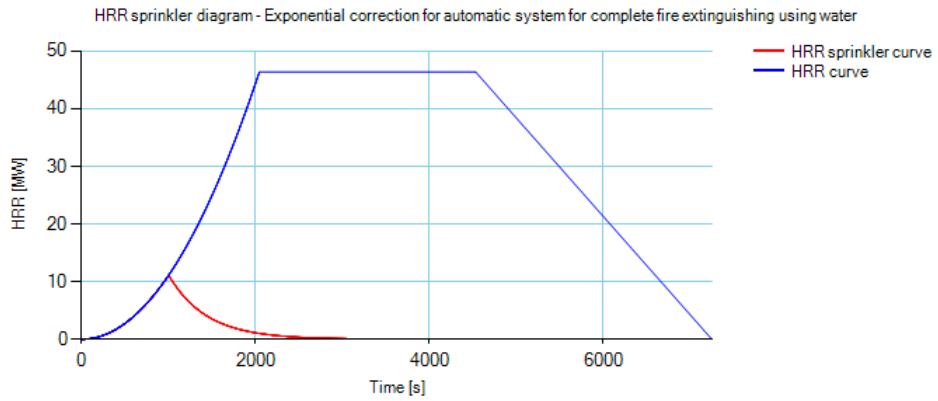
- **Ignition of nearby items:**
 - **Easily flammable items:** a 2.00 m maximum distance of calculus is allowed; for example for a distance equal to 1.00 m, the ignition of the item occurs in 210 s; for a distance equal to 1.50 m, the ignition occurs in 401 s;

- **Standard ignition resistant items:** a 2.00 m maximum distance of calculus is allowed; for example for a distance equal to 1.00 m, the ignition of the item occurs in 386 s; for a distance equal to 1.50 m, the ignition occurs in 469 s;
- **Hardly flammable items:** a 2.00 m maximum distance of calculus is allowed; for example for a distance equal to 1.00 m, the ignition of the item occurs in 547 s; for a distance equal to 1.50 m, the ignition occurs in 668 s;
- **Additional flashover information:** both methods - since they are not considering roof openings - show how roof ventilation reduces the value of maximum heat released ratio. Flashover values are, in fact, higher than the theoretical value of HRR_{max} calculated for this situation.
 - **The Thomas approach:** flashover occurs after 1562 s, with a heat released power equal to 21721 kW;
 - **The Babrauskas approach:** flashover occurs after 1400 s, with a heat released power equal to 21779 kW; for this approach, standard boundary conditions have been applied: surface emissivity equal to 0.5, hot gases specific heat equal to $1 \frac{kJ}{kg \cdot K}$, 40% of radiative power loss, environment temperature equal to 20°C and hot gases temperature equal to 600°C.

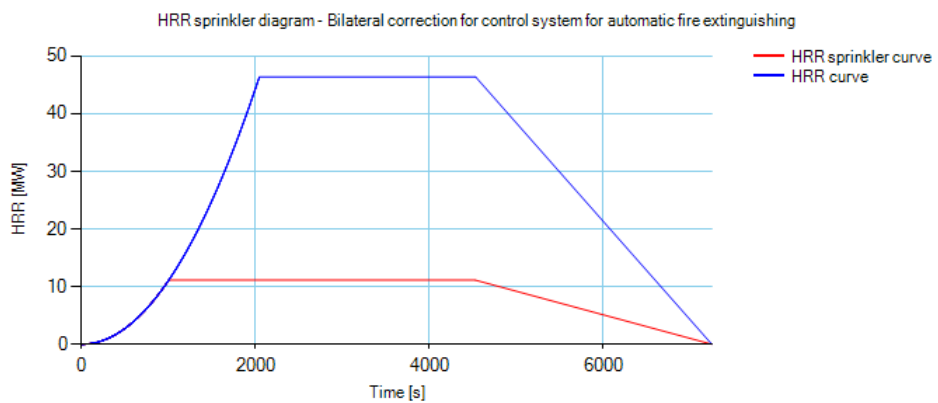
Note that in the same situation, when roof ventilation openings are not considered, there is a maximum heat release rate value equal to 52140 kW, with flashover that occurs approximately at 42% of the maximum releasable power; this value is reliable, since several experimental tests showed that flashover occurs between 30% and 70% of HRR_{max} .



(a) BS PD 7974-3 Correction - Automatic system for complete fire extinguishing using gas; Sprinkler hydraulic class §EN 12845: HHP3



(b) Exponential correction - Automatic system for complete fire extinguishing using water



(c) Bilateral correction - Control system for automatic fire extinguishing

Figure A.14: HRRSprinkler Gen - Output sprinkler diagrams for the example 4.1.7

A.3.1.11 Plotting modified diagrams

In this section it is possible to modify the HRR diagram in three different ways. Here it is also possible to estimate the sprinkler activation time. These are the settings:

- **EN 12845 HHP3 Sprinkler:** with a discharge density equal to 12.5 mm/min
- **NFPA 13 Quick response Sprinkler:** with a RTI equal to $50 \sqrt{m \cdot s}$;
- **Dimension of the burner:** assumed to be a cube with 1.50 m side;
- **Location of the sprinkler:** assumed to be 15 m far along the width direction (X axis) and 15 m far along the depth dimension (Y axis);
- **Location of the burner - center of mass:** assumed to be 10 m far along the width direction (X axis) and 10 m far along the depth dimension (Y axis);

With this data, the estimated activation time is equal to 60 s, but an alert occurs: since a medium growth speed fire has been defined, the software tells the user that this algorithm is stable for a faster growth speed of fire. For this example, the plotted diagrams have been plotted assuming an activation time of the sprinkler equal to 1000 s.

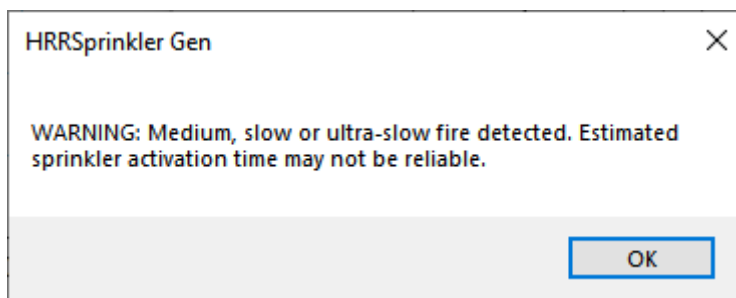


Figure A.15: HRRSprinkler Gen - Software instability for estimating sprinkler activation time with slower fire

At this point, it is possible to save or export the diagram and to work on it.

A.3.2 Parametric HRR - Simple approach

This approach is focused on generating an HRR parametric diagram, through a simplified method - that does not consider ventilation -, reported both in the Eurocode 1 and in the Italian Fire Prevention Standard. As previously said, there is a mathematical correlation between the maximum released heat rate and the value of the time of beginning of the steady-state phase of the fire:

$$t_A = \sqrt{RHR_{max} \cdot \frac{t_\alpha^2}{1000}} \quad (\text{A.11})$$

To select this approach, from the main screen, "Parametric HRR curve - Simple approach" button must be pressed.

Thus the user, depending on the available data, decides to type the value of t_A or RHR_{max} . The other parameters that the user must provide are the fire growth speed - t_α , the specific fire load - q_f , expressed in [$\frac{MJ}{m^2}$] - and the fire area - A_f , expressed in [m^2] - that can be the fire compartment area or the burner floor surface - in case of non-uniform distribution of combustible in the environment.

Once generated the graph, the user is able to:

- **Calculate the time of ignition of nearby items:** as explained in the **Paragraph 4.1.1**
- **Export the HRR diagram as an image:** as explained in the **Paragraph 4.1.3**
- **Open the HRR diagram on Microsoft Excel:** as explained in the **Paragraph 4.1.4**
- **Export the HRR diagram as data:** as explained in the **Paragraph 4.1.5**
- **Generate a HRR diagram with the correction of a sprinkler system**

A.3.2.1 Generating a HRR diagram with the correction of a sprinkler system

As this approach is very simplified compared to the complex approach, the correction models are simplified too. At first, in this section of the software it is not possible to estimate the sprinkler activation time. Therefore, the user has only two ways to modify an HRR diagram:

- **Control system for automatic fire extinguish:** this algorithm is the same as discussed in **Paragraph 4.1.6**, subparagraph **Bilateral correction - Control system for automatic fire extinguish**;
- **Automatic system for complete fire extinguish:** this algorithm is similar to the one explained in **Paragraph 4.1.6**, subparagraph **Exponential correction - Automatic system for complete fire extinguish using water**; in this case, when the sprinkler system activation occurs, a linear decrease of the heat during over time is embedded - unlike the exponential decrease of the aforementioned method. From the point $(t_{sprinkler}, RHR_{sprinkler})$, the linear decrease has the same angular coefficient as the natural fire decrease - the straight line passing through the points (t_B, RHR_{max}) and $(t_C, 0)$. This correction algorithm will be clearer in the next paragraph, in which an example of application of this method is fully explained.

A.3.2.2 Example of generation of a parametric HRR using simple approach

This example is on a fire compartment of a shopping centre.

A.3.2.3 Data to be stored

- **Dimensions of the fire compartment:** 700 m^2 ;
- **Dimensions of the burner:** industrial fridge with a 50 m^2 floor surface;
- **Specific fire load:** assuming $q_f = 550 \frac{\text{MJ}}{\text{m}^2}$;
- **Fire growth rate:** the fire is assumed to have a fast speed growth;
- **Time for reaching HRR_{max} :** 290 s are required to have a fully developed fire;
- **Kind of combustible:** combustible is a cellulosic material;
- **Sprinkler activation time:** from a FDS analysis, 150 s of time are needed to activate the system; both of the methods of sprinkler system are being analysed.

A.3.2.4 Setting the software

Once opened HRRSprinkler Gen, the user must choose for this application "Parametric HRR curve - Simplified approach". In this case, the data reported in the section **Data to be stored** can be simply reported in the User Interface. Once setted the software, "Generate HRR" button must be pressed.

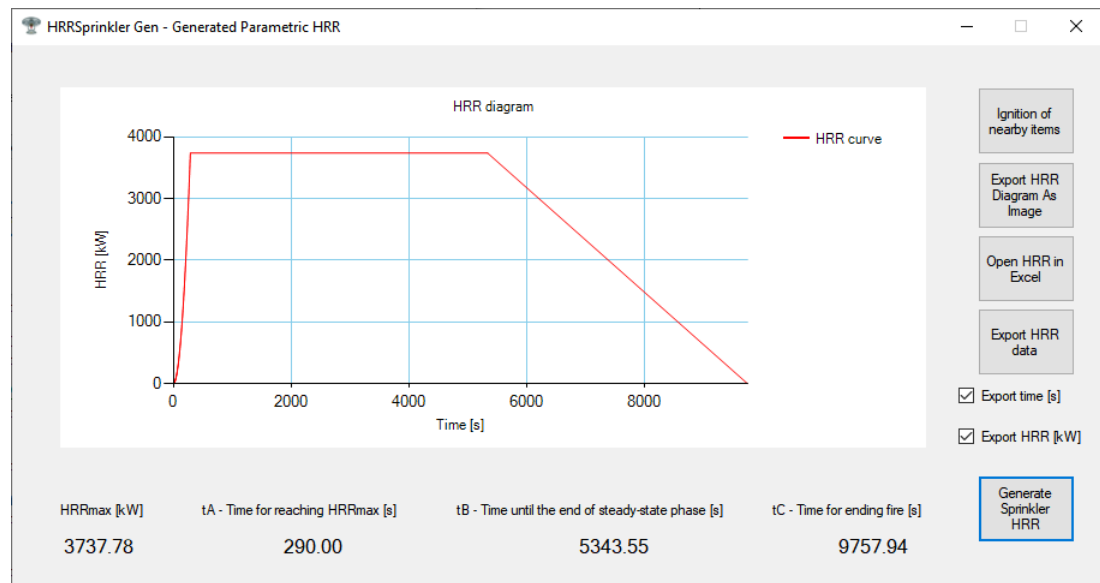
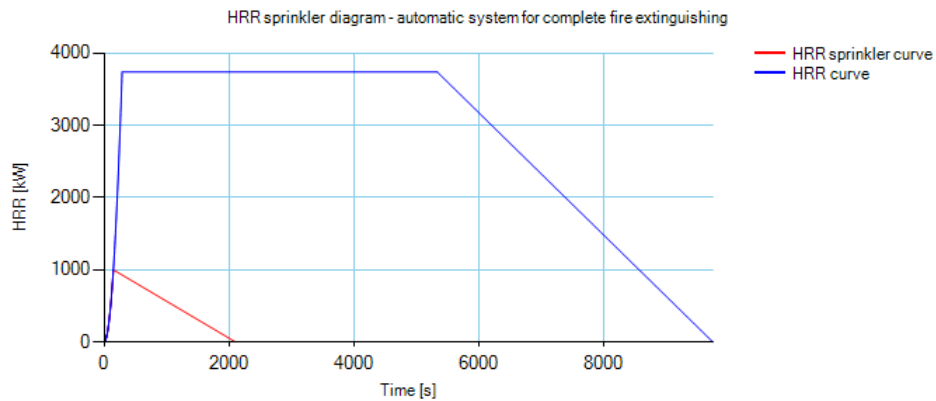


Figure A.16: HRRSprinkler Gen - Output HRR diagram for the example 4.2.2

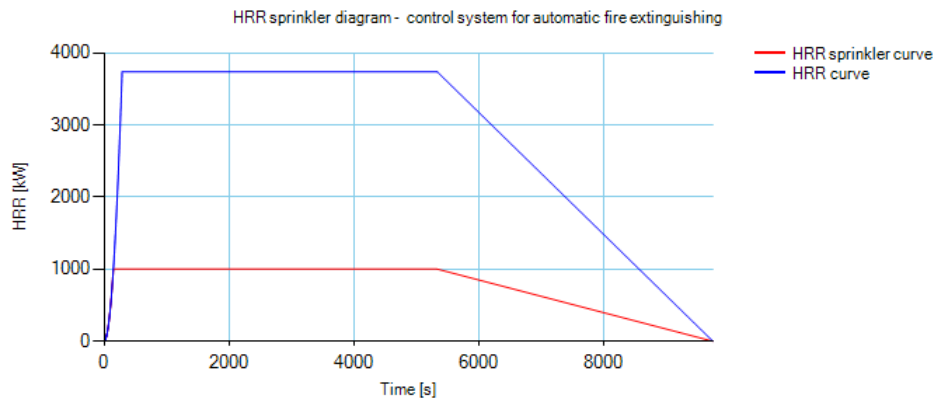
A.3.2.5 Output of the software

Once the diagram is generated, it is possible to export it or to calculate several details about the fire, as previously said. For this example:

- **HRR_{max}** : 3737.38 kW;
- **t_A** : 290.00 s for reaching maximum heat release rate;
- **t_B** : 5343.55 s for the end of the steady-state phase of the fire;
- **t_C** : 9757.94 s for the natural fire extinguish;
- **Ignition of nearby items:**
 - **Easily flammable items:** a 1.78 m maximum distance of calculus is allowed; for example for a distance equal to 1.00 m, the



(a) *HRRSprinkler Gen - Modified HRR for automatic system for complete fire extinguishing*



(b) *HRRSprinkler Gen - Modified HRR for control system for automatic fire extinguishing*

Figure A.17: HRRSprinkler Gen - Output diagram for the example 4.2.2

A.3.3 Premade parametric HRR

In this section, the user can quickly generate premade HRR diagrams and modify them to take account of the activation of a sprinkler system. To do this, from the main page, the "Premade parametric HRR curves" button must be pressed.

Two algorithms for modifying the diagrams have been embedded, since this section - as the previous one - is a simplified way to generate HRR diagrams. The user is able to understand values and distribution about the fire and maximum released heat rate can be limited through the application of the aforementioned two correction mathematics models.

Thus, the available diagrams have been divided in two groups: one for envi-

ronments and one for materials or items.

- **Environmental HRR diagrams:** these diagrams have been chosen from reliable literature and can be useful, since these kind of environments are very common and if the user is not provided with specific studies, this is a simple way to have a rough distribution of the heat over time. The following values have been taken from the Italian ClaRaF 3.0 Database and specific fire load values have been increased, applying the statistic Gumbel distribution, of the 80% fractile coefficient. The user has only to type the value of the floor surface and the time of activation of the sprinkler system.

| Environments | $RHR_{max,f} [\frac{kW}{m^2}]$ | $t_{\alpha} [s]$ | Specific fire load $q_f [\frac{MJ}{m^2}]$ | 80% fractile - Gumbel distribution | Effective specific fire load $q_f [\frac{MJ}{m^2}]$ |
|----------------------|--------------------------------|------------------|---|------------------------------------|---|
| Office building | 250 | 300 | 420 | 1.22 | 512.4 |
| Shopping centers | 250 | 150 | 600 | 1.22 | 732 |
| Hospital bedrooms | 250 | 300 | 230 | 1.22 | 280.6 |
| Hotel bedrooms | 250 | 300 | 310 | 1.22 | 378.2 |
| Library | 500 | 150 | 1500 | 1.22 | 1830 |
| School classrooms | 250 | 300 | 285 | 1.22 | 347.7 |
| Theaters and cinemas | 500 | 150 | 285 | 1.22 | 347.7 |
| Flats | 250 | 300 | 300 | 1.75 | 525 |

- **Materials or items HRR diagrams:** these diagrams have been chosen from "SFPE Handbook of Fire Protection Engineering" and represents the most common burner items or material that can be found in buildings. In order to be generated properly, these diagrams need the value of floor surface and the corresponding specific fire load value to be typed in. Note that when wooden pallets items have been chosen, no surface floor is allowed, since EPAL pallets have a standard dimension that has been provided yet to the calculator.

Once the required parameters are typed, the diagrams can be generated by the pressure of the "Generate HRR" button. As in the previous section, the basic function for the generated diagrams are:

- **Calculating the time of ignition of nearby items:** as explained in the Paragraph 4.1.1

| Materials or items | $RHR_{max,f} [\frac{kW}{m^2}]$ | $t_{\alpha} [s]$ |
|--|--------------------------------|------------------|
| Wooden pallets: 1,20x1,20 m, stacked for 0,46 m height | 1248 | 230 |
| Wooden pallets: 1,20x1,20 m, stacked for 1,52 m height | 3745 | 140 |
| Wooden pallets: 1,20x1,20 m, stacked for 3,05 m height | 6810 | 95 |
| Wooden pallets: 1,20x1,20 m, stacked for 4,88 m height | 10215 | 90 |
| Postal envelopes: stacked for 1.52m height | 397 | 180 |
| Carton box: stacked for 4,57 m height | 2270 | 57 |
| Letter tray: stacked for 1,52 m height | 8512 | 180 |
| Carton packed PE bins: stacked for 4,57 m height | 2837 | 52 |
| Carton packed glass fiber reinforced polyester shower cabin: stacked for 4,57 m height | 1298 | 80 |
| PET bottles | 6242 | 80 |
| Carton packed PET bottles: stacked for 4,57 m height | 1929 | 71 |
| Rigid foam insulating panels: stacked for 4,57 m height | 1929 | 8 |
| PS boxes | 13620 | 52 |
| Carton packed PS vats: stacked for 4,57 m height | 5107 | 100 |
| Carton packed PS toys stacked for 4,57 m height | 2043 | 104 |
| Rigid PS insulating panels: stacked for 4,57 m height | 3291 | 7 |
| PVC bottles | 3405 | 9 |
| PP vats | 4426 | 10 |
| PE and PS rolls of film: stacked for 4,57 m height | 3972 | 38 |

- **Exporting the HRR diagram as an image:** as explained in the **Paragraph 4.1.3**
- **Opening the HRR diagram on Microsoft Excel:** as explained in the **Paragraph 4.1.4**
- **Exporting the HRR diagram as data:** as explained in the **Paragraph 4.1.5**
- **Generating a HRR diagram with the correction of a sprinkler system**
 - **Control system for automatic fire extinguish:** this algorithm is the same discussed in the **Paragraph 4.1.6**, under the subparagraph **Bilateral correction - Control system for automatic fire extinguish**;
 - **Automatic system for complete fire extinguish:** this algorithm is the same discussed in the **Paragraph 4.2.1**, under the subparagraph **Automatic system for control fire extinguish**;

The behaviour of this section is really similar to the one described in the example discussed in the **Paragraph 4.2.2**: the user is advised to follow this chapter for setting the program and the **Paragraph 4.1.6** - subparagraph **Bilateral correction - Control system for automatic fire extinguish** and **Paragraph 4.2.1** - subparagraph **Automatic system for control fire extinguish** to generate the modified HRR.

A.3.4 Experimental HRR

In this section, it is possible to plot and modify experimental HRR diagrams. To access this function, from the main screen, the "Experimental HRR curves" button needs to be pressed.

When these commands appear, the user is able to import HRR experimental diagrams by points. To import the diagrams, it is advised to paste data from a dataset or a workbook. From the version 1.00 BETA, a graph digitizer has been embedded, in order to build the HRR diagram from an image. Finally, the fire growth rate needs to be set, in order to calculate secondary information about the fire.



Figure A.18: HRRSprinkler Gen - Experimental HRR diagrams importing

After pressing on "Generate HRR" button, the diagram will be generated and it is possible to:

- **Calculate the time of ignition of nearby items:** as explained in the **Paragraph 4.1.1**
- **Export the HRR diagram as an image:** as explained in the **Paragraph 4.1.3**
- **Open the HRR diagram on Microsoft Excel:** as explained in the **Paragraph 4.1.4**
- **Export the HRR diagram as data:** as explained in the **Paragraph 4.1.5**
- **Generate a HRR diagram with the correction of a sprinkler system**

The exporting function, that may seem useless, is provided because the software rebuilds the diagram - through a linear interpolation algorithm - in order to correct it with more accuracy, when applying the sprinkler system. Thus, an intermediate step before modifying the curve is provided, in which the user is able to export the new diagram by points.

A.3.4.1 Graph digitizer for an experimental HRR diagram

A graph digitizer has been embedded from the version 1.00 BETA, in order to build an experimental HRR diagram from an image. To use this function, the "Add HRR diagram from image" button must be pressed. Once the interface appears, the first step is importing the HRR diagram as an image, from a file or directly from the image URL.

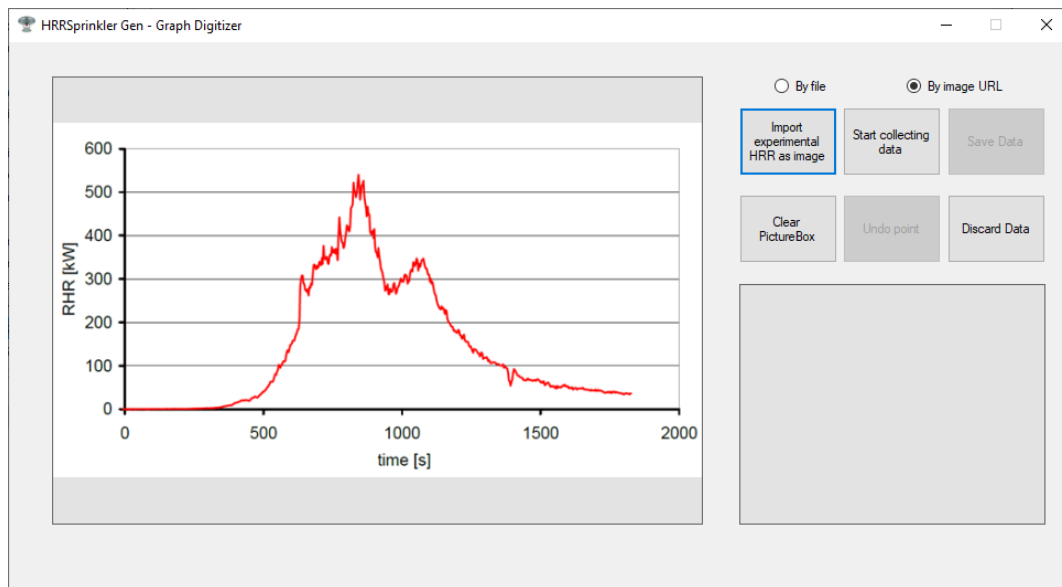


Figure A.19: HRRSprinkler Gen - Importing an HRR diagram from an image using the Graph Digitizer

For the next step, the "Start Collecting data" button must be pressed. A command string is reported on the bottom of the interface to help the user with the following steps. To pick points more easily, on the bottom right corner a cursor magnifier has been embedded. At first, the user has to pick, on the figure, the origin point of the XY reference system and, once prompted the dialog, the coordinates of the picked point must be typed. The following point to be picked is the X axis upper bound, for which the coordinates of the point on the figure must be typed too. Then, the Y axis upper bound, with the same procedure about the insertment of the coordinates points. After done this, the curve points must be picked and, once finished, the "End Collecting data" button must be pressed. Finally, the "Save Data" button needs to be pressed and a dialog is prompted, where the user has to choose the measure units of the imported diagram. The procedure has ended and the diagram can be generated from the window shown in the Figure 4.14, by the pressure of the "Generate HRR" button.

A.3.4.2 Generating a HRR diagram with the correction of a sprinkler system

The generation of a HRR diagram with a sprinkler system occurs with the same algorithms described in **Paragraph 4.1.6**, with a slightly modified interface, in order to make the user type all the parameters needed for the

analysis. Hence, it is possible to estimate the activation time for the activation of the sprinkler system and to correct the diagram with the aforementioned three models for the sprinkler systems. The following paragraph regards an example of correction of an experimental HRR diagram.

A.3.4.3 Example of generation of an experimental HRR

For this example, a supermarket warehouse is required to be investigated about the fire. A Fire Safety Engineer states that the most dangerous fire scenario is about the burning of wooden pallets, stacked for 1.44 m height. For this scenario, the HRR diagram is from the "SFPE Handbook of Fire Protection Engineering".

A.3.4.4 Data to be stored

- **Dimensions of the fire compartment:** 25 m wide, 5 m deep, 4 m high;
- **Fire growth rate:** the fire is assumed to have a fast speed growth;

A.3.4.5 Setting the software

Once HRRSprinkler Gen is opened, the user must choose for this application "Experimental HRR curve". On the next page, the heat transfer diagrams points are provided. Once the software is set, the "Generate HRR" button must be pressed.

A.3.4.6 Output of the software

Once generated the diagram, it is possible to export it or to calculate several details about the fire, as previously said. For this example:

- **HRR_{max} :** 3248.8 kW;

| Time [s] | HRR [kW] | Time [s] | HRR [kW] | Time [s] | HRR [kW] |
|-----------------|-----------------|-----------------|-----------------|-----------------|-----------------|
| 0 | 0 | 410.3 | 3001.3 | 604.81 | 2388.6 |
| 9.95 | 70.8 | 419.5 | 2760 | 615.52 | 2643.8 |
| 48.24 | 56.1 | 421.03 | 2646.5 | 623.17 | 2742.9 |
| 87.29 | 69.7 | 424.1 | 2547.2 | 631.59 | 2813.7 |
| 106.43 | 112 | 426.4 | 2490.4 | 644.61 | 2827.7 |
| 133.22 | 182.5 | 430.23 | 2476.2 | 651.51 | 2572.3 |
| 157.72 | 295.6 | 437.88 | 2575.3 | 659.94 | 2331.1 |
| 182.99 | 352 | 439.41 | 2646.2 | 663.77 | 2217.5 |
| 201.36 | 380.1 | 440.19 | 2277.4 | 675.27 | 2033 |
| 231.99 | 408.1 | 440.94 | 2660.4 | 679.87 | 1919.4 |
| 262.61 | 549.5 | 452.43 | 2404.9 | 686.76 | 1749.1 |
| 278.69 | 591.8 | 459.32 | 2433.2 | 696.72 | 1593 |
| 297.06 | 705 | 466.22 | 2390.6 | 708.98 | 1408.4 |
| 306.25 | 761.6 | 468.52 | 2277 | 733.49 | 1237.8 |
| 313.9 | 804.1 | 471.59 | 2163.5 | 751.11 | 1081.5 |
| 322.32 | 1030.9 | 476.18 | 2191.8 | 767.19 | 982 |
| 325.38 | 1130.1 | 483.07 | 2305.2 | 784.8 | 896.7 |
| 331.5 | 1271.9 | 486.13 | 2361.9 | 796.29 | 839.8 |
| 335.32 | 1456.2 | 496.09 | 2205.7 | 813.14 | 825.3 |
| 336.84 | 1626.4 | 502.99 | 2021.2 | 820.03 | 825.2 |
| 343.73 | 1839.1 | 513.71 | 1978.5 | 835.34 | 839.2 |
| 351.38 | 1938.3 | 521.36 | 1978.4 | 853.72 | 881.5 |
| 357.48 | 2548.1 | 525.19 | 1964.2 | 868.27 | 852.9 |
| 362.84 | 2746.6 | 533.62 | 1964.1 | 882.05 | 739.3 |
| 368.95 | 2973.5 | 545.87 | 1864.6 | 891.24 | 881 |
| 370.48 | 3115.3 | 553.53 | 1821.9 | 914.98 | 795.5 |
| 378.13 | 3228.7 | 562.72 | 1836 | 928.76 | 795.3 |
| 383.49 | 3242.8 | 583.39 | 1949.2 | 942.54 | 795.1 |
| 392.69 | 2987.3 | 591.04 | 2020 | 952.5 | 795 |
| 395.75 | 2930.6 | 594.1 | 2090.9 | 967.81 | 794.8 |
| 404.18 | 2887.9 | 597.16 | 2190.1 | 976.23 | 823 |
| 408 | 2958.8 | 601.75 | 2331.9 | 1002.26 | 865.2 |

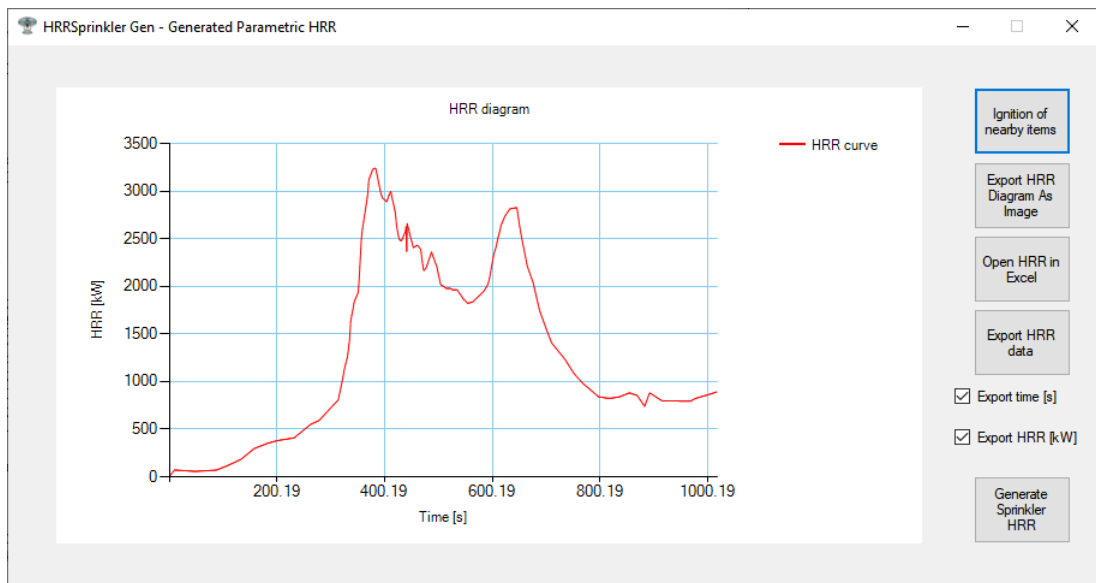
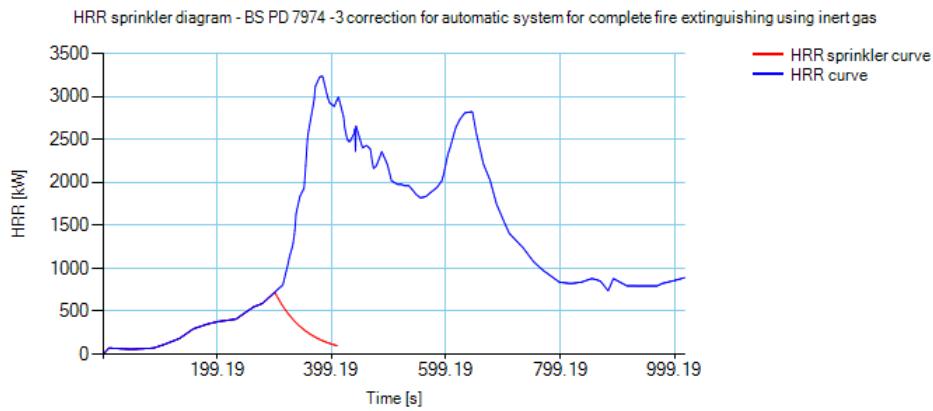


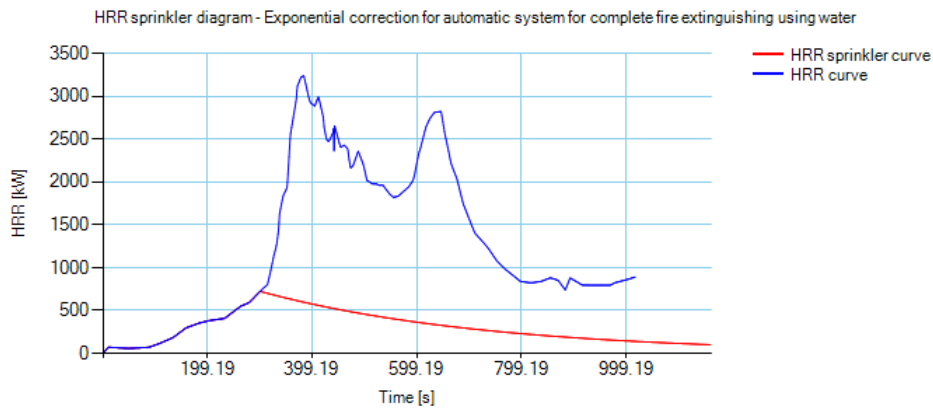
Figure A.20: HRRSprinkler Gen - Output HRR diagram for the example 4.4.2

- **Ignition of nearby items:**

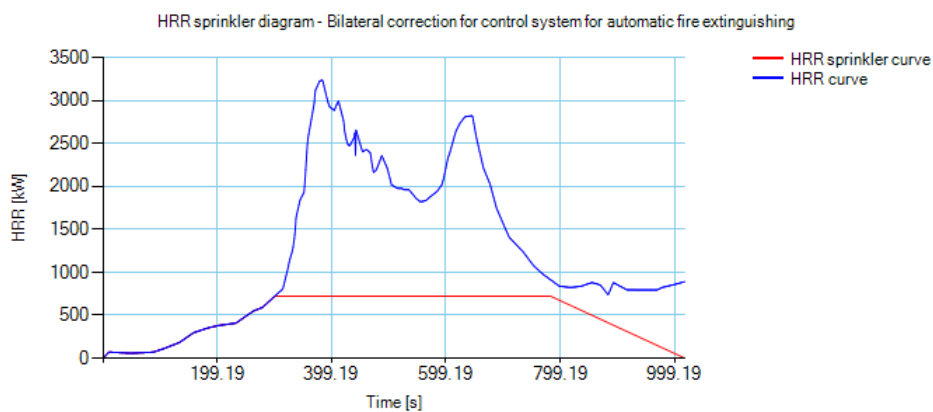
- **Easily flammable items:** a 1.73 m maximum distance of calculus is allowed; for example for a distance equal to 1.00 m, the ignition of the item occurs in 52 s; for a distance equal to 1.50 m, the ignition occurs in 100 s:
- **Standard ignition resistant items:** a 2.00 m maximum distance of calculus is allowed; for example for a distance equal to 1.00 m, the ignition of the item occurs in 97 s; for a distance equal to 1.50 m, the ignition occurs in 117 s:
- **Hardly flammable items:** a 0.98 m maximum distance of calculus is allowed; for example for a distance equal to 0.50 m, the ignition of the item occurs in 98 s; for a distance equal to 0.75 m, the ignition occurs in 119 s:



(a) BS PD 7974-3 Correction - Automatic system for complete fire extinguishing using gas; Sprinkler hydraulic class §EN 12845: HHP2



(b) Exponential correction - Automatic system for complete fire extinguishing using water



(c) Bilateral correction - Control system for automatic fire extinguishing

Figure A.21: HRRSprinkler Gen - Output sprinkler diagrams for the example 4.4.2

A.3.4.7 Plotting modified diagrams

In this section it is possible to modify the HRR diagram in three different ways. Here it is also possible to estimate the sprinkler activation time. These are the settings:

- **EN 12845 HHP2 Sprinkler:** with a discharge density equal to 10 mm/min
- **NFPA 13 Quick response Sprinkler:** with a RTI equal to $65 \sqrt{m \cdot s}$;
- **Dimension of the burner:** assumed to be a cube with 1.50 m size;
- **Location of the sprinkler:** assumed to be 17 m along the width direction (X axis) and 4 m along the depth dimension (Y axis);
- **Location of the burner - center of mass:** assumed to be 7 m along the width direction (X axis) and 4 m along the depth dimension (Y axis);

With this data, the estimated activation time is equal to 60 s and this time has been estimated successfully because the fire has a fast growth rate. For this example, the plotted diagrams have been plotted assuming an activation time of the sprinkler equal to 300 s.

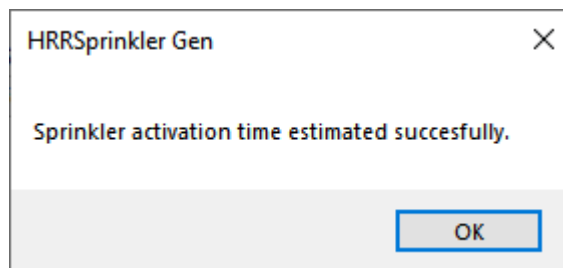
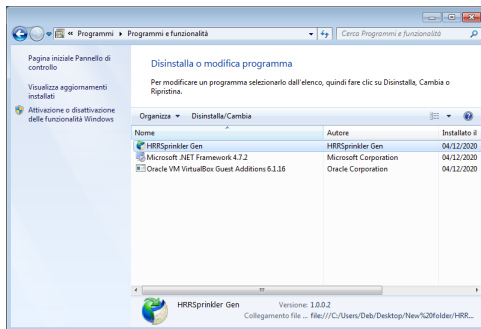


Figure A.22: HRRSprinkler Gen - Successful estimation of the sprinkler activation time

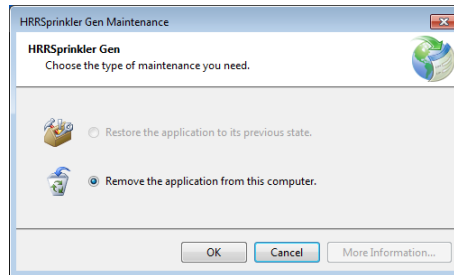
At this point, it is possible to save or export the diagram and to work on it.

A.4 Uninstalling HRRSprinkler Gen

To uninstall HRRSprinkler Gen, it is necessary to reach Windows Control Panel - through Start Menu on Windows 7 or by searching it on Windows 8 or newer - and select Programs and Functionalities. Then, select HRRSprinkler Gen and, when Uninstallation confirmation screen appears, select "Remove the application from this computer" and press OK.



(a) Program and functionalities



(b) HRRSprinkler Gen Uninstallation confirm

Figure A.23: HRRSprinkler Gen - Uninstallation steps

A.5 Error list

This appendix explain the errors that can occur while using the software:

- **Error 1: check input parameters.:** generic error. Check the input parameters to be sure that values are valid and will not cause any numerical instability.
- **Error 2: invalid t_B or t_C value:** this error occurs while generating parametric HRR diagrams, if the value of t_B is higher than or equal to the value of t_C .
- **Error 3: unable to generate an experimental HRR. Check input parameters.:** the user should check the typed points in the screen and be sure that there are not any null points.
- **Error 4: Unstable solution for values higher than or equal to the maximum distance for starting ignition. Check the distance of the item.:** this error occurs while calculating ignition of secondary items. The typed distance is unstable because it is higher than the maximum distance that the software calculates and shows.
- **Error 5: Unable to achieve convergence with chosen data input.:** this error occurs while calculating the modified HRR diagram with a sprinkler, using an advanced approach - **Paragraph 4.1.6**. Since both the BS PD 7974-3 approach and the exponential one are based on logarithmic equations, it is possible that the typed parameters will produce data that are out of the domain of the function.
- **Error 6: Roof openings cannot be initialized because of convergence instability. Check parameters.:** this error occurs while generating a parametric HRR diagram, through the complex approach, using the Kawagoe algorithm. The error occurs when, as the software makes a convergence control in order to give the user reliable results, the ratio $\frac{A_v \cdot \sqrt{d_H}}{A_v \cdot \sqrt{h}}$ returns a value out of the range from 0.3 to 1.5.
- **Error 7: Check image URL or Internet connection.:** this error occurs while importing an image from an URL into the Graph Digitizer, provided for generating experimental HRR diagrams. Check that the Internet connection is working and that the provided URL contains an image.

- **Error 8: Please check local reference coordinates.:** this error occurs while importing an image from an URL into the Graph Digitizer, provided for generating experimental HRR diagrams. Check to have typed valid coordinates - as integer numeric values.
- **Error 9: Too high density point. Repeat procedure picking less points on the image.:** this error occurs while using the Graph Digitizer, because point density is too high; in other words, points have been picked too near one from the other. Please repeat the picking point procedure, picking less points and picking them farer one to each other.

Appendix B

FDS2ANSYS User Manual

FDS2ANSYS is a freeware software which allows users to **study the structural behavior under the action of the fire**. In particular, this is a bridge-software which links the results of FDS - Fire Dynamics Simulator -, which is a CFD calculus engine optimised for low values of Mach number reactions (typical of the fire), and ANSYS, which is one of the most common commercial Finite Element suite for engineering analysis. This software has been developed for automatizing the procedures for coupling thermal and mechanical analysis, in order to gain as much as possible information on the structural response while a fire is occurring. To achieve this goal, the FDS2FTMI scripts^{1 2} has been implemented with a graphical user interface. Furthermore, the needed procedures to generate the geometries - for both FDS and the FEM code - have also been automatized, in order to simplify the whole thermal-mechanical approach.

FDS2ANSYS is the result of a research carried on with the Italian National Fire Brigade (CNVVF – Corpo Nazionale dei Vigili del Fuoco) - Piedmont Division -, in order to lay the foundation to update the Italian Technical Fire Prevention Standards³ on the structural security checks advanced methods, through the study of the local structural collapses. Moreover, a statistical survey on the activities which may need further security checks for the fire action has been carried on by the Italian National Fire Brigade and has shown that reinforced concrete structures - both with ordinary and pre-

¹SILVA J.C. (2017), "FDS2FTMI User's Guide - An automated code to one-way coupling between FDS and FEM using FTMI", National Institute of Standards and Technology

²ZHANG C., SILVA J.C., WEINSCHENK C., KAMIKAWA D., HEASEMI Y. (2017), "Simulation Methodology for Coupled Fire-Structure Analysis: Modeling localized fire tests on a steel column", National Institute of Standards and Technology

³Italian Technical Fire Prevention Standards - Ministerial Decree 3rd of August, 2015 and subsequent amendments and additions

stressed reinforcement steel configuration - are more diffused than the steel ones. For this reason, FDS2ANSYS is capable of computing scripts for solving the thermal-mechanical analysis issues for concrete structures only. Through the coupling of these two calculus engines, it is possible to predict accurately which is the effective structural behavior. What is needed to achieve this goal, is to perform coupled thermal-mechanical analysis, which is a relatively new area of research. The coupling procedure of these two kinds of analysis can be different.

- **One-way coupled analysis:** the fire scenario is modeled once and the temperature-time profiles are carried out from FDS. Then a time-history thermal-mechanical analysis is performed and all collapses configuration are considered;
- **Two-way coupled analysis:** the fire scenario is modeled once and the temperature-time profiles are carried out from FDS in order to perform thermal-mechanical analysis. During the structural analysis, when the first structural collapse occurs, the structure is remodeled, following the deformed-shape configuration and another FDS analysis is performed, restarting from the boundary condition of the collapse time-step. After this, the coupled thermal-mechanical analysis goes on until the second structural collapse occurs. This iterative procedure is carried on for a variable maximum number of structural failures (which corresponds to the number of iterations).

FDS2ANSYS is a one-way coupling bridge-software and generates the needed files to perform the following phases of analysis;

- **FDS analysis:** it is an exothermic analysis in which two boundary functions are enabled to perform the next steps of analysis: the Adiabatic Surface Temperature and the Heat Transfer Coefficient;
- **Heat Transfer analysis:** it is the transport of the output values of Adiabatic Surface Temperature the Heat Transfer Coefficient onto the FEM model;
- **Endothermic analysis:** starting from the results of the exothermic analysis results transferred inside the FEM environment, an endothermic analysis phase is performed to obtain the heat propagation time-history in the mean;
- **Structural analysis:** this procedure is called coupling and it consists to apply the thermal loads obtained from the previous step of anal-

ysis. Once performed the structural analysis, security checks can be approached.

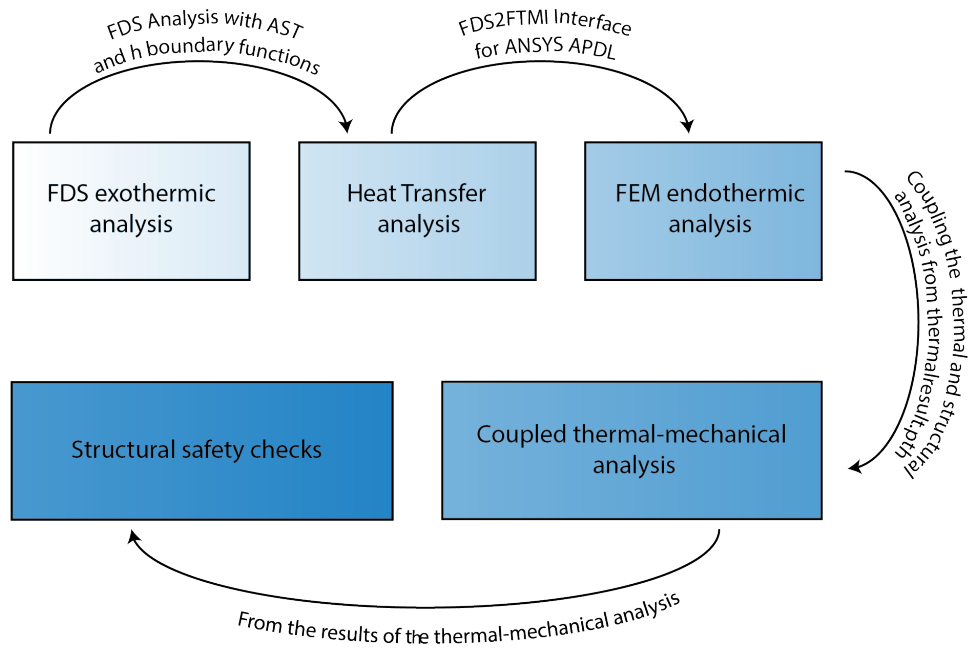


Figure B.1: Flowchart for one-way coupling

B.1 Limitations of FDS2ANSYS

On the FDS setting-up analysis phase, FDS2ANSYS has two main limitations: a cubic mesh is assumed for the calculus and it is not allowed to place any mesh refinement areas. In other words, all the geometrical model is studied with the same cubic mesh cell size and, even if it is highly recommended to set a cubic mesh, this aspect may represent a limitation, since the CPU time may increase significantly. On the FEM side, the main limitation of this software is due to the section of the structural members. Indeed, FDS2ANSYS is capable of recognizing rectangular or squared sections only. In case of more complex sections, it is advisable to calculate an equivalent cross-section as follows, by knowing the section surface and the moment of inertia:

$$\begin{cases} b_{new} \cdot h_{new} \approx A_{element} \\ \frac{b_{new} \cdot h_{new}^3}{12} \approx I_{x,element} \end{cases} \quad (B.1)$$

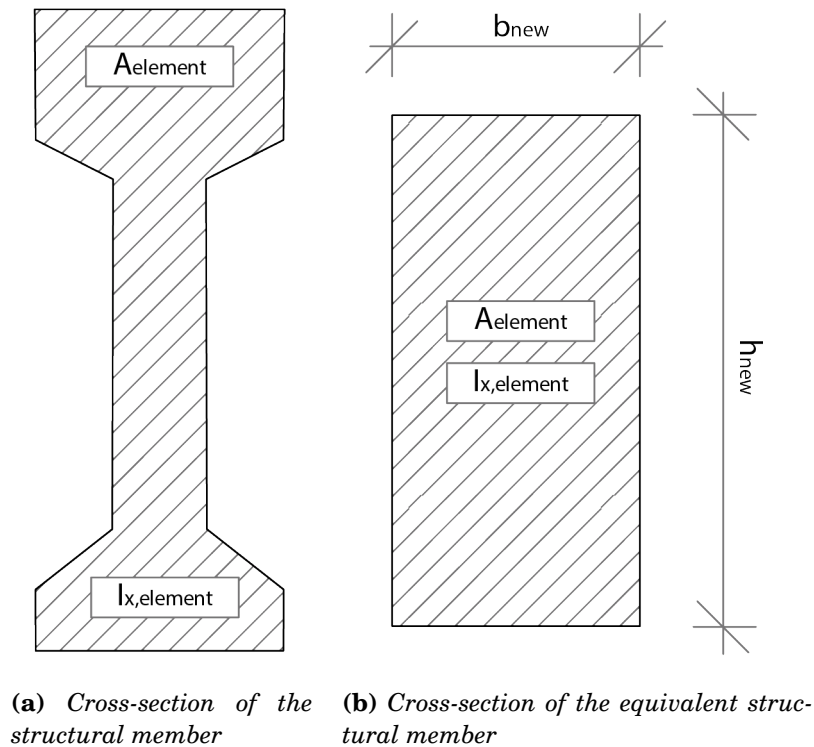


Figure B.2: Original and equivalent cross-sections of structural members

Another limitation is due to the FDS method of reading geometries. It

is not allowed to model any slopes (roof slabs, diagonal beams or braces). To overcome this limitation, an equivalent height of the structural members may be calculated. An advised method may be the averaged height of the columns.

B.2 Theory Reference on ANSYS Mechanical APDL Element Types

In order to understand the capability of this software, ANSYS Mechanical APDL, in the Help Section, is endowed of a Theory Reference where the theoretical definitions are explained. It is also important to distinguish two different ways of performing coupled thermal-mechanical analysis⁴:

- **Sequential coupling approach:** it consists in performing the endothermic analysis and then the structural analysis, which is obtained with the results of the first one. Furthermore, this technique allows users to take into consideration the non-linearity for both thermal - conductivity, specific heat, density - and mechanical material - stress-strain relationship for concrete compressive strength and reinforcement steel ultimate tension strength - properties. Despite this aspect, this approach does not take into account of the change of the temperature field, that may cause, once a failure occur - an extra-exposition of the inner core of the structural elements to the thermal stress.
- **Direct coupling approach:** it consists in a step-by-step thermal-mechanical analysis. In other words a thermal and then a mechanical analysis for the single time-step is performed. Unfortunately, with this technique, concrete cracking and crushing behavior may be neglected. On the other hand, it is possible to take into account of the variation of the after-failure temperature field, while the fire is still occurring.

To obtain reliable results from a sequential coupled thermal-mechanical model of a reinforced concrete structure, four different types of finite element needs to be defined:

- **Thermal behavior of concrete:** a **SOLID70** element type needs to be defined. It is a 3D thermal conductive element, with eight nodes and a single degree of freedom, temperature, at each node. This element is

⁴M. ELSHORBAGY, M. ABDEL-MOOTY (2019), "The coupled thermal-structural response of RC beams during fire events based on nonlinear numerical simulation", Engineering Failure Analysis, Volume 109

also capable of both steady-state and transient thermal analysis and it can compensate for mass transport heat flow from a constant velocity field. For this kind of analysis, the material properties for concrete that need to be defined are thermal conductivity, density and specific heat.

- **Thermal behavior of rebar and stirrups:** a **LINK33** element type is capable of representing the thermal behavior of rebar and stirrups. It is a uniaxial conductive element with two nodes, a starting one and an ending one, with a single degree of freedom per node - temperature. Besides, a section needs to be defined for this element, in order to set the cross section surface of the bar. For this kind of analysis, the material properties for reinforcing steel that need to be defined are thermal conductivity, density and specific heat.
- **Mechanical behavior of concrete:** a **SOLID65** element type needs to be defined, because it is the most suitable way to simulate and calculate the nonlinear structural behavior of concrete. It is a 3D solid element, with eight nodes and three degrees of freedom per each node - translations along X, Y and Z direction. Rotational DOFs can be added by calling an instance of the specific command. The SOLID65 element type is capable of foreseeing cracking - in tension - and crushing - in compression - of concrete. For this kind of analysis, the material properties for concrete that need to be defined are Young modulus, Poisson coefficient, cylindrical compression strength and thermal elongation. The stress-strain diagram is represented by a Multilinear Kinematic Hardening model. Therefore, some parameters are needed to be defined for the cracking/crushing concrete behavior. Thus, ANSYS is also capable of allowing spalling parameters - that for these analysis are set equal to zero. These mechanical features are not related to Standard and Codes and the values are referred to guidelines, forum threads and tutorials⁵ and for this reason are not editable from the FDS2ANSYS GUI. Here follow the list:

- **Open Shear Transfer Coefficient:** 0.3
- **Closed Shear Transfer Coefficient:** 1
- **Uniaxial Cracking Stress:** 2.7E+6 [Pa]
- **Uniaxial Crushing Stress:** -1
- **Biaxial Crushing Stress:** 0

⁵<https://www.youtube.com/watch?v=0JiKNWt095I>

- **Hydrostatic Pressure:** 0
- **Hydrostatic Biaxial Cracking Stress:** 0
- **Hydrostatic Uniaxial Crushing Stress:** 0
- **Tensile Cracking Factor:** 0
- **Mechanical behavior of rebar and stirrups:** a **LINK180** element type needs to be defined. It is a two-node element, with three degrees of freedom per each node - translations along X, Y and Z direction. It is the LINK33 homologue element for modeling mechanical behavior and, so, LINK180 too needs the definition of a section to quantify the cross section surface. For this kind of analysis, the material properties for reinforcing steel that need to be defined are Young modulus, Poisson coefficient, yielding strength and thermal elongation. The stress-strain diagram is represented by a Multilinear Isotropic Hardening model.

In order to obtain reliable results from a direct coupled thermal-mechanical analysis, another element type needs to be defined:

- **Thermal-mechanical behavior of concrete:** a **SOLID226** element type needs to be defined in order to perform a direct-coupled thermal mechanical analysis. It is a twenty-node element, with up to six degrees of freedom per each node - for this analysis, only four of them are considered: translations along X, Y and Z direction and temperature. Even in this case, rotational DOFs can be added by invoking an instance of the specific command. For this kind of analysis, the material properties are the same to the ones defined for both the SOLID70 and SOLID65 element types;
- **Thermal-mechanical behavior of rebar and stirrups:** it is defined with a **LINK180**, neglecting the thermal behavior of the reinforcement steel.

Thus, there is a sixth element type that needs to be defined in order to couple the FDS output solution with ANSYS Mechanical APDL and it is the **SURF152** element type, that has neither thermal nor mechanical behavior, but it is needed just to perform the Heat Transfer Analysis. It is a 2D planar thermal element, with variable number of nodes - from four to eight, depending on the element type keyoptions. Since this is a thermal element, temperature is the main degree of freedom per each node. It has also a top temperature and a bottom temperature, that may be enabled or disabled,

depending on the element type keyoptions. To allow the heat transfer, a real constant for this element type needs to be defined and it is equal to the Stefan-Boltzmann constant: $\sigma = 5.67 \cdot 10^{-8} \frac{W}{m^2 \cdot K^4}$

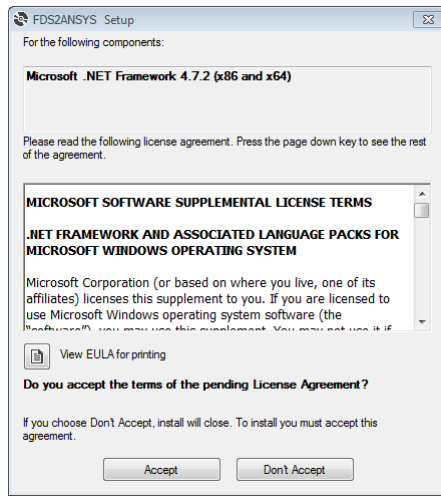
B.3 Installing FDS2ANSYS

FDS2ANSYS can be easily downloaded from <https://github.com/NicTunFSE/FDS2ANSYS>. On this page, it is possible also to updated the software and consulting changelog. It is also possible to report any bugs or issues about the program by sending an email to: nictunfse@engineer.com.

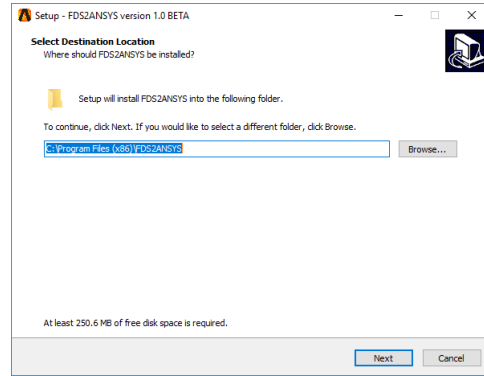
In order to exploit all the functionalities, here follows the **system requirements** for FDS2ANSYS:

- OS: Microsoft Windows 7, Microsoft Windows 8, Microsoft Windows 8.1, Microsoft Windows 10
- CPU: AMD or Intel 2 GHz x64 processor
- RAM: 16 GB
- Graphics: 2 GB of video RAM
- Screen resolution: at least 1280x960 pixels
- HDD: at least 50 GB of free space
- .NET Framework 4.7.2
- An internet connection is required
- A working installation of ANSYS is required
- *Highly recommended: a FDS-based modeling engine and calculator*

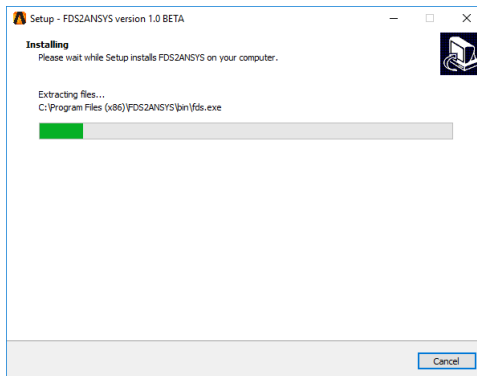
The installation proceeds with the simple following steps. At first, it may be asked the user to install the .NET Framework, v4.7.2, to make FDS2ANSYS working properly. Once the setup is run, it is needed to define an installation path. Then it is asked to create - or not - a shortcut of FDS2ANSYS on the desktop. After this, the installation starts.



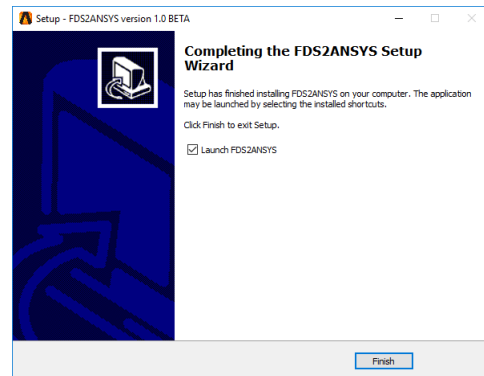
(a) .NET Framework 4.7.2 installation



(b) Installation path



(c) Installation phase



(d) Installation complete

Figure B.3: FDS2ANSYS - Installation steps

B.4 Running and using FDS2ANSYS

Once opened, the FDS2ANSYS splash screen appears. **IMPORTANT: in order to exploit all the functionalities, it is highly recommended to run FDS2ANSYS as Administrator.**



Figure B.4: FDS2ANSYS - Splash screen

At first, in order to make FDS2ANSYS running successfully, the point "." must be set as decimal separator. To do this, a message is prompt when FDS2ANSYS is started. Three actions can be done: the decimal separator can be set automatically as point, the international settings tab in the Microsoft Windows Control Panel can be called or FDS2ANSYS can be closed.

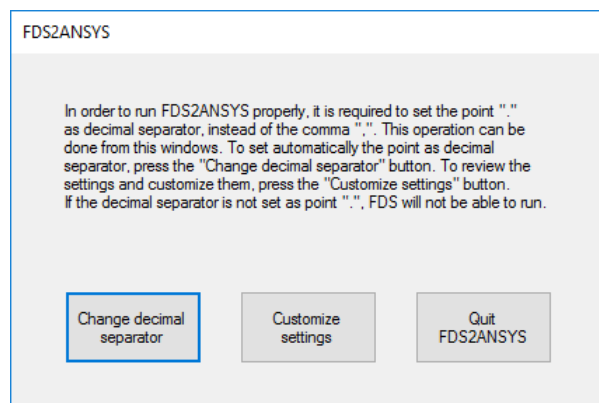


Figure B.5: FDS2ANSYS - Decimal separator alert

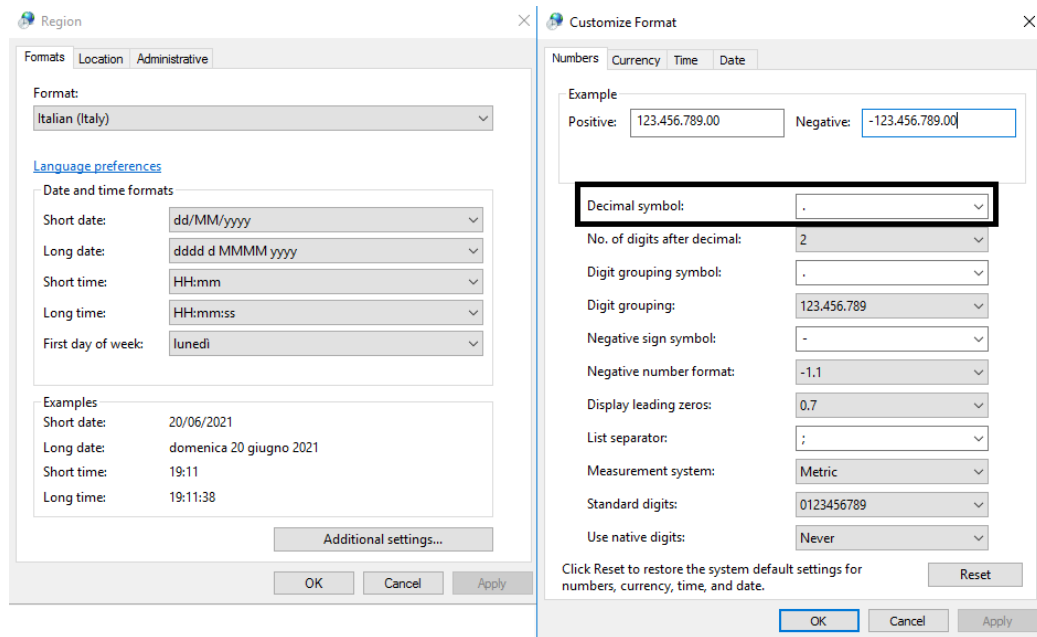


Figure B.6: Decimal separator setting tab - Microsoft Windows 10 Control Panel

At this point, a welcome pop-up window is shown to briefly describe the functionalities and the limitations of FDS2ANSYS. By pressing OK, a runtime control on the Windows Key Registry is started in order to find a working installation of ANSYS on the computer on which FDS2ANSYS is running.

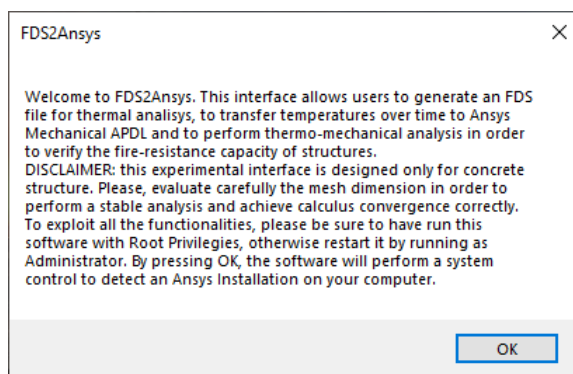
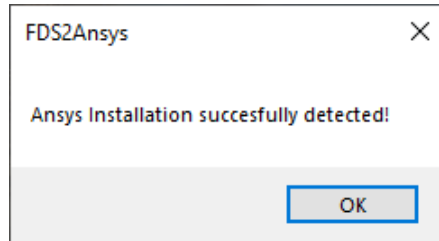


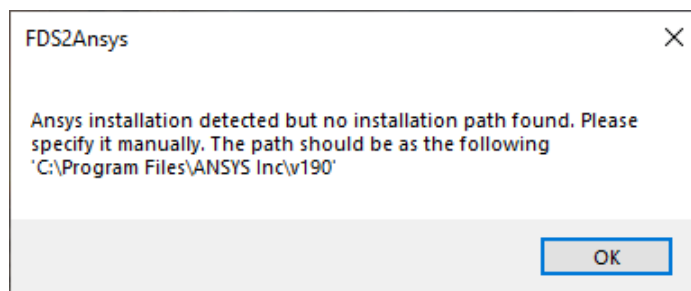
Figure B.7: FDS2ANSYS - Welcome screen

Then three different scenarios may occur:

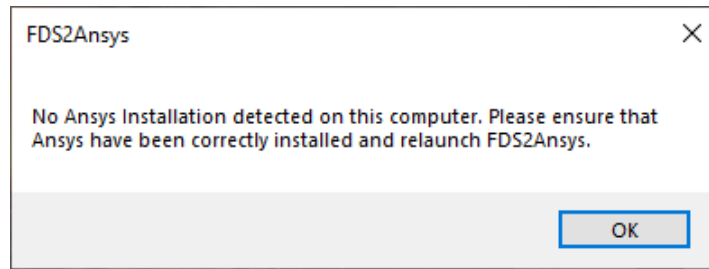
- **The ANSYS installation and the installation path have been found successfully:** FDS2ANSYS starts normally.



- **The ANSYS installation have been found successfully but the software has not been able to find a valid installation path:** FDS2ANSYS starts but a valid installation path needs to be provided from the user in the following form: C:\Program Files\ANSYS Inc\v190. Please note that if ANSYS was previously installed and then uninstalled and the Windows Registry Key has not been wiped from the useless Registry Entry, this alert may appear. In order to solve, before installing ANSYS again, reach the Start Menu, locate the Search command, find for "run" (or press  + ) and digit "regedit.exe". Then the HKEY_CURRENT_USER\Software\ANSYS, Inc.\ANSYS\ and HKEY_LOCAL_MACHINE\SOFTWARE\ANSYS, Inc.\ Windows Registry Keys should be deleted. In the end, the ANSYS installation may proceed.



- **The ANSYS installation has not been found:** an alert appears and FDS2ANSYS closes, since the Software\ANSYS, Inc.\ANSYS\ Windows Registry Key has not been found.



Once FDS2ANSYS is running properly, two phases of work can be distinguished:

- **Step I: Generation of an FDS base file:** all the needed procedures for the generation of an FDS file with the structural geometries, which may be added of further details for the fire simulation;
- **Step II: Generation of a base file for thermal-mechanical analysis:** all the needed procedures for the generation of some input files for ANSYS Mechanical APDL.

These two steps are illustrated in detail in the following paragraphs.

B.4.1 Generation of an FDS base file

Once FDS2ANSYS is running successfully, the main screen of the Step I is shown. The first step, in order to start the software working, is to provide a geometrical model of the structure, which can be in IGES, ACIS SAT or Parasolid format, since these are the supported models from ANSYS Mechanical APDL. When the working directory and the 3D model extension have been selected and the CHID (case-sensitive and without spaces) have been typed, a control to find the geometry file is executed.

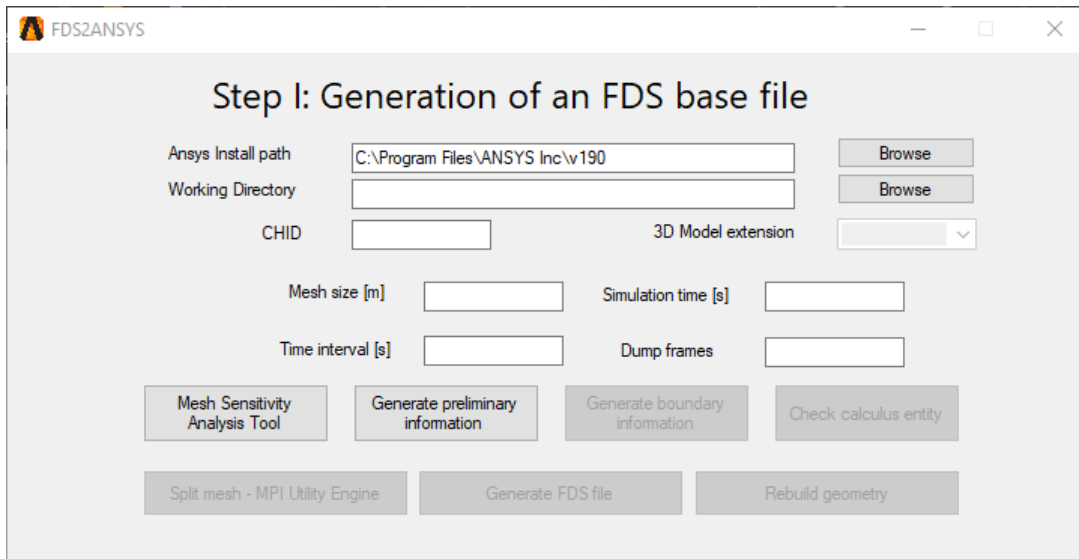
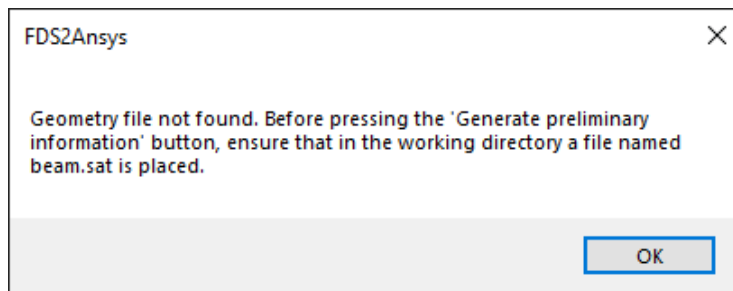
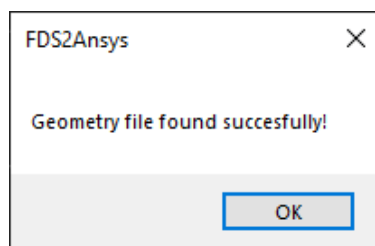


Figure B.8: FDS2ANSYS - Main screen for Step I



(a) Geometry file not found alert



(b) Geometry file found successfully alert

Figure B.9: FDS2ANSYS - Control to find the geometry file

Then, some data are required to set up the analysis phases:

- **Working directory:** the folder in which there is the geometry and where all the generated files are located;

- **CHID:** name of the file, which must be the same name of the geometrical model, case-sensitive and without spaces;
- **3D Model extension:** the format of the provided geometrical model (IGES, ACIS SAT or Parasolid);
- **Simulation time:** the duration of the simulation;
- **Mesh cell size:** the FDS discret size, assuming a cubic mesh;
- **Dump frames:** the number of output dumps per calculation;
- **Time interval:** the rate of output dumps for the heat transfer - **Paragraph 4.2.4. Heat Transfer Analysis.**

B.4.1.1 Mesh Sensitivity Analysis Tool

In order to run the whole analysis properly, the mesh cell size needs to be evaluated carefully. Indeed, the FDS calculator deformats the mesh and calculates the boundaries as mesh cell integer multiples. This means that if the bound of a structural member does not match with the edge of a mesh cell, the structural element is deformed and no reliable data on the bearing capacity can be considered. This deformation may occur in three different ways:

- **Element longer than the half of the mesh cell:** the side is approximated to the maximum integer number of mesh cells;
- **Element shorter than the half of the mesh cell:** the side is approximated to the minimum integer number of mesh cells;
- **Element as long as the half of the mesh cell:** the side may be approximated to the minimum or the maximum integer number of mesh cells, depending on the allocation mode of numbers on the RAM.

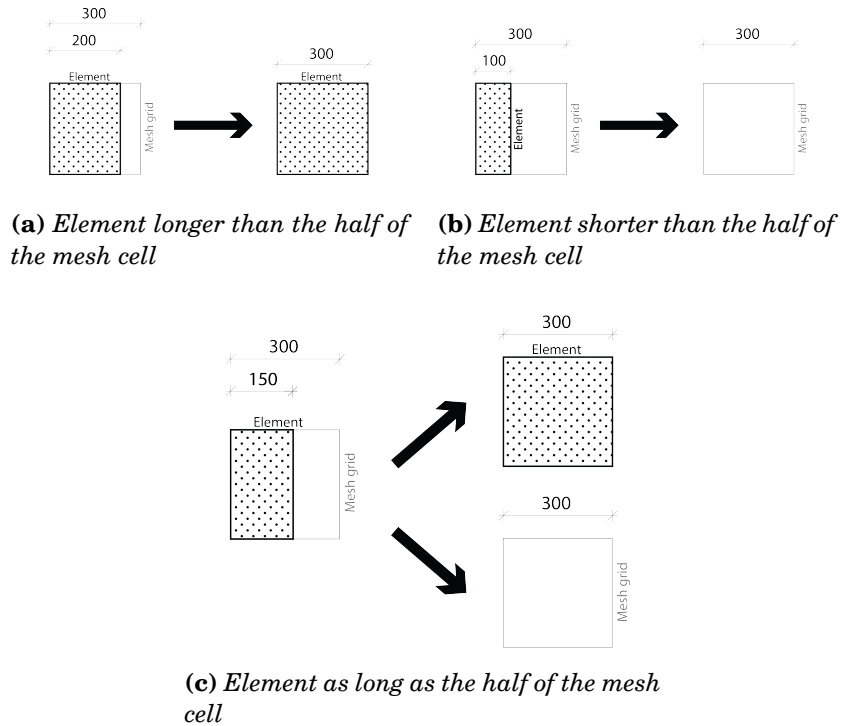


Figure B.10: FDS reading method of geometries. LEFT: how the element is - RIGHT: how the element is read by FDS

In order to evaluate correctly the mesh size, the MSAT - Mesh Sensitivity Analysis Tool - Utility has been implemented. It consists in a greatest-common-factor-based algorithm which calculates the most suitable size for the mesh, depending on the provided dimensional information. Many details are typed, more detailed may the analysis be, with a consequent increase of the CPU time. This means that FDS2ANSYS may be used both for global and local analysis, with different levels of details. The MSAT Utility requires the following information:

- **Side of structural members**
- **Clear spans**
- **Concrete cover**
- **Spacing between stirrups**

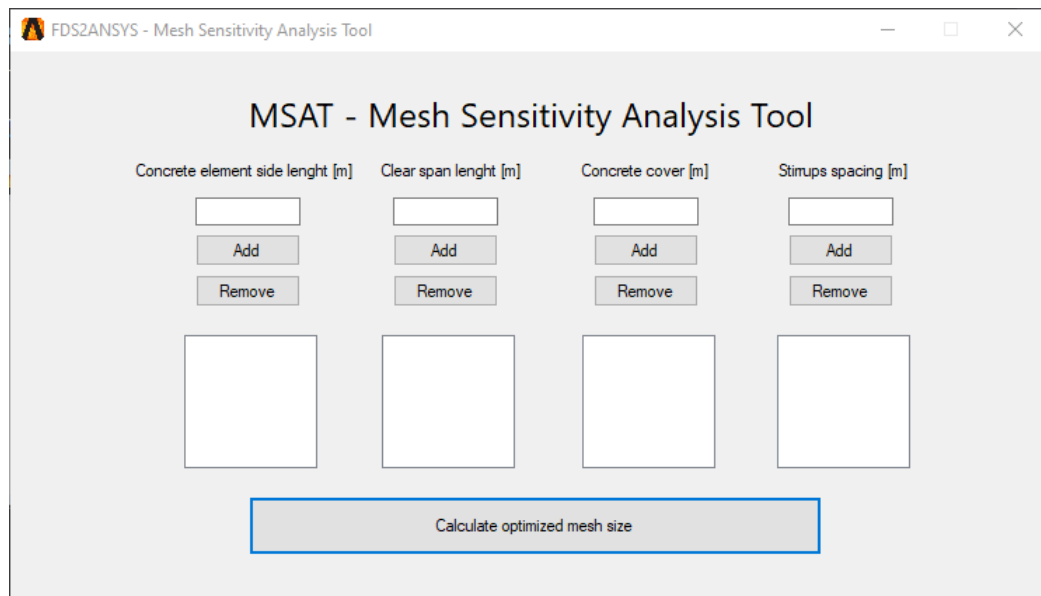
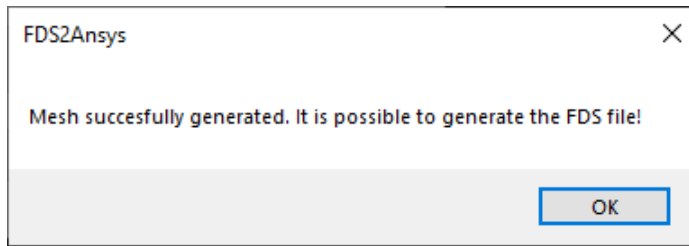


Figure B.11: FDS2ANSYS - Mesh Sensitivity Analysis Tool

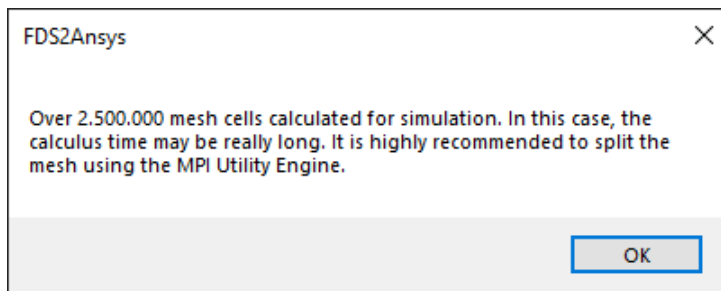
B.4.1.2 Generation of FDS geometric boundaries

However it is possible to type a user-defined mesh cell size, without using the MSAT Utility. Then, on the main screen, the "Generate preliminary information" and the "Generate boundary information" buttons must be pressed in this order to start FDS2ANSYS working. In this phase, a batch session of ANSYS Mechanical APDL is started to import the geometric model (IGES, ACIS SAT or Parasolid file format) and to run the "ANSYS2FDS.geom" APDL macro, developed by professor Julio Cesar Silva⁶, in order to generate the obstructions strings for the FDS file. Then, this input file is added of the simulation settings (mesh boundaries depending on the cell size, simulation time and dump frames). Then the "Check calculus entity" button needs to be pressed, in order to state the entity of the analysis: if over 2.500.000 cells are computed, a pop-up window suggests the user to run the Split Mesh Utility, whereas if the cells number is less than 2.500.000, an alert tells the user that it is possible to generate the FDS file.

⁶SILVA J.C. (2017), "FDS2FTMI User's Guide - An automated code to one-way coupling between FDS and FEM using FTMI", National Institute of Standards and Technology



(a) Mesh cells less than 2.500.000



(b) Mesh cells more than 2.500.000

Figure B.12: FDS2ANSYS - Check of the entity calculus

B.4.1.3 Splitting the mesh through the MPI Utility Engine

As previously said, despite the level of details may be high and the results of the calculation reliable, the CPU time may be very long (as the mesh cell size decreases and as the simulation time and the dimensions of the model increase). As the FDS analysis are run by default onto a single thread of the CPU, it is possible to exploit the parallel computing principle, in order to load "pieces" of the model onto different threads of the CPU. This is possible, since FDS is endowed of a parallel computing interface, called FDS Parallel, based on the Intel MPI - Message Passing Interface - Libraries. It is possible to divide the geometry directly in FDS2ANSYS, through a Python script ⁷ transposed on Visual Basic .NET Language and implemented. This script divides the geometry in user-defined parts and this number needs to be higher than the employed logical processors - user-defined number too. This utility can be run in two ways:

- **Local resources:** a runtime control finds the number of the logical processors, which is the maximum allowable number.

⁷COLLINS D.C. (2015), "Dividing and Conquering Meshes within the NIST Fire Dynamics Simulator (FDS) on Multicore Computing Systems", Master of Science Degree Thesis, University of Tennessee, Knoxville

- **Remote resources:** all the files contained in the working directory are prepared to be copied in a workstation/server/cluster which is not the PC that is running FDS2ANSYS. To this purpose, a maximum number of 64 threads can be set.

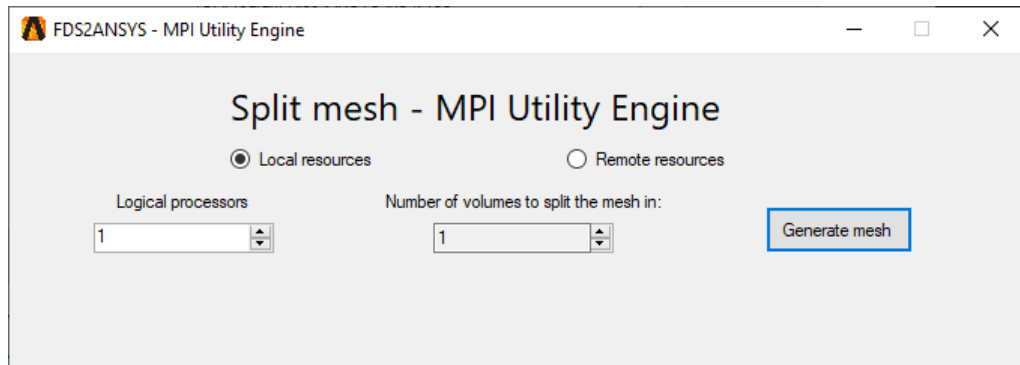


Figure B.13: FDS2ANSYS - MPI Utility Engine

B.4.1.4 Generation of FDS file

At this point, the "Generate FDS file" button needs to be pressed. Since the FDS file has been generated, it is possible to edit it and to perform the analysis. When the FDS analysis is complete, the "Rebuild geometry" button needs to be pressed. If the FDS analysis has not been performed successfully, an error on the Smokeview file missing occurs.

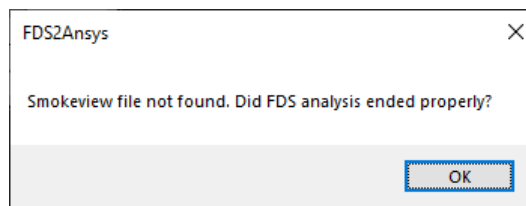


Figure B.14: FDS2ANSYS - Smokeview file not found error

In this phase, all the obstructions which have the "CONCRETE" surface tag are recognised as structural members and rebuilt from FDS2ANSYS. If an FDS analysis has been performed onto a single mesh FDS file, by pressing the "Rebuild geometry" button reads the external geometry and rebuilds it. Otherwise, if the MPI Utility Engine has been used, the user is asked to follow the procedure as follows, since the Heat Transfer Analysis - that occurs in the next following steps - needs to be performed on

the FDS file which has been modified and launched for the numerical solving. Furthermore, the FDS2FTMI scripts support the MPI calculation but it is difficult to rebuild geometries from a MPI-calculated Smokeview file, whereas for the temperature association no limitations are presented. For this reason, if the MPI Utility Engine is invoked, it is necessary to build an alternative Smokeview file - as a single mesh - just for reading the geometric input and it is generated by an instance of the ended FDS analysis. So, it is asked to:

1. Press the "Rebuild Geometry" button. This task consists in importing the run-analysis FDS input file - the procedure is automatized and it is done by placing the FDS file into the working folder and naming it as CHID.fds. Please, remember that all the geometric structural obstructions need to have the "CONCRETE" surface tag. Once imported, it is asked to press again the button, which is showing the "Step I" text.
2. By pressing the "Step I" button, all the mesh boundaries are rebuilt as a single merged mesh and all the structural obstruction are added to this file. Once the procedure is completed, it is asked to press the button again, which is showing the "Step II" text.
3. By clicking the aforementioned button, a batch session of FDS starts, in order to generate a Smokeview file to read the geometry boundaries. This is necessary in order to avoid any issues - that could occur because of the mesh division - on the reading geometry phase and to have congruence with the geometry boundaries when running the Heat Transfer Analysis
4. By clicking the "Rebuild Geometry" button, the procedure of geometry rebuilding starts.

Two examples of FDS scripts can be found in the **Appendix C.1.1 - Case Study A. - Raw FDS Code** and in the **Appendix C.1.2 - Case Study A. - Pyrosim FDS Code**. The first example is the base code, directly generated from FDS2ANSYS, whereas the second code has been generated through editing the first one.

B.4.2 Generation of a base file for thermal-mechanical analysis

At this point it is needed to select the coupling procedure method (sequential or direct) and enabling or disabling the reinforcement. The "Rebuild

geometry" button works with the Smokeview file, generated from the FDS analysis. In particular, this file is useful to rebuild the geometrical boundaries, since it contains the information on the effective analyzed geometry, which needs to be ported into ANSYS Mechanical APDL through a specific input file. The following operations, indeed, have the goal to write automatically the /PREP7 input files, needed to perform both the endothermic and the coupled thermal-mechanical analysis phases.

If the boundaries have been read successfully, when the Step II screen is loaded, a green string reporting "Geometry rebuilt successfully" is printed on screen, otherwise a red string reporting "Error while rebuilding geometry. Check working directory and CHID" appears and the user is not allowed to do any operation.

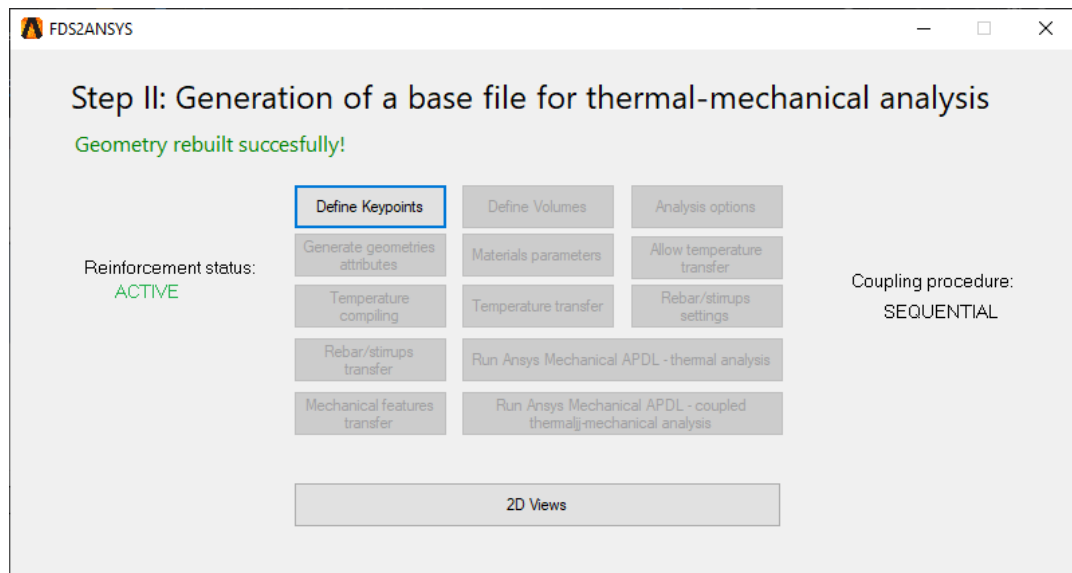


Figure B.15: FDS2ANSYS - Main screen for Step II

B.4.2.1 2D Views Panel

On this screen, several buttons are reported. The "2D Views" button may be noticed on the bottom part of the interface. It consists in a useful utility which allows the user to check if the geometry boundaries have been rebuilt in the right way, through the plot of 2D views of the geometric model. It is possible to check the geometrical configuration by placing a XY, XZ or YZ section planes, whose quote can be selected by the relative track-bar. Then, the "Plot view" button must be pressed. A light gray grid can be noticed and it is the mesh cell discretization. It is also possible to save the view as an

image through the specific button.

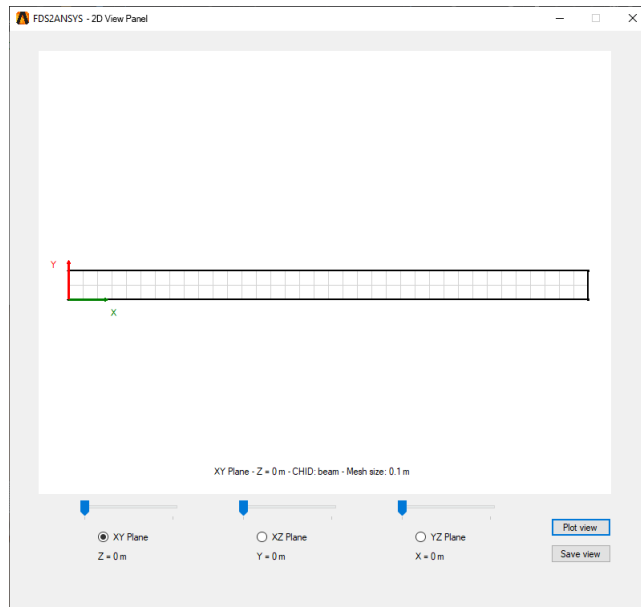


Figure B.16: FDS2ANSYS - 2D View Panel, example for a simply supported beam

B.4.2.2 Generation of /PREP7 files

Referring to the **Figure 4.10**, as previously said, the interface has been designed to be intuitive as much as possible. Indeed, the buttons in the panel get enabled just in the moment that needs to be used to do a certain operation and then disabled.

The procedure may be a little different if the reinforcement is enabled or not, and the coupling method of the analysis:

- **Sequential coupling approach:** this technique allows users to take into consideration the non-linearity for both thermal - conductivity, specific heat, density - and mechanical material - stress-strain relationship for concrete compressive strength and rebar ultimate strength-properties and, so, to model the thermal-mechanical behavior with an high precision. This approach is achieved by performing separately the whole time-history thermal analysis, for the entire simulation time, and then, for the same time interval, the whole time-history mechanical analysis needs to be performed by coupling the results of the thermal analysis. For this reason, on the FEM code, appropriate finite

element types need to be chosen, both for thermal and mechanical behavior. Despite this technique is really accurate on the results, it does not take into account of the change of the temperature field, that may occur with collapses - which may expose more the inner core of the structural elements to the thermal stress.

- **Direct coupling approach:** this technique consists in a step-by-step thermal-mechanical analysis. The coupling procedure, indeed, is not reached at the end of the endothermic analysis but at each time-step. In other words, whereas in the sequential coupled analysis appropriate finite element types need to be chosen, both for thermal and mechanical behavior, in the direct coupling technique a single element type - one for the concrete and one for the rebar - needs to be chosen and it may be capable of performing both thermal and structural analysis. This would mean that the concrete cracking and crushing behavior may be neglected with this kind of coupling procedure. On the other hand, it is possible to take into account any variation of the temperature field while the fire is occurring.

The sequential coupling technique can be divided in the following steps:

- **Procedures for exothermic analysis:** to generate a FDS input file needed to the exothermic analysis;
- **Procedures for heat transfer analysis:** to transfer the temperature profile over time in ANSYS Mechanical APDL;
- **Procedures for endothermic analysis:** to analyze - for the whole simulation time - the heat propagation into the concrete inner core
- **Procedures for coupling thermal and mechanical analysis:** from the temperature field, it is possible to carry on a mechanical analysis with the thermal and inertial forces.

On the direct coupling technique, several steps may be identified:

- **Procedures for exothermic analysis:** performed in the same way of the sequential coupling approach;
- **Procedures for heat transfer analysis:** performed in the same way of the sequential coupling approach;
- **Procedures for direct-coupled thermal-mechanical analysis:** thermal and structural analysis are performed together step-by-step.

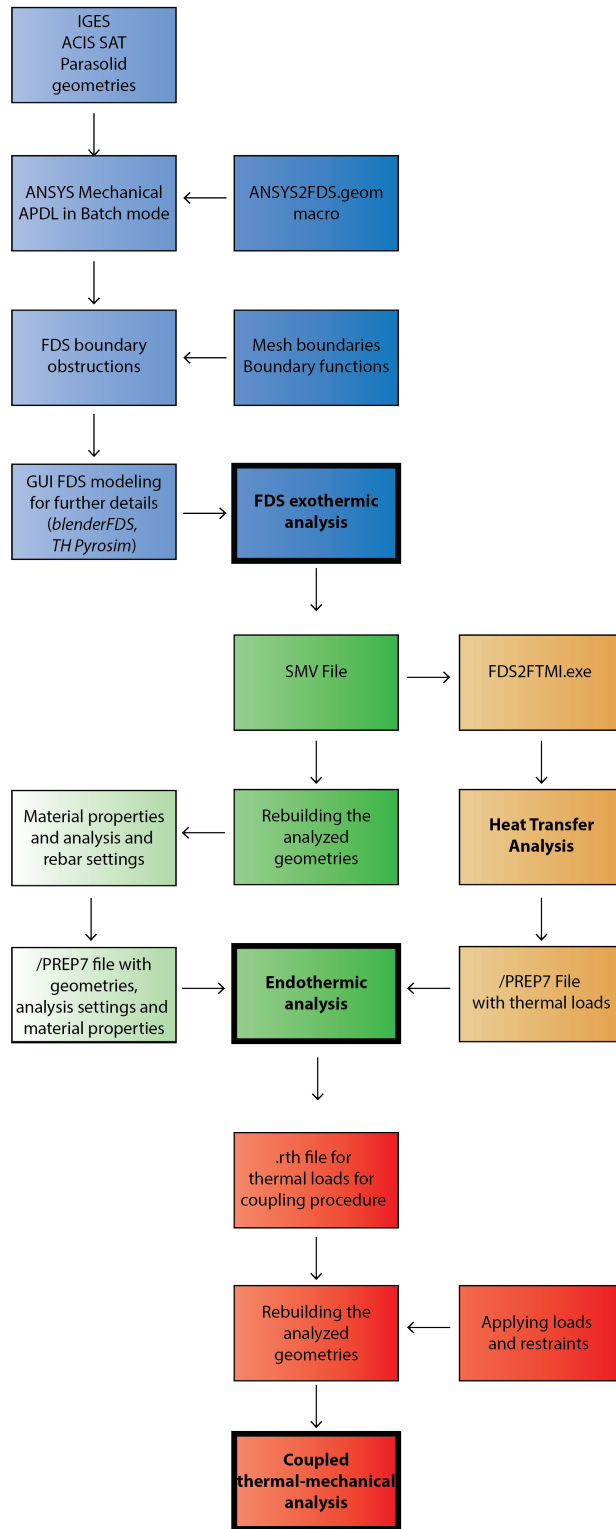


Figure B.17: Complete flowchart for sequential coupling procedures in FDS2ANSYS

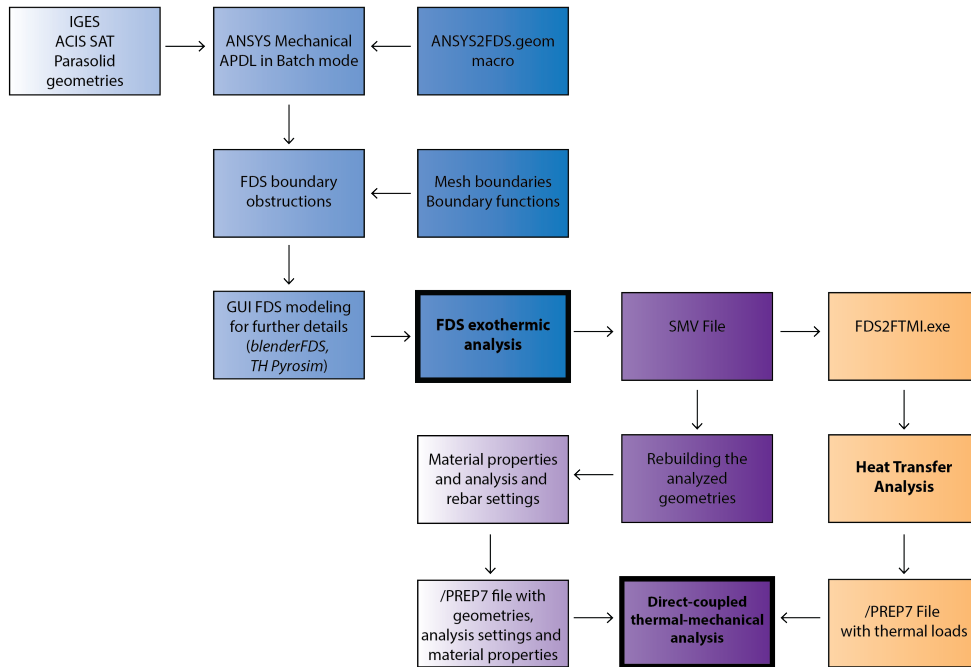


Figure B.18: Complete flowchart for direct coupling procedures in FDS2ANSYS

The first button that needs to be pressed is the "Define Keypoints" button, which defines the vertexes of the volumes into ANSYS Mechanical APDL input file. Then, from this keypoints the solid elements - for concrete - are created and meshed - with the provided mesh cell size in the Step I - by pressing the "Define Volumes" button. At this point, some analysis options need to be defined through the homonym button. It is important to understand which element types have been chosen in order to fill the /PREP7 input files. These features change with the coupling method:

- **Sequential coupled analysis settings:**

- **Concrete thermal behavior - SOLID70 element type:**

- * **Evaluation of film coefficient** can be set as:

- Evaluate film coefficient (if any) at average film temperature, $(T_S + T_B)/2$ (KEYOPT(2)=0)
 - Evaluate at element surface temperature, T_S (KEYOPT(2)=1)
 - Evaluate at fluid bulk temperature, T_B (KEYOPT(2)=2)

- Evaluate at differential temperature $|TS-TB|$ (KEYOPT(2)=3)
- * **Element coordinate system defined** can be set as:
 - Element coordinate system is parallel to the global coordinate system (KEYOPT(4)=0)
 - Element coordinate system is based on the element I-J side (KEYOPT(4)=1)
- * **Nonlinear fluid option** can be set as:
 - Standard heat transfer element (KEYOPT(7)=0)
 - Nonlinear steady-state fluid flow analogy element - Temperature degree of freedom interpreted as pressure - (KEYOPT(7)=1)
- * **Mass transport effects** can be set as:
 - No mass transport effects (KEYOPT(8)=0)
 - Mass transport with VX, VY, VZ (KEYOPT(8)=1)
- **Reinforcement thermal behavior - LINK33 element type:**
no keyoptions needed to be set.
- **Concrete mechanical behavior - SOLID65 element type:**
 - * **Extra displacement shapes** can be set as:
 - Including extra displacement shapes (KEYOPT(1)=0)
 - Suppressing extra displacement shapes (KEYOPT(1)=1)
 - * **Behavior of totally crushed unreinforced elements** can be set as:
 - Base behavior (KEYOPT(3)=0)
 - Suppress mass and applied loads, and warning message (KEYOPT(3)=1)
 - Features of 1 and apply consistent Newton-Raphson load vector (KEYOPT(3)=2)
 - * **Concrete linear solution output** can be set as:
 - Print concrete linear solution only at centroid (KEYOPT(5)=0)
 - Repeat solution at each integration point (KEYOPT(5)=1)
 - Nodal stress printout (KEYOPT(5)=2)
 - * **Concrete nonlinear solution output** can be set as:
 - Print concrete nonlinear solution only at centroid (KEYOPT(6)=0)
 - Print solution at each integration point (KEYOPT(6)=1)
 - * **Stress relaxation after cracking** can be set as:

- No tensile stress relaxation after cracking (KEYOPT(7)=0)
- Include tensile stress relaxation after cracking to help convergence (KEYOPT(7)=1)
- * **Warning message for totally crushed unreinforced element** can be set as:
 - Print the warning (KEYOPT(8)=0)
 - Suppress the warning (KEYOPT(8)=1)
- **Reinforcement mechanical behavior - LINK180 element type:**
 - * **Cross-section scaling** (which applies only if large-deflection effects - NLGEOM,ON - are specified) can be set as:
 - By default, enforce incompressibility; cross section is scaled as a function of axial stretch (KEYOPT(2)=0)
 - Section is assumed to be rigid (KEYOPT(2)=1)
 - * **Hydrodynamic output** can be set as:
 - By default, none (KEYOPT(12)=0)
 - Additional hydrodynamic printout (KEYOPT(12)=1)
- **Direct coupled analysis:**
 - **Concrete thermal-structural behavior - SOLID226 element type:**
 - * **Element degrees of freedom for coupled-field analysis** always set for coupled thermal-structural analysis (KEYOPT(1)=11);
 - * **Coupling DOFs matrix** can be set equal to:
 - **Strong (matrix) coupling:** produces an unsymmetric matrix. In a linear analysis, a coupled response is achieved after one iteration (KEYOPT(2)=0);
 - **Weak (load vector) coupling:** produces a symmetric matrix and requires at least two iterations to achieve a coupled response (KEYOPT(2)=1);
 - * **Integration method** can be set equal to:
 - **Full integration:** it uses 14 integrations points. This method can cause volumetric locking in the models with nearly incompressible materials. It is primary employed for purely linear analyses (KEYOPT(6)=0);
 - **Uniform reduced integration:** it uses a 2 x 2 x 2 integration scheme. This method helps prevent volumetric mesh locking in the models with nearly incompressible

materials. It is recommended for analyses with structural nonlinearities. To avoid the propagation of hour-glass mode associated with the reduced integration, the model must have at least two layers of elements in each direction (KEYOPT(6)=1);

* **Specific heat matrix** can be set equal to:

- **Consistent:** (KEYOPT(10)=0);
- **Diagonalized:** (KEYOPT(10)=1);
- **Diagonalized:** in this case, the specific heat or enthalpy is evaluated at element centroid (KEYOPT(10)=2);

* **Element formulation** can be set equal to:

- **Pure displacement:** (KEYOPT(11)=0);
- **Mixed displacement-forces formulation:** (KEYOPT(11)=1);

– **Reinforcement mechanical behavior - LINK180 element type:**
see the keyoptions feature above.

Once saved the desired settings, the Option panel gets closed and the Step II interface is shown again. At this point the "Generate geometries attributes" button needs to be pressed, in order to transfer the element types features onto the /PREP7 file. Then, it is needed to set the concrete and the reinforcement steel thermal and mechanical features.

B.4.2.3 Material parameters

The thermal and mechanical features of the materials needs to be set by pressing the "Material Parameters" button on the Step II screen. For the mathematical functions that describe the variation of the parameters and the reference to the current Standards, the **Chapter 5. Engineering Data** of this essay is invoked.

B.4.2.4 Heat Transfer Analysis

Once the geometry and the material features have been defined into ANSYS Mechanical APDL, it is needed to associate the temperature boundaries from FDS into the FEM code. An example of the code generated so far can be found in the **Appendix C.1.3. Case Study A: /PREP7 Code for ANSYS Mechanical APDL #1.**

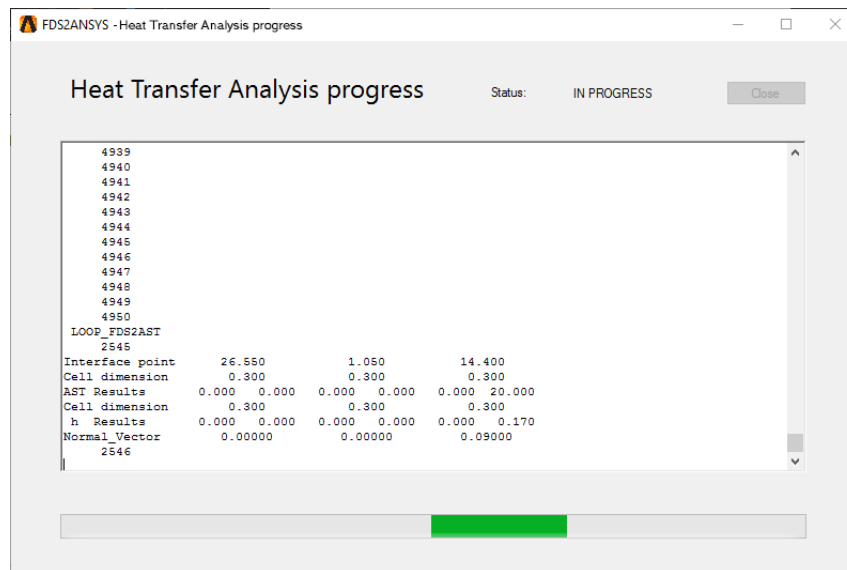


Figure B.19: FDS2ANSYS - Heat Transfer Analysis progress window

This phase is possible through the FDS2FTMI scripts^{8 9}. In order to make this interface working properly, there must be an absolute correspondence between the FDS and the FEM geometry. This association occurs with another element type, defined into the /PREP7 file and needed to perform the Heat Transfer - with neither thermal nor mechanical behavior. This coupling procedure is obtained through the definition of the **SURF152** element type, that is a 2D planar thermal element, with variable number of nodes - from four to eight, depending on the element type keyoptions. Since this is a thermal element, temperature is the main degree of freedom per each node. It has also a top temperature and a bottom temperature, that may be enabled or disabled, depending on the element type keyoptions. To allow the heat transfer, a real constant for this element type needs to be defined and it is equal to the Stefan-Boltzmann constant: $\sigma = 5.67 \cdot 10^{-8} \frac{W}{m^2 \cdot K^4}$. The Heat Transfer is achieved by pressing the "Allow temperature transfer" and "Temperature compiling" buttons in the order. During the execution of the Heat Transfer Analysis, the output log is shown in a specific window. At the end of the analysis, the shown log is saved as textfile - called *HTAoutput.dat* - and the information on the computing time are reported. Once this phase is completed, the temperatures are transferred into the ANSYS model

⁸SILVA J.C. (2017), "FDS2FTMI User's Guide - An automated code to one-way coupling between FDS and FEM using FTMI", National Institute of Standards and Technology

⁹ZHANG C., SILVA J.C., WEINSCHENK C., KAMIKAWA D., HEASEMI Y. (2017), "Simulation Methodology for Coupled Fire-Structure Analysis: Modeling localized fire tests on a steel column", National Institute of Standards and Technology

(containing all the features generated so far) through a batch-script that is executed by pressing the "Temperature transfer" button. An example of the Heat Loads /PREP7 file for ANSYS Mechanical APDL can be found in the **Appendix C.1.4. Case Study A: /PREP7 Code for ANSYS Mechanical APDL #2.**

B.4.2.5 Rebar and stirrups settings

Once the temperatures on the external faces of the obstructions have been transferred successfully, it is possible to set the rebar and stirrups configuration for the structural members, through pressing the "Rebar/stirrups settings" button on the Step II interface. These features are defined after the Heat Transfer Analysis, in order to avoid any mismatch with the transport of the temperatures from FDS. Please, note that actually it is not possible to set a different reinforcement steel for rebar and stirrups.

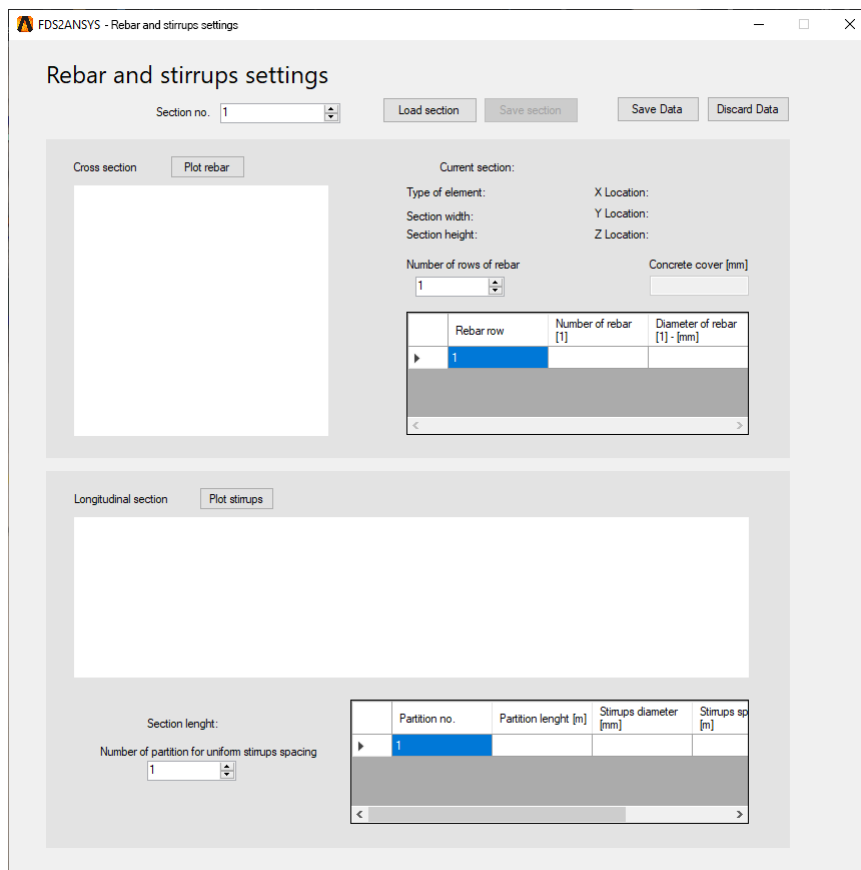
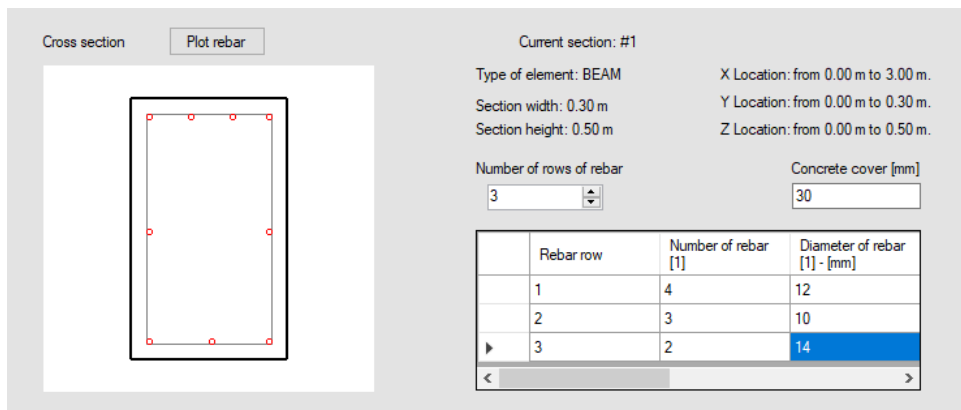


Figure B.20: FDS2ANSYS - Rebar/stirrups settings panel

In order to make the interface working properly, please follow in the order the following instructions:

1. On the upper left part of the interface can be noticed a NumericUp-Down box, in which the number of the structural member sections is reported. Press the "Load Section" button to load the element. Then, both the cross and the longitudinal section are drawn.
2. Focusing the attention on the Cross section panel, the features of the structural members are reported. The first operations that need to be done are setting the concrete cover distance (in millimeters) and the number of the rows of rebar. Please, pay attention to the table to fill with rebar: number and diameter of bending-resistant bars need to be typed. As can be noticed in the following figure, the first row of the table represents the upper row of bars. Then, the second row of the table is the bottom row of bars. Finally, from the third row of the table, the central rows of bars are defined (from the top to the bottom). When the rebar features have been defined, press the "Plot rebar" button.

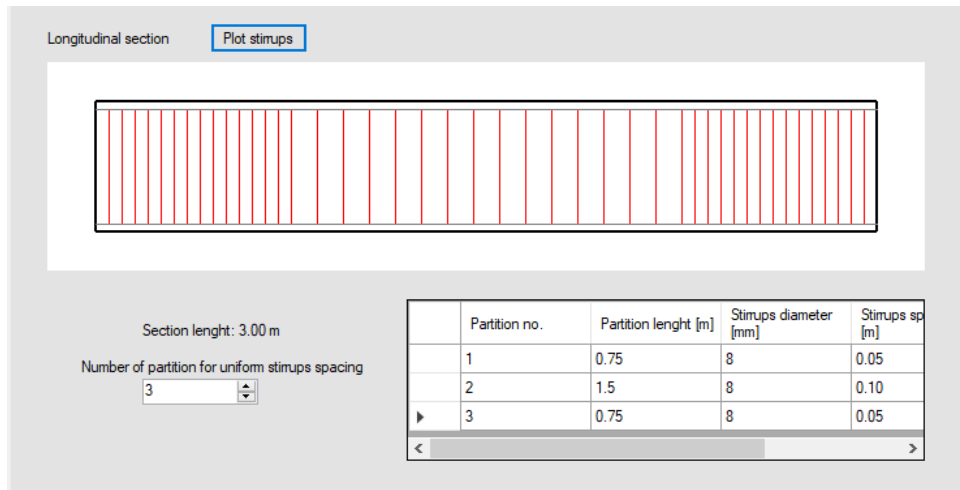


3. Focusing the attention on the Longitudinal section panel, first of all, it is needed to define the number of partitions with uniform spacing of stirrups, in order to define any critical zones - for example the beam-column nodes. These divisions are defined from the left to the right of the longitudinal section and some parameters for each division must be typed:

- Partition length [m]
- Stirrups diameter [mm]
- Stirrups spacing [m]

- Number of stirrup legs

Obviously, the sum of the provided partition lengths must be equal to the section length, reported to the left side of the table. When the stirrups features have been defined, press the "Plot stirrups" button.



4. Once these features have been defined, press the "Save section" button. A message box appears to warn the user that the section has been saved successfully.
5. Repeat these steps for each structural member, following the step 1 to 4 of this list. If saved, it is possible to load a section in order to see the typed features, following the step 1 of this list.
6. Once the reinforcement properties have been defined for each section, the "Save Data" button, in the upper right corner of the rebar/stirrups settings panel must be pressed. A message box warns the user that these data have been saved successfully. These data are typed into a specific /PREP7 file, containing the reinforcement features.

B.4.2.6 Endothermic analysis on ANSYS Mechanical APDL

Once the rebar/stirrups settings have been saved successfully, it is needed to import these features into the ANSYS Mechanical APDL model. This aim is achieved through a batch-script, executed by pressing the "Rebar/stirrups transfer" button. At this point, it is possible to start ANSYS Mechanical APDL model. If the direct coupling analysis method has been chosen, in this phase it is needed to set the mechanical loads and restraint. It is also

possible to set the Load Cases and the Load Combinations for the security checks. If the sequential coupling analysis has been chosen, it is possible to start the thermal analysis by pressing the homonym button. A pop-up windows explains the user how to proceed once ANSYS Mechanical APDL is running: once ANSYS Mechanical APDL is started, the user must reach, from the left bar, the following path: Solution > Solve > Current LS. At this point the endothermic analysis starts. For the structural analysis for sequential couplead analysis, see the next paragraph. Once the endothermic analysis is finished, it is possible to investigate on the obtained results from both the General Postprocessor (POST1) and the Time-History Postprocessor (POST26).

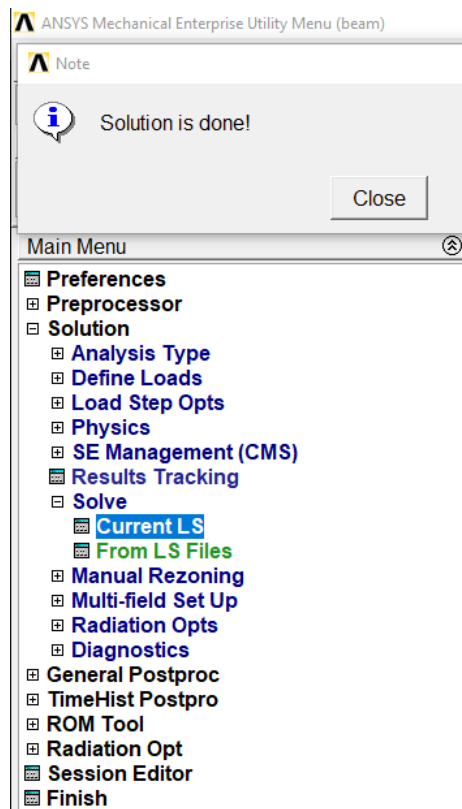


Figure B.21: Running the Endothermic analysis in ANSYS Mechanical APDL

B.4.2.7 Coupled thermal-mechanical Analysis on ANSYS Mechanical APDL

Since the direct coupling procedure is finished with the previous step of generation of the /PREP7 files, this paragraph regards only the sequential coupling approach. This procedure is done once the Endothermic Analysis phase is completed. The coupling procedure between thermal and mechanical analysis is achieved through another /PREP7 input file, which is generated automatically. An example of this code can be found in **Appendix C.1.6. Case Study A. - /PREP7 Code for ANSYS Mechanical APDL #4**. This input source is needed to:

- **Switching the analysis from thermal to mechanical:** this is done through the switching options which converts the geometries from thermal behavior - SOLID70 for concrete and LINK33 for reinforcement steel and relative keyoptions - to structural behavior - SOLID65 for concrete and LINK180 for reinforcement steel and relative keyoptions.
- **Material properties:** for mechanical behavior of both concrete and reinforcement steel.
- **Coupling the analysis:** the .rth file, which reports the results of the thermal analysis, is loaded onto ANSYS↑ Mechanical APDL as loads.

Then, load and restraint conditions needs to be set. This phase has not been automatized from FDS2ANSYS and it can be done directly on ANSYS Mechanical APDL, by prompting in the command-line or by the graphical interface. Once done this, the coupled-thermal analysis can be performed and the result may be discussed.

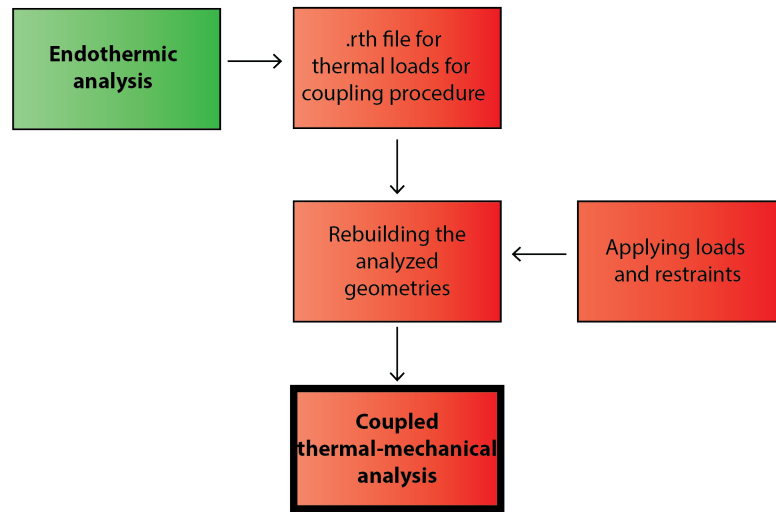


Figure B.22: Flowchart for FDS2ANSYS procedures to couple thermal and mechanical analysis for sequential coupled thermal-mechanical analysis

In order to perform a thermal-mechanical analysis, the coupling procedure needs to be executed. This is possible in a very simple way, since from the thermal analysis an output file, which is named CHID.rth and is going to be applied as load, is exported. The coupling procedure consists in applying these overloads and then in importing the structural material properties and the analysis settings and in switching from the thermal to the mechanical element types. This step occurs by pressing the "Mechanical features transfer" button. Once completed, it is possible to start ANSYS Mechanical APDL with the thermal-mechanical input file, by pressing the "Run ANSYS Mechanical APDL - coupled thermal-mechanical analysis" button. At this point, all the structural loads and the restraint configuration need to be defined, directly in ANSYS Mechanical APDL. **It is highly recommended to apply the loads and the restraints per nodes or elements and not per lines, keypoints, areas or volumes.**

B.5 Dissertation on validation procedures for FDS2ANSYS

For the validation procedures used for FDS2ANSYS, please consult the **Chapter 7. Validation** of this essay.

B.6 Uninstalling FDS2ANSYS

To uninstall FDS2ANSYS, it is necessary to reach the Microsoft Windows Control Panel - through Start Menu on Windows 7 or by searching it on Windows 8 or newer - and select Programs and Functionalities. Then, select FDS2ANSYS and, when Uninstallation confirmation screen appears, select "Remove the application from this computer" and press Yes to confirm. The uninstallation will be performed in a while.

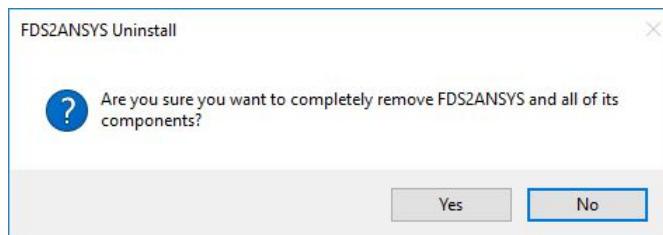


Figure B.23: FDS2ANSYS - Uninstallation message prompt

Appendix C

Script text of the examined case studies

In this section there are the script text that FDS2ANSYS generates - and the adjustments done - in order to perform a thermal-mechanical analysis.

C.1 Case Study A. - Simply supported beam

The first case study is a simply supported beam, reported in a reliable paper ¹ and taken as term of comparison. For further information, please see **Figure 7.1 - Case Study A. geometrical features for validating the Heat Transfer and Endothermic analysis phases [quotes in millimeters]**.

C.1.1 Case Study A. - Raw FDS Code

```
&HEAD CHID= 'beam' , /
&TIME T_END=1000 /
&DUMP NFRAMES=1000 /
&MESH ID= 'Mesh01' , IJK=180 , 12 , 19 ,
XB= 0.000 , 3.600 , 0.000 , 0.240 , 0.000 , 0.380 /

&SURF ID= 'CONCRETE' , COLOR= 'GRAY_40' /
&OBST XB= 0.000 , 3.600 , 0.000 , 0.240 , 0.380 ,
0.380 , SURF_ID= 'CONCRETE' , BNDF_OBST= .TRUE. /
```

¹M. ELSHORBAGY, M. ABDEL-MOOTY (2019), "The coupled thermal-structural response of RC beams during fire events based on nonlinear numerical simulation", Engineering Failure Analysis, Volume 109

```

&OBST XB= 0.000, 3.600, 0.000, 0.240, 0.000,
0.000, SURF_ID='CONCRETE', BDNF_OBST=.TRUE. /
&OBST XB= 0.000, 0.000, 0.000, 0.240, 0.000,
0.380, SURF_ID='CONCRETE', BDNF_OBST=.TRUE. /
&OBST XB= 0.000, 3.600, 0.240, 0.240, 0.000,
0.380, SURF_ID='CONCRETE', BDNF_OBST=.TRUE. /
&OBST XB= 3.600, 3.600, 0.000, 0.240, 0.000,
0.380, SURF_ID='CONCRETE', BDNF_OBST=.TRUE. /
&OBST XB= 0.000, 3.600, 0.000, 0.000, 0.000,
0.380, SURF_ID='CONCRETE', BDNF_OBST=.TRUE. /

&BNDF QUANTITY='ADIABATIC_SURFACE_TEMPERATURE' /
&BNDF QUANTITY='HEAT_TRANSFER_COEFFICIENT' /

&TAIL /

```

C.1.2 Case Study A. - Pyrosim FDS Code

```

beam.fds
Generated by PyroSim - Version 2019.3.1204
8-apr-2021 15.11.15

&HEAD CHID='beam' /
&TIME T_END=1000.0 /
&DUMP DT_RESTART=1000.0, DT_SL3D=0.25 /

&MESH ID='Mesh01', IJK=180,12,50,
XB=0.0,3.6,0.0,0.24,0.0,1.0 /

&REAC ID='POLYURETHANE_GM27',
FYI='SFPE_Handbook,GM27',
FUEL='REAC_FUEL',
C=1.0,
H=1.7,
O=0.3,
N=0.08,
CO_YIELD=0.042,
SOOT_YIELD=0.198,
RADIATIVE_FRACTION=0.35 /

```

```
&DEVC ID='SOLID01',
QUANTITY='ADIABATIC_SURFACE_TEMPERATURE',
XYZ=2.9,0.04,0.74, IOR=-3/
&DEVC ID='SOLID02',
QUANTITY='ADIABATIC_SURFACE_TEMPERATURE',
XYZ=2.9,0.08,0.74, IOR=-3/
&DEVC ID='SOLID03',
QUANTITY='ADIABATIC_SURFACE_TEMPERATURE',
XYZ=2.9,0.12,0.74, IOR=-3/
&DEVC ID='SOLID04',
QUANTITY='ADIABATIC_SURFACE_TEMPERATURE',
XYZ=2.9,0.16,0.74, IOR=-3/
&DEVC ID='SOLID05',
QUANTITY='ADIABATIC_SURFACE_TEMPERATURE',
XYZ=2.9,0.2,0.74, IOR=-3/
&DEVC ID='SOLID06',
QUANTITY='ADIABATIC_SURFACE_TEMPERATURE',
XYZ=2.2,0.2,0.74, IOR=-3/
&DEVC ID='SOLID07',
QUANTITY='ADIABATIC_SURFACE_TEMPERATURE',
XYZ=2.2,0.04,0.74, IOR=-3/
&DEVC ID='SOLID08',
QUANTITY='ADIABATIC_SURFACE_TEMPERATURE',
XYZ=2.2,0.08,0.74, IOR=-3/
&DEVC ID='SOLID09',
QUANTITY='ADIABATIC_SURFACE_TEMPERATURE',
XYZ=2.2,0.12,0.74, IOR=-3/
&DEVC ID='SOLID10',
QUANTITY='ADIABATIC_SURFACE_TEMPERATURE',
XYZ=2.2,0.16,0.74, IOR=-3/
&DEVC ID='SOLID11',
QUANTITY='ADIABATIC_SURFACE_TEMPERATURE',
XYZ=1.4,0.16,0.74, IOR=-3/
&DEVC ID='SOLID12',
QUANTITY='ADIABATIC_SURFACE_TEMPERATURE',
XYZ=0.7,0.04,0.74, IOR=-3/
&DEVC ID='SOLID13',
QUANTITY='ADIABATIC_SURFACE_TEMPERATURE',
XYZ=0.7,0.08,0.74, IOR=-3/
&DEVC ID='SOLID14',
```

```

QUANTITY= 'ADIABATIC_SURFACE_TEMPERATURE',
XYZ=0.7,0.12,0.74, IOR=-3/
&DEVC ID= 'SOLID15',
QUANTITY= 'ADIABATIC_SURFACE_TEMPERATURE',
XYZ=0.7,0.16,0.74, IOR=-3/
&DEVC ID= 'SOLID16',
QUANTITY= 'ADIABATIC_SURFACE_TEMPERATURE',
XYZ=0.7,0.2,0.74, IOR=-3/
&DEVC ID= 'SOLID17',
QUANTITY= 'ADIABATIC_SURFACE_TEMPERATURE',
XYZ=1.4,0.2,0.74, IOR=-3/
&DEVC ID= 'SOLID18',
QUANTITY= 'ADIABATIC_SURFACE_TEMPERATURE',
XYZ=1.4,0.04,0.74, IOR=-3/
&DEVC ID= 'SOLID19',
QUANTITY= 'ADIABATIC_SURFACE_TEMPERATURE',
XYZ=1.4,0.08,0.74, IOR=-3/
&DEVC ID= 'SOLID20',
QUANTITY= 'ADIABATIC_SURFACE_TEMPERATURE',
XYZ=1.4,0.12,0.74, IOR=-3/

&SURF ID= 'CONCRETE',
COLOR= 'GRAY_40'/
&SURF ID= 'BURNER',
COLOR= 'RED',
HRRPUA=1000.0/

&OBST ID= 'Obstruction_#1',
XB=0.0,3.6,0.0,0.24,1.0,1.0,
SURF_ID= 'CONCRETE'/
&OBST ID= 'Obstruction_#2',
XB=0.0,3.6,0.0,0.24,0.76,0.76,
SURF_ID= 'CONCRETE'/
&OBST ID= 'Obstruction_#3',
XB=0.0,0.0,0.0,0.24,0.76,1.0,
SURF_ID= 'CONCRETE'/
&OBST ID= 'Obstruction_#4',
XB=0.0,3.6,0.24,0.24,0.76,1.0,
SURF_ID= 'CONCRETE'/
&OBST ID= 'Obstruction_#5',
XB=3.6,3.6,0.0,0.24,0.76,1.0,

```

```

SURF_ID='CONCRETE'/
&OBST ID='Obstruction_#6',
XB=0.0,3.6,0.0,0.0,0.76,1.0,
SURF_ID='CONCRETE'/
&OBST ID='Obstruction',
XB=0.64,2.94,0.0,0.24,0.0,0.5,
SURF_IDS='BURNER','INERT','INERT'/
&OBST ID='Obstruction', XB=0.62,0.64,0.0,0.24,0.0,0.76,
SURF_ID='INERT'/
&OBST ID='Obstruction', XB=2.94,2.96,0.0,0.24,0.0,0.76,
SURF_ID='INERT'/

&VENT ID='Mesh_Vent:Mesh01[XMIN]',
SURF_ID='OPEN',
XB=0.0,0.0,0.0,0.12,0.0,1.0/
&VENT ID='Mesh_Vent:Mesh01[YMIN]',
SURF_ID='OPEN',
XB=0.0,1.8,0.0,0.0,0.0,1.0/
&VENT ID='Mesh_Vent:Mesh01[ZMAX]',
SURF_ID='OPEN',
XB=0.0,1.8,0.0,0.12,1.0,1.0/
&VENT ID='Mesh_Vent:Mesh02[XMIN]',
SURF_ID='OPEN',
XB=0.0,0.0,0.12,0.24,0.0,1.0/
&VENT ID='Mesh_Vent:Mesh02[YMAX]',
SURF_ID='OPEN',
XB=0.0,1.8,0.24,0.24,0.0,1.0/
&VENT ID='Mesh_Vent:Mesh02[ZMAX]',
SURF_ID='OPEN',
XB=0.0,1.8,0.12,0.24,1.0,1.0/
&VENT ID='Mesh_Vent:Mesh03[XMAX]',
SURF_ID='OPEN',
XB=3.6,3.6,0.0,0.12,0.0,1.0/
&VENT ID='Mesh_Vent:Mesh03[YMIN]',
SURF_ID='OPEN',
XB=1.8,3.6,0.0,0.0,0.0,1.0/
&VENT ID='Mesh_Vent:Mesh03[ZMAX]',
SURF_ID='OPEN',
XB=1.8,3.6,0.0,0.12,1.0,1.0/
&VENT ID='Mesh_Vent:Mesh04[XMAX]',
SURF_ID='OPEN',

```

```

XB=3.6,3.6,0.12,0.24,0.0,1.0/
&VENT ID='Mesh_Vent:Mesh04[YMAX]',
SURF_ID='OPEN',
XB=1.8,3.6,0.24,0.24,0.0,1.0/
&VENT ID='Mesh_Vent:Mesh04[ZMAX]',
SURF_ID='OPEN',
XB=1.8,3.6,0.12,0.24,1.0,1.0/

&BNDF QUANTITY='ADIABATIC_SURFACE_TEMPERATURE'/
&BNDF QUANTITY='HEAT_TRANSFER_COEFFICIENT'/

&TAIL /

```

C.1.3 Case Study A. - /PREP7 Code for ANSYS Mechanical APDL #1

```

/VUP,1,Z
/PREP7
K, 1, 0.000, 0.000, 1.000
K, 2, 0.000, 0.240, 1.000
K, 3, 3.600, 0.000, 1.000
K, 4, 3.600, 0.240, 1.000
K, 5, 0.000, 0.000, 0.760
K, 6, 0.000, 0.240, 0.760
K, 7, 3.600, 0.000, 0.760
K, 8, 3.600, 0.240, 0.760
!*
V,1,3,4,2,5,7,8,6
!*
!*
ET,1,70
!*
KEYOPT,1,2,0
KEYOPT,1,4,0
KEYOPT,1,7,0
KEYOPT,1,8,0
!*
R, 1, , , , , ,
RMORE, , , , , ,
RMORE, ,

```

```
!*
ESIZE ,0.02
MSHAPE ,0,3D
MSHKEY ,1
VMESH ,1
!*
EPLLOT
!*
TOFFST ,273
!*
MPTEMP , , , , , , ,
MPTEMP ,1,20
MPTEMP ,2,100
MPTEMP ,3,200
MPTEMP ,4,300
MPTEMP ,5,400
MPTEMP ,6,500
MPTEMP ,7,600
MPDATA ,DENS ,1, , ,2400
MPDATA ,DENS ,1, , ,2400
MPDATA ,DENS ,1, , ,2352
MPDATA ,DENS ,1, , ,2316
MPDATA ,DENS ,1, , ,2280
MPDATA ,DENS ,1, , ,2259
MPDATA ,DENS ,1, , ,2238
MPTEMP , , , , , , ,
MPTEMP ,1,20
MPTEMP ,2,100
MPTEMP ,3,200
MPTEMP ,4,300
MPTEMP ,5,400
MPTEMP ,6,500
MPTEMP ,7,600
MPDATA ,KXX ,1, , ,1.333028
MPDATA ,KXX ,1, , ,1.2297
MPDATA ,KXX ,1, , ,1.1108
MPDATA ,KXX ,1, , ,1.0033
MPDATA ,KXX ,1, , ,0.9072
MPDATA ,KXX ,1, , ,0.8225
MPDATA ,KXX ,1, , ,0.7492
MPTEMP , , , , , , ,
```

```
MPTEMP , 1 , 20
MPDATA ,EMIS ,1 , ,0.8
MPTEMP , , , , , ,
MPTEMP ,1 ,20
MPTEMP ,2 ,100
MPTEMP ,3 ,200
MPTEMP ,4 ,300
MPTEMP ,5 ,400
MPTEMP ,6 ,500
MPTEMP ,7 ,600
MPDATA ,C ,1 , ,900
MPDATA ,C ,1 , ,900
MPDATA ,C ,1 , ,1000
MPDATA ,C ,1 , ,1050
MPDATA ,C ,1 , ,1100
MPDATA ,C ,1 , ,1100
MPDATA ,C ,1 , ,1100
!*
MPTEMP , , , , , ,
MPTEMP ,1 ,20
MPTEMP ,2 ,1000
MPDATA ,DENS ,2 , ,7850
MPDATA ,DENS ,2 , ,7850
MPTEMP , , , , , ,
MPTEMP ,1 ,20
MPTEMP ,2 ,100
MPTEMP ,3 ,200
MPTEMP ,4 ,300
MPTEMP ,5 ,400
MPTEMP ,6 ,500
MPTEMP ,7 ,600
MPTEMP ,8 ,700
MPTEMP ,9 ,800
MPTEMP ,10 ,900
MPTEMP ,11 ,1000
MPDATA ,KXX ,2 , ,47.56
MPDATA ,KXX ,2 , ,45.8
MPDATA ,KXX ,2 , ,43.6
MPDATA ,KXX ,2 , ,41.4
MPDATA ,KXX ,2 , ,39.2
MPDATA ,KXX ,2 , ,37
```

```

MPDATA ,KXX ,2 , ,34.8
MPDATA ,KXX ,2 , ,32.6
MPDATA ,KXX ,2 , ,30.4
MPDATA ,KXX ,2 , ,28.2
MPDATA ,KXX ,2 , ,28.2
MPTEMP , , , , , , ,
MPTEMP ,1 ,20
MPTEMP ,2 ,100
MPTEMP ,3 ,200
MPTEMP ,4 ,300
MPTEMP ,5 ,400
MPTEMP ,6 ,500
MPTEMP ,7 ,600
MPTEMP ,8 ,700
MPTEMP ,9 ,800
MPTEMP ,10 ,900
MPTEMP ,11 ,1000
MPDATA ,C ,2 , ,430.573248407643
MPDATA ,C ,2 , ,471.337579617834
MPDATA ,C ,2 , ,522.292993630573
MPDATA ,C ,2 , ,573.248407643312
MPDATA ,C ,2 , ,624.203821656051
MPDATA ,C ,2 , ,675.15923566879
MPDATA ,C ,2 , ,726.114649681529
MPDATA ,C ,2 , ,1184.71337579618
MPDATA ,C ,2 , ,579.617834394904
MPDATA ,C ,2 , ,579.617834394904
MPDATA ,C ,2 , ,579.617834394904
MPTEMP , , , , , , ,
MPTEMP ,1 ,20
MPDATA ,EMIS ,2 , ,0.8

```

C.1.4 Case Study A. - /PREP7 Code for ANSYS Mechanical APDL #2

```

/PREP7
N, 30590, 0.010, 0.010, 1.000, , , ,
N, 30591, 0.000, 0.010, 0.990, , , ,
N, 30592, 0.010, 0.000, 0.990, , , ,
N, 30593, 0.010, 0.030, 1.000, , , ,

```

```
N, 30594, 0.000, 0.030, 0.990, , , ,
```

```
[...]
```

```
N, 39514, 3.590, 0.210, 0.760, , , ,
```

```
N, 39515, 3.590, 0.240, 0.770, , , ,
```

```
N, 39516, 3.600, 0.230, 0.770, , , ,
```

```
N, 39517, 3.590, 0.230, 0.760, , , ,
```

```
!*
```

```
ET, 2, SURF152
```

```
!*
```

```
KEYOPT, 2, 1, 0
```

```
KEYOPT, 2, 2, 0
```

```
KEYOPT, 2, 3, 0
```

```
KEYOPT, 2, 4, 0
```

```
KEYOPT, 2, 5, 1
```

```
KEYOPT, 2, 6, 0
```

```
KEYOPT, 2, 7, 0
```

```
KEYOPT, 2, 8, 4
```

```
KEYOPT, 2, 9, 1
```

```
!*
```

```
!*
```

```
R, 2, 1, 5.67E-08, , , ,
```

```
RMORE, , , ,
```

```
RMORE, , , ,
```

```
!*
```

```
!*
```

```
TYPE, 2
```

```
MAT, 1
```

```
REAL, 2
```

```
ESYS, 0
```

```
SECNUM,
```

```
TSHAP, LINE
```

```
!*
```

```
nsel, S, node, , 384
```

```
nsel, A, node, , 1
```

```
nsel, A, node, , 3
```

```
nsel, A, node, , 385
```

```
ESURF, 30590
```

```
!*
```

```
nsel, S, node, , 1
```

```
nselect, A, node, , 384
nselect, A, node, , 6841
nselect, A, node, , 2556
ESURF, 30591
!*
nselect, S, node, , 3
nselect, A, node, , 1
nselect, A, node, , 2556
nselect, A, node, , 2557
ESURF, 30592
!*
nselect, S, node, , 383
nselect, A, node, , 384
nselect, A, node, , 385
nselect, A, node, , 386
ESURF, 30593
!*

[...]

!*
nselect, S, node, , 8929
nselect, A, node, , 8930
nselect, A, node, , 4548
nselect, A, node, , 4547
ESURF, 39514
!*
nselect, S, node, , 6829
nselect, A, node, , 4527
nselect, A, node, , 4526
nselect, A, node, , 4671
ESURF, 39515
!*
nselect, S, node, , 4527
nselect, A, node, , 4669
nselect, A, node, , 4548
nselect, A, node, , 4526
ESURF, 39516
!*
nselect, S, node, , 8930
nselect, A, node, , 4671
```

```

nset ,A,node , ,      4526
nset ,A,node , ,      4548
ESURF ,      39517
!*
ALLSEL ,ALL
!*
*DIM ,A      30590 ,TABLE ,      501 ,1 ,1 , TIME , TEMP ,
!*
*DIM ,H      30590 ,TABLE ,      501 ,1 ,1 , TIME , ,
!*
*DIM ,A      30591 ,TABLE ,      501 ,1 ,1 , TIME , TEMP ,
!*
*DIM ,H      30591 ,TABLE ,      501 ,1 ,1 , TIME , ,
!*
*DIM ,A      30592 ,TABLE ,      501 ,1 ,1 , TIME , TEMP ,
!*
*DIM ,H      30592 ,TABLE ,      501 ,1 ,1 , TIME , ,
!*
*DIM ,A      30593 ,TABLE ,      501 ,1 ,1 , TIME , TEMP ,
!*
*DIM ,H      30593 ,TABLE ,      501 ,1 ,1 , TIME , ,
!*
*DIM ,A      30594 ,TABLE ,      501 ,1 ,1 , TIME , TEMP ,
!*
*DIM ,H      30594 ,TABLE ,      501 ,1 ,1 , TIME , ,
!*

[...]

!*
*DIM ,A      39513 ,TABLE ,      501 ,1 ,1 , TIME , TEMP ,
!*
*DIM ,H      39513 ,TABLE ,      501 ,1 ,1 , TIME , ,
!*
*DIM ,A      39514 ,TABLE ,      501 ,1 ,1 , TIME , TEMP ,
!*
*DIM ,H      39514 ,TABLE ,      501 ,1 ,1 , TIME , ,
!*
*DIM ,A      39515 ,TABLE ,      501 ,1 ,1 , TIME , TEMP ,
!*
*DIM ,H      39515 ,TABLE ,      501 ,1 ,1 , TIME , ,

```

```

!*
*DIM ,A      39516 , TABLE ,      501 , 1 , 1 , TIME , TEMP ,
!*
*DIM ,H      39516 , TABLE ,      501 , 1 , 1 , TIME , ,
!*
*DIM ,A      39517 , TABLE ,      501 , 1 , 1 , TIME , TEMP ,
!*
*DIM ,H      39517 , TABLE ,      501 , 1 , 1 , TIME , ,
!*
*set ,A      30590(      1 , 0) , 0.00000E+00
*set ,A      30590(      1 , 1) , 0.20000E+02
*set ,A      30590(      2 , 0) , 0.20005E+01
*set ,A      30590(      2 , 1) , 0.20000E+02

[... ]

*set ,H      39517(      500 , 0) , 0.99800E+03
*set ,H      39517(      500 , 1) , 0.25559E+01
*set ,H      39517(      501 , 0) , 0.10000E+04
*set ,H      39517(      501 , 1) , 0.25559E+01
!*
D,      30590 , , %A      30590% , , , , TEMP , , , , ,
!*
D,      30591 , , %A      30591% , , , , TEMP , , , , ,
!*
D,      30592 , , %A      30592% , , , , TEMP , , , , ,
!*
D,      30593 , , %A      30593% , , , , TEMP , , , , ,
!*
D,      30594 , , %A      30594% , , , , TEMP , , , , ,
!*

[... ]

!*
D,      39514 , , %A      39514% , , , , TEMP , , , , ,
!*
D,      39515 , , %A      39515% , , , , TEMP , , , , ,
!*
D,      39516 , , %A      39516% , , , , TEMP , , , , ,
!*

```

```

D, 39517, , %A 39517% , , , ,TEMP, , , , ,
!*
SFE, 25921,1,CONV,0,%H 30590%
SFE, 25922,1,CONV,0,%H 30591%
SFE, 25923,1,CONV,0,%H 30592%
SFE, 25924,1,CONV,0,%H 30593%

[...]

SFE, 34845,1,CONV,0,%H 39514%
SFE, 34846,1,CONV,0,%H 39515%
SFE, 34847,1,CONV,0,%H 39516%
SFE, 34848,1,CONV,0,%H 39517%

```

C.1.5 Case Study A. - /PREP7 Code for ANSYS Mechanical APDL #3

```

/VUP,1,Z
/UIS,MSGPOP,4
/PREP7
MAT,2
!*
ET,3,33
!*
TYPE,3
!*
N,741,1.4,0.9,0.8
N,742,1.5,0.9,0.8
N,743,1.6,0.9,0.8

[...]

N,879,4.7,1,1
N,880,4.8,1,1
!*
MAT,2
SECTYPE,1,LINK,,R1,
SECDATA,0.000113,
SECCONTROL,0,1
SECNUM,1

```

```
E,741,742  
E,742,743  
E,743,744
```

```
[...]
```

```
E,808,809  
E,809,810  
MAT,2  
SECTYPE,2,LINK,,R2,  
SECDATA,0.000572265,  
SECCONTROL,0,1  
SECNUM,2  
E,811,812  
E,812,813  
E,813,814
```

```
[...]
```

```
E,878,879  
E,879,880  
MAT,2  
SECTYPE,3,LINK,,R3,  
SECDATA,0.0001578,  
SECCONTROL,0,1  
SECNUM,3  
E,741,776  
E,742,777  
E,743,778
```

```
[...]
```

```
E,809,879  
E,810,880  
NUMMRG,NODES  
FINISH  
SAVE
```

C.1.6 Case Study A. - /PREP7 Code for ANSYS Mechanical APDL #4

```

/VUP , 1 , Z
/UIS , MSGPOP , 4
/PREP7
K , 1 , 3.600 , 0.000 , 0.000
K , 2 , 3.600 , 0.000 , 0.400
K , 3 , 3.600 , 0.300 , 0.000
K , 4 , 3.600 , 0.300 , 0.400
K , 5 , 0.000 , 0.000 , 0.000
K , 6 , 0.000 , 0.000 , 0.400
K , 7 , 0.000 , 0.300 , 0.000
K , 8 , 0.000 , 0.300 , 0.400
!*
V , 5 , 1 , 3 , 7 , 6 , 2 , 4 , 8
!*
MAT , 1
!*
ET , 1 , 65
!*
KEYOPT , 1 , 1 , 0
KEYOPT , 1 , 3 , 0
KEYOPT , 1 , 5 , 0
KEYOPT , 1 , 6 , 0
KEYOPT , 1 , 7 , 0
KEYOPT , 1 , 8 , 0
!*
R , 1 , , , , , ,
!*
ESIZE , 0.1
MSHAPE , 0 , 3D
MSHKEY , 1
VMESH , 1
!*
EPLLOT
!*
TOFFST , 273
!*
ANTYPE , 4

```

```

!*
TRNOPT , FULL
LUMPM , 0
!*
DELTIM , 1 , 0 , 0
OUTRES , ERASE
OUTRES , ALL , 1
KBC , 0
TIME , 9000
!*
TUNIF , 20 ,
TREF , 20 ,
!*
LDREAD , TEMP , , , , , 'beam' , 'rth' , '□'
!*
MAT , 2
!*
ET , 2 , 180
!*
KEYOPT , 2 , 2 , 0
KEYOPT , 2 , 12 , 0
NLGEOM , ON
!*
MAT , 1
MPTEMP , , , , , , ,
MPTEMP , 1 , 20
MPTEMP , 2 , 100
MPTEMP , 3 , 200
MPTEMP , 4 , 300
MPTEMP , 5 , 400
MPTEMP , 6 , 500
MPTEMP , 7 , 600
MPDATA , EX , 1 , , 55000000
MPDATA , EX , 1 , , 55000000
MPDATA , EX , 1 , , 35200000
MPDATA , EX , 1 , , 19800000
MPDATA , EX , 1 , , 8800000
MPDATA , EX , 1 , , 2200000
MPDATA , EX , 1 , , 0
MPDATA , PRXY , 1 , , 0.2
MPDATA , PRXY , 1 , , 0.1733333333333333

```

```
MPDATA ,PRXY ,1 , ,0.14
MPDATA ,PRXY ,1 , ,0.1066666666666667
MPDATA ,PRXY ,1 , ,0.073333333333333333
MPDATA ,PRXY ,1 , ,0.04
MPDATA ,PRXY ,1 , ,0.04
TB ,KINH ,1 ,13 ,3 ,
TBTEMP ,20
TBPT , ,0.0025 ,55000000
TBPT , ,0.02 ,0
TBTEMP ,100
TBPT , ,0.004 ,55000000
TBPT , ,0.0225 ,0
TBTEMP ,200
TBPT , ,0.0055 ,52250000
TBPT , ,0.025 ,0
TBTEMP ,300
TBPT , ,0.007 ,46750000
TBPT , ,0.0275 ,0
TBTEMP ,400
TBPT , ,0.01 ,41250000
TBPT , ,0.03 ,0
TBTEMP ,500
TBPT , ,0.015 ,33000000
TBPT , ,0.0325 ,0
TBTEMP ,600
TBPT , ,0.025 ,24750000
TBPT , ,0.035 ,0
TBTEMP ,700
TBPT , ,0.025 ,16500000
TBPT , ,0.0375 ,0
TBTEMP ,800
TBPT , ,0.025 ,8250000
TBPT , ,0.04 ,0
TBTEMP ,900
TBPT , ,0.025 ,3300000
TBPT , ,0.0425 ,0
TBTEMP ,1000
TBPT , ,0.025 ,2200000
TBPT , ,0.045 ,0
TBTEMP ,1100
TBPT , ,0.025 ,550000
```

```

TBPT , , 0.0475 , 0
TB , CONC , 1 , 1 , 9 ,
TBTEMP , 20
TBDATA , , 0.3 , 0.6 , 2.7e+6 , -1 , 0 , 0
TBDATA , , 0 , 0 , 0 , , ,
MPTEMP , , , , , , ,
UIMP , 1 , REFT , , , 20
MPTEMP , 1 , 20
MPDATA , ALPX , 1 , , 6.16E-06
!*
MAT , 2
MPTEMP , , , , , , ,
MPTEMP , 1 , 20
MPTEMP , 2 , 100
MPTEMP , 3 , 200
MPTEMP , 4 , 300
MPTEMP , 5 , 400
MPTEMP , 6 , 500
MPTEMP , 7 , 600
MPTEMP , 8 , 700
MPTEMP , 9 , 800
MPTEMP , 10 , 900
MPTEMP , 11 , 1000
MPDATA , EX , 2 , , 200000000000
MPDATA , EX , 2 , , 200000000000
MPDATA , EX , 2 , , 180000000000
MPDATA , EX , 2 , , 160000000000
MPDATA , EX , 2 , , 140000000000
MPDATA , EX , 2 , , 120000000000
MPDATA , EX , 2 , , 62000000000
MPDATA , EX , 2 , , 26000000000
MPDATA , EX , 2 , , 18000000000
MPDATA , EX , 2 , , 14000000000
MPDATA , EX , 2 , , 8000000000
MPDATA , PRXY , 2 , , 0.309376
MPDATA , PRXY , 2 , , 0.311936
MPDATA , PRXY , 2 , , 0.315136
MPDATA , PRXY , 2 , , 0.318336
MPDATA , PRXY , 2 , , 0.321536
MPDATA , PRXY , 2 , , 0.324736
MPDATA , PRXY , 2 , , 0.327936

```

```
MPDATA ,PRXY ,2 , ,0.331136
MPDATA ,PRXY ,2 , ,0.334336
MPDATA ,PRXY ,2 , ,0.337536
MPDATA ,PRXY ,2 , ,0.3
MPTEMP , , , , , ,
MPTEMP ,1 ,20
UIMP ,2 ,REFT , , ,20
MPDATA ,ALPX ,2 , ,1.208E-05
TB ,MISO ,2 ,11 ,4 ,
TBTEMP ,20
TBPT , ,0.02 ,450000000
TBPT , ,0.15 ,450000000
TBPT , ,0.2 ,0
TBTEMP ,100
TBPT , ,0.02 ,450000000
TBPT , ,0.15 ,450000000
TBPT , ,0.2 ,0
TBTEMP ,200
TBPT , ,0.02 ,450000000
TBPT , ,0.15 ,450000000
TBPT , ,0.2 ,0
TBTEMP ,300
TBPT , ,0.02 ,450000000
TBPT , ,0.15 ,450000000
TBPT , ,0.2 ,0
TBTEMP ,400
TBPT , ,0.02 ,450000000
TBPT , ,0.15 ,450000000
TBPT , ,0.2 ,0
TBTEMP ,500
TBPT , ,0.02 ,351000000
TBPT , ,0.15 ,351000000
TBPT , ,0.2 ,0
TBTEMP ,600
TBPT , ,0.02 ,211500000
TBPT , ,0.15 ,211500000
TBPT , ,0.2 ,0
TBTEMP ,700
TBPT , ,0.02 ,103500000
TBPT , ,0.15 ,103500000
TBPT , ,0.2 ,0
```

```
TBTEMP ,800
TBPT , ,0.02 ,49500000
TBPT , ,0.15 ,49500000
TBPT , ,0.2 ,0
TBTEMP ,900
TBPT , ,0.02 ,27000000
TBPT , ,0.15 ,27000000
TBPT , ,0.2 ,0
TBTEMP ,1000
TBPT , ,0.02 ,18000000
TBPT , ,0.15 ,18000000
TBPT , ,0.2 ,0
!*
MAT ,2
!*
ET ,2 ,180
!*
KEYOPT ,2 ,2 ,0
KEYOPT ,2 ,12 ,0
NLGEOM ,ON
!*
TYPE ,2
!*
N ,741 ,1.4 ,0.9 ,0.8
N ,742 ,1.5 ,0.9 ,0.8
N ,743 ,1.6 ,0.9 ,0.8

[... ]

N ,879 ,4.7 ,1 ,1
N ,880 ,4.8 ,1 ,1
!*
MAT ,2
SECTYPE ,1 ,LINK , ,R1
SECDATA ,0.000113 ,
SECCONTROL ,0 ,1
SECNUM ,1
E ,741 ,742
E ,742 ,743
E ,743 ,744
```

[...]

```
E,808,809
E,809,810
MAT,2
SECTYPE,2,LINK,,R2
SECDATA,0.000572265,
SECCONTROL,0,1
SECNUM,2
E,811,812
E,812,813
E,813,814
```

[...]

```
E,878,879
E,879,880
MAT,2
SECTYPE,3,LINK,,R3
SECDATA,0.0001578,
SECCONTROL,0,1
SECNUM,3
E,741,776
E,742,777
E,743,778
```

[...]

```
E,809,879
E,810,880
NUMMRG,ALL
ACEL,0,0,9.806
!*
FINISH
SAVE
```

Bibliography

- Abdel-Mooty M., Elshobargy M. *The coupled thermal-structural response of RC beams during fire events based on nonlinear numerical simulation* Engineering Failure Analysis 109 - 2020
- Agrawal A., Kodur V.K.R. *An approach for evaluating residual capacity of reinforced concrete beams exposed to fire* Engineering Structures 110 - 2016
- Albostan U. *Implementation of Coupled Thermal and Structural Analysis Methods for Reinforced Concrete Structures* M.Sc. Thesis, Middle East Technical University, Ankara, Turkey - 2013
- Allam S.M., Shoukry M.S., Rashad G.E., Hassan A.S. *Evaluation of tension stiffening effect on the crack width calculation of flexural RC members* Alexandria Engineering Journal 52 - 2013
- American Society of Civil Engineers *Manual of Practice no.78* 1992
- Anson M., Lau A. *Effect of high temperatures on high performance steel fibre reinforced concrete* Cement and Concrete Research 36 - 2006
- ASTM F2170-18 *Standard Test Method for determining Relative Humidity in Concrete Floor Slabs Using in Situ Probes* 2018
- ANSYS, Inc. *ANSYS Mechanical APDL Introductory Tutorials* 2017
- ANSYS, Inc. *ANSYS Mechanical APDL Command Reference Guide* 2019
- ANSYS, Inc. *ANSYS Mechanical APDL Theory Reference Guide* 2019
- ANSYS, Inc. *ANSYS Mechanical APDL Element Reference Guide* 2020
- Babrauskas V. *COMP2 - A Program for Calculating Post-Flashover Fire Temperatures* NBS Technical Note 991 - 1979

- Babrauskas V., Clark H.M., Harris R.H., Gann R.G. Jr, Levin B.C., Lee B.T., Peacock R.D., Paabo M., Twilley W., Yoklavich M.F. *Fire Hazard Comparison of Fire-Retarded and Non-Fire-Retarded Products* NBS Special Publication 749 - 1988
- Babrauskas V., Krasny J.F., Parker W.J. *Fire Behavior of Upholstered Furniture and Mattresses* William Andrew Publishing, Norwich, England - 2007
- Bahr O., Schaumann P., Bollen B., Bracke J. *Young's modulus and Poisson's ratio of concrete at high temperatures: Experimental investigations* Materials and Design 45 - 2013
- Banerjee D., Gross J., Hess W., Olano M., Terrill J. *Visualization of Structural Behavior under Fire* NISTIR 7619 - 2009
- Baum H.R. *Simulating Fire Effects on Complex Building Structures* Fire Safety Science - Proceedings of the Eighth International Symposium - 2005
- Baum H.R., Prasad K. *Coupled fire dynamics and thermal response of complex building structures* Proceedings of the Combustion Institute 30 - 2005
- Breunese A., Fellingner J. *Fire Safe Design: Make it Concrete!* 2004
- Buchanan A. H. *Structural Design for Fire Safety* John Wiley & Sons, New York City, United States - 2002
- Buchanan A. H., Abu A. K. *Structural Design for Fire Safety – Second Edition* John Wiley & Sons, New York City, United States - 2017
- Burgess I., Huang Z., Plank R. *Behaviour of reinforced concrete structures in fire* 2014
- Chan A., Kumar S., Lemaire T., Miles S., Welch S. *FIRESTRUC – Integrating Advanced Three-dimensional Modelling Methodologies for Predicting Thermo-mechanical Behaviour of Steel and Composite Structures Subjected to Natural Fires* Fire Safety Science - Proceedings of the Ninth International Symposium - 2008
- Chen L., Liu P., Lua J., Luo C. *Abaqus Fire Interface Simulator Toolkit (AFIST) For Coupled Fire and Structural Response Prediction* American Institute of Aeronautics and Astronautics, Inc. - 2010

- Chen L., Lua J., Luo C. *FDS and Abaqus Coupling Toolkit for Fire Simulation and Thermal and Mass Flow Prediction* Fire Safety Science - Proceedings of the Tenth International Symposium - 2011
- Choe G., Hwang E., Kim G., Kim Y., Lee T., Nam J., Yoon M. *Creep Behavior of High-Strength Concrete Subjected to Elevated Temperatures* Materials 10 - 2017
- Colajanni P., Papia M., Spinella N. *Stress-Strain Law for Confined Concrete with Hardening or Softening Behavior* Dipartimento di Ingegneria Civile, Informatica, Edile, Ambientale e Matematica Applicata, Università di Messina, Contrada di Dio, Villaggio Sant'Agata, 98166 Messina, Italy; Dipartimento di Ingegneria Civile, Ambientale, Aerospaziale e dei Materiali (DICAM), Università di Palermo, Viale delle Scienze, 90128 Palermo, Italy - 2013
- Collins D.C. *Dividing and Conquering Meshes within the NIST Fire Dynamics Simulator (FDS) on Multicore Computing Systems* Master's Thesis, University of Tennessee - 2015
- Concrete Construction Staff *Failure of a high-rise system* 1969
- Cosi F. *Antincendio. Casi pratici di progettazione* Wolters Kluwer - 2017
- Dahmani L., Kouane M. *Thermal Cracking Response of Reinforced Concrete Beam to Gradient Temperature* World Academy of Science, Engineering and Technology International Journal of Civil and Environmental Engineering Vol:6 - 2012
- de Boer J. G. G. M., Hofmeyer H., Maljaars J., van Herpen, R. *Two-way coupled CFD fire and thermomechanical FE analyses of a self-supporting sandwich panel façade system* Fire Safety Journal 105 - 2019
- De Wit A. *Behaviour and structural design of concrete structures exposed to fire* Master of Science Thesis, Stockholm, Sweden - 2011
- Denoël J.F. *Fire Safety and Concrete Structures* FEBELCEM - Federation of Belgian Cement Industry - 2007
- Drysdale D. *An introduction to fire dynamics, second edition* John Wiley & Sons, New York City, United States - 1998
- Duthinh D., McGrattan K., Khaskia A. *Recent advances in fire-structure analysis* Fire Safety Journal 43 - 2008

- Duthinh D., McGrattan K., Wickstrom U. *Adiabatic Surface Temperature For Calculating Heat Transfer To Fire Exposed Structures* NIST Publication - 2007
- El-Shayeb M. *Fire Resistance of Concrete-Filled And Reinforced Concrete Columns* University of New Hampshire, Durham, New Hampshire - 1986
- El-Zohairy A., Hammontree H., Oh E., Moler P. *Temperature Effect on the Compressive Behavior and Constitutive Model of Plain Hardened Concrete* Materials 13 - 2020
- EN 1991-1-2:2004 Standard *Eurocode 1: Actions on structures – Part 1-2: General actions – Actions on structures exposed to fire* 2004
- EN 1992-1-2:2019 Standard *Eurocode 2: Actions on concrete structures – Part 1-2: General actions – Actions on structures exposed to fire* 2019
- EN 1993-1-2:2005 Standard *Eurocode 3: Actions on steel structures – Part 1-2: General actions – Actions on structures exposed to fire* 2005
- Fédération internationale du béton *Fire Design of concrete structures – structural behavior and assessment* fib Bulletin 46 - 2008
- Feenstra J. *FDS-2-Abaqus, C++ Managed automated Python scripted CFD-FEM Coupling* Master of Science Degree Thesis, Eindhoven University of Technology - 2016
- Floyd J., Hostikka S., McDermott R., McGrattan K., Vanella M. *Fire Dynamics Simulator Technical Reference Guide; Volume 1: Mathematical Model* NIST Special Publication 1018-1 - Sixth Edition - 2020
- Floyd J., Hostikka S., McDermott R., McGrattan K., Vanella M. *Fire Dynamics Simulator User's Guide* NIST Special Publication 1019 - Sixth Edition - 2020
- Forney G. *Smokeview, A Tool for Visualizing Fire Dynamics Simulation Data - Volume I: User's Guide* NIST Special Publication 1017-1 - Sixth Edition - 2020
- Forney G. *Smokeview, A Tool for Visualizing Fire Dynamics Simulation Data - Volume II: Technical Reference Guide* NIST Special Publication 1017-2 - Sixth Edition - 2020

- Gernay T., Franssen J.M., Millard A. *A multi-axial constitutive model for concrete in the fire situation: Theoretical formulation* International Journal of Solids and Structures 50 - 2013
- Gomex P, Hernandez J., Lopez J., Zanzi C. *Analysis of Heat and Smoke Propagation and Oscillatory Flow through Ceiling Vents in a Large-Scale Compartment Fire* Applied Sciences 9 - 2019
- Guven I., Madenci E. *The Finite Element Method and Applications in Engineering Using ANSYS - Second Edition* Springer, United States - 2015
- Hager I., Mroz K. *An overview of concrete modulus of elasticity evolution with temperature and comments to European code provisions* IFireSS – International Fire Safety Symposium Coimbra, Portugal - 2015
- Halahla A. *Study the Behavior of Reinforced Concrete Beam Using Finite Element Analysis* Proceedings of the 3rd World Congress on Civil, Structural, and Environmental Engineering (CSEE'18) Budapest, Hungary - 2018
- Hurley M. J. *SFPE Handbook of Fire Protection Engineering - Fifth edition* Springer, United States - 2016
- Husain A., Ahmad J., Mujeeb A., Ahmed R. *Effects of Temperature on Concrete* International Journal of Advance Research in Science and Engineering - 2016
- INAIL *Il Codice di Prevenzione Incendi* Collana Ricerche - 2018
- INAIL *Gestione della Sicurezza e Operatività Antincendio* 2018
- INAIL *La Resistenza Al Fuoco Degli Elementi Strutturali* 2019
- INAIL *Metodi per l'ingegneria della sicurezza antincendio* 2019
- ISO Technical Report 16738 *Fire-safety engineering — Technical information on methods for evaluating behaviour and movement of people* 2009
- Italian Ministerial Decree 31 July 2012 *Approvazione delle Appendici nazionali recanti i parametri tecnici per l'applicazione degli Eurocodici* Decreto Ministeriale 31 luglio 2012 - 2012

- Italian Ministerial Decree 18 October 2019 *Codice di Prevenzione Incendi* Decreto Ministeriale 18 Ottobre 2019 - 2019
- Italian Ministerial Decree 18 October 2019 *Technical fire prevention standards* Decreto Ministeriale 18 Ottobre 2019 - Traduzione in lingua inglese - 2019
- Italian Ministerial Decree 20th february 2018 *Aggiornamento delle «Norme tecniche per le costruzioni»*. Decreto Ministeriale 20 febbraio 2018 - 2018
- Kent, D.C., Park, R. *Flexural Members with Confined Concrete* Journal of the Structural Division, ASCE, Vol. 97 - 1971
- Khoury G.A. *Passive fire protection of concrete structures* Proceedings of the Institution of Civil Engineers, Structures & Buildings 161, Issue SB3 - 2008
- Kodur V.K.R., Shakya A.M *Modeling the response of precast, prestressed concrete hollow-core slabs exposed to fire* PCI Journal - 2014
- La Malfa A., La Malfa R., La Malfa S. *Ingegneria della Sicurezza Antincendio* Legislazione Tecnica, Rome, Italy - 2020
- La Malfa A., La Malfa S. *Prevenzione Incendi - Problemi pratici risolti - Metodo prestazionale* Legislazione Tecnica, Rome, Italy - 2008
- Marechal J. C. *Variations In The Modulus Of Elasticity And Poisson's Ratio With Temperature* ACI Library - 1972
- McNamee R.J. *Fire spalling of concrete – A historical overview* MATEC Web of Conferences 6 - 2013
- Molay T.G.G., Leroy M.N.L., Fidele T., Franck H.G., Bienvenu N.J.M. *Mechanical and physical performances of concretes made from crushed sands of different geological nature subjected to high temperatures* Engineering Science and Technology - 2019
- Naser M. Z., Hawileh R.A., Abdalla J. *Modeling Strategies of Finite Element Simulation of Reinforced Concrete Beams Strengthened with FRP: A Review* Journal of Composite Science, 5 - 2021
- Naus D.J. *A Compilation of Elevated Temperature Concrete Material Property Data and Information for Use in Assessments of Nuclear Power Plant Reinforced Concrete Structures* Office of Nuclear Regulatory Research - 2010

- NFPA 13 *Standard for the Installation of Sprinkler Systems* NFPA, 1 Batterymarch Park, Quincy, Massachusetts - 2016
- NFPA 92 *Standard for Smoke Control Systems* NFPA, 1 Batterymarch Park, Quincy, Massachusetts - 2013
- Persson B. *Poisson's ratio of high-performance concrete* Cement and Concrete Research 29 - 1999
- Phan L. T., McAllister T. P., Gross J. L., Hurley M. J. *Best Practice Guidelines for Structural Fire Resistance Design of Concrete and Steel Buildings* NIST Technical Note 1681 - 2010
- Scott B.D. *Stress - Strain Relationships for Confined Concrete: Rectangular Sections* 1980
- Siddique R., Kaur D. *Properties of concrete containing ground granulated blast furnace slag (GGBFS) at elevated temperatures* Journal of Advanced Research - 2012
- Silva J.C. *FDS2FTMI User's Guide - An automated code to one-way coupling between FDS and FEM using FTMI* National Institute of Standards and Technology - 2017
- Silva R. *Direct Coupled Thermal-Structural Analysis in ANSYS WorkBench* ESSS Conference & ANSYS Users meeting, Atibaia, SP, Brazil - 2013
- UNI 10779:2014 *Fire fighting equipment - Hydrant systems* 2014
- UNI EN 12845:2009 *Fixed firefighting systems - Automatic sprinkler systems* 2009
- Yang Y. *Temperature-Dependent Thermoelastic Analysis of Multi-Dimensional Functionally Graded Materials* Ph.D. Thesis, University of Pittsburgh, Pennsylvania - 2015
- Zhang C., Silva J. G., Weinschenk C., Kamikawa D., Hasemi Y. *Simulation Methodology for Coupled Fire-Structure Analysis: Modeling localized - retests on a steel column* NIST Publication - 2016
- Zhang C., Silva J.C., Weinschenk C., Kamikawa D., Heasemi Y. *Simulation Methodology for Coupled Fire-Structure Analysis: Modeling localized fire tests on a steel column* National Institute of Standards and Technology - 2017